THE APPLICATION OF NANOMATERIALS FOR THE DELIVERY OF NATURAL ANTIMICROBIALS IN ENGINEERED SYSTEMS



Dissertation submitted for the degree of

DOCTOR OF PHILOSOPHY

Department of Engineering Science

UNIVERSITY OF OXFORD

ANDREA C. CHAN

Supervisor: Professor Ian P. Thompson

Brasenose College

Michaelmas Term 2013

THE APPLICATION OF NANOMATERIALS FOR THE DELIVERY OF NATURAL ANTIMICROBIALS IN ENGINEERED SYSTEMS

Biofouling is the undesired biofilm formation on surfaces at a liquid interface that interferes with the affected substrate's function. It is a ubiquitous problem in many engineered systems in industry. Biofouling causes contamination, essential damage to materials, and impedances to crucial industrial processes. These adverse effects lead to health hazards, gross increase in energy consumption, and significant decrease in overall productivity, all of which result in higher operational costs and environmentally destructive consequences.

Interest in discovering effective alternatives to conventional antimicrobial agents has gained momentum. Current anti-biofouling strategies have significant disadvantages, such as the generation of toxic by-products, harmful bioaccumulation in humans and animals, indiscriminate corrosion of surrounding materials and the environment, and promotion of resistance development. Alternative anti-biofouling methods are in high demand because present-day solutions are far from sustainable.

Plant secondary metabolites have been used as antiseptic, medicinal, and food preservation agents since antiquity. They are promising candidates as novel biocides because they are (i) highly effective in killing microbes while being non-toxic to humans at antimicrobially active concentrations, and (ii) safer and non-damaging to the natural environment since they are originally sourced from plant material. Herein, antimicrobial efficacies of five plant-derived compounds were assessed against various species of planktonic bacteria as well as biofilms at various maturity stages. Allyl isothiocyanate (AIT) and cinnamaldehyde (CNAD) displayed the greatest inhibitory effects against all planktonic species tested. The minimum inhibitory concentration is defined as the lowest concentration of a substance that inhibits visible microbial growth, and the MBC is defined as the lowest concentration at which 99.9% of the population is killed. AIT yielded MICs of 156.25 mg/L and MBCs of 156.25 to 312.5 mg/L, and CNAD yielded MICs of 78.125 to 156.25 mg/L and MBCs of 78.125 to 312.5 mg/L. Furthermore, 312.5 mg/L AIT and 625 mg/L CNAD successfully reduced > 80% of biofilm adhesion as compared to negative controls. AIT and CNAD were therefore further

evaluated extensively. Currently, interest in utilising plant-derived compounds has garnered interest in medicine and the agricultural sector, but they have not been explored as anti-biofouling agents.

Hindered by their volatile nature, immiscibility, and tendency to degrade in aqueous solutions, plant secondary metabolites typically do not reach their maximum antimicrobial capacity due to loss and low bioavailability. Thus, they would greatly benefit from being protected, stabilised, and delivered in compatible, easily functionalisable, nano-sized carriers. In this study, mesoporous silica nanoparticles (MSNs) were designed and evaluated as a novel method of delivering AIT and CNAD in order to enhance their biocidal efficacy. In one hour of exposure, employment of MSNs as carriers doubled the antibacterial efficacy of free form AIT and increased kill rate of free form CNAD by six times. Furthermore, free form AIT caused ~70% of 60 day-old biofilm to detach, whereas AIT-loaded MSNs essentially removed all of the mature biofilm. As for CNAD, its free form had no significant effect, whereas CNAD-loaded MSNs caused ~80% reduction in biofilm biomass.

MSNs were further engineered to incorporate lactose pore caps to achieve specific, on-command delivery of the plant antimicrobials. These MSNs were designed to respond to external stimuli intelligently, with gatekeepers that degrade only in the vicinity of certain target bacteria that are able to metabolise lactose. Capped AIT-loaded MSNs reduced bacterial viability by ~85% as compared to the negative control, while capped CNAD-loaded versions reduced viability by ~40%. For both AIT- and CNAD-loaded MSNs, the un-capped variety reduced a larger fraction of cells than the lactose-capped variety in both cases, most likely due to the < 100% de-capping efficiency of the lactose-capped MSNs. Despite these results, lactose-capped AIT- and CNAD-loaded MSNs were still more effective in killing than the two compounds as free agents.

This stimuli-triggered MSN delivery technology would be more sustainable than current methods because resistance development would be lowered, and the delivery vehicles could be recycled and reused. Herein, the complete AIT- or CNAD-loaded, lactose-capped MSNs delivery complex proved to be an effective, well engineered, and environmentally conscientious system for killing unwanted bacteria.

ACKNOWLEDGEMENTS

As I sit here under a cloudless blue expanse, watching the sunlight dance atop the waves of the San Francisco Bay while finishing up this last bit of my dissertation, I find myself intensely missing the grey, the cold, the drama, and the Gothic beauty that is Oxford. My time at Oxford was the best, most defining three years yet, both in academic development and self discovery. I feel ever so blessed to have the opportunity to expand my scientific knowledge and sharpen my engineering sense, with the guidance of the brightest, kindest, and most inspiring people I've ever had the humble pleasure to meet.

Many thanks to Professor Ian Thompson, for your relentless support, understanding, honesty, and brilliant scientific insights from which I have undoubtedly learned and benefitted immensely. Dr. Duane Ager, thank you for your generosity of spirit and unfailingly sharp advice: technical, scientific, and otherwise. Mentorship from both of you has certainly sparked sustained meaning and excitement in my work. I felt that you both truly believed in me, and I can't stress how grateful I am for that.

Steven M., Mark F., Helen T., Cordelia R., Fazriz F., Cindy H., Ke Y., Meg U., Gabi G., Rachel M., Cheng C., and Andrew W., I hope you maintain the synergy of intellectual exchange and continue to encourage each other in your respective ambitions, which was the atmosphere I was fortunate to have experienced in your company.

Annie, you are my steam during times of lost momentum and my anchor during times of total aimless drift. You've been my constant inspiration, scientifically and personally, during my highest highs and lowest lows. Under the warmth of the California sun, I miss and thank gloomy Oxford for providing the backdrop to our amazing friendship.

And of course, thanks Mom, you're amazing. And thank you, Baba.

Proverbs 3:5-6

TABLE OF CONTENTS

1. Introduction 14

1.1 Introduction 14

1.2 Biofilms: An Overview 15

1.2.1 Extracellular Polymeric Substance (EPS) 16

1.2.2 Biofilm Survival Strategies 17

1.2.3 Problems Caused by Biofilms 21

1.3 Disadvantages of Current Antimicrobial Strategies 24

1.3.1 Chlorine and Chlorinated Compounds 24

1.3.2 Ozone Treatment 25

1.3.3 Ultraviolet Light Irradiation 26

1.4 Resistance Development 27

1.5 Two Classes of Bacteria: Gram-positive and Gram-negative 28

1.6 Plant-Derived Compounds 29

1.6.1 Five Plant-Derived Natural Compounds to be Investigated 32

1.7 Nanoparticles as Delivery System 37

1.7.1 Mesoporous Silica Nanoparticles (MSNs) 38

1.7.2 Controlled Release 39

1.8 Aims and Objectives 40

2. Relative Antimicrobial Efficacies of Five Plant-Derived Compounds 41

2.1 Introduction 41

2.1.1 Antimicrobial Susceptibility Testing (AST) 41

2.1.2 Conventional Antimicrobial Agents as Reference Standards 43

2.1.3 Classes of Bacteria 45

2.1.4 Aims and Objectives 46

2.2 Materials and Methods 47

2.2.1 Chemicals and Antimicrobial Agents 47
2.2.2 Bacterial Cultures 47
2.2.3 Antimicrobial Susceptibility Tests (ASTs) 48
2.2.4 General Statistical Analysis 50
2.3 Results 51
2.3.1 Determining Relative Antimicrobial Activity 51
2.3.2 MIC and MBC Determination 54
2.3.3 Susceptibility of Gram-Negative and Gram-Positive Bacteria 56
2.4 Discussion 57
2.4.1 Relative Antimicrobial Activity of Five Natural Compounds 57
2.4.2 Volatility and Low Solubility of Natural Compounds 58
2.4.3 Carvacrol, Thymol, and Citral 59
2.4.4 Tolerance and Susceptibility of Different Bacterial Species 60
2.4.5 Conclusion 61
3. Resolving the Mechanism of Bacterial Inhibition by AIT and CNAD Employing Complementary Whole-Cell Biosensors 62
3.1 Introduction 62
3.1.1 Biosensors 62
3.1.2 Lux Genes 63
3.1.3 Metabolic Biosensor: Escherichia coli HB101_pUCD607_lux 65
3.1.4 Biosensor for the Detection of Genotoxicity: Acinetobacter baylyi ADP1_recA_lux 67
3.1.5 Transcriptional Analysis of recA 68
3.1.6 Aims and Objectives 69
3.2 Materials and Method 70
3.2.1 Bacterial Cultures 70
3.2.2 Biosensor Assays 71
3.2.3 Transcriptional Analysis of recA 73
3.2.4 Statistical Analysis 75
3.3 Results 76

3.3.1 Metabolic Biosensor: Incongruent Results from Bioluminescence Study & Plate Count Experiment 76

3.3.2 RecA Biosensor: Results from Bioluminescence Study Show No Induction of DNA Repair Response 77

3.3.3 Transcriptional Analysis of recA 79

3.4 Discussion 82

3.4.1 Metabolic Biosensor: Reduction of Intracellular ATP and $NADPH_2$ Not Solely Due to Loss of Barrier Function of the Cell Membrane 82

3.4.2 RecA Biosensor: AIT & CNAD Unlikely to be Genotoxic 83

3.4.3 Conclusion 86

4. Synthesis and Characterisation of Mesoporous Silica Nanoparticles 87

4.1 Introduction 87

4.1.1 Non-porous Silica Nanospheres 87

4.1.2 Mesoporous Silica Nanoparticles (MSNs) 88

4.1.3 Particle Characterisation 89

4.1.4 Loading and Release of Guest Compounds 92

4.1.5 Aims and Objectives 95

4.2 Materials and Methods 96

4.2.1 Synthesis of MSNs with Hexagonally-Ordered Mesopores 96

4.2.2 MSN Characterisation 96

4.2.4 Calcein Studies 100

4.2.3 Loading and Release of AIT and CNAD 102

4.2.4 GC-FID 103

4.3 Results and Discussion 106

4.3.1 MSN Characterisation 106

4.3.2 Release of Guest Molecules 112

4.3.3 Conclusion 117

5. Improving Antimicrobial Efficacy of AIT and CNAD via MSN Encapsulation and Delivery 118

5.1 Introduction 118

5.1.1 Viability Assays for Planktonic Bacteria 119

5.1.2 Biofilm Analysis 121

5.1.3 Aims and Objectives 124

5.2 Materials and Methods 125

5.2.1 Escherichia coli Culture Conditions 125

5.2.2 Calibration curve for LIVE/DEAD® BacLight™ Bacterial Viability Stain 125

5.2.3 Effect on Planktonic Bacteria 127

5.2.4 Pseudomonas aeruginosa Culture Conditions 129

5.2.5 Effect on Bacterial Biofilms 130

5.2.6 Statistical Analysis 136

5.3 Results and Discussion 137

5.3.1 Planktonic Bacteria 137

5.3.2 Biofilm Bacteria 162

5.3.3 Conclusion 186

6. Lactose-Capped MSNs for Directed, On-Command Release of AIT and CNAD 188

6.1 Introduction 188

6.1.1 Lactose and the Lac Operon 190

6.1.2 Trialkoxysilane Lactose Derivative as Gatekeepers 193

6.1.3 β-Galactosidase 194

6.1.4 Dye-Loading in MSNs Prior to Capping 195

6.1.5 AIT- and CNAD-Loading in MSNs Prior to Capping 195

6.1.6 Aims and Objectives 196

6.2 Materials and Methods 197

6.2.1 Synthesis of MSN Scaffold 197

6.2.2 Synthesis of Trialkoxysilane Lactose Derivative 197

6.2.3 Loading and Subsequent Lactose-Capping of MSNs 198

6.2.4 Characterisation of Dye-Loaded, Lactose-Capped MSNs using CPS Disc Centrifuge™. 199

6.2.5 Dye-Release Study: Enzyme-Triggered De-Capping of MSNs 199

6.2.6 Bacterial Growth using Trialkoxysilane Lactose Derivative as Carbon Source 202

6.2.7 Employment of Lactose-Capped, AIT- and CNAD-loaded MSNs to Kill Bacteria 205

6.3 Results and Discussion 206

6.3.1 CPS Disc Centrifuge™ 206

6.3.2 Enzyme-triggered De-capping and Release of Ruthenium Dye $[Ru(bpy)_3]Cl_2$ 206

6.3.3 Bacterial Growth using Trialkoxysilane Lactose Derivative as Carbon Source 208

6.3.4 Employment of Lactose-Capped, AIT- and CNAD-loaded MSNs to Kill Bacteria 210

6.3.5 Conclusion 213

7. Discussion 214

7.1 Discussion 214

7.1 Whole-Cell *Lux*-Based Biosensors to Assess Antimicrobial Mechanism of Action 216

7.2 MSNs as a Delivery Platform 217

7.3 Controlled Release by Capped MSNs 220

7.4 Strategies to Combat Biofilms 223

7.5 Future Work 224

7.6 Conclusion 226

References 228

LIST OF FIGURES

1.1	Scanning electron micrograph of *P. aeruginosa* biofilm	15
1.2	Schematic of biofilm behavior and survival strategies	17
1.3	Structural comparison between Gram-positive and Gram-negative bacteria	29
2.1	Photo of agar plates from the disk diffusion assay showing different sizes of inhibition zones	49
2.2	Results from the broth microdilution test using four plant-derived compounds against four different bacterial species	55
3.1	The *luxCDABE* operon and the enzymes it produces	65
3.2	The bioluminescence reactions catalysed by enzymes encoded by *luxCDABE*	65
3.3	The pUCD607 plasmid containing the *luxCDABE* operon	66
3.4	Bioluminescence output and plate count results for *E. coli* HB101_pUCD607_*lux*	77
3.5	Bioluminescence response of *A. Baylyi* ADP1_*recA_lux* to AIT treatment	78
3.6	Bioluminescence response of *A. Baylyi* ADP1_*recA_lux* to CNAD treatment	78
3.7	Gel electrophoresis of RT-PCR products from amplification of *recA* mRNA	80
3.8	NanoDrop® quantification of RT-PCR products from amplification of *recA* mRNA	81
4.1	Schematic of the sol-gel synthesis of MSNs	89
4.2 a	Typical TEM image of MSNs showing particle size measurements	97
4.2 b	Histogram generated from TEM image for particle size measurements	97
4.3 a	Typical TEM image of a MSN showing pore size measurements	98
4.3 b	Histogram generated from TEM image for pore size measurements	98
4.4 a	Typical TEM image of a MSN showing pore size measurements	98
4.4 b	Histogram generated from TEM image for pore size measurements	98
4.5 a	Typical TEM image of a MSN showing channel size measurements	98
4.5 b	Histogram generated from TEM image for channel size measurements	98
4.6	Calibration curve for the fluorescence of calcein	101
4.7 a	Calibration curve of AIT determined by GC-FID quantification	105
4.7 b	Calibration curve of CNAD determined by GC-FID quantification	105
4.8	Typical TEM image of MSNs showing spot contrast and line contrast view	107
4.9	TEM image displaying adjacent MSNs in spot contrast and line contrast view	107
4.10	TEM image showing pores aligned in a hexagonal pattern	107
4.11	Size distribution of MSNs obtained from measurements of TEM images	108
4.12	Overlay of size distribution of MSNs obtained from CPS Disc Centrifuge™	109
4.13	Particle size vs. concentration plot created by NanoSight™ analysis	109
4.14 a	BET nitrogen sorption isotherms of MSNs	111

4.14 b	BJH nitrogen sorption for MSN pore size determination	111
4.15 a	Surface area plots of MSNs obtained from BET theory	112
4.15 b	Surface area plots of MSNs obtained from Langmuir theory	112
4.16	Release profile of calcein from loaded-MSNs	113
4.17	Overlay of two chromatographs of AIT obtained via GC-FID	114
4.18	AIT release profile from 20 mg AIT-loaded MSNs	114
4.19	Overlay of two chromatographs of CNAD obtained via GC-FID	115
4.20	CNAD release profile from 20 mg CNAD-loaded MSNs	115
5.1	Photo of agar plate from the Miles and Misra plate count method	120
5.2	Principles of confocal laser scanning microscopy (CLSM)	123
5.3	Images of Bio-Blok® 100 matrices for growing mature biofilms	124
5.4	Calibration curve for LIVE/DEAD® *Bac*Light™ viability staining	127
5.5	Photo of apparatuses used to grow 60-day old biofilms	134
5.6	Photo of the biofilm-growing setup used to grow 60-day old biofilms	135
5.7	Results from Miles and Misra place count assay after AIT treatments	138
5.8	Results from Miles and Misra plate count assay after various CNAD treatments	143
5.9	Results from Miles and Misra plate count assay after various CNAD-loaded MSN treatments	143
5.10	Results from LIVE/DEAD® *Bac*Light™ viability staining after AIT treatments	147
5.11	Chemical structure of PI and an isothiocyanate compound	148
5.12	Reaction between isothiocyanates and primary amines to form thiourea products	148
5.13	Chemical structure of the cyanaine dye Cy2	140
5.14	Discrepancy between results from the plate count method and LIVE/DEAD® *Bac*Light™ viability staining for reference control samples	152
5.15	Results from LIVE/DEAD® *Bac*Light™ viability staining after CNAD treatments	153
5.16	Reaction between PI with aldehyde-containing compounds to form azomethine	155
5.17	Results from the plate count method and LIVE/DEAD® staining after CNAD-loaded MSN treatments	157
5.18	TEM images of negative control *E. coli* cells	159
5.19	Representative TEM image of *E. coli* undergoing binary fission	160
5.20	TEM images of *E. coli* exposed to empty MSNs	160
5.21	TEM images of *E. coli* exposed to 2 mg/ml AIT-loaded MSNs	161
5.22	TEM images of *E. coli* exposed to 2 mg/ml CNAD-loaded MSNs	162
5.23	Schematic of plasmolysis in hypertonic environments	162
5.24	Effects of AIT and CNAD on *P. aeruginosa* biofilm formation in 24 h	163
5.25	Thickness of 48 h-old *P. aeruginosa* biofilms after various treatments for 24 h	166
5.26 a to d	CLSM images of negative control biofilms	167

5.27 a to d	CLSM images of biofilms treated with empty MSNs (vehicle control)	168
5.28 a to h	CLSM images of biofilms exposed to various concentrations of AIT	170
5.29 a to l	CLSM images of biofilms exposed to various concentrations of AIT-loaded MSNs	172, 173
5.30 a to l	CLSM images of biofilms exposed to various concentrations of CNAD	176, 177
5.31 a to l	CLSM images of biofilms exposed to various concentrations of CNAD-loaded MSNs	180, 181
5.32	Thickness of 48 h-old biofilms resulting from various concentrations of AIT- and CNAD-loaded MSNs	182
5.33	Wet weight of 60 day-old *P. aeruginosa* biofilms after various treatments for 24 h	184
5.34	Photos of 60 day-old biofilms grown on Bio-Blok® polyethylene coupons	184
6.1	Chemical structure of lactose	191
6.2	Schematic of the *lac* operon and its regulatory mechanisms	192
6.3	Synthesis reaction of trialkoxysilane lactose derivative	193
6.4	Schematic of MSNs capped with lactose and the enzyme-triggered de-capping action	193
6.5	Calibration curve for the fluorescence of $[Ru(bpy)_3]Cl_2$	200
6.6	Overlay of size distribution of lactose-capped MSNs from CPS Disc Centrifuge™	206
6.7	Release profile of $[Ru(bpy)_3]Cl_2$ from lactose-capped MSNs	207
6.8	*E. coli* growth curve using glucose and trialkoxysilane lactose derivative as carbon source	209
6.9	*P. aeruginosa* growth curve using glucose and trialkoxysilane lactose derivative as carbon source	209
6.10	*E. coli* growth using various concentrations of lactose derivative as carbon source	210
6.11	Results from plate count assay after exposing *E. coli* to 2 mg/ml lactose-capped, AIT- and CNAD-loaded, and unloaded MSNs	211
6.12	Results from plate count assays comparing antimicrobial efficacies of lactose-capped and un-capped, AIT- and CNAD-loaded MSNs	212

LIST OF TABLES

1.1	Industries hindered by spontaneous biofilm formation	22
1.2	Comparison chart for current methods of disinfection	27
1.3	Five plant-derived compounds presently investigated	32
2.1	Four bacterial species used in susceptibility tests and their various classifications	46
2.2	Mean diameters of growth inhibition zones obtained from the disk diffusion assay	53
2.3	MICs and MBCs of four plant-derived compounds against four bacterial species	56
4.1	Calibration curve for the fluorescence of calcein	100
4.2 a	Parameters and methods developed to analyse AIT by GC-FID	104
4.3 b	Parameters and methods developed to analyse CNAD by GC-FID	104
5.1	Various of live- and dead-cell volumes to calibrate LIVE/DEAD® staining	123
5.2	Various treatments that *P. aeruginosa* biofilms were subjected to prior to CLSM	132, 169
6.1	Calibration curve for the fluorescence of $[Ru(bpy)_3]Cl_2$	199

Chapter One

1. INTRODUCTION

1.1 Introduction

Biofouling is the interference caused by unwanted microbial adhesion on materials and equipment in engineered systems (Chapman, Weir, & Regan, 2010; Weir, Lawlor, A., & F., 2008). It is prevalent in the water industry and its associated technological processes, such as ultra-filtration, reverse osmosis, desalination, and water-based temperature control systems (Ludensky, 2003). It is a serious problem with potentially significant health, environmental, and economic repercussions. Unwanted microbial growth and associated biofilm formation cause harmful contamination, irreversible corrosion and biodegradation of crucial materials (e.g. membranes and sensors), and significant impedances in processes such as heat exchange, diffusion and others involving fluid kinematics and dynamics (Bernhard, 2003; Weir *et al.*, 2008; Yasunori, Takaaki, & Kazuhiko, 2007; Zhao, Wang, Liu, & Wang, 2007). These complications lead to health hazards, gross increase in energy and fuel consumption, more frequent maintenance and replacement of equipment, and lower overall productivity, all of which lead to higher operational costs and direct harm to our environment.

Current anti-biofouling strategies have significant drawbacks and are no longer fit for purpose as modern drivers toward energy efficiency and sustainability. Concerns with conventional biocides include exposure and disposal issues due to toxicity toward humans, indiscriminate reaction and corrosion of surrounding materials (D. Kim, Jung, Sohn, Kim, & Lee, 2009), and the ever-evolving problem of microbial resistance development (Bernhard, 2003; Davies, 2003). Traditional biocides used in industrial water systems are incompatible with sustainable end-of-life biological treatment processes since biocide persistence in the

system leads to increasing microbial tolerance over time (Ludensky, 2003). The European Commission's Biocidal Products Directive (98/8/EC) seeks to abolish the most hazardous biocides in the short term, and eventually all harmful ones in the long term. The Commision has since accepted a new regulation to replace the then-current Directive (98/8/EC), which aims to stiffen permissive active substances in biocides over a transitional period of time (European Parliament, 2012). Alternative and effective methods of controlling biofouling are urgently needed because present-day solutions are not sustainable.

1.2 Biofilms: An Overview

Biofilms are highly ubiquitous communities of bacteria that colonise on essentially all surfaces in an aqueous environment (Davies, 2003). They form when unicellular microorganisms collectively attach onto solid surfaces at a liquid interface, and subsequently embed themselves in a matrix of self-secreted extracellular polymeric substance (EPS) (Davies, 2003; Mah & O'Toole, 2001) (Figure 1.1).

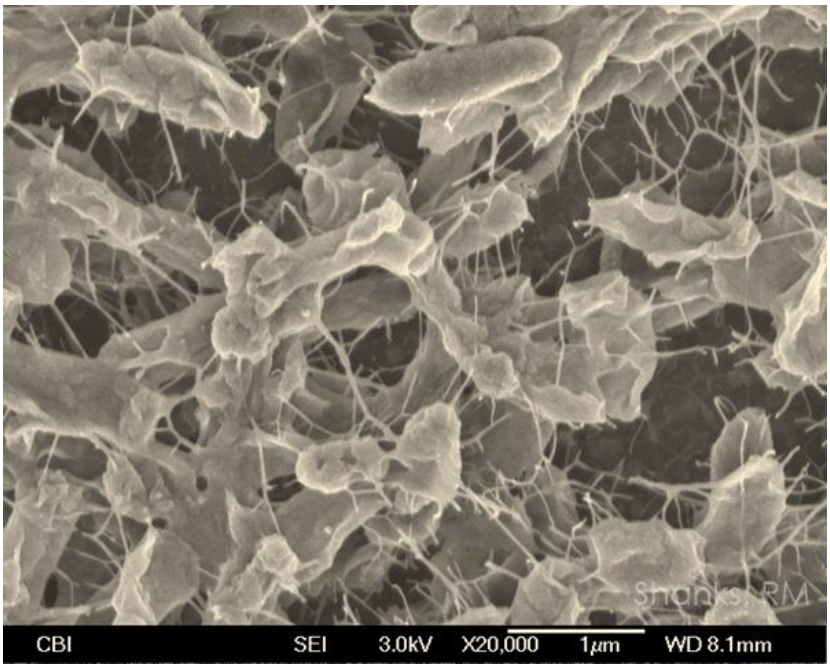


***FIGURE 1.1*: Scanning electron micrograph (SEM) of *Pseudomonas aeruginosa* biofilm**

(University of Pittsburgh Schools of the Health Sciences; available at http://eyemicrobiology.upmc.com/PhotoGalleryBiofilms.html)

Bacterial biofilms consist of single or multiple bacterial species that exist in clusters of microcolonies within the EPS, separated by open water channels acting as a basic circulatory system for delivery of nutrients, expulsion of metabolic wastes, and transport of intercellular messenger molecules for communication (Davies, 2003; L. Ma *et al.*, 2009) . Biofilms are responsible for the majority of biofouling in water-based technological processes (Ludensky, 2003; Yasunori *et al.*, 2007).

1.2.1 Extracellular Polymeric Substance (EPS)

The EPS is composed of polysaccharides, proteins, and nucleic acids. This matrix plays several crucial roles in enhancing the survival of constituent cells. Firstly, the EPS acts as a physical barrier that protects the encased bacteria from environmental stress, and antimicrobial treatments (Bernhard, 2003; Davies, 2003; L. Ma *et al.*, 2009; Weir *et al.*, 2008). Furthermore, the EPS facilitates horizontal gene transfer between constituent cells, and hence promotes the spread of resistance in persister cells to otherwise susceptible neighbours (Fux, Costerton, Stewart, & Stoodley, 2005). The network of channels within the matrix helps intercellular transport of secreted molecules that induce transcription of certain genes in neighbouring cells. The targeted genes are often associated with cellular defence mechanism, and switching them on leads to the production and release of degradative extracellular enzymes and cytotoxins that neutralise potentially biocidal agents (Davey & O'Toole, 2000; Davies, 2003) .

1.2.2 Biofilm Survival Strategies

Several studies have reported that bacterial biofilm cells are 10 to 1000 times more resistant to antibacterial agents as compared to their planktonic (free-living/vagile) counterparts (M. R. W. Brown & Gilbert, 1993; Davies, 2003; Mah & O'Toole, 2001). There are multiple properties and mechanisms discussed below that contribute to biofilm's overall high tolerance to antagonistic treatments, some of which are summarised in Figure 1.2.

1. **Inability of antimicrobial agents to penetrate EPS**
2. **Reduced growth rate of biofilm cells**
3. **Heterogeneity of biofilm's internal environment**
4. **Activation of biofilm-specific phenotypes**
5. **Horizontal gene transfer**

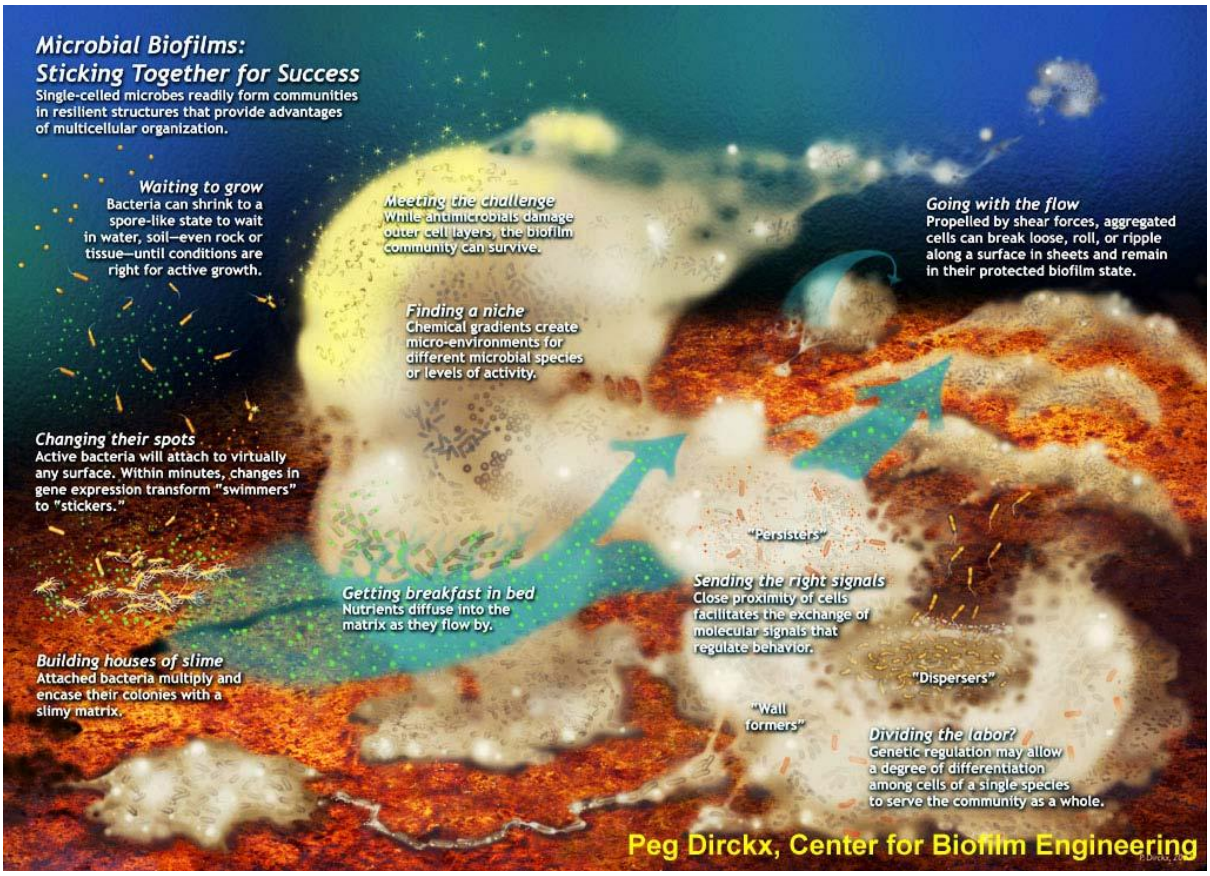


***FIGURE 1.2*: Schematic of biofilm behaviors and survival strategies**

(Center for Biofilm Engineering; also published in Nature Reviews Microbiology 2, 95-108 (2004); available at http://www.centerforgenomicsciences.org/research/biofilm.html)

1.2.2.1 Inability of Antimicrobial Agents to Penetrate EPS

As mentioned previously, the EPS matrix plays a large part in the increased resistance in biofilms. As a physical barrier, the matrix prevents free diffusion of antimicrobial agents to embedded bacterial cells, and therefore restricts access of antibiotics, immune response cells (such as antibodies and phagocytes), and other biocidal chemicals to constituent cells (Cheow, Chang, & Hadinoto, 2010; Davies, 2003; Fux *et al.*, 2005). In addition, the EPS is commonly negatively charged and thus prevents the penetration of positively charged compounds by binding to them via electrostatic attraction. This retards the penetration of important antibacterial compounds like aminoglycosidic molecules, which include many conventionally used antibiotics such as streptomycin and tobramycin (Fux *et al.*, 2005). In addition to the potential to form ionic bonds with positively charged elements, the EPS can also act as an adsorbent, binding to other classes of antimicrobial agents and reducing their bioavailability (Davies, 2003; Suci, Mittelman, Yu, & Geesey, 1994). Prolonged diffusion of microbially antagonistic compounds may also contribute to resistance by providing more time for the constituent bacteria to implement adaptive stress responses (Fux *et al.*, 2005).

1.2.2.2 Reduced Growth Rate of Biofilm Cells

Biofilms are dense and slow-growing, which are properties that confer tolerance to antimicrobial treatments. The compact, layered structure together with the obstructive nature of the EPS matrix limits the availability of nutrients to constituent cells, especially those in the depths of the biofilm. This causes biofilm cells to arrest in growth and to reduce respiratory activity, behaving very similarly to planktonic cells in stationary phase (Davies, 2003; Fux *et al.*, 2005). It has been reported that reduced rates of bacterial growth, most often caused by starvation, directly correlate to increased antibiotic resistance (M. R. Brown, Allison, & Gilbert, 1988; Fux *et al.*, 2005; Mah & O'Toole, 2001). Many antibiotics target

growth-specific factors in bacteria, so cells with lowered metabolic activity, such as those that are nutritionally deprived within biofilms, are more resistant to treatment by such antagonists (Cheow *et al.*, 2010; Davies, 2003). Also, many studies attribute heightened resistance to high cell densities. There is increased accumulation of extracellular signalling molecules (*N*-acylated homoserine lactones, or AHLs) among highly-dense cells, and therefore protective cell-to-cell signalling, known as quorum sensing, is much more active in tightly packed bacteria (Davies, 2003; Fux *et al.*, 2005). Quorum sensing leads to transcription of certain density-dependent genes, thereby upregulating the expression of many cellular defence mechanisms, which include the release of degradative extracellular enzymes and cytotoxins (Cheow *et al.*, 2010; Davies, 2003; Fux *et al.*, 2005).

1.2.2.3 Heterogeneity of Biofilms' Internal Environment

The heterogeneity of a biofilm's internal environment contributes to their increased resistance. A given cell within a biofilm will occupy a slightly different micro-environment compared to other cells within the same biofilm due to varying gradients of nutrients, waste products and signalling factors (Mah & O'Toole, 2001). Thus, cells at different locations of the biofilm grow, respire and metabolise to different degrees, causing patches of varying susceptibility in relation to another area in the same community. Antimicrobial treatment of biofilm will not be equally effective against all constituent cells, often leaving persister cells behind to re-colonise (Davies, 2003; Y. Liu, Li, Qiu, & Burda, 2007). This sub-population of persister cells, which was resistant to the initial antimicrobial treatment in the first place, may respond by further strengthening its resistance. Furthermore, this surviving subpopulation will repopulate the biofilm with new cells that possess the same resistant phenotypes as the parent persister cells (vertical gene transfer). This results in the resurgence of the biofilm that is more robust and resistant than before the initial antimicrobial treatment (Y. Liu *et al.*, 2007; Stewart, 2002).

1.2.2.4 Biofilm-Specific Phenotypes

Not only do biofilm cells passively protect themselves via mechanisms mentioned above, but they also engage in active defence against biocidal attacks. Biofilm cells have unique gene expression profiles that differ from their planktonic counterparts, and the resulting phenotypes contribute to their increased resistance. Biofilm formation is often a cellular coping mechanism induced by unfavourable changes in environmental conditions. Vagile cells attach and colonise onto a solid substrate during the initial stage of biofilm formation, and this initiates the expression of specific genes that ultimately renders biofilm cells morphologically and biochemically distinct from its previous existence as free-floating cells. The resulting physiological changes are related to cellular stress response that act to protect the cell from deleterious effects, such as heat and cold shock, changes in pH and pressure, oxidative stress, anaerobiosis, and exposure to toxic substances and detergents (Conlon, Humphreys, & O'Gara, 2002; Cramton, Ulrich, Gotz, & Doring, 2001; Hengge-Aronis, 1996; Y. Liu *et al.*, 2007; Mah & O'Toole, 2001; Rachid, Ohlsen, Witte, Hacker, & Ziebuhr, 2000). Mechanisms to actively combat antibacterial agents are also engaged; such mechanisms include: increased expression of multi-drug efflux pumps and stress response regulons (M. R. Brown *et al.*, 1988; Gilbert, Das, & Foley, 1997); alterations to membrane-protein composition (i.e. porin proteins) (M. R. Brown *et al.*, 1988); deployment of extracellular biocide-degrading enzymes such as catalase (targets hydrogen peroxide) (Cochran, McFeters, & Stewart, 2000) and β-lactamase (targets β-lactam antibiotics such as penicillin and ampicillin) (Anderl, Franklin, & Stewart, 2000).

1.2.2.5 Horizontal Transfer of Resistance Genes

All the factors mentioned above work together synergistically to set the stage for efficient horizontal gene transfer (Fux *et al.*, 2005). The EPS matrix, high cell density,

acquired resistance, increased genetic competence, and accumulated intercellular communicative elements all highly encourage the transfer of fit genetic material from one bacterial cell to another. The ability to transfer genes laterally is crucial in the development of such high resistance in biofilm.

1.2.3 Problems Caused by Biofilms

The features of biofilm that affect the function and efficiency of various industries can be summarised in three facets: biological, physical, and chemical.

1. **Biological aspect**: Biofilm is a substantial biological threat not only because it causes the majority of human infections, but also due to its potential to contaminate commercial products and spread infections to consumers.
2. **Physical aspect**: The EPS matrix causes increased physical obstruction, such as fluid friction, heat transfer resistance, and decreased flux in pipelines and membranes.
3. **Chemical aspect**: The metabolic activity of biofilm cells causes corrosion, changes in chemistry, and irreversible damage to materials.

It is important to note that the industries adversely affected by biofilm aggregation are not limited to those discussed below (summarised in Table 1.1). Although biofilms account for over 80% of microbial infections of the body (United States National Institute of Health), their role in disease and infection will not be covered in the scope of this thesis.

***TABLE 1.1*: Industries hindered by spontaneous biofilm formation.**

AREAS AFFECTED BY BIOFOULING	IMPACT OF BIOFILM FORMATION
Engineered Systems	- Lower overall efficiency and productivity - Increase energy and fuel consumption - Increase of waste generated - Increase cost of operation
I. Heat Exchange Systems	- Heat transfer resistance - Fluid frictional resistance - Bio-corrosion of materials
II. Membrane Systems	- Occlusion and clogging of membranes - Reduced permeability and flux - Irreversible damage and deformation to membranes
III. Manufacturing	- Bio-corrosion of equipment and pipework - Bio-contamination of final consumer products with possibly resistant strains of microbes

1.2.3.1 Biofilm in Cooling Water Systems

Water-cooling towers in industrial plants are ideal for biofilm formation because these systems provide an abundance of nutrients, high agitation and aeration, optimal temperature for bacterial proliferation, and substrata with high surface area-to-volume ratio to which bacteria can easily adhere and colonise (Ludensky, 2003; Saeed *et al.*, 2000). Re-circulating cooling water tower systems is an integral part of any industrial process because they keep all components at low, functional temperatures so that operations carry on smoothly and efficiently (Ludensky, 2003). Biofilms cause both heat transfer resistance and fluid frictional resistance at power plant condensers and process heat exchangers, which result in massive

energy loss (Ludensky, 2003; Yasunori *et al.*, 2007). To explain, thermal conductivity of biofilm is significantly less than that of metal heat transfer materials, and thus rates of heat transfer substantially decrease when biofouling occurs on heat exchange columns. Furthermore, biofilms increase fluid friction due to the roughness and bulk generated on the surface of equipment in liquid-based plants, thus reducing flux and efficiency. Replacement of equipment, along with the effort and time exerted to clean and replace contaminated parts contribute to the increased cost of operation. Taking into account all of the aforementioned factors, the economic impact that biofilm contamination has is substantial.

1.2.3.2 Biofilm in Reverse Osmosis Technology

Desalination plants are also highly susceptible to biofouling. Sea water reverse osmosis technology (SWRO) accounts for half of the global desalination market, but the prevalence of biofouling poses a serious issue. Biofilm colonisation on reverse osmosis (RO) membranes causes reduced flux due to decreased permeability and clogging of the membrane (D. Kim *et al.*, 2009). Moreover, biofilms cause bio-corrosion, deformation, discoloration, and changes in physicochemical and electrical activities of RO membranes (Chapman *et al.*, 2010). This type of irreversible damage can only be remedied by replacing the degraded membrane with a new one. All of this is true for membranes used in water purification plants as well. Again, all these factors ultimately lead to increase in operational costs, lowered efficiency, and gross energy loss. It is important to note that biofilm formation in water-based processes can occur even with a carbon source limitation – even ultra-pure water systems are found to support biofilm colonisation (Schaule & Flemming, 1997).

1.2.3.3 Biofilm in the Manufacturing Industry

The manufacturing of consumer products, including household goods, cosmetics, and paper products, is also affected by biofouling (Elsmore, Ludensky, & Coulburn, 1999;

Ludensky, 2003). Biofilms commonly occur in pipelines, dead legs, water storage tanks, and other machinery elements in contact with liquid in production lines. These biofilm cells are often sloughed off due to mechanical agitation, thereby bio-contaminating ingredients that end up in the final product, causing serious health and safety issues (Ludensky, 2003). Because the biofilm would have been exposed to many chemicals and preservatives, the constituent bacteria that end up in consumer products would most likely have developed resistance to a range of chemicals, which poses significant health risks. To minimise contamination, biofilm-susceptible parts must be frequently discarded and replaced. This causes a tremendous decrease in overall productivity and extra effort must be exerted in the quality control aspect of production. Also, frequent replacements of equipment are expensive.

1.3 Disadvantages of Current Antimicrobial Strategies

1.3.1 Chlorine and Chlorinated Compounds

Although effective in killing, conventional applications for controlling biofouling have significant drawbacks. Biocides are chemical disinfection agents used to eradicate unfavourable biological growth and infestation. Currently, the most prevalent biocide in the industrial sector is free chlorine, a strong oxidising agent that is relatively cost-effective (D. Kim *et al.*, 2009). Free chlorine (i.e. HOCl, OCl^-) is commonly administered in the form of chlorine gas (Cl_2) or sodium hypochlorite (NaOCl), and is highly bacteriostatic and bactericidal. Free chlorine owes its high inhibitory effect to its strong oxidative potential; unfortunately, it is the same oxidative power that makes chlorine very problematic as a disinfectant because it chemically corrodes surrounding materials indiscriminately (D. Kim *et al.*, 2009). Because of its high toxicity, US Government regulates that if NaOCl solution is to be used to disinfect anything in contact with food, it is required that the solution does not exceed 200 ppm available chlorine, which is an extremely small amount. In the case of RO

technology, HOCl and OCl^- attacks amide functional groups in the polyamide RO membrane and can destroy it (Al-Ahmad, Abdul Aleem, Mutiri, & Ubaisy, 2000; D. Kim *et al.*, 2009; Kwon & Leckie, 2006). Another downside of using free chlorine as a biocide is that it generates carcinogenic by-products like trihalomethanes (THM) and halo acetic acids (HAA). Also, de-chlorination processes are required after chlorine treatment. Not only do de-chlorination steps add time and cost to the overall process, but it can also cause even more severe biofouling as a result (D. Kim *et al.*, 2009). Additional drawbacks include its ineffectiveness at pH values above 7.5, danger in working with pressurised gas, and environmental risks with chlorinated hydrocarbons. Environmental legislation now limits chlorine residual exposure, imposing a requirement for de-chlorination of the water, prior to discharge (Department for Environment, 1995). This is an expensive and very energy demanding process.

Other chlorinated compounds have been used to circumvent the disadvantages of using Cl_2 and NaOCl. One alternative is chloramine, which is less corrosive and damaging on materials, but has poor killing activity compared to free chlorine because its oxidation potential is much lower (D. Kim *et al.*, 2009). Another option is chlorine dioxide (ClO_2), which is relatively harmless on membranes and surrounding surfaces. However, chlorite is a dominant by-product of ClO_2 treatment and is acutely toxic to humans and animals (D. Kim *et al.*, 2009).

1.3.2 Ozone Treatment

Ozone treatment is another disinfection strategy that has been widely used for drinking water. The advantages of ozone include its very strong oxidation potential, its preferential reaction with organic matter through electrophilic attacks on carbon double bonds, and the low levels of halogenated by-products generated (D. Kim *et al.*, 2009).

However, hydroxyl radicals, products of ozone degradation, are much stronger oxidising agents and react non-selectively with its surroundings (Perrins, Cooper, van Leeuwen, & Herwig, 2006). Both ozone and hydroxyl radicals break down RO membrane surfaces. In salt water reverse osmosis (SWRO) specifically, hypobromite anions are generated from ozonation, which leads to rapid degradation of SWRO membranes (Perrins *et al.*, 2006). Furthermore, carcinogenic bromate is formed as a result of ozonation of sea water (Tyrovola & Diamadopoulos, 2005).

1.3.3 Ultraviolet Light Irradiation

Another method used to inhibit microbes in industrial settings is ultraviolet light (UV) irradiation. This approach is a physical process, as compared to the chemical reactions discussed above. UV irradiation at 254 nm breaks down bacterial DNA and thwarts their reproduction (D. Kim *et al.*, 2009). Although no hazardous chemicals are used and no harmful by-products are formed, this method is limited to only small areas, so this approach is ineffective in large scale operations (Lopez-Ramirez, Sahuquillo, Sales, & Quiroga, 2003). Also, UV irradiation is susceptible to scale formation in mineral-rich water (D. Kim *et al.*, 2009), which requires extra steps for maintenance and thus drastically lowering efficiency.

TABLE 1.2: **Comparison chart for current methods of disinfection.**

DISINFECTION	ADVANTAGE	DISADVANTAGE
Free chlorine (i.e. HOCl, OCl^-)	- High killing efficiency	- Extremely corrosive to materials, including RO membranes - Generates toxic and carcinogenic by-products (THMs, HAAs) - Ineffective at pH above 7.5 - Dangerous when working with pressurised gas
Chloramine (NH_2Cl)	- Less corrosive than free chlorine	- Poor killing efficiency
Chlorine dioxide (ClO_2)	- Relatively harmless on membranes	- Generates chlorite as by-product, which is highly toxic
Ozone	- Good killing efficiency	- Chemically react with surrounding materials; destroys materials - Generates bromate, which is carcinogenic
Ultraviolet light irradiation (UV)	- Good killing efficiency - No harmful by-products	- Scale formation - Application limited to small areas

1.4 Resistance Development

In addition to the severe disadvantages of present-day biocides, the mounting problem of resistance development (Davies, 2003; Fux *et al.*, 2005), an issue that has developed into a serious health concern worldwide, is a major reason for such urgent demand for alternative methods of antimicrobial control (Ludensky, 2003). Antibiotic/biocide resistance is an ever-evolving problem: to eradicate resistant bacteria, elevated dosages of biocides are administered, which yields even greater resistance either through acquired tolerance, or through the vertical and lateral passage of genetic material from surviving persister cells to

other cells. New strategies for combating microbes are needed to end this worsening, self-propagating cycle of growing resistance, which has led to highly dangerous health risks like MRSA-related infections (Fux *et al.*, 2005). Ideally, the new generation of antimicrobial agents would only be activated when control action is required, but are inactivated or removed when their biocidal action is no longer desired. This would reduce exposure and increase compatibility with downstream biological treatment processes.

1.5 Two Classes of Bacteria: Gram-positive and Gram-negative

Bacteria can be categorised into two groups based on physicochemical properties of their cell walls via the Gram stain method (Schleifer & Kandler, 1972). The key distinction between the two groups is that the cell wall of Gram-negative bacteria consists of: 1) an additional outer phospholipid membrane apart from the inner cytoplasmic membrane (which both Gram-stain types possess), which contains exterior-facing lipopolysaccharide (LPS) chains, and 2) a thinner peptidoglycan layer as compared to Gram-positive cells. The cell wall of Gram-positive bacteria is largely composed of peptidoglycan (50 - 90% of cell envelope) (Schleifer & Kandler, 1972), which is stained purple/blue by crystal violet. Gram-negative bacteria are unable to retain the crystal violet since the cell wall consists of a much thinner peptidoglycan layer (only 10% of cell envelope) and is thus stained pink by the counter-stain. The cell wall structures of both Gram classifications are depicted in Figure 1.3.

The greater tolerance of Gram-negative bacteria is attributed to the presence of the outer membrane consisting of hydrophilic LPS chains that serve as a barrier to hydrophobic agents (S.P. Denyer & Maillard, 2002; Mann, Cox, & Markham, 2000; Mayaud, Caricajo, Zhiri, & Aubert, 2008). Hydrophobicity is generally a favourable property in antibacterial agents because it enables the agent to partition into the phospholipid bilayer of the cell membrane. However, the outer layer of Gram-negative bacteria decreases the permeability to

lipophilic compounds and protects the cell from certain antibiotics, detergents, and chemicals that would normally damage the outermost, peptidoglycan layer of Gram-positive cells. The outer membrane also acts as a molecular sieve that regulates traffic into the cell; molecules with mass exceeding 600-1000 Da cannot penetrate the LPS outer membrane (S.P. Denyer, 1995; S.P. Denyer & Maillard, 2002).

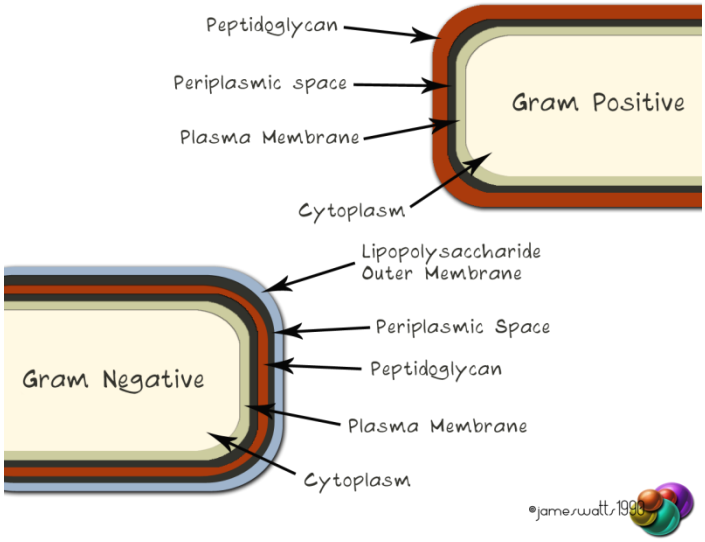


FIGURE 1.3: **Structural comparison between Gram-positive and Gram-negative bacteria**

(Available at http://vetsci.co.uk/2011/01/03/bacteria-basics/)

1.6 Plant-Derived Compounds

Plant essential oils (EOs) are natural, aromatic, oily liquids isolated from plant materials like flowers, buds, seeds, leaves, wood, herbs, fruits, and roots (Prabuseenivasan, Jayakumar, & Ignacimuthu, 2006). Three thousand EOs are known to exist (Jones, 1996). They are variable mixtures composed of mainly terpenoids: specifically monoterpenes (C_{10}), sesquiterpenes (C_{15}), and their oxygenated derivatives (Calsamiglia, Busquet, Cardozo, Castillejos, & Ferret, 2007; Gallucci *et al.*, 2009; Prabuseenivasan *et al.*, 2006).

EOs and their constituent compounds have been used as antiseptic, medicinal, and food preservation agents for thousands of years (Jones, 1996). These plant secondary

metabolites could potentially serve as effective alternatives to conventional antimicrobial agents. It has been demonstrated that these plant-derived substances and their constituent chemicals display antibacterial, antimycotic, antiviral, anticancer, and antiparasitic properties (Aruoma *et al.*, 1996; S.P. Denyer, 1995; Kurita, Miyaji, Kurane, Takahara, & Ichimura, 1981; Moleyar & Narasimham, 1986; Monzote, Montalvo, Scull, Miranda, & Abreu, 2007; Suhr & Nielsen, 2003; Sylvestre, Pichette, Longtin, Nagau, & Legault, 2006) without conferring resistance in targeted microbes (S. Chao, Young, C., & Nakaoka, 2008). Although not fully elucidated, plant compounds have been reported have a multi-targeted mechanism of action against microbes (Luciano & Holley, 2009), unlike many current antimicrobial and antibiotic strategies.

In addition to their excellent ability to inhibit and/or kill microbes, natural plant-derived compounds are promising candidates as novel antimicrobial agents for two major reasons. Firstly, these secondary plant metabolites are safer and non-damaging for the natural environment, since they are originally sourced from plant material. Natural compounds may be effective alternatives to current biocides such as chlorine and ozone, which are strong oxidizing agents that indiscriminately react with and destroy the surrounding environment (D. Kim *et al.*, 2009). Secondly, natural compounds are safe for human exposure at antimicrobially-active concentrations, unlike current antimicrobial strategies that produce toxic and carcinogenic by-products (Bernhard, 2003; D. Kim *et al.*, 2009). The plant compounds of present interest are registered by the European Commission for use in foodstuffs as they present no risk to consumers and are classified as Generally Recognised as Safe (GRAS) by the U.S. Food and Drug Administration (Gomes, R.G., & Castell-Perez, 2011).

Currently, interest in utilising plant-derived substances in areas of alternative medicine (C. S. Liu *et al.*, 2007), pharmacology (Jones, 1996; Sherry, Boeck, & Warnke,

2001), infection and disease control (Prabuseenivasan *et al.*, 2006) , as well as food and agricultural spoilage control (Burt, 2004; Delaquis & Mazza, 1995; Ouattara, Simard, Holley, Pitte, & Begin, 1997) is gaining momentum due to their availability, organic and non-toxic nature, and better biodegradability as compared to conventional antibiotics and preservatives (Kalemba & Kunicka, 2003). However, limited work has been done on expanding the application of natural compounds to control bacterial biofouling.

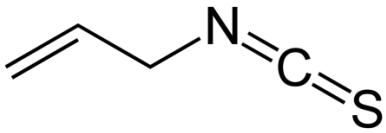
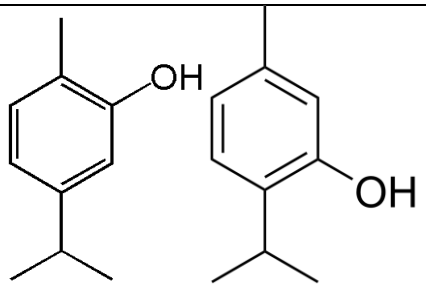
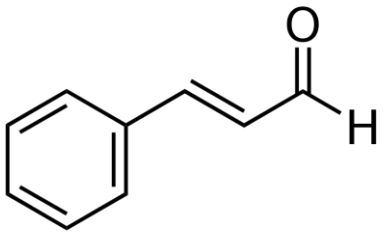
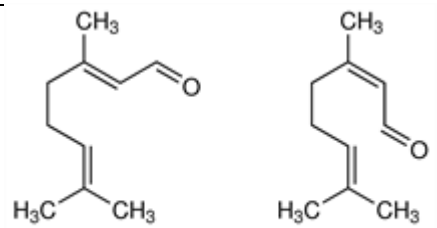
Several studies have ranked aldehyde and phenolic terpenes highest in antimicrobial activity compared to other terpenoid classes (Dorman & Deans, 2000; Gallucci *et al.*, 2009; Gomes *et al.*, 2011; Mayaud *et al.*, 2008). Therefore, two aldehyde terpenes, cinnamaldehyde (CNAD) and citral, and two phenolic terpenes, carvacrol and thymol, were selected as test compounds due to their reported effectiveness in inhibiting microbes (Gallucci *et al.*, 2009; Inouye, Abe, Yamaguchi, & Asakura, 2003; Tunc, Chollet, Chalier, Preziosi-Belloy, & Gontard, 2007). Additionally, allyl isothiocyanate (AIT), a potent organosulfur of the essential oil of mustard, was also included in the panel of compounds to be tested.

A crucial characteristic of these plant secondary metabolites is the hydrophobic character of their hydrocarbon skeleton and the hydrophilic character of their functional groups, which enables them to partition the lipid bilayer of microbial cell membranes, mitochondria, and other cell structures (Gomes *et al.*, 2011; Sikkema, DeBont, & Poolman, 1994). Their accumulation causes swelling of the cytoplasmic membrane, increased membrane fluidity and permeability, increased flux of protons, and leakage of potassium ions (S.P. Denyer, 1995; Sikkema *et al.*, 1994). All of these factors contribute to the dissipation of the pH gradient and the electrical potential across the membrane, resulting in the collapse of a cell's proton motive force, the driving factor of energy-transduction in cells (Sikkema *et al.*, 1994).

1.6.1 Five Plant-Derived Natural Compounds to be Investigated

The five plant-derived compounds to be assessed for their antimicrobial activity, along with their respective parent essential oils, chemical classifications, and chemical structures, are listed in Table 1.3.

***TABLE 1.3*: Five plant-derived compounds presently investigated.**

MAJOR CONSTITUENTS	ESSENTIAL OIL	TYPE OF COMPOUND	CHEMICAL STRUCTURE
Allyl isothiocyanate (AIT)	Mustard oil, horseradish oil	Organosulfur	
Carvacrol & Thymol	Thyme oil, oregano oil	Aromatic phenolic terpenes	 Carvacrol Thymol
Cinnamaldehyde (CNAD)	Cinnamon oil	Aromatic aldehyde terpene	
Citral (*E*-isomer: Geranial; *Z*-isomer: Neral)	Lemongrass oil	Non-aromatic aldehyde terpene	 Geranial Neral

1.6.1.1 Allyl Isothiocyanate

Allyl isothiocyanate (AIT) is a volatile, low molecular weight organosulfur detected in all plants belonging to the *Brassicaceae* family (C. M. Lin, Preston, & Wei, 2000 ; Turgis, Han, Caillet, & Lacroix, 2009). AIT is the primary component of both mustard oil and horseradish oil, constituting 90-99% of their total content (Nedorostova, Kloucek, Kokoska, Stolcova, & Pulkrabek, 2009; C. M. Park, Taormina, & Beuchat, 2000; Suhr & Nielsen, 2003). This aliphatic compound is a major product of the hydrolytic reaction between endogenous myrosinase, an enzyme involved with plant defence, and sinigrin, a glucosinolate found in cruciferous plants such as mustard, horseradish, Brussels sprouts, and broccoli (Delaquis & Mazza, 1995).

It has been reported to exhibit higher antibacterial activity than some conventional antibiotics (streptomycin, penicillin G, and polymyxin B) (C. M. Lin *et al.*, 2000 ; C. M. Park *et al.*, 2000) and biocidal agents (sulphur dioxide and ethanol) (Tunc *et al.*, 2007). Natural compounds containing sulphur, such as AIT, have been reported to demonstrate greater bactericidal activity as compared to other plant-derived chemicals, including aldehyde and phenolic terpenes (Koroch, Juliana, & Zygadio, 2007; Nedorostova *et al.*, 2009; Suhr & Nielsen, 2003; Tunc *et al.*, 2007).

With a polar isothiocyanate end and a non-polar allyl side chain, AIT is an amphiphilic compound that can pass through the hydrophilic outer cell wall of Gram-negative bacteria and also partition into the hydrophobic phospholipid bilayer of the cell membrane (C. M. Lin *et al.*, 2000). The loss of barrier function of the membrane not only causes the loss of vital cellular components and metabolites (Burt, 2004; Turgis *et al.*, 2009), but also leads to influx of protons which lowers intracellular pH, disrupting crucial cellular processes such as DNA transcription, protein synthesis, and enzyme activity (C. M. Lin *et al.*, 2000 ;

Turgis *et al.*, 2009). AIT possesses a highly electrophilic central carbon atom that can be reactive with amino acids, peptides, and aromatic and aliphatic amines; thus, it may be able to alter protein structure and inactivate enzymes via reaction with free amino groups and oxidative cleavage of disulphide bonds (Delaquis & Mazza, 1995; Kawakishi & Kaneko, 1987; Luciano, Hosseinian, Beta, & Holley, 2008). In addition, previous studies demonstrating low internal ATP pool and weak ATP efflux infer that AIT shunts production of ATP production and drives ATP hydrolysis inside the cell (S. Chao *et al.*, 2008; Turgis *et al.*, 2009).

1.6.1.2 Carvacrol & Thymol

The aromatic phenolic terpenes carvacrol and thymol are major constituents of thyme oil and oregano oil (Mayaud *et al.*, 2008; Suhr & Nielsen, 2003; Ultee, Kets, & Smid, 1999). Reports of antibacterial activities of thyme and oregano date back several decades, and it is been well-established that the antimicrobial activities of both these oils are due to the high content of carvacrol (up to 80%) and thymol (up to 57%) (Oussalah, Caillet, & Saucier, 2007).

The antimicrobial effects of carvacrol and thymol encompass a wide spectrum of microorganisms, including bacteria, yeast, fungi, insects, and mites, while exhibiting zero toxicity to humans (Ben Arfa, Combes, Preziosi-Belloy, Gontard, & Chalier, 2006; Dorman & Deans, 2000; Ultee *et al.*, 1999). Thyme oil and oregano oil, along with carvacrol and thymol, have demonstrated comparable antimicrobial efficiencies to those of cinnamon oil and cinnamaldehyde, often sharing the position as top performers in bactericidal activity (Didry, Dubreuil, & Pinkas, 1994; Dorman & Deans, 2000; Gallucci *et al.*, 2009; Inouye *et al.*, 2003; Inouye, Takizawa, & Yamaguchi, 2001; Mayaud *et al.*, 2008; Warnke *et al.*, 2009).

Carvacrol and thymol are relatively stable, moderately soluble in water, and relatively low in volatility as compared to other plant-derived compounds, all which are properties that favour high antimicrobial activity (Inouye *et al.*, 2001). According to studies on the chemistry and configuration of terpenoids, the presence and position of hydroxyl groups in phenolic compounds are important in the interference of cell membranes and proteins (Dorman & Deans, 2000; Gallucci *et al.*, 2009; Ultee *et al.*, 1999). The free hydroxyl group and delocalised electron system of carvacrol and thymol structurally destabilises the cytoplasmic membrane and inactivates crucial membrane-embedded enzymes such as ATPases (Ben Arfa *et al.*, 2006; Gill & Holley, 2006; Helander *et al.*, 1998). The compounds act as transmembrane carriers of monovalent cations by exchanging hydroxyl protons for potassium ions, thereby lowering the electrical gradient across the membrane (Ultee, Bennik, & Moezelaar, 2002). Also, the presence of the aromatic ring significantly increases the compound's bioactivity, as shown in the lack of inhibiting effects of menthol while carvacrol and thymol are highly bactericidal (Gallucci *et al.*, 2009).

1.6.1.3 Cinnamaldehyde

Cinnamaldehyde (CNAD), an aldehyde terpene, is the major constituent of cinnamon oil, ranging from 52-70% of total content (Inouye *et al.*, 2003; Mayaud *et al.*, 2008; Prabuseenivasan *et al.*, 2006). In studies where composite EOs and their major constituent terpenoids were evaluated, cinnamon oil and CNAD exhibited similar levels of killing efficiency, inferring that the overall antimicrobial activity of cinnamon oil is derived mainly from CNAD (Didry *et al.*, 1994; Inouye *et al.*, 2001; Mayaud *et al.*, 2008). When compared to a number of other EOs, several reports have demonstrated cinnamon oil to display greatest efficacy against a broad range of microbes, including Gram-positive and Gram-negative bacteria, fungi, yeast, and bacteriophages (S. C. Chao, Young, & Oberg, 2000; Inouye *et al.*, 2001; Tunc *et al.*, 2007; Warnke *et al.*, 2009). Cinnamon oil have also exhibited greater

antimicrobial activity than some conventional antimicrobial agents such as streptomycin, sulphur dioxide, ethanol, providone iodine, chlorhexidine, hydrogen peroxide, triclosan, and gentamicin (Nuryastuti *et al.*, 2009; Prabuseenivasan *et al.*, 2006; Tunc *et al.*, 2007; Warnke *et al.*, 2009). Furthermore, bacterial strains resistant to these agents are found to be susceptible to cinnamon oil (Alil *et al.*, 2005; Nuryastuti *et al.*, 2009; Warnke *et al.*, 2009).

CNAD inhibits bacteria largely by disrupting the phospholipid bilayer of the cell membrane. Cyclic monoterpenes like CNAD preferentially partition from aqueous phase into the hydrophobic domain of the cytoplasmic membrane and between the lipid acyl chains of the outer membrane (in Gram-negative bacteria), which lead to a cascade of deteriorating events associated with membrane damage (Ben Arfa *et al.*, 2006; Gill & Holley, 2006). Injury to cell membrane can lead to the uncoupling of oxidative phosphorylation, shut down of active transport, inhibition of protein translocation, loss of vital metabolites and cellular components, and interference of DNA-, RNA-, protein-, lipid-, and polysaccharide-synthesis (S.P. Denyer, 1995; Knobloch, Weigand, Weis, Schwarm, & Vigenschow, 1986). The functional aldehyde group conjugated to a carbon-carbon double bond is highly electronegative, which could explain CNAD's ability to interfere with biological processes involving electron transfer (Knobloch *et al.*, 1986; Koroch *et al.*, 2007).

1.6.1.4 Citral

Citral is a non-aromatic aldehyde monoterpene consisting of structural isomers, geranial and neral. It is the major constituent of lemongrass oil, with composition of 38-46% geranial and 29-35% neral (Aruoma *et al.*, 1996; S. Chao *et al.*, 2008; Inouye *et al.*, 2001; Mayaud *et al.*, 2008).

Several reports have demonstrated lemongrass oil to exhibit excellent antimicrobial activity against various bacterial and fungal species, including resistant strains (Inouye *et al.*,

2003; Inouye *et al.*, 2001; Mayaud *et al.*, 2008; Warnke *et al.*, 2009). When evaluated against 91 other EOs, lemongrass oil displayed the greatest inhibitory effect against methicillin-resistant *Staphylococcus aureus* (MRSA) (S. Chao *et al.*, 2008). Another study ranked citral second only to CNAD in antibacterial efficiency against respiratory tract pathogens among other major constituents of 14 other EOs (Inouye *et al.*, 2001).

As a hydrophobic liquid, not only does citral compromise the integrity of cell membranes and thus lead to subsequent adverse effects associated with membrane damage as previously discussed, but the functional aldehyde group of the compound also facilitates in the denaturation of proteins and nucleic acids (Kurita, Miyaji, Kurane, Takahara, & Ichimura, 1979). Similar to CNAD, the aldehyde group of citral is highly electronegative, which explains the high bioactivity of this class of compounds (Moleyar & Narasimham, 1986).

1.7 Nanoparticles as Delivery System

Despite natural the potential of plant compound to be effective antimicrobial agents, their hydrophobicity, volatile nature, and low solubility and tendency to degrade in aqueous environments prevent them from reaching their maximum inhibitory capacity. Therefore, such compounds may benefit from being protected and stabilised in nano-sized carriers to control unwanted microbial growth. The low dissolution capacity of hydrophobic substances, such as plant compounds, is usually overcome by employing emulsifiers or solvents, which often lower the inhibitory effect of the agent (Barbé *et al.*, 2004). In order to harness the full antibacterial power of natural plant compounds, loading them into compatible nanoparticles (NPs) may be an effective and novel method to treat unwanted bacterial growth, especially biofilm. Specifically of interest in this study are mesoporous silica nanoparticles (MSNs).

1.7.1 Mesoporous Silica Nanoparticles (MSNs)

Mesoporous silica nanoparticles (MSNs) are inorganic, nanoscale materials that may be promising candidates for the delivery of natural compounds in order to improve their antimicrobial effect. According to the International Union of Pure and Applied Chemistry (IUPAC) dentition (McCusker, Liebau, Engelhardf, & Schuth, 2003), MSNs have pores ranging from 2-50 nm in diameter in which compounds of interest can be loaded. In recent years, MSNs have received growing scientific interest as carriers for many applications, including pharmaceutical drug delivery, gene therapy, enzyme immobilisation, catalytic chemistry, ion exchange, biosensing , and bioimaging (Davis, 2002; Hom *et al.*, 2010; Ispas, Sokolov, & Andreescu, 2009; Knopp, Tang, & Niessner, 2009; Lu, Liong, Zink, & Tamanoi, 2007; Ozin & Arsenault, 2005). Silica is appealing because it is chemically inert, thermally stable, harmless, and inexpensive (Nandiyanto, Kim, Iskander, & Okuyama, 2009).

The channels that form the nanosized pores within MSNs act as physical, protective barriers that surround volatile guest molecules such as natural plant compounds; hence, MSNs are capable of stabilising volatile antimicrobial agents, minimising their loss through vaporisation, and enhancing the effectiveness of each antimicrobial treatment by retaining more of the loaded agent in the system (Lu *et al.*, 2007). Also, the high surface area-to-volume ratio along with MSNs' accessible reaction sites on pore surfaces help to maximise the bioavailability of the loaded compound during exposure to microbes (Ispas *et al.*, 2009).

Due to the immiscibility of natural plant compounds, they are largely isolated in discrete oil phases separated from the aqueous environment where the target microbes are usually located. As carriers, MSNs can mitigate this problem and increase the bioavailability of natural compounds because they can freely disperse evenly in aqueous solutions without

the use of additional emulsifiers or solvents, and thus enhance the delivery of hydrophobic agents to target cells (Barbé *et al.*, 2004).

Another advantageous feature of MSNs is that particle size, porosity, and surface properties can be predictably controlled and tailored to match the physicochemical properties of guest compounds as well as the overall needs of specific applications (Ispas *et al.*, 2009). Functional groups, targeting ligands, and stimuli-sensitive molecules can be conjugated to surfaces of pores and particles themselves in order to optimise loading of guest compounds, control the release profile, improve dispersity, and direct the carriers to targeted sites (Knopp *et al.*, 2009; Xia *et al.*, 2009; Zhu, Fang, Bordchardt, & Kaskel, 2011). Thus, employment of MSNs to deliver antimicrobial compounds can decrease the amount of agent used in each dose because less of the compound through non-specific diffusion to areas with no cells. In summary, in order to harness the full antimicrobial potential of natural plant compounds, loading them into MSNs is a fitting and novel method to improve their lethality.

1.7.2 Controlled Release

Pores of MSNs can be gated or capped with biodegradable molecules to control the release of loaded compounds in response to surrounding micro-environment (Bernardos *et al.*, 2010; C. Park, Lee, & Kim, 2009). Of particular interest presently is to cap pores with carbohydrate molecules to retain antimicrobial plant compounds within the nano-spheres (Bernardos *et al.*, 2009; C. Park, Kim, Kim, & Kim, 2009). The loaded MSNs in this state are antimicrobially inactive, avoiding issues of over-exposure which would typically lead to resistance development. Upon exposure to specific microorganisms, the saccharide caps will be metabolically degraded by the target microbes themselves in a "Trojan horse," self-killing approach. Such nanoparticles are thus a good means of delivering toxic doses of plant-derived antimicrobial agents to undesired microbes, such as those involved in biofouling.

1.8 Aims and Objectives

The principal aim of this project was to evaluate the feasibility and effectiveness of plant secondary metabolites as antimicrobial agents, especially in the context of controlling unwanted microbial growth in both planktonic and biofilm forms, as this is representative of biofouling in engineered systems. Another overall objective was to develop a novel delivery system for select plant antimicrobial compounds, employing bespoke MSNs as carriers. This nanoparticle-mediated delivery approach would enhance the killing efficiency and control the release of loaded plant-derived agents. Aims of each phase of this research are as follows:

- To evaluate the effects on growth and viability of *E. coli, P. aeruginosa, B. subtilis,* and *S. aureus* that exposure to AIT, carvacrol, CNAD, citral, and thymol have in order to identify the compound(s) with the greatest relative antimicrobial activity.
- To perform two complementary bioluminescence-based bacterial biosensor assays to evaluate the antimicrobial mechanism of action of the two most potent plant compounds selected.
- To synthesise hexagonal MSNs and characterise the size, size distribution, morphology, porosity, and surface area.
- To load synthesised MSNs with AIT and CNAD and to determine release profiles of the two natural compounds loaded in the pores of MSNs.
- To assess the antimicrobial efficiency of AIT- and CNAD-loaded MSNs as compared to that of AIT and CNAD as free agents against planktonic and biofilm bacteria.
- To modify MSN surface with lactose in order to cap the mesopores for controlled release of guest compounds.
- To enzymatically trigger the degradation of lactose caps on MSNs for directed release of AIT and CNAD.

Chapter Two

2. Relative Antimicrobial Efficacies of Five Plant-Derived Compounds

2.1 Introduction

The focus of this chapter is the response of four species of bacteria challenged by five different natural plant-based compounds to determine whether they can be effective and more sustainable alternatives to current antimicrobial agents. Specifically, allyl isothiocyanate (AIT), carvacrol, cinnamaldehyde (CNAD), citral, and thymol were selected to be investigated because they span different classes of plant-derived compounds, each with distinct chemistry. Although the exact antimicrobial mechanisms of natural compounds have not been fully determined, it is likely to be attributed to their chemical structure. The reactivity of each compound's functional groups, its aqueous solubility, and its ability to form intermolecular bonds is directly linked to its antimicrobial potency (Koroch *et al.*, 2007).

All five diverse test compounds had demonstrated their ability to inhibit a range of microorganisms in separate studies under varying experimental parameters, but no work has been done to compare their efficacy in a single study using the four bacterial strains presently selected, which are species implicated in biofouling (López, Vlamakis, & R., 2010).

2.1.1 Antimicrobial Susceptibility Testing (AST)

Two widely used antimicrobial susceptibility tests (ASTs) were employed in this study: 1) the disk diffusion assay and 2) broth microdilution test. Both methods were performed in accordance with the procedures outlined by the Clinical and Laboratory Standards Institute (CLSI) and in "*Antimicrobial Susceptibility Testing: A Review of General*

Principles and Contemporary Practices" (Jorgensen & Ferraro, 2009), by which sizes of inhibition zones, minimum inhibitory concentrations (MICs), and minimum bactericidal concentrations (MBCs) were determined. The MIC is defined as the lowest concentration of a substance that inhibits visible microbial growth, and the MBC is defined as the lowest concentration at which 99.9% of the population is killed (J.M. Andrews, 2001).

2.1.1.1 Disk Diffusion Assay

The disk diffusion assay is conventionally used to determine relative antimicrobial efficiency between test compounds (J.M. Andrews, 2001). It is performed by applying bacterial inoculum onto the surface of agar growth medium, then placing filter disks impregnated with known concentrations of an antimicrobial agent onto the inoculated agar. The agar plates are incubated at optimal microbial growth temperature, and the zones of growth inhibition around each disk are subsequently measured. The diameter of the zone is related to the antimicrobial strength of the test compound and the diffusion rate of the compound through the agar medium. The detailed protocol specific to this study is described in the "Materials and Methods" section of this chapter (Section 2.2.3.1).

2.1.1.2 Broth Microdilution Test

The broth microdilution test involves preparing two-fold serial dilutions of antimicrobial test compounds in liquid growth medium dispensed in wells of a 96-well microplate (Nunc, UK). The wells containing test agents are inoculated with a standardised bacterial suspension. Following incubation, the wells are examined for visible microbial growth as evidenced by turbidity. The lowest concentration of test compound that thwarted any microbial growth represents the MIC. The precision of this method is considered to be plus or minus one two-fold concentration, due largely to inherent error in manually preparing serial dilutions of the test compounds (J.M. Andrews, 2001; Jorgensen & Ferraro, 2009).

To determine the MBC, all wells showing no growth are sub-cultured onto fresh agar growth medium and incubated. The concentration at which the number of resulting microbial colonies corresponded to a 1000-fold reduction as compared to the colony count of the control was determined to be the MBC (J.M. Andrews, 2001). Detailed protocol specific to this study is described in the "Materials and Methods" section of this chapter (Section 2.2.3.2).

2.1.2 Conventional Antimicrobial Agents as Reference Standards

Streptomycin (an antibiotic), triclosan (an antibacterial and antifungal chemical), and NaOCl (a disinfectant) were included as reference standards in the disk diffusion assay in order to compare the activity of the five natural compounds to that of conventional antibacterial strategies. All three antimicrobial substances have significant drawbacks that may be mitigated with the use of natural compounds as novel alternatives.

2.1.2.1 Streptomycin

Streptomycin is an aminoglycosidic antibiotic drug commonly used not only to treat infections, but also as a pesticide to control bacteria, fungi, and algae in foodstuffs. Since this broad spectrum antibiotic binds to a single site on the 30S subunit of the ribosome, high level resistance can result from single step mutations in the chromosomal gene encoding the ribosomal protein S12, *rpsL* (Honoré & Cole, 1994; Springer *et al.*, 2001). Base substitutions at position 904 in the 16S rRNA gene also confer streptomycin resistance in bacteria. In addition to ribosome alteration, other mechanisms of resistance to streptomycin include reduced cell permeability and enzyme-mediated modification of the streptomycin compound (Kucers, Bennett, & Kemp, 1997).

2.1.2.2 Triclosan

Triclosan is a chlorinated aromatic compound used as an antibacterial and antifungal agent in wastewater treatment as well as in many consumer products such as toothpastes, detergents, soaps, and pesticides. Its safety is currently under review by the US Food and Drug Administration (FDA) and Health Canada (US Food and Drug Administration, 2010).

Triclosan is a chlorophenol compound known to form carcinogenic and toxic products such polychlorinated dibenzodioxins (dioxins) upon exposure to UV (commonly from sunlight) or degradation by microorganisms (Rule, Ebbett, & Vikesland, 2005). Dioxins are mutagenic, carcinogenic, teratogenic, immunotoxic, endocrine disruptive, and hepatotoxic according to the US Environmental Protection Agency (EPA) (US Environmental Protection Agency, 2010). Dioxins are chemically stable; not only do they persist in the environment for a long time, but they also bioaccumulate in fatty tissues in the human body and other living organisms (especially aquatic organisms), possibly reaching dangerous levels over time (Van den Berg *et al.*, 2006). Another by-product of triclosan is trihalomethanes (THMs), which are classified by the EPA to be a carcinogen and serious environmental pollutant (Rule *et al.*, 2005). Chloroform, a THM compound, is produced when triclosan reacts with free chlorine, often in drinking water (Fiss, Rule, & Vikesland, 2007). It is designated by the International Agency for Research in Cancer (IARC) to be a probable human carcinogen, mostly associated with hepatocellular carcinoma. Furthermore, triclosan has been reported to be an endocrine disruptor in the North American bullfrog, indicating that this biocide can alter hormone regulation in other multi-cellular life forms as well (Veldhoen *et al.*, 2006).

Triclosan is toxic to aquatic microbiota and inhibits photosynthesis in diatom algae in the environment, which accounts for a significant amount of photosynthesis on Earth (Ricart *et al.*, 2010). Resistance development is also a concern, as observed in *E. coli* and *S. aureus*

via mutations or over-expression of the fatty acid biosynthesis gene, *fabI* (Heath *et al.*, 1999; Slater-Radosti *et al.*, 2001). Also, innate resistance to triclosan was reported in *P. aeruginosa* and some *Bacillus* genus (Chuanchuen, Karkhoff-Schweizer, & Schweizer, 2003).

2.1.2.3 Sodium Hypochlorite

Sodium hypochlorite (NaOCl), more commonly known as bleach, is used to disinfect point-of-use drinking water, swimming pools, and wastewater. A 12% solution is commonly used for chlorination of drinking water, and a 15% solution is typical for use in treatment plants (Metcalf & Eddy, Tchobanoglous, Burton, & Stensel, 2002).

NaOCl is a strong oxidizing agent that is not only corrosive to surrounding materials and the environment, but also hazardous to human health. Use of NaOCl in drinking water can oxidize constituent organic matter to produce carcinogenic THMs and haloacetic acids (HAA) (Smith, 1994; US Environmental Protection Agency, 2012), both of which are carcinogens. Also, mixing of NaOCl with organic chemicals or ammonia can generate toxic and carcinogenic volatile, gaseous compounds (Odabasi, 2008). Therefore, the use of NaOCl and the levels of THMs in water are closely regulated by the EPA.

2.1.3 Classes of Bacteria

In this chapter, *Escherichia coli* and *Pseudomonas aeruginosa* were chosen as representative Gram-negative bacteria, and *Bacillus subtilis* and *Staphylococcus aureus* were chosen as representative Gram-positive forms to be tested against. Selected for their diversity, the four strains represent both Gram-stain classifications, both major cell shape classes (cocci and bacilli), and three different orders in biological classification (Enterobacteriales, Pseudomonadales, and Bacillales) (Table 2.1). Additionally, the four strains exhibit a range of tolerance levels to stress and varying potential to become pathogenic. All four species are prevalent in the environment and in biofouling (López *et al.*, 2010).

***TABLE 2.1*: Four bacterial species used in susceptibility tests and their various classifications.**

	GRAM STAIN	CELL SHAPE	BIOLOGICAL CLASSIFICATION: ORDER
Escherichia coli	Gram-negative	Rod	Enterobacteriales
Pseudomonas aeruginosa	Gram-negative	Rod	Pseudomonadales
Bacillus subtilis	Gram-positive	Rod	Bacillales
Staphylococcus aureus	Gram-positive	Cocci	Bacillales

2.1.4 Aims and Objectives

The aim of the studies within this chapter was to evaluate the effect on growth and viability that AIT, carvacrol, CNAD, citral, and thymol have on *E. coli, P. aeruginosa, B. subtilis,* and *S. aureus* in order to identify the compound(s) with the greatest relative antimicrobial activity. The objective was to be achieved by performing two complementary susceptibility tests: (i) the disk diffusion assay and (ii) the broth microdilution method.

2.2 Materials and Methods

2.2.1 Chemicals and Antimicrobial Agents

Analytical grade allyl isothiocyanate (AIT) (95% purity), carvacrol (99%), cinnamaldehyde (CNAD) (> 93%), citral (> 95%) and thymol (99.5%) were selected as test antimicrobial agents. The solvent dimethyl sulfoxide (DMSO) (≥ 99.9%) was used to dissolve the natural compounds in aqueous solution when appropriate. Streptomycin, sodium hypochlorite (NaOCl), and ethidium bromide (EtBr) were used as positive reference standards. All chemicals were supplied by Sigma-Aldrich Company Ltd. (Dorset, UK).

2.2.2 Bacterial Cultures

Two Gram-negative bacterial strains, *E. coli* (National Collection of Industrial Bacteria (NCIMB) 8879) and *P. aeruginosa* (NCIMB 950), and two Gram-positive strains, *S. aureus* (NCIMB 6571) and *B. subtilis* (NCIMB 3610), were tested for their ability to grow and survive in the presence of the five selected natural compounds. Cultures of all four strains were prepared by streaking frozen glycerol stocks (-80˚C) of each onto Mueller-Hinton agar (MHA) (Sigma-Aldrich Company Ltd., Dorset, UK) and were left to grow for 16 h at 37°C until visible colonies appeared. One colony of each species was then picked to start primary seed cultures in 5 ml sterile Mueller-Hinton broth (MHB) (Sigma-Aldrich Company Ltd., Dorset, UK). After growth for 6 h at 37˚C with 150 rpm agitation, seed cultures were added to 100 ml sterile MHB and incubated at 37°C with 150 rpm agitation until cultures reached mid-exponential growth phase. Resulting cultures were harvested, washed twice with phosphate buffered saline (PBS) (Sigma-Aldrich Company Ltd., Dorset, UK), and then resuspended in PBS. The turbidity of each bacterial suspension was adjusted to match 0.5 McFarland standard (OD_{600} = 0.132), which corresponds to bacterial density of 10^8 CFU/ml.

The resulting bacterial suspensions were used in both the disk diffusion assay and broth microdilution test.

2.2.3 Antimicrobial Susceptibility Tests (ASTs)

All AST experiments were performed using MHA and MHB as growth media, the standard media recommended by CLSI for its consistent reproducibility (Clinical and Laboratory Standards Institute, 2009a, 2009b). The media contains 2.0 g/L beef infusion solids, 17.5 g/L casein hydrolysate, and 1.5 g/L starch at pH 7.3 ± 0.2 at 25 ˚C.

2.2.3.1 Disk Diffusion Assay

The assay was performed by streaking each bacterial suspension (turbidity adjusted to 0.5 McFarland units as described earlier) onto MHA with a sterile cotton swab to obtain uniform lawn growth. Series of two-fold dilutions of each natural compound, ranging from 100 to 6.25 mg/ml, were prepared with DMSO sterilized by filtration through a 0.22 µm membrane filter. Under aseptic conditions, sterile filter disks (Whatman no. 5, 6 mm diam; Fisher Scientific Ltd., Loughborough, UK) were saturated with 20 µl of each respective test compound at five serially diluted concentrations (100, 50, 25, 12.5, and 6.25 mg/ml) and placed onto inoculated agar with sterilized tweezers. For a positive reference standard, the same was done using streptomycin at the same concentrations. A second reference standard, 15% NaOCl solution, was also included. DMSO served as vehicle control since it was used to dissolve the natural compounds. Concentrations of each reference standard were chosen to be relevant to levels used commercially and industrially today.

Because DMSO was used as the solvent for the natural compounds, filter disks impregnated with 20 µl of DMSO served as a vehicle control. Once the moistened filter disks were placed onto the seeded agar, they were sealed with parafilm and left at room temperature for 30 min to allow for the diffusion of the natural compounds, and then

incubated at 37°C for 16 h. After incubation, the circular zones of inhibition were measured and rounded to the nearest 0.5 mm. Studies were performed in biological and technical triplicates at the least, and the diameters of inhibition zones were averaged. The test compound that yielded the largest zone of inhibition was taken to be the most effective antibacterial agent, and others were ranked accordingly.

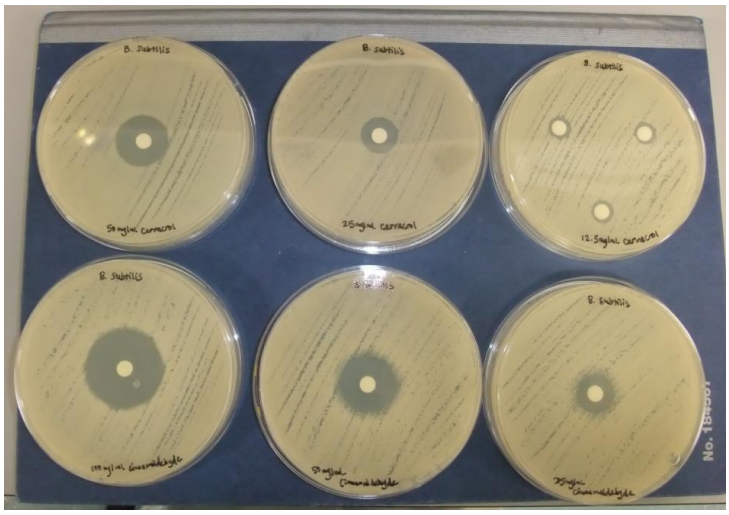


FIGURE 2.1: **Disk diffusion assay in which *B. subtilis* was subjected to varying concentrations of carvacrol (top three plates) and CNAD (bottom three plates). Different sizes of inhibition zones are visible around the filter disks. Photo by Andrea Chan.**

2.2.3.2 Broth Microdilution Method

Based on the previous screening, citral demonstrated the lowest overall antimicrobial activity and therefore was not included in further experiments. The MICs and MBCs of AIT, CNAD, carvacrol, and thymol were determined using the broth microdilution method. Stock solutions of 5000 mg/L of each natural compound were prepared with DMSO(20%)-MHB solution as solvent. Series of two-fold dilutions of each compound, ranging from 2500 to 4.88 mg/L final concentration, were prepared across sterile 96-well microtitre plates. Each well was then inoculated with 100 µl of the bacterial suspensions prepared as described earlier (turbidity adjusted to 0.5 McFarland units). MHB with no inoculum served as negative control. DMSO(20%)-MHB with no test compound served as vehicle control, MHB with

inoculum served as positive control. Plates were sealed with microporous tape sheets (AirPore® Tape Sheets, Qiagen, UK) and incubated at 37°C for 16 h at 150 rpm agitation. Experiments were repeated three times, with eight technical replicates per experiment. Using a Synergy HT Multi-detection Microplate Reader (Bio-Tek, UK), inhibition of growth was judged by comparing absorbance values before and after incubation. The MIC is defined as the difference in absorbance values (DA), expressed by the following equation: $DA = A - A_o$, where A is the absorbance value at wavelength of 600 nm (OD_{600}) after incubation, and A_o is the OD_{600} of the initial inoculum. The MIC of each compound is defined as the lowest concentration inhibiting any visible growth (J.M. Andrews, 2001), where $DA \leq 0$.

After incubation, the contents in the clear wells of the microplate were then diluted 20-fold. Three µl of such diluted samples were spread onto fresh MHA plates using sterile glass beads (3 mm diam; VWR, Leicestershire, UK) and then incubated at 37°C overnight to allow colonies to form. The experiment was repeated three times, with eight MHA plates inoculated with contents from eight separate wells per experiment. The initial inocula before incubation were also plated. The resulting colonies were counted using Stuart SC6PLUS colony counter. The MBC is defined as the lowest concentration at which 99.9% of bacteria are killed (J.M. Andrews, 2001). The concentration at which the number of resulting colonies was 0.1% that of the the colony count of the starting inoculum was determined to be the MBC.

2.2.4 General Statistical Analysis

F-test, *t*-test and analyses of variance (ANOVA) followed by Tukey's test were applied when appropriate. *P* values of 0.05 and 0.01 were used to determine statistical significance.

2.3 Results

2.3.1 Determining Relative Antimicrobial Activity

The antibacterial activity of five selected natural compounds, expressed as sizes of inhibition zones, against four bacterial species is summarized in Table 2.2. All five compounds exhibited inhibitory effects of varying magnitudes against *E. coli*, *B. subtilis*, and *S. aureus*. *P. aeruginosa* was susceptible to only AIT and CNAD. There was no inhibition observed with the vehicle control (DMSO) in either assays.

Overall, AIT performed much better than the other selected compounds in inhibiting all four bacterial strains. It produced the largest zones of inhibition in all cases except at concentrations ≤ 25 mg/L against *B. subtilis and P. aeruginosa*. AIT was the only compound to completely inhibit growth of all four species on the entire agar plate (86 mm diam) at one or more concentrations used in this study. However, the activity of AIT abruptly dropped to zero as its concentration decreased by just one dilution step, demonstrating maximum inhibitory capacity at 12.5 mg/L and then suddenly no inhibition at all at 6.25 mg/L against *E. coli* and *S. aureus*.

CNAD also displayed excellent antibacterial activity, generating the largest inhibition zones against *P. aeruginosa* at concentrations ≤ 25 mg/L. Otherwise, in most cases CNAD produced the second-largest zones of inhibition following AIT (except in the case against *B. subtilis*, in which citral performed second-best).

For all species tested, the reference standard streptomycin produced inhibitions zones that were smaller than all of the natural compounds at the same concentrations, with the exception of citral against *S. aureus*, in which case streptomycin exhibited greater antibacterial activity for all concentrations tested. One percent triclosan exhibited no detectable inhibition against *P. aeruginosa* and *B. subtilis*, while at least one natural

compound was able to inhibit growth to some degree at ≥ 12.5 mg/ml for *P. aeruginosa* and ≥ 6.25 mg/ml for *B. subtilis*. In the case of *E. coli* and *S. aureus,* the natural compounds generally displayed greater antibacterial activity than 1% triclosan at concentrations ≥ 12.5 mg/ml, except in the following cases: citral exhibited greater inhibition at ≥ 25 mg/ml against *S. aureus* and CNAD exhibited greater inhibition at ≥ 6.25 mg/ml against *E. coli*. Detectable inhibition in all four species resulted from treatment with 15% NaOCl. At least two of the natural compounds yielded larger inhibition zones at ≥ 50 mg/ml as compared to 15% NaOCl.

Carvacrol and thymol displayed moderate and similar levels of inhibition against three bacterial strains, but had no detectable effect on *P. aeruginosa*. Although citral showed good inhibition against *B. subtilis,* it displayed the poorest antibacterial activity against all other strains. Because of its overall low efficacy, citral was not included in the broth microdilution test.

TABLE 2.2: **Mean diameters of growth inhibition zones obtained from the disk diffusion assay. Mean values presented in millimetres ± SD of at least three biological and technical replicates. 0 = no observed inhibition. * = Positive reference standards.**

	E. COLI						***P. AERUGINOSA***					
Concentration (mg/ml)	100	50	25	12.5	6.25		100	50	25	12.5	6.25	
Compound												
AIT	>86	>86	>86	>86	0		>86	>86	0	0	0	
CNAD	42 ± 0	36 ± 1.7	28.7 ± 0.6	16.7 ± 0.6	8 ± 0		19 ± 0	13.7 ± 0.3	11.2 ± 0.3	8.2 ± 0.7	0	
Carvacrol	30 ± 0	21.75 ± 0.4	14.7 ± 0.5	11.3 ± 0.3	0		0	0	0	0	0	
Citral	10.5 ± 0.5	11.18 ± 0.6	8 ± 0	8 ± 0	0		0	0	0	0	0	
Thymol	33.8 ± 0.6	20.78 ± 0.8	13.8 ± 0.2	12.7 ± 0.6	0		0	0	0	0	0	
Streptomycin*	9.3 ± 0.3	1 ± 0	0	0	0		0	0	0	0	0	
1% Triclosan*						5.72 ± 0.2						0
15% NaOCl*						10.5 ± 1.3						19 ± 0.3
	S. AUREUS						***B. SUBTILIS***					
Concentration (mg/ml)	100	50	25	12.5	6.25		100	50	25	12.5	6.25	
Compound												
AIT	>86	>86	>86	>86	0		>86	>86	15 ± 0.2	0	0	
CNAD	39.8 ± 0.4	32.4 ± 1.3	20.5 ± 0.5	15.7 ± 0.4	0		37.4 ± 4.2	29.3 ± 2.9	14 ± 0	8.3 ± 0.3	0	
Carvacrol	34.6 ± 0.8	28.2 ± 0.9	25.5 ± 0.8	9.2 ± 0.4	0		30.8 ± 0.7	22.8 ± 0.3	14.2 ± 0.1	8.5 ± 0	0	
Citral	22.2 ± 0.8	15.3 ± 0.5	9.3 ± 0.5	0	0		53.5 ± 3.0	36.9 ± 1.4	24 ± 0	20 ± 1.0	11.3 ± 0.3	
Thymol	33.2 ± 0.4	23 ± 0.3	12.8 ± 0.7	8.5 ± 0.3	0		34 ± 0.5	23 ± 0.8	15.4 ± 0.3	9.8 ± 0.1	6.5 ± 0	
Streptomycin*	28 ± 0	26 ± 0	14 ± 0	6.8 ± 0.2	0		7 ± 0	0	0	0	0	
1% Triclosan*						6.5 ± 0.3						0
15% NaOCl*						21 ± 0.3						21.3 ± 0.3

2.3.2 MIC and MBC Determination

Results of the broth microdilution method (displayed in DA values) for AIT, CNAD, carvacrol, and thymol against four bacterial species are presented in Figure 2.2. DA values of 0.0528, 0.0407, -0.0073, and -0.0078 were obtained when *E. coli* suspensions were treated with 19.531, 39.063, 78.125, and 156.25 mg/L of CNAD, respectively. *E. coli* cells incubated with CNAD at concentrations ≥ 78.125 mg/L resulted in DA values ≤ 0, meaning that the OD_{600} of such samples after incubation were significantly less than OD_{600} of the initial inocula ($P < 0.05$). Thus, according to the definition of MIC described earlier, the MIC of CNAD against *E. coli* was determined to be 78.125 mg/L. It should be noted that although concentrations ranging from 2500 to 4.88 mg/L of all four compounds were used in this assay, only four concentrations of each compound are shown in Figure 2.2 in order to concisely show the MIC in each case, which is the point at which DA values transition from positive to negative.

Subsequent plate count experiments demonstrated that *E. coli* treated with 78.125 mg/L CNAD resulted in ≥ 99.9% reduction in CFU/ml as compared to the colony counts of the initial inoculum. Therefore, based on the definition of MBC given earlier, the MBC of CNAD against *E. coli* was determined to be 78.125 mg/L. Similarly, the MICs and MBCs of AIT, CNAD, carvacrol, and thymol against *E. coli*, *P. aeruginosa*, *S. aureus*, and *B. subtilis* were determined (Table 2.3).

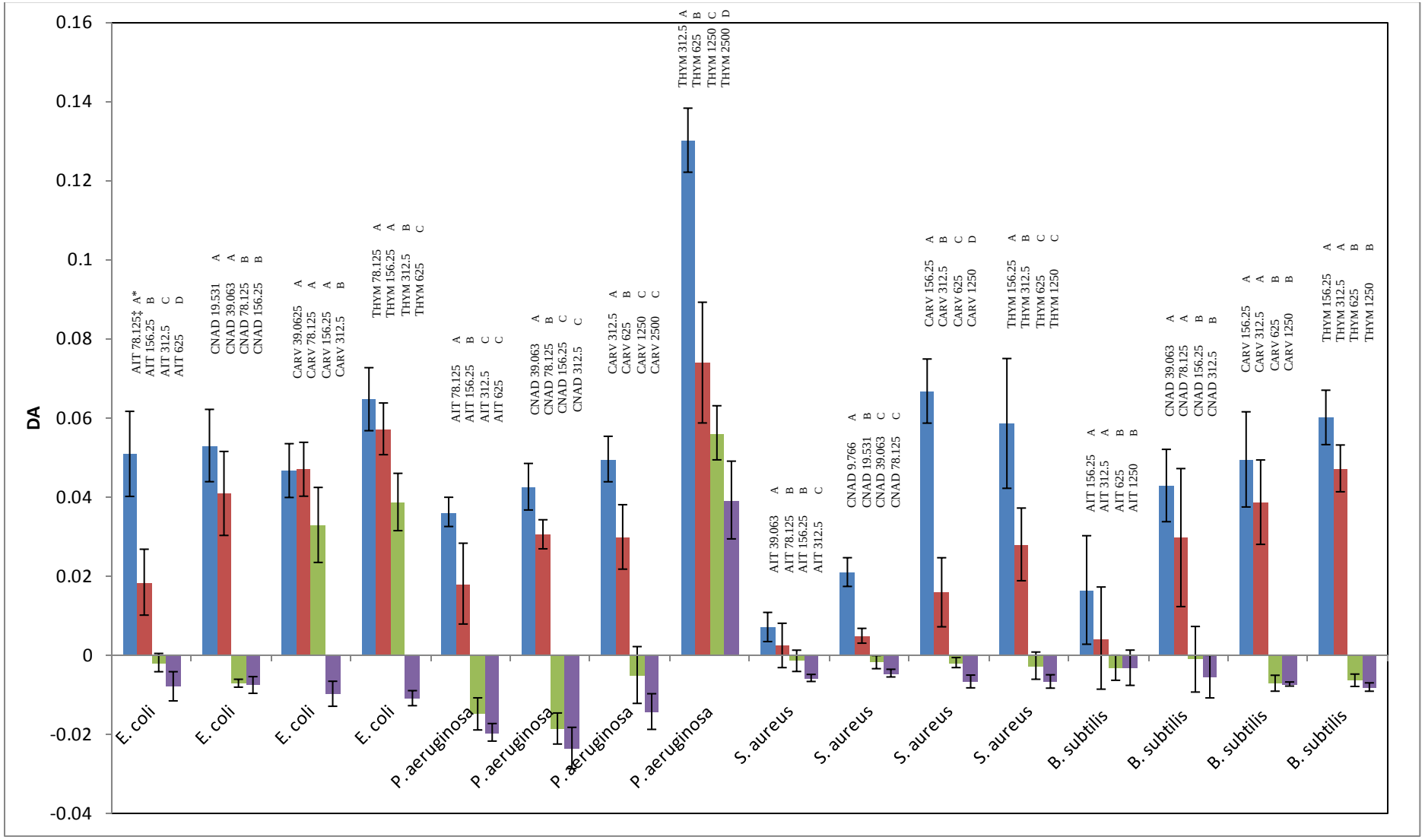


FIGURE 2.2: **Results from the broth microdilution method, in which *E. coli*, *P. aeruginosa*, *S. aureus*, and *B. Subtilis* were treated with serial dilutions of allyl isothiocyanate (AIT), carvacrol (Carv), cinnamaldehyde (CNAD), and thymol (Thym). Results are expressed in differences in absorbance (DA); DA = A - A_o, where A is OD_{600} after incubation, and A_o is the OD_{600} of the initial inoculum. MIC of each compound is the lowest concentration inhibiting any visible growth, where DA ≤ 0 (point at which DA values transition from positive to negative). "‡" = Units of concentration are expressed in mg/L. "*" = Mean values within the same cluster with different letters are significantly different ($P < 0.05$). Error bars represent ± SD (technical and biological triplicates).**

TABLE 2.3: **Minimum inhibitory concentrations (MICs) and minimum bactericidal concentrations (MBCs) of four natural compounds, obtained from broth microdilution method, for four bacterial species. Units of concentration are expressed in mg/L. Experiment was repeated three times, with eight technical replicates per experiment.**

	Bacterial Species							
Compound	***E. coli***		***P. aeruginosa***		***S. aureus***		***B. subtilis***	
	MIC	MBC	MIC	MBC	MIC	MBC	MIC	MBC
AIT	156.25	156.25	156.25	312.5	156.25	156.25	156.25	312.5
CNAD	78.125	78.125	156.25	312.5	78.125	78.125	156.25	312.5
Carvacrol	312.5	312.5	1250	2500	625	1250	625	625
Thymol	625	625	> 2500	> 2500	625	1250	625	625

In the broth microdilution assay, CNAD exhibited the greatest inhibitory effect against all bacterial strains, yielding the lowest MICs ranging from 78.125 to 156.25 mg/L and the lowest MBCs ranging from 78.125 to 312.5 mg/L. AIT displayed the second-highest activity, presenting MICs of 156.25 and MBCs ranging from 156.25 mg/L to 312.5 mg/L. Carvacrol and thymol generated very similar MIC and MBC values except with *P. aeruginosa*, in which case carvacrol resulted in MIC of 1250 mg/L and MBC of 2500 mg/L while thymol's MIC and MBC were beyond the highest concentration used in this study (> 2500 mg/L).

2.3.3 Susceptibility of Gram-Negative and Gram-Positive Bacteria

No obvious difference in susceptibility was detected between Gram-negative and Gram-positive bacteria. *P. aeruginosa* was the most resistant to antibacterial treatments employed in these two assays, followed by *B. subtilis*. This is in accordance to previous studies claiming *P. aeruginosa* to be highly tolerant to antimicrobial agents (S.P. Denyer & Maillard, 2002; Mann *et al.*, 2000; Mayaud *et al.*, 2008). No inhibition of growth was observed with DMSO control samples.

2.4 Discussion

Four species of bacteria were challenged with five different plant-based compounds to determine whether they could serve as effective and more sustainable alternatives to current antimicrobial agents. All five test compounds exhibited inhibitory effects against the selected bacteria at varying degrees, with the antimicrobial order being AIT > CNAD > carvacrol ≥ thymol > citral.

2.4.1 Relative Antimicrobial Activity of Five Natural Compounds

Of the five compounds (AIT, carvacrol, CNAD, citral, and thymol), AIT and CNAD displayed the greatest biocidal activity against the broadest range of bacteria used in this study. Carvacrol and thymol exhibited moderate inhibitory activity against three bacterial strains, but were ineffective against *P. aeruginosa*. Lastly, although citral performed well against *B. subtilis,* it was the overall poorest inhibitor against all other strains tested. Results of this study are in line with a previous study which reported the antimicrobial order to be carvacrol ≈ thymol > citral for all four strains presently used (Gallucci *et al.*, 2009). Similarly, another study reported the same antimicrobial order as this present study (AIT ≈ CNAD > carvacrol) using the fungus *Penicillium notatum* as the target microbe (Tunc *et al.*, 2007). However, current findings contrast with other studies that have reported CNAD, carvacrol, and thymol to exhibit similar levels of antibacterial activity against *E. coli* (Helander *et al.*, 1998; Palaniappan & Holley, 2010; Pei, Zhou, Ji, & Xu, 2009). Also, findings of Mahmoud *et al.* differ from those of this study; they reported that the antimicrobial order against microflora of carp to be carvacrol ≈ CNAD ≈ thymol > citral >> AIT (Mahmoud *et al.*, 2004). The discrepancies between these reports may be explained by factors such as the varying susceptibility methods used to screen the natural compounds and more importantly, the different types of target microorganisms used. The parameters of the

experiments such as temperature, culture media, incubation time, pH, volume of inocula, volume of sample (microdilution versus macrodilution), and agitation rate could also individually or in combination affect the results of different studies. Commonly, only one method of testing bacterial susceptibility is employed to evaluate the antimicrobial activities of different test substances. On the contrary, three different techniques (disk diffusion assay, broth microdilution method, and plate count experiments) were performed in this present study to yield multi-dimensional results that are less likely to be skewed by the limitations of any one particular test method.

2.4.2 Volatility and Low Solubility of Natural Compounds

AIT exhibited the greatest antimicrobial activity against all four bacterial species by a significant margin ($P < 0.05$) in the disk diffusion assay. CNAD produced the second-largest zones of inhibition against three out of the four strains in the disk diffusion assay and presented the lowest MIC and MBC values for all four bacterial strains. AIT did not produce the lowest MIC and MBC values as would have been expected based on the results from the disk diffusion assay. A possible explanation for CNAD performing better than AIT in the broth microdilution test was the difference in volatility between the test compounds. The vapour pressure of AIT (4.6 mmHg at 25˚C) is greater than that of CNAD (0.03 mmHg at 25˚C), meaning a greater amount of AIT compared to CNAD would have been lost from the media into the atmosphere during the incubation period, since the microtitre plates were not sealed air-tight. Also, the initial concentration of AIT dispensed in samples may have rapidly declined even before the start of incubation due to exposure to air during preparation of the entire 96-well microplate. The high volatility of the natural compounds may also explain the lack of observable inhibition at the lowest concentration (6.25 mg/ml) for all five natural compounds in most cases of the disk diffusion assay. Furthermore, the sudden drop in activity of AIT within just one dilution step in the disk diffusion assay may also be attributed to

AIT's highly volatile nature (T.-T. Liu & Yang, 2010). There may be a threshold concentration at which AIT stayed in solution, and below this threshold, AIT molecules may have been immediately lost through vaporisation, leaving none available in the media to react with target cells.

Another factor contributing to why MIC and MBC values may not fully reflect natural compounds' maximum inhibitory capacity is their low solubility in aqueous solution. To better dissolve AIT and CNAD, DMSO was used in this study. Polar aprotic solvents such as DMSO dissolve both polar and nonpolar compounds. However, the use of emulsifiers or solvents in combination with natural compounds has been shown to lower the inhibitory effect of the compound (Mann & Markham, 1998). The degree to which they mute antimicrobial activity of each compound is unknown, which may explain why the same compound may yield varying degrees of bacterial inhibition in different types of susceptibility tests.

2.4.3 Carvacrol, Thymol, and Citral

The moderately active compounds were carvacrol and thymol and the two displayed very similar levels of inhibition against all four bacterial strains. Carvacrol and thymol are both major constituents of the same EOs, and apart from the positions of the hydroxyl groups, they share the same chemical structure. Therefore, their similar degrees of antimicrobial efficacy were not surprising. Contrary to previous reports (Dorman & Deans, 2000; Gallucci *et al.*, 2009; Mayaud *et al.*, 2008), carvacrol and thymol had zero inhibitory capacity against *P. aeruginosa*.

Citral, the major constituent of lemongrass oil, exhibited the lowest overall activity in this study. Although lemongrass oil has previously been reported to be a potent killer of

microbes (S. Chao *et al.*, 2008; Ultee *et al.*, 2002), citral performed poorly under the experimental parameters of this study.

2.4.4 Tolerance and Susceptibility of Different Bacterial Species

In general, the MBCs were greater than the MICs for each corresponding strain (Table 2.3), indicating that a higher concentration was needed to kill the bacteria as compared to inhibiting their growth. However, in the case of *E. coli*, the MBC and MIC values were equal for three of four test compounds (CNAD, carvacrol, and thymol), which suggested that the tolerance for natural compounds at inhibitory concentrations is low for *E. coli*.

In this study, Gram-negative and Gram-positive bacteria were found to be equally susceptible to treatment of natural antimicrobial compounds, which correlates to some previous findings (Dorman & Deans, 2000; Friedman, Henika, & Mandrell, 2002; Inouye *et al.*, 2001) while contradicting others (Palaniappan & Holley, 2010; Pei *et al.*, 2009; Prabuseenivasan *et al.*, 2006). The low susceptibility of *P. aeruginosa* in this study is not surprising since it has been well-documented to be extremely resistant to antibacterial treatment relative to other bacterial species (Dorman & Deans, 2000; Gallucci *et al.*, 2009; Inouye *et al.*, 2001; Warnke *et al.*, 2009).

2.4.5 Conclusion

In summary, the results of this study demonstrated that AIT and CNAD have strong antimicrobial activity against the representative bacterial strains presently selected. The MIC and MBC of CNAD against four selected bacterial species were found to be 78.125 for both; the MIC and MBC of AIT against the same species were 156.25 mg/L (MIC) and between 156.25 mg/L to 312.5 mg/L (MBC), respectively. However, these values may not truly reflect the full antimicrobial capacity of these compounds due to their volatility and low solubility. To explore the application of AIT and CNAD as novel antimicrobial agents, further research would be needed to alleviate the problem of volatility and low solubility in order to harness the full bactericidal potentials of these compounds.

Chapter Three

3. Resolving the Mechanism of Bacterial Inhibition by AIT and CNAD Employing Complementary Whole-Cell Biosensors

3.1 Introduction

3.1.1 Biosensors

Biosensors are sensitive biological materials (e.g. multicellular organisms, microorganisms, tissue, enzymes, antibodies, nucleic acid probes) that interact with analytes under study to provide information-linked response via a suitable transducer (Turner, Wilson, & Kaube, 1987). The transducer transforms the interaction of the analyte with the biological element into a measurable and quantifiable signal (e.g. optical, electrochemical, etc.). Of particular interest to the studies of this chapter are whole-cell bacterial biosensors that assess acute toxicity of analytes using bioluminescence genes (*luxCDABE*) as the transducer (Close *et al.*, 2012; Simpson *et al.*, 1998).

There are two classes of whole-cell biosensors: the metabolic (non-specific) type and the catabolic (specific) type. Metabolic biosensors operate in a constitutive manner where the reporter gene is fused to promoters that are continuously expressed as long as the organism is alive and metabolically active. This type of biosensor is effective for evaluating the global toxicity of analytes of interest (F. Zhang & Keasling, 2011). Catabolic biosensors function in an inducible manner where the reporter gene is fused to a promoter regulated by the concentration of a catabolic compound of interest (F. Zhang & Keasling, 2011). By sensing

levels of a particular product from cellular breakdown reactions, this type of biosensor is suitable for detecting the activity of a specific catabolic pathway as a result of exposure to analytes under study (Yu, Chen, & Mulchandani, 2006).

Although certain antimicrobial modes of attack by plant-derived compounds have been proposed (Koroch *et al.*, 2007), the complex mechanisms of action of such compounds are not well understood. Bacterial whole-cell biosensors reflect the multi-dimensional response to toxic stimuli launched by a host strain that is representative of target bacterial communities. Therefore, such assays may be able to provide not only a measure of toxicity of plant compounds, but also a dynamic perspective on their respective antibacterial mechanisms.

3.1.2 Lux Genes

Luciferase is an enzyme that catalyses a light-emitting chemical reaction. Such enzymes are endogenous in various organisms, including bacteria, fungi, algae, jellyfish, and insects (Baldwin, 1996; Baldwin *et al.*, 1995). Bacterial luciferase is a heterodimeric enzyme comprising α and β subunits with molecular masses of 40 kDA and 37 kDA, respectively (Baldwin *et al.*, 1995). *Lux* genes code for the luciferase enzyme and are therefore responsible for the bioluminescence of naturally luminescent bacteria. The *lux* operon consists of five genes, *luxCDABE*, and is approximately 7 kb long (Burlage & Kuo, 1994). *LuxA* and *luxB* encode the α- and β-subunits of luciferase, respectively (Figure 3.1). The enzyme catalyses the light-emitting reaction (Figure 3.2, Equation 1), which involves the oxidation of a reduced riboflavin phosphate ($FMNH_2$) and a long-chain aliphatic aldehyde (R-CHO) to produce blue-green light with maximum intensity at 490 nm (Burlage & Kuo, 1994; Meighen, 1991). The second step of the bioluminescent reaction involves the reduction of a fatty acid (R-COOH) back to an aldehyde (R-CHO) (Figure 3.2, Equation 2). A multi-

enzyme fatty acid reductase complex uses $NADPH_2$ and ATP to regenerate the aldehyde substrate (R-CHO) required in the light-emitting reaction (Burlage & Kuo, 1994; Meighen, 1991). The reductase complex is composed of three proteins: a reductase (54 kDa), a transferase (42 kDa), and a synthase (33 kDa), which are encoded by *luxC*, *luxD*, and *luxE* of the *lux* operon, respectively (Figure 3.1). The continued expression of the *lux* gene cassette occurs through autocatalysis, where by the products of the light-emitting reaction also drive the reaction from which they were derived.

In the present study, two genetically-modified bacterial biosensors were employed to detect microbial response to AIT and CNAD treatment through the use of the *lux* cassette as a reporter gene. In one system (*E. coli* HB101_pUCD607_*lux)*, the production of light was directly linked to metabolic activity (Belas *et al.*, 1982; Tiensing, Preston, Strachan, & Paton, 2001). In the other bioreporter system (*Acinetobacter baylyi* ADP1_*recA_lux*), the *lux* operon was fused to the inducible promoter of an essential gene involved in the DNA repair.

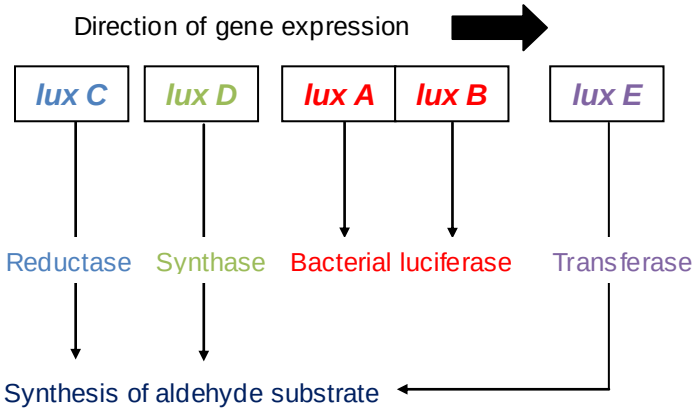


***FIGURE 3.1*: The *luxCDABE* operon consists of two genes for luciferase (*luxA* and *luxB)*, the enzyme that catalyses the light-emitting reaction, and three genes for the multi-enzyme fatty acid reductase complex (*luxC*, *luxD* and *luxE)* that catalyses the production of the aldehyde substrate required in the light-emitting reaction. Schematic by Andrea Chan.**

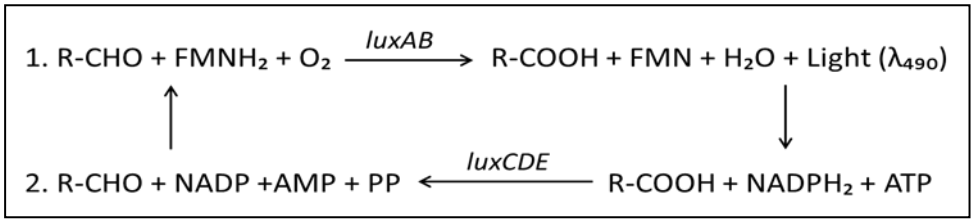


***FIGURE 3.2*: The bioluminescence reactions are catalysed by enzymes encoded by the *luxCDABE* operon. The *luxAB* genes code for luciferase, which converts an aldehyde substrate (R-CHO) to a fatty acid (R-COOH), generating visible light (Equation 1). The *luxCDE* genes collectively encode a reductase complex, which uses $NADPH_2$ and ATP to regenerate the aldehyde (Equation 2). Schematic by Andrea Chan.**

3.1.3 Metabolic Biosensor: Escherichia coli HB101_pUCD607_lux

In the first biosensor assay, *E. coli* HB101 transformed with the multi-copy pUCD607 plasmid containing the *luxCDABE* gene cassette from *Vibrio fischeri* (Figure 3.3) (Belas *et al.*, 1982) was used to detect impairment of cellular metabolism in bacteria. *V. fischeri* are naturally luminescent Gram-negative marine bacteria. The *lux* reporter genes are constitutively expressed, resulting in the constant production of visible light during normal, healthy cell cycles.

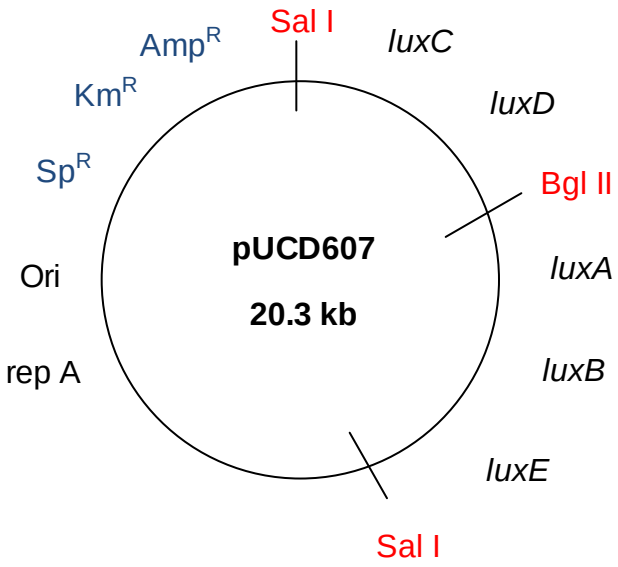


FIGURE 3.3: **The high copy pUCD607 plasmid containing the *V. fischeri luxCDABE* operon. Schematic by Andrea Chan**

The coenzymes ATP and $NADPH_2$ are products of cellular respiration and are units of intracellular energy that drives the majority of cellular functions (Campbell *et al.*, 2008b; Knowles, 1980). Since $NADPH_2$ and ATP are needed for the regeneration of the aldehyde substrate required in the light-emitting reaction (Figure 3.2), the bioluminescence of the bioreporter cells is intrinsically tied to their metabolic activity (Keane, Phoenix, Ghoshal, & Lau, 2002; Meighen, 1991). Thus, any injury to cellular metabolism caused by a test compound is reflected in the decrease of cellular light output, in which the degree of toxicity is directly proportional to the reduction in light intensity (Keane *et al.*, 2002; Kurvet, Ivask, Bondarenko, Sihtmäe, & Kahru, 2011; Meighen, 1991; Simpson *et al.*, 1998).

3.1.4 Biosensor for the Detection of Genotoxicity: Acinetobacter baylyi ADP1_recA_lux

The second bioluminescence-based biosensor employs the bioreporter *Acinetobacter baylyi* ADP1_*recA_lux*, in which *luxCDABE* genes cloned from *Photorhabdus luminescens* have been chromosomally integrated into *recA* of *A. baylyi* ADP1 (Song *et al.*, 2009). This biosensor has been used previously to detect plant secondary metabolites, specifically salicylic acid in tobacco leaves (Huang *et al.*, 2006). *RecA* is an essential gene in bacterial DNA repair and is induced after DNA damage occurs, as indicated by the accumulation of single-stranded DNA (ssDNA) regions (Chen, Yang, & Pavletich, 2008). Activated upon binding to ssDNA, the functional product of the *recA* gene (RecA protein) facilitates the expression of a suite of genes, collectively known as SOS response genes, involved in the global response to DNA damage. The presence of DNA-damaging stimulus causes r*ecA* expression to rise above basal level, resulting in the de-repression of the SOS regulon, thereby inducing protection, repair, replication, mutagenesis, and metabolism of DNA. Furthermore, RecA protein also directly participates in recombinational DNA repair (Chen *et al.*, 2008).

With the *lux* operon inserted under the *recA* promoter, *A. baylyi* ADP1_*recA*_lux cells are activated to produce light in the presence of DNA-damaging toxicants. The fusion of *lux* genes under the regulatory region of this essential DNA repair gene provides a quantifiable optical signal that is directly linked to the cells' transcriptional response to DNA damage (Ben-Israel, Ben-Israel, & Ulitzur, 1998).

RecA is universally present in all species (Kawabata, Kawabata, & Nishibori, 2005); thus, this biosensor system is not only a good indicator of whether a test compound is genotoxic to bacteria, but it also sheds light on the DNA-damaging potential of the compound in higher, multicellular organisms.

3.1.5 Transcriptional Analysis of recA

Transcription of genomic DNA to create messenger RNA (mRNA) is the first step in the mechanism of gene expression. Expression levels of the inducible *recA* gene can be monitored by quantifying the amount of corresponding mRNA transcript in the cell. Such quantification can be achieved by first isolating total RNA from cells, then targeting and amplifying the *recA* mRNA via reverse transcription polymerase chain reaction (RT-PCR), and lastly, determining the abundance of the RT-PCR product. The *A. baylyi* ADP1_*recA_lux* bioluminescence study claims that the level of light emitted by the bioreporter cells is directly proportional to the degree of *recA* expression. To corroborate the results from this luminescence-based assay, RNA from *A. baylyi* ADP1_*recA_lux* cells were isolated after various treatments and subsequently reverse-transcribed, amplified, and quantified.

3.1.5.1 Reverse Transcription Polymerase Chain Reaction (RT-PCR)

RT-PCR is a variant of the PCR technique commonly used to detect RNA expression levels (Freeman, Walker, & Vrana, 1999). With extracted total RNA as the template (instead of DNA in the case of traditional PCR), specific primers target the mRNA transcript of interest, which is subsequently reverse transcribed into its DNA complement (cDNA) by reverse transcriptase. The newly synthesized strand of cDNA is then amplified via traditional PCR. For quantitative transcriptional analysis, the number of PCR cycles is optimised and reduced so that the reaction terminates at the exponential phase of amplification, during which the copies of amplicon produced is proportional to the amount of starting mRNA template (Freeman *et al.*, 1999). The plateau phase of amplification should be avoided since the PCR products will be in saturation and thus unrepresentative of the amount of starting mRNA.

To confirm that amplicons contain the expected number of base pairs, the RT-PCR product can be visualised via DNA gel electrophoresis, a technique that separates DNA fragments according to size and charge (Sambrook & Russel, 2001). In this method, an electric field is applied across an agarose matrix through which negatively charged nucleic acids differentially travel based on their size. Once the desired product is confirmed, the abundance of amplified DNA can be quantified spectrophotometrically.

3.1.6 Aims and Objectives

The first objective of this study was to perform two complementary bioluminescence-based bacterial biosensor assays to evaluate the toxic effects of AIT and CNAD. Since the *lux* reporter gene is linked to different cellular functions that toxic antagonists may target, using the two biosensors in combination could elucidate the mechanisms by which AIT and CNAD inhibit or kill bacteria. This is the first study to combine complementary *lux*-based bacterial biosensor systems to assess cytotoxicity and genotoxicity of plant secondary metabolites.

The second aim of this chapter was to confirm findings from the genotoxicity-sensing *A. baylyi* ADP1_*recA*_*lux* biosensor assay using molecular techniques. To determine the relative transcription levels of *recA* after exposure to AIT and CNAD, semi-quantitative RT-PCR was performed on extracted mRNA of *A. baylyi* ADP1_*recA*_*lux* bioreporter cells. This molecular-based validation study would provide an added dimension in determining whether CNAD and AIT were genotoxic or not.

3.2 Materials and Method

3.2.1 Bacterial Cultures

3.2.1.1 *E. coli* HB101_pUCD607_*lux* Bioreporters

Stock suspensions of the *E. coli* HB101_pUCD607_ *lux* (Belas *et al.*, 1982; Simpson *et al.*, 1998) biosensor were prepared as follows. Five ml of an overnight culture were added to 100 ml of sterile lysogeny broth-Miller with 1 g/L glucose (LBG) with 50 µg/ml ampicillin. Antibiotic was added to select for bacterial cells that contain the pUCD607 plasmid after growth. The culture was incubated at 37°C at 150 rpm agitation for 8 h until the cells reached mid-exponential growth phase. The culture was immediately placed on ice to prevent further growth, and then centrifuged at 3000 rpm at 4°C for 20 min. The resulting cell pellet was resuspended in sterile *Mist dessicans*, which is 1:3 (vol:vol) solution of LBG with additional 10 g/L glucose : horse serum. One ml of this suspension was dispensed into each sterile freeze-drying vial, partially sealed with rubber stoppers, frozen at -80°C overnight, and freeze-dried for 24 h at -55°C.

3.2.1.2 *A. baylyi* ADP1_*recA*_*lux* Bioreporters

Stock suspensions of the *A. baylyi* ADP1_*recA_lux* biosensor (Song *et al.*, 2009) were prepared as follows. One colony was inoculated into 100 ml of lysogeny broth-Miller (LB) and incubated at 37°C at 150 rpm agitation for 14 h until the cells reached mid-exponential growth phase. Cells were then harvested by centrifugation at 3000 rpm for 20 min. The resulting cell pellet was freeze-dried in the same procedure as described above. The resulting freeze-dried products of both *E. coli* HB101_pUCD607_ *lux* and *A. baylyi* ADP1_*recA_lux* were sealed and stored at -20°C until use in the biosensor assays.

3.2.2 Biosensor Assays

3.2.2.1 *E. coli* HB101_pUCD607_*lux* Assay

3.2.2.1.1 Bioluminescence Study

The *E. coli* HB101_pUCD607_*lux* biosensor assay was performed at respective MICs of the AIT and CNAD against *E. coli* (156.25 mg/L AITC and 78.125 mg/L CNAD; determined previously via broth microdilution method in Chapter 2, Table 2.4). In addition, treatment of 156.25 mg/L CNAD (2MIC) was also included in this assay in order to directly compare the cytotoxic effects of AIT and CNAD when used at the same concentration. Freeze-dried stock suspensions of *E. coli* HB101_pUCD607_*lux* cells (prepared as described earlier) were resuscitated by dispensing 2 ml of sterile de-ionised water (DW) into each vial and incubating at 25°C for 2 h. The cell suspensions were then centrifuged at 3000 rpm for 5 min, followed by removal of supernatant and resuspension of cells in 2 ml of sterile DW. The resulting resuscitated cells were diluted 10-fold in solutions of 156.25 mg/L AIT (corresponding to 1MIC for *E. coli*), 78.125 mg/L CNAD (1MIC), 156.25 mg/L CNAD (2MIC), and sterile DW which served as the control. The bioreporter cells were exposed to the designated concentrations of AIT and CNAD for 30 min and then transferred to a 96-well black microplate (Nunc, UK), with 200 µl of sample dispensed in each well. Light output was measured using a Synergy HT Multi-detection Microplate Reader (Bio-Tek, UK). Luminescence values were expressed as relative light units (RLU), and the intensity of light emitted by the treated bioreporter cells were expressed as percentages of the untreated control. Sixteen readings (two rows of a 96-well microplate) were taken for each sample during each run, and the experiment as a whole was repeated at least three times.

3.2.2.1.2 Post-Exposure Recovery Plate Count Experiment

After exposure to the natural compounds, serial 10-fold dilutions of the *E. coli* HB101_pUCD607_*lux* samples from the bioluminescence study were immediately prepared and sub-cultured onto LBG agar with 50 µg/ml ampicillin. Inoculated agar plates were incubated at 37°C for 16 h and visible colonies were subsequently counted to determine the CFU/ml resulting from exposure to specified concentrations of AIT and CNAD. In order to directly compare RLU values from the bioluminescence study with CFU/ml values from plate count experiments, colony counts were normalized to percentages of the control wells. Plate counts for each sample were performed in biological and technical triplicates at the least.

3.2.2.2 *A. baylyi* ADP1_*recA*_*lux* Assay: Bioluminescence Study

Resuscitated *A. baylyi* ADP1_*recA*_*lux* bioreporter cells were diluted 10-fold in solutions of AIT (at final concentrations of 2 mg/L, 0.2 mg/L, and 0.1 mg/L) and CNAD (at final concentrations of 4 mg/L, 2 mg/L and 0.2 mg/L) in a 96-well black microplate (Nunc, UK), with 20 µl of cell suspension and 180 µl of treatment in each well. Cells were also similarly diluted in sterile DW, which served as negative control. Two µM ethidium bromide (EtBr) (Sigma-Aldrich Company Ltd., Dorset, UK) and 0.001% NaOCl served as positive reference controls. Light output was measured immediately after sample preparation using a Synergy HT Multi-detection Microplate Reader (Bio-Tek, UK) at 10-min intervals for 4.25 h and at 15-min intervals for 3 h thereafter. The intensity of light emitted by the treated bioreporter cells were expressed as percentages of the untreated negative control. Sixteen readings (two rows of a 96-well microplate) were taken for each sample during each run, and the experiment as a whole was repeated at least three times.

3.2.3 Transcriptional Analysis of recA

3.2.3.1 RNA Extraction

A. baylyi ADP1_*recA_lux* bioreporter cells were grown to mid-exponential growth phase in LB and harvested when culture reached OD_{600} between 0.5 and 0.6. Cells were washed twice with PBS and resuspended in PBS, so that final OD_{600} of the suspension was 0.3. Using sterile 15-ml centrifuge tubes, 1-ml aliquots of the bacterial suspension were diluted 10-fold in solutions of 0.2 mg/L AIT, 2 mg/L CNAD, 2 µM EtBr, 0.001% NaOCl, and sterile DW, respectively. Cells treated with EtBr and NaOCl served as positive reference controls; cells in DW served as the negative control. Samples were incubated at 20 rpm on an orbital rotator at room temperature for 0 h, 5 h, and 7 h. At these designated time points, samples were centrifuged (4100 rpm, 15 min) and supernatant was discarded. For immediate RNA stabilisation and protection, cell pellets were resuspended in 1 ml of 2:1 (vol:vol) solution of RNAprotect® Bacteria Reagent (Qiagen Ltd., West Sussex, UK) : PBS, incubated at room temperature for 5 min, and then centrifuged (4100 rpm, 15 min). The resulting bacteria pellets were enzymatically lysed using lysozyme (Sigma-Aldrich Company Ltd., Dorset, UK) and total RNA was extracted using RNeasy® Mini Kit (Qiagen Ltd., West Sussex, UK). To remove any contaminating genomic DNA from the RNA samples, on-column DNase digestion was performed using DNase I (RNase-Free DNase Set, Qiagen Ltd., UK). To elute the isolated RNA within the spin column, 30 µl of RNase-free water were added and left for 10 minutes before the final centrifugation step. Experiment was repeated three times. Extracted RNA samples were stored at -20˚C.

3.2.3.2 RT-PCR

Based on the coding DNA sequence of *recA* for *A. baylyi* ADP1 (GenBank accession number L26100.1, nucleotide positions 403 to 1452), two 24-mer oligonucleotide primers

were designed and synthesised (Integrated DNA Technologies, London, UK). The forward primer (5'-TTG GTG GCT TAC CTA AAG GGC GTA-3') and reverse primer (5'-ACA GGT ACC ACC TGC TTT CTG ACA-3') were employed to target *recA* mRNA and amplify its cDNA.

Reverse transcription and PCR were performed sequentially in the same tube using OneStep RT-PCR Kit (Qiagen Ltd., West Sussex, UK). For all samples, 1 µl of extracted total RNA (template) was added to a 25 µl reaction mixture consisting of OneStep RT-PCR Enzyme Mix (containing both reverse transcriptase and HotStarTaq® DNA polymerase), 1X reaction buffer (2.5mM Mg^2), 400 µM of each deoxynucleoside triphosphate (dNTP), and 0.6 µM of forward and reverse primers. RT-PCR reactions were carried out using a MJ Mini™ Thermo Cycler (Bio-Rad Laboratories, Inc., UK) as described below:

1.	Reverse transcription	50˚C for 30 min
2.	Initial PCR activation	95˚C for 15 min
3.	Denaturation	94˚C for 30 s
4.	Annealing	55˚C for 30 s
5.	Extension	72˚C for 1 min
	Repeat steps 3-5 ten times	
6.	Final extension	72˚C for 10 min

Using a 50 bp DNA ladder (New England BioLabs Inc., Hitchin, UK) as a reference, RT-PCR products were visualised via 1.8% agarose (Invitrogen, Paisley, UK) gel electrophoresis for amplicon size verification. The gel was stained after electrophoresis with SYBR® Gold Nucleic Acid Gel Stain (Invitrogen, Paisley, UK) diluted 10,000-fold in 1X Tris/Borate/EDTA (TBE) for 15 min at 12 rpm on an orbital rotator, then visualised using a Visi-Blue™ Transilluminator (UVP Ltd., Cambridge, UK). Once amplicons were verified to contain the expected number of base pairs, RT-PCR products were quantified using

NanoDrop® 2000 Micro-Volume UV-Vis Spectrophotometer (Thermo Scientific, Nortumberland, UK).

3.2.4 Statistical Analysis

F-test, *t*-test and ANOVA followed by Tukey's test were applied when appropriate. *P* values of 0.05 were used to determine statistical significance.

3.3 Results

3.3.1 Metabolic Biosensor: Incongruent Results from Bioluminescence Study & Plate Count Experiment

Results from the *E. coli* HB101_pUCD607_*lux* biosensor assay are shown in Figure 3.4. Exposure of luminescent *E. coli* cells to 156.25 mg/L AIT (1MIC), 156.25 mg/L CNAD (2MIC), and 78.125 mg/L CNAD (1MIC) for 30 min resulted in light output that were 2.1%, 8.3%, and 9.4% of control cells, respectively. Parallel plate count experiments demonstrated that when the samples from the bioluminescence study (1MIC AIT-treated, 2MIC CNAD-treated, and 1MIC CNAD-treated cells) were sub-cultured onto fresh agar media, the resulting colony counts were 14.0%, 23.9%, and 80.0% of the control, respectively. Both the bioluminescence study and the plate count experiment reflected that AIT was more toxic than CNAD when used at the same concentration (156.25 mg/L) (Figure 3.4). Also, both methods demonstrated the order of relative toxicity to be 1MIC AIT > 2MIC CNAD > 1MIC CNAD. However, in all three treatments, the results from the bioluminescence study were significantly lower ($P \leq 0.05$) than those from the plate count method performed in parallel. Furthermore, the difference in toxicity observed between 2MIC CNAD and 1MIC CNAD in the bioluminescence study was insignificant ($P \leq 0.05$), whereas in the plate count method, CNAD at 2MIC inhibited approximately four times more cells than CNAD did at 1MIC ($P \leq 0.01$).

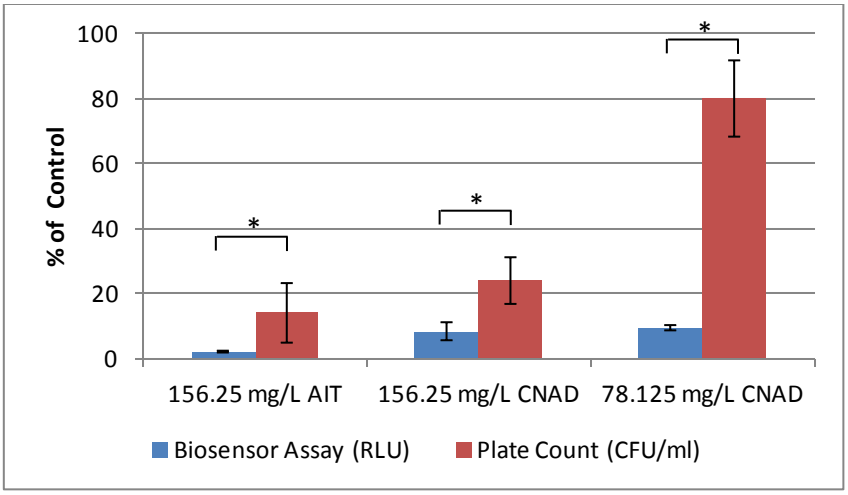


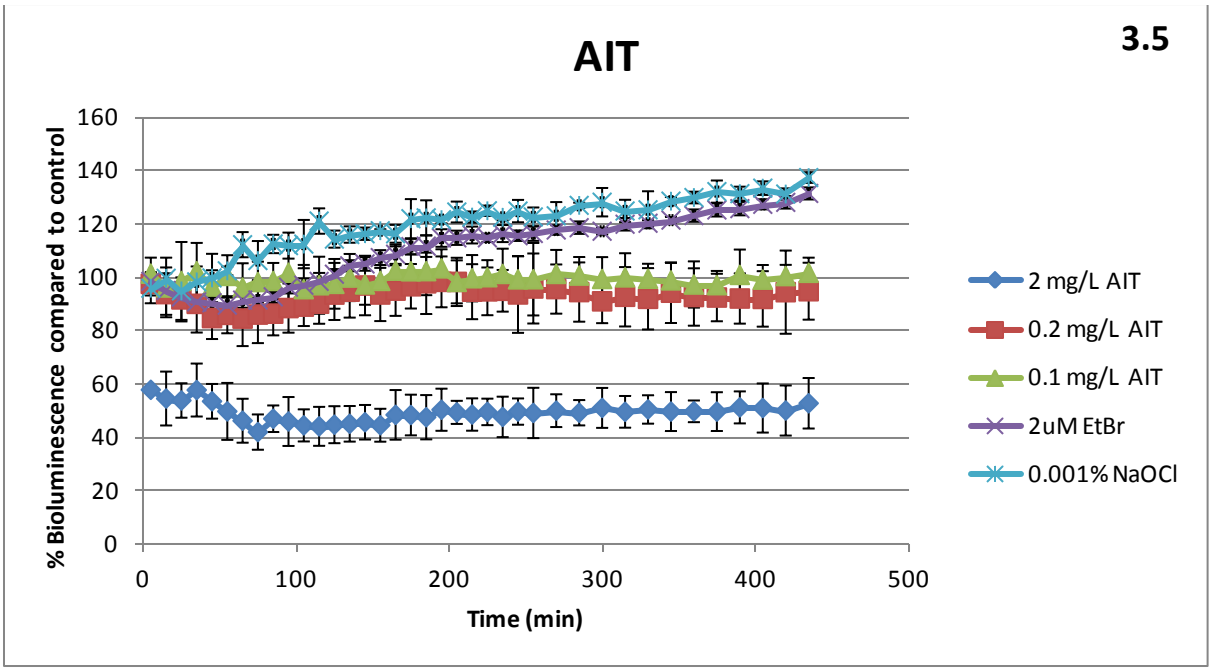
FIGURE 3.4: **Bioluminescence output and plate count results for *E. coli* HB101_pUCD607_*lux*. Values presented are all normalised as percentages of the negative control. Error bars represent ± SD. Asterisks (*) denote significant difference ($P \leq 0.05$). Experiments were performed in biological and technical triplicates at the least.**

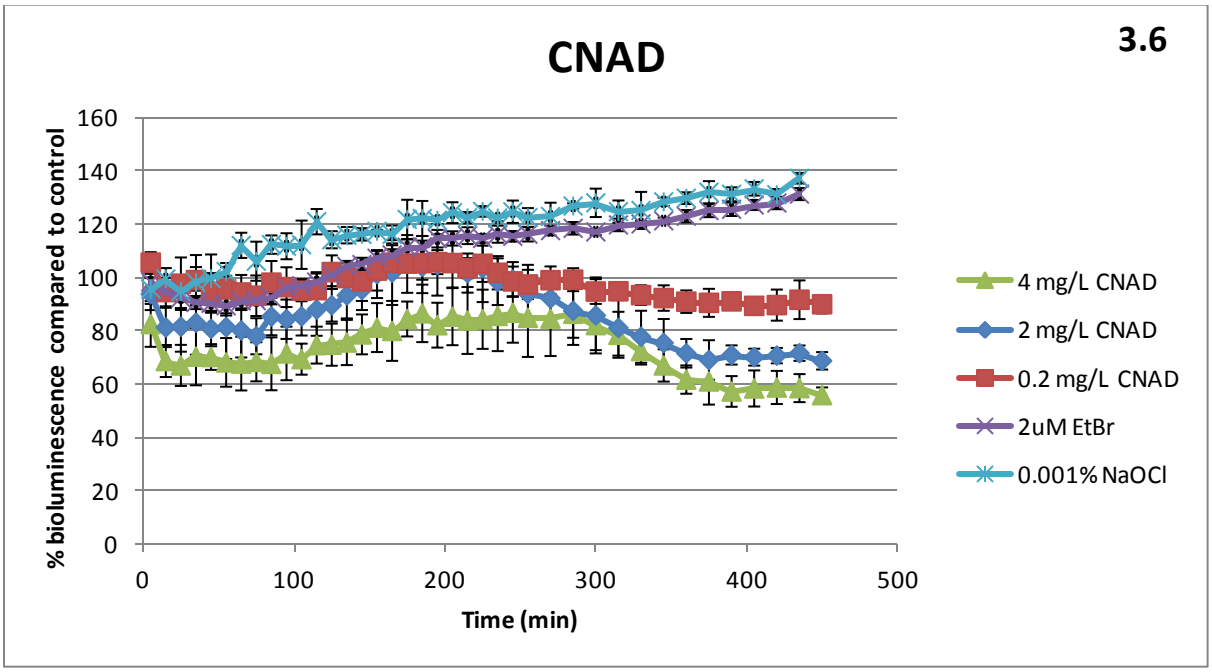
3.3.2 RecA Biosensor: Results from Bioluminescence Study Show No Induction of DNA Repair Response

The results from the *A. baylyi* ADP1_*recA_lux* biosensor assay are shown in Figures 3.5 and 3.6. Light emitted by the treated bioreporter cells was standardised as percentages of the negative control. Since *A. baylyi* ADP1_*recA_lux* cells have a baseline expression of *recA* and therefore produced a constant level of bioluminescence under normal conditions, a decrease in light output below basal level would indicate that the bioreporter cells were inhibited or killed, while an induction of bioluminescence above the baseline indicated that the cells had been exposed to DNA damaging toxicants. The baseline expression of bioluminescence was represented as the amount of light emitted by the untreated negative control samples and thus expressed as 100% in Figures 3.5 and 3.6.

To determine the appropriate concentrations of all compounds to be employed in this bioluminescence study, preliminary titration experiments were performed (data not shown). Concentrations of AIT, CNAD, EtBr, and NaOCl, designated in the legends of Figures 3.5 and 3.6, were chosen because treatment at any higher concentration (for all compounds)

caused light output to fall below 20% of the negative control, indicating that severe cell injury and/or death had occurred to the point where activation of cell repair systems (i.e. SOS response) could not be detected. Therefore, *recA* induction could not be measured at higher concentrations than those indicated in Figures 3.5 and 3.6.





FIGURES 3.5 & 3.6: **Bioluminescence response of *A. Baylyi* ADP1_*recA*_*lux* biosensor to different concentrations of AIT (Figure 3.5) and CNAD (Figure 3.6), expressed as percentages of the negative control. 2µM EtBr and 0.001% NaOCl served as served as positive reference controls. Error bars represent ± SD. Experiment was repeated three times, with eight technical replicates per experiment.**

AIT at 0.1 mg/L and 0.2 mg/L did not cause any detectable genotoxic effects as the treated cells emitted light at levels consistent with the baseline at all time points, never reaching levels significantly greater than 100% of control ($P \leq 0.05$). Similarly, 0.2 mg/L and 2 mg/L CNAD did not cause detectable damage to DNA since treatments at both concentrations did not result in bioluminescence levels that significantly exceeded 100% of control ($P \leq 0.05$) at any time point. AIT at 2 mg/L and CNAD at 4 mg/L significantly reduced light output below 100% of control ($P \leq 0.01$) and failed to induce expression of bioluminescence above the baseline. This suggests that 2 mg/L AIT and 4 mg/L CNAD successfully inhibited or killed the bioreporter cells, but not by damaging genetic material, since the essential DNA repair gene *rec*A was not activated even at sub-inhibitory concentrations of both compounds, as discussed earlier.

Bioreporter cells treated with CNAD at all three concentrations experienced a steady decline in bioluminescence expression starting at 225 min (Figure 3.6), which implies that the cells proceeded to die gradually after exposure to CNAD sustained for at least 225 min. NaOCl at 0.001% caused the bioreporter cells to emit light at levels that gradually exceeded 100% of the negative control, starting at 65 min ($P \leq 0.05$) (Figures 3.5 and 3.6). EtBr at 2 µM, serving as positive control, also caused a steady increase in bioluminescence expression that climbed beyond the baseline starting at 125 min. This suggests that 0.001% NaOCl and 2 µM EtBr are both damaging to DNA, since *rec*A was activated upon both treatments.

3.3.3 Transcriptional Analysis of recA

DNA gel electrophoresis of RT-PCR products resulting from amplification of *recA* mRNA isolated from *A. baylyi* ADP1_*recA_lux* after designated treatment for 7 h is presented in Figure 3.7. This visualization, via 470 nm blue light transillumination, achieved three objectives: (i) confirmed that the amplicons were of the expected size (113 bp) and

therefore products were indeed amplified from *recA* mRNA; (ii) demonstrated that no induction of *recA* occurred upon treatment with 0.2 mg/L AIT and 2 mg/L CNAD since there was no visually significant difference among band intensities of the control, AIT, and CNAD samples (Figure 3.7); and (iii) showed that treatment with 2 µM EtBr and 0.001% NaOCl triggered upregulation of *recA* since band intensities of EtBr and NaOCl samples were relatively darker than those of the control (Figure 3.7). Intensity of band fluorescence upon staining with a DNA-intercalating agent (i.e. SYBR® Gold) was directly proportional to the quantity of nucleic acid present; therefore, the darker bands of the EtBr and NaOCl samples indicated that greater concentrations of RT-PCR products were present in those lanes than in the lanes of the other samples and the control.

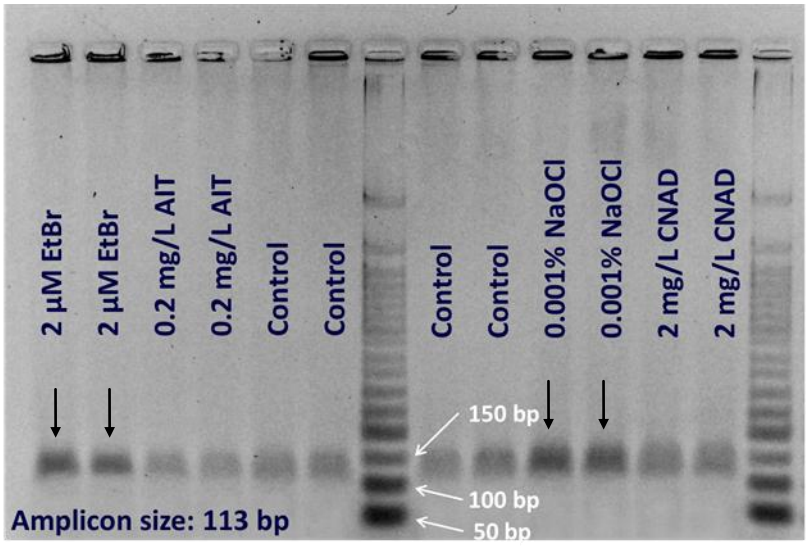


FIGURE 3.7: **Gel electrophoresis of RT-PCR products (113 bp) from amplification of *recA* mRNA from *A. baylyi* ADP1_recA_lux after various treatments for 7 h. Black arrows highlight relatively darker bands of EtBr- and NaOCl-treated samples, indicating induction of *recA* above basal level following treatment with 2 µM EtBr and 0.001% NaOCl.**

Spectrophotometric (NanoDrop®) quantification of the RT-PCR products is shown in Figure 3.8. The results were consistent with the semi-quantitative findings of the DNA gel electrophoresis run: (i) treatment with 0.2 mg/L AIT and 2 mg/L CNAD did not induce *recA* expression above basal level since the concentrations of RT-PCR products for both samples

were not significantly different than those of the control; (ii) exposure to 2 µM EtBr and 0.001% NaOCl caused an increase in *recA* transcription, specifically at 5 h and even more so at 7 h, revealed by the significantly greater amplicon concentrations ($P \leq 0.05$) for both EtBr and NaOCl reference controls as compared to those of the negative control (Figure 3.8). The findings of the transcriptional studies of *recA* validated the results from the *A. baylyi* ADP1_*recA*_*lux* luminescence biosensor study (Figures 3.5 and 3.6).

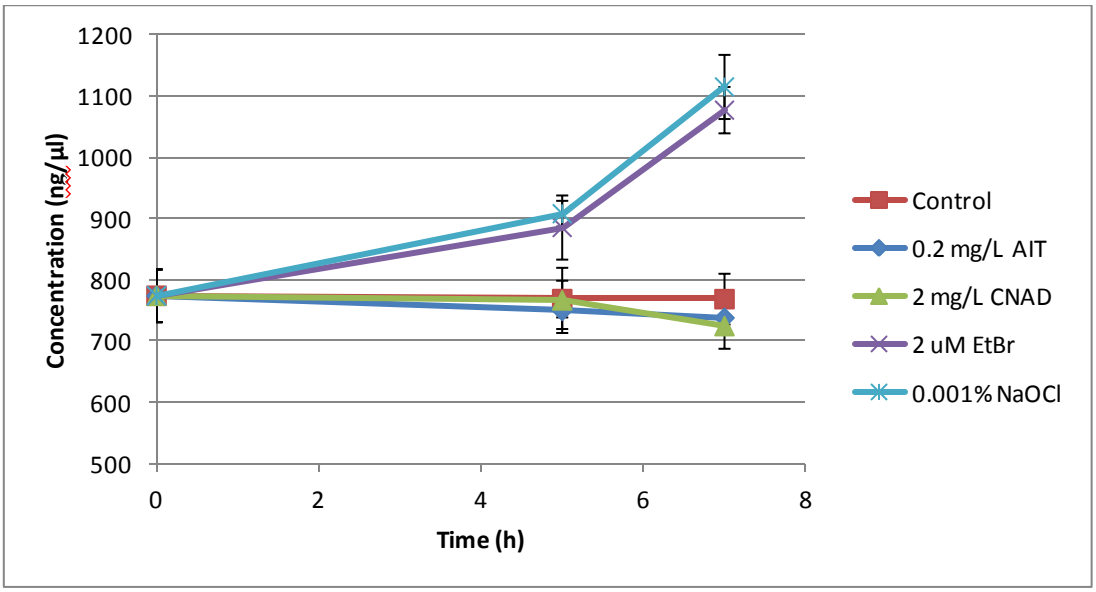


FIGURE 3.8: **NanoDrop® quantification of RT-PCR products from amplification of *recA* mRNA from *A. baylyi* ADP1_recA_lux after exposure to various compounds for 0 h, 5 h, and 7h. Values presented are means ± SD. RT-PCR was performed three times for all samples; four NanoDrop® readings were performed per sample for all RT-PCR runs.**

3.4 Discussion

3.4.1 Metabolic Biosensor: Reduction of Intracellular ATP and $NADPH_2$ Not Solely Due to Loss of Barrier Function of the Cell Membrane

Results from the *E. coli* HB101_pUCD607_*lux* biosensor assay revealed dose-response relationships of AIT and CNAD against *E. coli,* and also provided some information regarding the mechanism of kill and cytotoxic effects of the compounds. Findings from both the bioluminescence study and the plate count experiment corroborate the results from the disc diffusion assay (Chapter 2), which confirmed that AIT was more toxic to bacteria than CNAD when both were applied at the same concentration. These results from three separate assays increased the confidence level of identifying AIT as the most potent antimicrobial compound in this study.

In this metabolic biosensor, light emitted from bacterial cells was directly linked to energy products of cellular respiration, and therefore the significant decrease ($P \leq 0.01$) in bioluminescence of both CNAD-treated and AIT-treated cells compared to the control suggest that the availability of intracellular ATP and/or $NADPH_2$ in treated samples were < 10% that of healthy control samples. If these two coenzymes were depleted due to the rupturing of the cell membrane alone, then the corresponding number of culturable colonies should have also been < 10% of the control since membrane damage to that degree (causing the exit of > 90% intracellular ATP and/or $NADPH_2$) is likely to be irreversible. However, in fact, the resulting colony counts from parallel plate count experiments (expressed as percentages of the control) were greater than the light output (also normalized as percentages of the control) for each respective sample. This suggests that the significant decrease in bioluminescence of treated samples were due to impairment of metabolic activity reflected in the decline of ATP and $NADPH_2$ production, and not solely due to the loss of barrier

function of the cell membrane leading to the exit of ATP and $NADPH_2$. It is important to note that the antimicrobial activity of EOs and terpenoids is not simply due to the physicochemical effect of an oily substance on cell membranes, as proven by the inability of olive oil, paraffin oil, and canola oil to kill bacteria and fungi.

When the treated samples were sub-cultured onto fresh growth agar media in which the inhibitory pressures of AIT and CNAD were removed, a fraction of the cells were able to recover from their metabolically stunted state (Figure 3.4), return to producing higher levels of ATP and $NADPH_2$, and form healthy colonies.

3.4.2 RecA Biosensor: AIT & CNAD Unlikely to be Genotoxic

A. baylyi ADP1 is typical of water and soil bacteria occurring in the natural environment, and so *A. baylyi* ADP1_*recA_lux* bioreporter cells are ideal for assessing bacterial response to AIT- and CNAD- treatment in the environmental context (Tiensing *et al.*, 2001). By exploiting bacteria's inherent SOS response to DNA damage, the *A. baylyi* ADP1_*recA_lux* biosensor assay showed that bacterial exposure to AIT and CNAD did not activate *rec*A, indicating that neither compound compromised the integrity of bacterial genomes. Because *rec*A homologs exist in all species, it can be deduced that these natural compounds are unlikely to be genotoxic or mutagenic to multicellular organisms as well. In contrast, EtBr, a known mutagen that deforms DNA and thus chosen as positive reference control for this study, and NaOCl, a conventional biocide frequently used in water disinfection, both induced the transcription of *rec*A, indicating that both chemicals were DNA damaging toxicants. NaOCl has been shown to exhibit genotoxicity in microbes (Buschini, Carboni, Furlini, Poli, & Rossi, 2004), and based on the results of this current study, NaOCl may also have similar genetically deleterious effects on human cells since the same *rec*A-related response to DNA damage is present in mammalian cells as well. As an

antimicrobial agent, it is advantageous that the compound be lethal against target microbes but safe for higher organisms, so that damage and toxicity towards multicellular life forms are minimised.

A gradual increase of bioluminescence was observed between 15 min and 185 min in *A. baylyi* ADP1_*recA_lux* cells treated with CNAD at all three concentrations tested (Figure 3.6), but the intensity of light emitted never surpassed the baseline expression of bioluminescence. This suggests that cellular activity was initially inhibited upon exposure to CNAD, but the bioreporter cells were able to recover to some degree, as indicated by the steady increase of bioluminescence toward the baseline. Although having increased over time, the light output never significantly exceeded 100% of the control ($P \leq 0.05$); therefore, it can be inferred that CNAD did not activate *rec*A at any point, meaning DNA damage did not occur as a result of CNAD treatment. A steady decline in bioluminescence followed thereafter without any spikes in light output above the baseline, which again is indicative of gradual cell inhibition or death via mechanisms independent of DNA disruption.

3.4.2.1 Transcriptional Studies of *recA*

The same RNA extraction protocol was followed for all samples and controls at all time points, so RNA yield should have only depended on gene transcription levels that resulted from exposure to the various compounds of this study. RT-PCR was carried out using the same volume (1 µl) of extracted RNA for all samples. Therefore, the amount of RT-PCR product was directly proportional to the amount of *recA* mRNA present in the initial 1 µl of template, which is why this method is appropriate for the quantification of *recA* transcript levels upon various treatments.

Temporal *recA* expression profiles obtained from NanoDrop® quantification of RT-PCR products (Figure 3.8) were similar to the bioluminescence profiles from the *A. baylyi*

ADP1_*recA*_*lux* biosensor study (Figures 3.5 and 3.6). This validates the genotoxicity-sensing mechanism of the *A. baylyi* ADP1_*recA*_*lux* biosensor, where the intensity of light produced by the bioreporter cells was directly proportional to their level of *recA* expression, which itself was directly related to the degree of DNA damage. Since there was no rise in *recA* transcript abundance at any point during treatment with 0.2 mg/L AIT and 2 mg/L CNAD, these two compounds did not cause DNA damage. On the contrary, 2 µM EtBr and 0.001% NaOCl caused increased *recA* expression, which indicates that both were genotoxic compounds.

3.4.2.2 DNA Damage is Linked to Resistance Development

Development of resistance in bacteria often occurs through spontaneous or induced mutation(s) after exposure to the toxicant. It is relatively easier for a compound to confer resistance if its mechanism of inhibition is DNA disruption because cells may overcome the damage by inducing the standard SOS response to DNA damage, which involves error-prone DNA repair and mutagenesis. Because the inhibitory mechanism of AIT and CNAD seem to be related to structural and metabolic injury rather than to DNA damage, the likelihood of resistance development against these two natural compounds is likely to be lower than that of genotoxic toxicants that target DNA. Based on current findings of this *rec*A-dependent biosensor assay, AIT and CNAD may be good alternatives to widely-used, but genotoxic, antimicrobial agents such as NaOCl.

3.4.3 Conclusion

In summary, the *E. coli* HB101_pUCD607_*lux* metabolic biosensor assay demonstrated that the mechanism of action of AIT and CNAD did not simply involve membrane partitioning and damage by an oily substance, but also included other process(es) that injured and compromised cellular metabolism and energy production. A second complementary biosensor assay, which employed the genotoxicity-sensing strain *A. baylyi* ADP1_*recA*_*lux*, revealed that AIT and CNAD did not activate the essential DNA repair gene *recA*, which is evidence that it is unlikely that these two natural compounds caused damage to bacterial and higher genomes, and resistance development via mutagenesis is reduced.

Chapter Four

4. SYNTHESIS AND CHARACTERISATION OF MESOPOROUS SILICA NANOPARTICLES

4.1 Introduction

4.1.1 Non-porous Silica Nanospheres

Silica nanoparticles are inorganic, nanoscale (≤ 100 nm diam) materials that have received much attention in recent years due to their inert, biocompatible, biodegradable, thermally and chemically stable properties (Barbé *et al.*, 2004; Y.-S. Lin & Haynes, 2009; Lu, Liong, Li, Zink, & Tamanoi, 2010; Trewyn, Nieweg, Zhao, & Lin, 2008). As mentioned before, MSNs (non-porous and porous) have received growing scientific interest as carriers for many applications, including pharmaceutical drug delivery, gene therapy, enzyme immobilisation, catalytic chemistry, ion exchange, biosensing, and bioimaging (Davis, 2002; Heikkila *et al.*, 2007; Horn *et al.*, 2010; Ispas *et al.*, 2009; Knopp *et al.*, 2009; Ozin & Arsenault, 2005; F. Wang, Guo, Yang, & Liu, 2010).

Since Stöber *et al.* first introduced a robust process for fabricating monodispersed amorphous, non-porous silica nanoparticles (Stöber, Fink, & Johnston, 1968), a number of synthesis methods of non-porous silica nanospheres have been published (Rao, El-Hami, Kodaki, Matsuhige, & Makino, 2005), most of which employ a sol-gel system based on the Stöber process.

4.1.2 Mesoporous Silica Nanoparticles (MSNs)

Specific to this study, silica nanoparticles consisting of mesopores are promising candidates for the stabilisation and delivery of plant-derived compounds in order to improve their antimicrobial effect. Pore size, pore arrangement, and particle size of MSNs can be customised to suit their application (Nandiyanto *et al.*, 2009).

There are various synthesis methods that result in different morphologies, dimensions, and porosities of MSNs, e.g. "blackberry-like" (Nandiyanto *et al.*, 2009) or "chrysanthemum-like" (H. Zhang *et al.*, 2010) particles. In the present work, MSNs having pores with hexagonal symmetry (Hom *et al.*, 2010; Trewyn, Slowing, Giri, Chen, & Lin, 2007) are of particular interest as carriers for the plant compounds due to their uniform and regular physical properties as well as reproducibility of the synthesis method.

According to the sol-gel process of synthesis (Figure 4.1), the amphiphilic molecule cetyltrimethylammonium bromide (CTAB) acts as the surfactant and forms the template of mesopores. With vigorous agitation at a high temperature, the silica precursor tetraethylorthosilicate (TEOS) is then hydrolysed and condensed around the pore template to form silica nanospheres. In order to reduce aggregation and increase stability of the MSNs, the silica surface can be modified with phosphonate groups after particle formation (Hom *et al.*, 2010).

The organic template is removed after synthesis by refluxing in acidic methanol, leaving the inorganic silica framework as nanoparticles with hexagonally ordered pores. Thereafter, nanoscale cargo (from 1 Å to 20 Å) such as drugs, fluorescent dyes, quantum dots, or other compounds of low molecular weight can be loaded into the mesopores of the MSNs (Liong *et al.*, 2008).

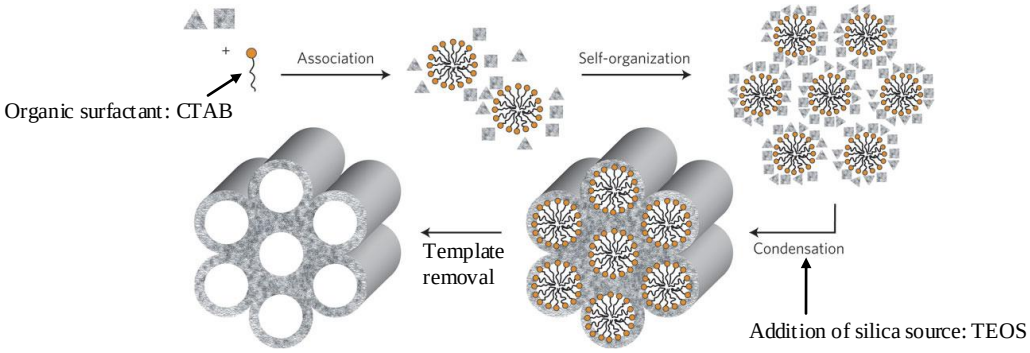


FIGURE 4.1: **Sol-gel synthesis of MSNs. CTAB molecules form spherical micelles, and CTAB micelles assemble into hexagonal bundles, which create the template for internal pore structure. Hexagonally-ordered porous nanospheres are produced by selectively removing the organic CTAB template by reflux. The remaining inorganic silica framework becomes the MSN.**

(Schematic from Tolbert, SH. *Mesoporous Silica: Holey Quasicrystals.* Nature, 2012. **11**: 749-751.)

4.1.3 Particle Characterisation

It is important to characterise particles synthesised in-house to ensure product quality, uniformity, and regularity between different batches. The behavior and activity of particulate materials are largely influenced by the physical properties of constituent particles, therefore it is important to measure properties such as size, shape, and surface area.

4.1.3.1 Transmission Electron Microscopy (TEM)

Transmission electron microscopy (TEM) is a method of visually imaging samples that are in micro- and nanoscale. This technique is similar to optical microscopy, except instead of light, an electron beam is used to image the sample (Williams & Carter, 1996). In TEM, images are formed when the transmitted electron beam interacts with an ultra-thin specimen on a mesh grid and subsequently detected in magnified form by a charge-coupled device (CCD) camera (Fultz & Howe, 2007). The maximum resolution d is represented by the following equation, where λ is the wavelength of the directed beam and NA is the numerical aperture of the optical system: $d = \frac{\lambda}{2n\sin\alpha} \approx \frac{\lambda}{2\,\mathrm{NA}}$.

Because the wavelength of electrons is extremely short in high voltage (typically 200 kV for TEM), the maximum resolution can be as low as 1 Å (Fultz & Howe, 2007).

4.1.3.2 Disc Centrifuge Photosedimentometry

Disc centrifuge photosedimentometry measures particle size distributions based on the principle of differential centrifugal sedimentation in a liquid medium (CPS Instruments Inc.; Hewitt, Mulcahy, Ralston, & Wilkinson, 1991). It is an effect approach for measuring materials from 10 nm to 50 µm. According to Stoke's law, particles settle in viscous fluid under a gravitational field depending on their size (Batchelor, 1967). In this technique, particles settle within an optically clear, rotating disc. When particles approach the outside edge of the rotating disc, they block/scatter a portion of a light beam that passes through the disc. The change in light intensity is continuously recorded and converted into particle size distribution of the sample (CPS Instruments Inc.).

A density gradient of the viscous liquid is usually used to allow for reproducible and accurate results, and this gradient is usually 2% to 8%, 4% to 12%, or 8% to 24% w/v sucrose or dextran solution (CPS Instruments Inc., 2005). It is important that the highest density layer in any gradient is lower in density than the particles in the sample; otherwise, particles may never arrive at the detector.

4.1.3.3 NanoSight™

NanoSight™ is an instrument used to analyse nanoparticle size between 1 nm to 1 µm. This technique uses a laser diode to illuminate particles in liquid suspension to track individual particle's motion by video (NanoSight, 2009). Subsequently, Nanoparticle Tracking Analysis (NTA) software analyses the video and measures the Brownian motion of particles whose speed of motion, with diffusion coefficient *D*, is related to particle size through the

Stokes-Einstein equation: $D = \frac{kT}{6\pi\eta R}$, where k is the Boltzmann constant, T is the temperature, η is the viscosity of the liquid, and R is the hydrodynamic radius of the particle (Carr *et al.*, 2008; Carr & Wright, 2013; NanoSight, 2009).

4.1.3.4 Nitrogen sorption

The Gemini™ VI Surface Area Analyzer (Micromeritics Instrument Corporation, US) is an instrument that measures surface area and porosity of nanoparticles based on physical adsorption and desorption of nitrogen gas (N_2) molecules on particle and pore surfaces (Micromeritics, 2013a, 2013b). The analyser monitors the saturation volume of gas adsorbed on the surface of the sample under a series of stable pressures on a continuous basis. A sorption isotherm, which is a description of the amount of adsorbate (N_2 gas) on the adsorbent (nanoparticles) as a function of pressure under constant temperature (Brunauer, Emmett, & Teller, 1938; Leddy, 2012), is subsequently generated. The analyser produces surface area results using the Brunauer, Emmet, and Teller (BET) theory, which is a multilayer molecular adsorption concept that is an extension of the Langmuir monolayer adsorption theory, contingent with the hypotheses that 1) gas molecules physically adsorb on a solid in layers infinitely, 2) there is no interaction between each layer adsorbed, and 3) the Langmuir theory can be applied to each layer (Brunauer *et al.*, 1938; Leddy, 2012; Sing, 2001).

The analyser determines porosity via the Barrett, Joyner, and Halenda (BJH) method (Micromeritics, 2013a) . This theory follows the hypothesis that gas molecules first condense in the pores with the smallest dimensions as pressure increases until all pores are filled to saturation (Barrett, Joyner, & Halenda, 1951; Leddy, 2012). The adsorptive gas pressure then is reduced incrementally, evaporating the condensed gas from the system. Evaluation of the

adsorption and desorption branches of these isotherms and the hysteresis between them yields information regarding size, volume, and area (Barrett *et al.*, 1951).

4.1.4 Loading and Release of Guest Compounds

Once MSNs are synthesised and properly characterised, the next step is to load guest molecules within the pores and determine the release profile of such molecules.

4.1.4.1 Proof of Concept: Calcein

Calcein ($C_{30}H_{26}N_2O_{13}$, molecular weight of 622.55 g/mol) is a fluorescent dye with excitation/emission maxima of 495/515 nm, respectively (Patel, Tscheka, & Heerklotz, 2009). Calcein was selected as a model compound to be loaded into synthesised MSNs because its release from the MSNs can easily be monitored by fluorescence readings over time. Calcein was chosen especially for its self-quenching property even at concentrations below 100mM (Patel *et al.*, 2009), which is important because the dye will only fluoresce when released out from the nanoparticles and not when it is residing inside the mesopores. This ensures an accurate release profile of the dye, in which the fluorescence measurements correlate only to the amount of calcein released.

4.1.4.2 Diffusion

Diffusion is a transport mechanism in which flux naturally goes from regions of higher concentration to areas of lower concentration until diffusive equilibrium is reached, where concentrations of the diffusing substance in the two compartments become equal. As proof of concept to show that compounds can be loaded within MSNs and result in sustained release over time, calcein was loaded into the mesopores via diffusion (procedure for loading guest molecules in MSNs are described in the Materials and Methods portion of this chapter (Section 4.2)). Its subsequent release in solution, also via diffusion, was continuously

monitored kinetically in a fluorescence microplate reader (details are further described in the Materials and Methods section (Section 4.2)). The procedure established for calcein became the basis for loading and unloading of AIT and CNAD in MSNs.

4.1.4.2 Gas Chromatography (GC)

Gas chromatography (GC) is a technique in analytical chemistry used presently to identify and quantify the amount of AIT and CNAD released from the MSNs over time, since monitoring change in fluorescence (in the case of calcein) is not a feasible method of tracking their release (both compounds do not auto-fluoresce strongly enough). The basis of chromatography is the principle that an analyte (or analytes in a mixture) dissolved in a mobile phase travels at a particular speed through a stationary phase, resulting in retention time on the stationary phase that is characteristic of that particular analyte (Harris, 1999; Higson, 2004). This technique can be used to identify and separate unknown constituents of a mixture and, more relevant to the present application, to identify and quantify a known compound in solution.

In GC, the mobile phase is an inert or unreactive carrier gas while the stationary phase is a liquid or polymer on a solid support inside a tube-like glass or metal column. During analysis, the analyte(s) is vaporised without decomposing and is carried through the column in the gaseous mobile phase (Harris, 1999; Higson, 2004). The compound(s) to be analysed then interacts with the stationary phase inside the column, and their rate of progress through the column is determined by the strength of adsorption between the compound(s) and the stationary phase, causing the analyte(s) to elute at a specific time (Harris, 1999; Higson, 2004). The distinct retention time of a compound enables the identification of a particular analyte.

A method is a set of conditions in which the chromatograph (instrument that performs GC) operates for a given analysis (Harris, 1999). Depending on the analyte(s), the solvent, the

type of detector, the type of column, and the type of instrument used, a specific method must be developed for a given analysis to acquire accurate data and results. Conditions that can be varied to accommodate a required analysis include: inlet temperature, detector temperature, column temperature, temperature program, carrier gas and carrier gas flow rates, inlet type and flow rates, sample size, and injection technique (Harris, 1999; Higson, 2004).

Data is generally presented in a chromatogram after each run of an established GC method. A chromatogram is a graph of detector response (*y*-axis) versus retention time (*x*-axis), which displays peaks for a sample that represent analytes present eluting from the column at particular times (Higson, 2004). The area under a peak (or area under the curve, AUC) is proportional to the amount of analyte present. By calculating the AUC using the mathematical function of integration, the concentration of an analyte in the original sample can be determined (Higson, 2004). Concentration can be calculated using a calibration curve, established experimentally by determining the detector response for a series of known concentrations of the analyte.

Different types of detectors are available for use in GC to detect and measure concentrations of compounds in a gas stream at the end of the column. In this study, a flame ionisation detector (FID), one of two most commonly used (the other being a thermal conductivity detector (TCD)), was employed for the quantification of AIT and CNAD. TCDs are essentially universal, but FIDs are more suitable for the analysis of hydrocarbons (Halasz & Schneider, 1961; Harris, 1999). Since both plant compounds are organic, a FID was selected because of its sensitivity to organic species. FIDs can measure organic/hydrocarbon substance concentrations at very low and very high levels, having a linear response of 10^6. In FID, electrodes are placed adjacent to a flame fuelled by nitrogen or air near the exit of the column. When carbon-containing compounds elute from the column, they are pyrolysed by the flame, causing the carbons to form cations and electrons (Harris, 1999; Higson, 2004). This

generates a current between the electrodes, and this spike in current is translated into a peak in the chromatogram (Halasz & Schneider, 1961).

4.1.5 Aims and Objectives

The objectives of this portion of the study were to: (i) synthesise hexagonal MSNs and characterise their size, size distribution, morphology, porosity, and surface area; and (ii) to load the mesopores with calcein, AIT, and CNAD and determine the release profiles of these guest compounds from bespoke MSNs. This is the first reported study to use silica nanoparticles of any morphology as a delivery system for these plant secondary metabolites.

4.2 Materials and Methods

4.2.1 Synthesis of MSNs with Hexagonally-Ordered Mesopores

MSNs were synthesised via hot hydrolysis in an aqueous, base-catalysed sol-gel system as described in Hom *et al.*, 2010 (Hom *et al.*, 2010), with some modifications. In a typical synthesis, 200 mg CTAB (surfactant) (99%; Sigma Aldrich, UK) was dissolved in a 96 ml DW and 700 µl 2M NaOH in a 250-ml round-bottom flask at 80˚C (pH 12.4) with stirring at 500 rpm. Once the temperature stabilised, 1 ml TEOS (silica precursor) (Sigma Aldrich, UK) was added into the system. After stirring for 15 min, 254 µl 3-(trihydroxysilyl)propylmethylphosphonate (THPMP) was added to the suspension in order to modify the silica surface with phosphonate groups to reduce aggregation. After stirring for another 2 h at 80˚C, the suspension was centrifuged at 9000 rpm for 5 min. The resulting nanoparticles that were collected were washed twice with methanol (Sigma Aldrich, UK). The surfactant CTAB was subsequently removed by refluxing in 40 ml methanol plus 2 ml 37% hydrochloric acid (HCl) (Sigma Aldrich, UK) overnight at 80˚C using a water-cooled coil condenser.

4.2.2 MSN Characterisation

4.2.2.1 TEM Analysis

Synthesised MSNs were imaged via TEM with JEOL JEM 2010 operating at 200 kV for bright field imaging, with small angle tilts (-20˚ to +20˚) to inspect pore orientation. Specimens were prepared by drop-casting MSNs onto holey carbon-coated TEM copper grids (carbon film on 3mm 300 mesh, Agar Scientific, UK), allowing them to air dry overnight before imaging.

Particle and pore sizes were measured using DigitalMicrograph™ software. An MSN was measured in two directions perpendicular to each other by analysing the region of

interest on a histogram of the TEM image in line plot display (Figures 4.2 a and b). The size of each individual nanoparticle was the mean value of the two measurements, and the mean size of all collective MSNs was the average of all particle sizes measured. Furthermore, pore/channel diameters were also measured similarly (Figures 4.3, 4.4, and 4.5). Standard deviation was given for reference of uniformity.

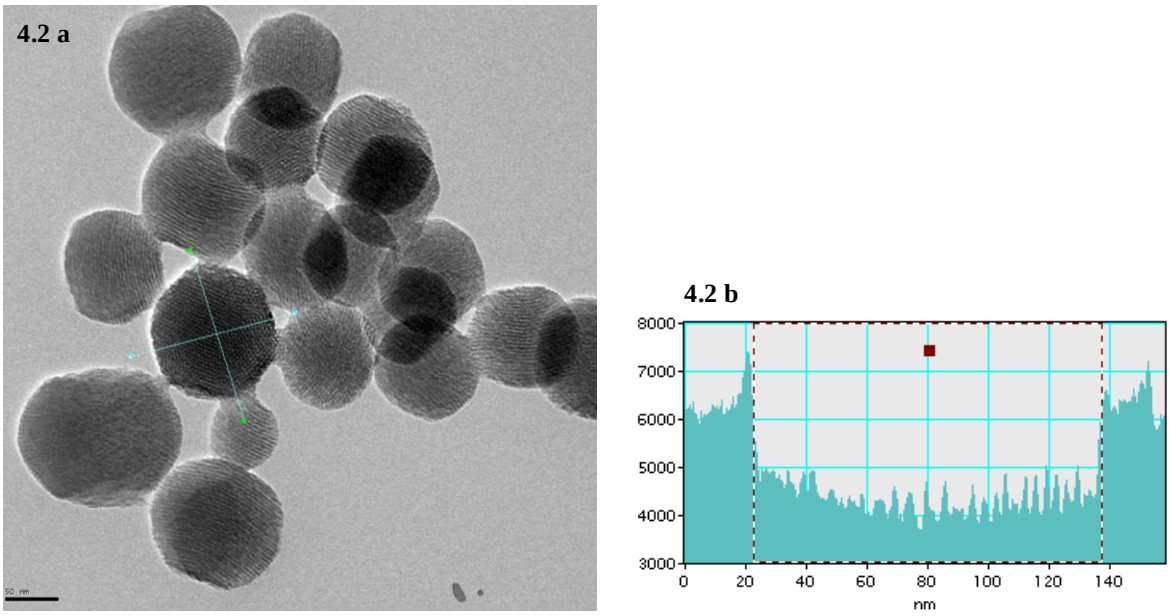


FIGURE 4.2 A & B: **Typical TEM image of MSNs. Nanoparticles were measured in two perpendicular directions, as indicated by the blue lines (4.2 a). Measurements were made using the histogram generated by building a contrast profile along the blue lines (4.2 b). Scale bar represents 50 nm.**

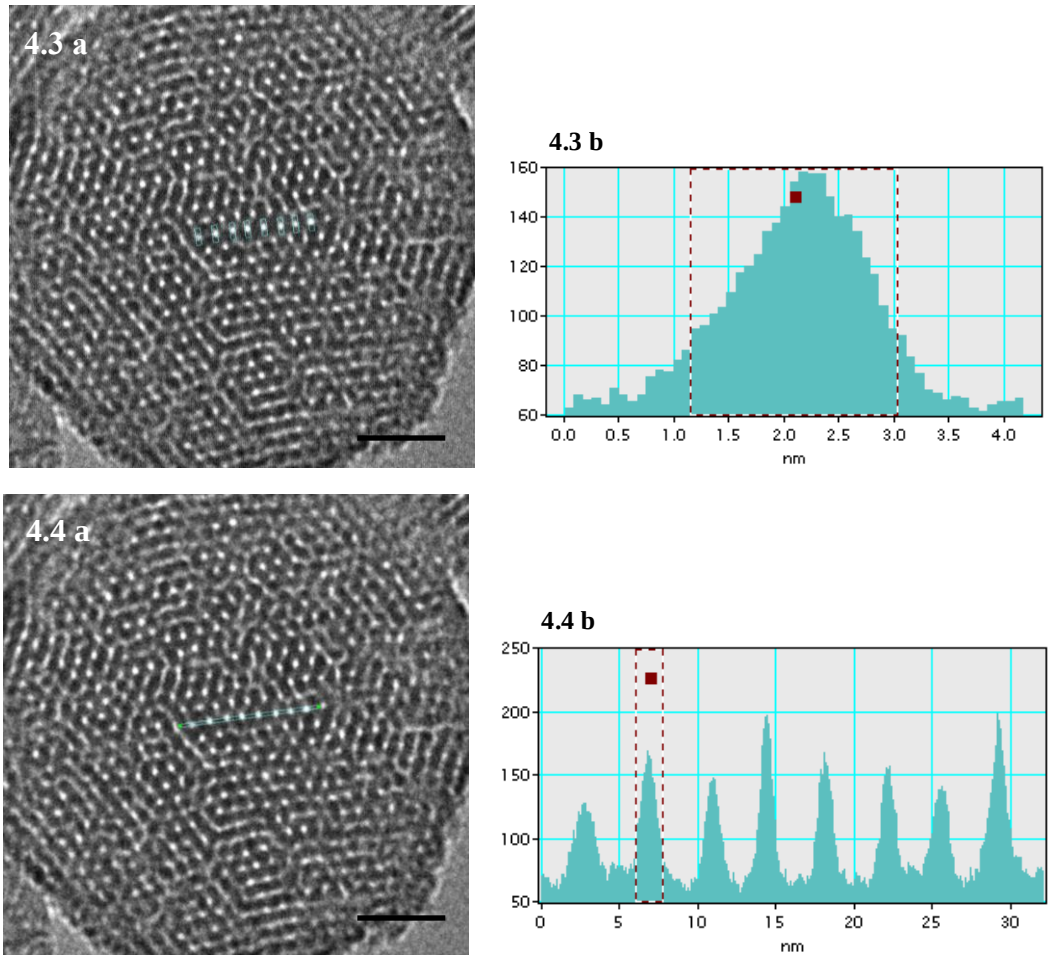


FIGURE 4.3 A & B, 4.4 A & B: **Typical TEM images of a MSN. Pores were measured in two directions, as indicated by blue rectangular selected regions (4.3 a & 4.4 a). Measurements were made using histograms generated by building a contrast profile along the blue lines (4.3 b & 4.4 b). Scale bars represent 20 nm.**

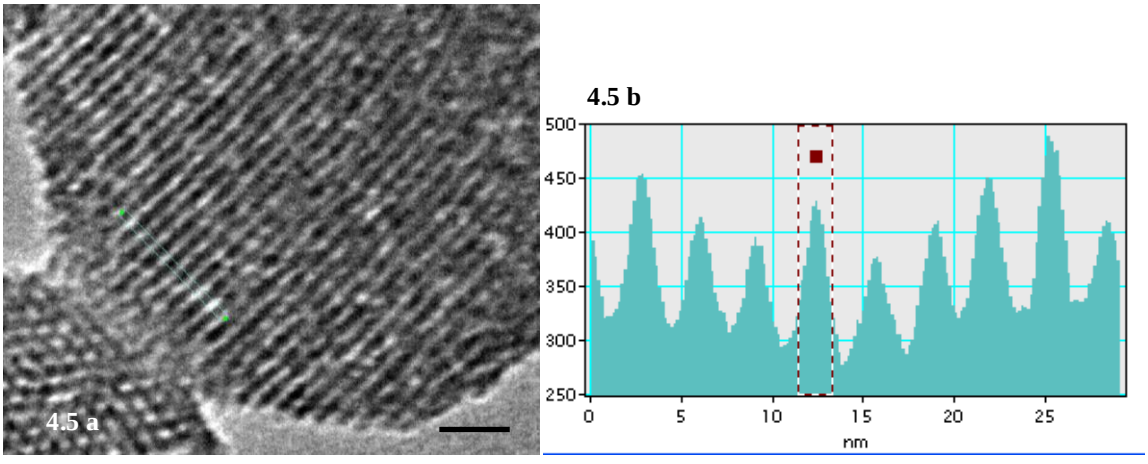


FIGURE 4.5 A & B: **Typical TEM images of a MSN. Cross-sections of pore channels were measured, as indicated by blue rectangular selected regions (4.5 a). Measurements were made using histograms generated by building a contrast profile along the blue lines in line plot display (4.5 b). Scale bar represents 10 nm.**

4.2.2.2 CPS Disc Centrifuge™

The CPS Disc Centrifuge™ operated with fluids that formed a density gradient inside the disc. Aqueous solutions ranging from 4% to 12% sucrose were prepared with DW, and the density gradient was created by injecting 2 ml of each solution into the disc in order of decreasing concentration. This allowed the sedimentation of the MSNs to remain stable.

With the disc centrifuge set to 24,000 rpm, the instrument was calibrated against known particle size standards before analysing MSN samples. Dilute suspensions of MSNs (200 µl aliquots) were injected into the instrument with a syringe, and three separate samples were measured.

4.2.2.3 NanoSight™

NanoSight™ LM10 instrument (2009) was used to visualise 0.3 ml sample of MSNs suspended in PBS. The associated Nanoparticle Tracking Analysis (NTA) software tracked the light scattered by the MSNs from frame to frame. NTA and related particle movement to particle size of each individual MSN from direct observations of diffusion under Brownian motion via video.

4.2.2.4 Gemini™ VI Surface Area Analyser

Gemini™ VI Surface Area Analyser utilised an adaptive rate, static volumetric technique that adjusted the rate at which N_2 gas is delivered to the MSNs to the rate at which it was adsorbed. Each pressure point was allowed to equilibrate before the next point is taken. The instrument has two gas reservoirs which are filled with equal volumes of N_2. From the reservoirs, gas was metered into the sample and balance tubes via a servo valve that reacts to the rate of adsorption.

4.2.4 Calcein Studies

4.2.4.1 Calibration Curve

A calibration curve of calcein was established by measuring fluorescence signal of six standard samples of known concentrations prepared in PBS (Table 4.1). Triplicate samples were prepared for each concentration and readings were done in a 96-well flat-bottom black microplate (Nunc, UK), with 200 µl of sample dispensed in each well.

TABLE 4.1: **Calibration curve for the fluorescence of calcein**

CALCEIN CONCENTRATION (mg/ml)	FLUORESCENCE
1.11×10^{-05}	3
2.22×10^{-05}	15
1.11×10^{-04}	239
5.56×10^{-04}	1465
2.78×10^{-03}	7138
5.56×10^{-03}	12852

Fluorescence was measured using a Synergy HT Multi-detection Microplate Reader (Bio-Tek, UK) at excitation and emission wavelengths of 485/20 nm and 528/20 nm, respectively. The data is fit to a straight line using linear regression analysis, yielding a model described by the equation $y = 2E6x + 85.522$ with an R^2 value of 0.9971 (Figure 4.6).

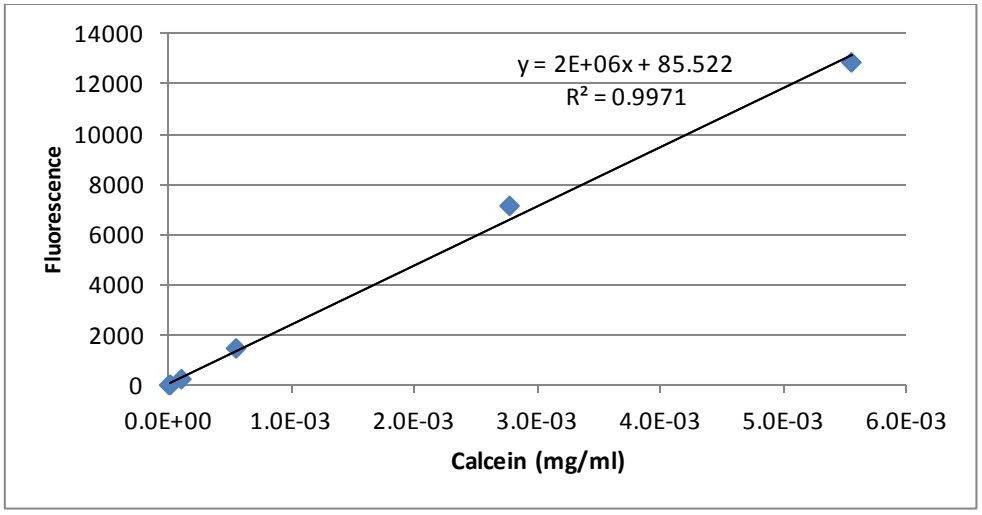


FIGURE 4.6: **Calibration curve for the fluorescence of calcein. Each point represents the mean of three samples, with each sample measured three times. The line is a least-squares fit of the relationship between concentration of calcein (*x*) and fluorescence value (*y*).**

4.2.4.2 Loading and Release of Calcein from MSNs

Calcein salt (18 mg) was first dissolved in 2 ml DMSO, and then loaded into 20 mg MSNs in 7 ml PBS via diffusion in a 15 ml glass vial (Fisher Scientific, UK). Contents were sonicated with a probe for 3 min at 5 sec intervals, then left to stir at 250 rpm for 24 h in the dark. After loading, MSNs were transferred into six 1.5-ml microfuge tubes (Fisher Scientific, UK) and centrifuged at 120,000 rpm for 3 min. MSNs were washed twice with 1.3 ml 50:50 (vol:vol) methanol:de-ionised water (DW) and once with 1.3 ml PBS to remove any excess calcein on surface of the MSNs.

Washed MSNs were resuspended in 1.5 ml fresh PBS and 200 µl aliquots of this suspension were dispensed into a 96-well black microplate (Nunc, UK). Fluorescence signal was measured for 12 h at 30 min intervals at excitation and emission wavelengths of 485/20 nm and 528/20 nm, respectively.

4.2.3 Loading and Release of AIT and CNAD

AIT (250 µl) was dissolved in 1.75 ml DMSO, and then loaded into 20 mg of MSNs in 7 ml PBS using the same protocol as was done for calcein (Section 4.2.4.2). In the case of CNAD, 500 µl CNAD was dissolved in 1.5 ml DMSO. Loaded MSNs were washed with 50:50 (vol:vol) methanol:DW and PBS as described previously.

Washed MSNs were resuspended in 10 ml PBS in 15-ml centrifuge tubes (Fisher, UK). The resulting AIT-loaded and CNAD-loaded MSN suspensions were incubated at 30˚C at 150 rpm agitation. Release was monitored every 30 min for 4 h and then again at 24 h, via liquid-liquid extraction and subsequent GC-FID analysis. Five separate release experiments were performed for each plant compound, and three samples per time point were prepared in each experiment.

4.2.3.1 Liquid-Liquid Extraction

Liquid-liquid extraction is a method of extracting a substance from one liquid phased to another, based on relative solubilities in two different immiscible liquids such as an aqueous solution and an organic solvent. In this case, ethyl acetate (EtOAc) was used as the organic solvent to extract AIT and CNAD from PBS solution because 1) both hydrophobic plant compounds are more soluble in EtOAC than in aqueous PBS solution, and 2) EtOAc is a compatible solvent to be injected into the GC directly after sampling for identification and quantification.

At each sampling time point, 550 µl MSN suspension was transferred into a 1.5-ml microfuge tube and centrifuged at 13,000 rpm for 2 min. The PBS supernatant (500 µl) was then transferred to a new microfuge tube, in which 500 µl (equal volume) EtOAc was added. This 1:1 (vol:vol) EtOAc:PBS solution was shaken at 220 rpm for 20 min to extract the plant compounds out from aqueous solution into the organic phase. Samples were then centrifuged

at 130,000 rpm for 2 min to separate the two immiscible liquids, and 220 µl of the top EtOAc layer was carefully transferred into a GC vial. The sample was then injected into the GC-FID instrument to be analysed.

4.2.4 GC-FID

A GC-2010 (Shimadzu) GC-FID instrument with Perkin Elmer Clarus GC ovens was used to quantify the release of AIT and CNAD from 20mg of loaded MSNs. The analytical methods for both compounds were developed experimentally and are detailed in Tables 4.2a and b.

TABLE 4.2 A & B: **Parameters and methods developed to analyse AIT and CNAD by GC-FID, respectively.**

TABLE 4.2A: AIT	
Item	**Condition**
Instrument	Shimadzu GC-2010, Perkin Elmer Clarus GC ovens
Detector	Flame ionization detector (FID)
Detector temperature	300°C
Injector temperature	200°
Injection volume	1µl
Injection mode	Splitless
Carrier gas, total flow rate	Nitrogen, 5ml/min
Hydrogen flow rate, air flow rate	40ml/min, 400ml/min
Flow control mode, column flow rate	Linear velocity, 0.98ml/min
Column	Shim-5MS 5% Phenyl (equiv.) Polysilphenylene-siloxane
Column temperature	55°C
Column oven temperature program	55°C for 2 min 55°C to 75°C at rate of 25°C/min 75°C for 3 min 75°C to 85°C at rate of 4°C/min
Solvent	Ethyl acetate
Retention time for AITC	6.668 min

TABLE 4.2B: CNAD	
Item	**Condition**
Instrument	Shimadzu GC-2010, Perkin Elmer Clarus GC ovens
Detector	Flame ionization detector (FID)
Detector temperature	300°C
Injector temperature	240°
Injection volume	1µl
Injection mode	Splitless
Carrier gas, total flow rate	Nitrogen, 58.5ml/min
Hydrogen flow rate, air flow rate	40ml/min, 400ml/min
Flow control mode, column flow rate	Linear velocity, 1.07ml/min
Column	Shim-5MS 5% Phenyl (equiv.) Polysilphenylene-siloxane
Column temperature	65°C
Column oven temperature program	65°C for 1 min 65°C to 155°C at rate of 25°C/min 155°C for 2 min 155°C to 170°C at rate of 4°C/min
Solvent	Ethyl acetate
Retention time for CNAD	7.078 min

Calibration curves of AIT and CNAD were established by preparing solutions of known concentrations ranging from 0.5 to 3000 mg/L in EtOAc for both compounds. Each standard solution of known concentration was analysed (in triplicate) with GC-FID under the respective analytical methods described above. Using the GCsolution™ software (Shimadzu), the AUC obtained at particular retention times were determined and calibration curves for both compounds were subsequently established, as shown in Figures 4.7 a and b.

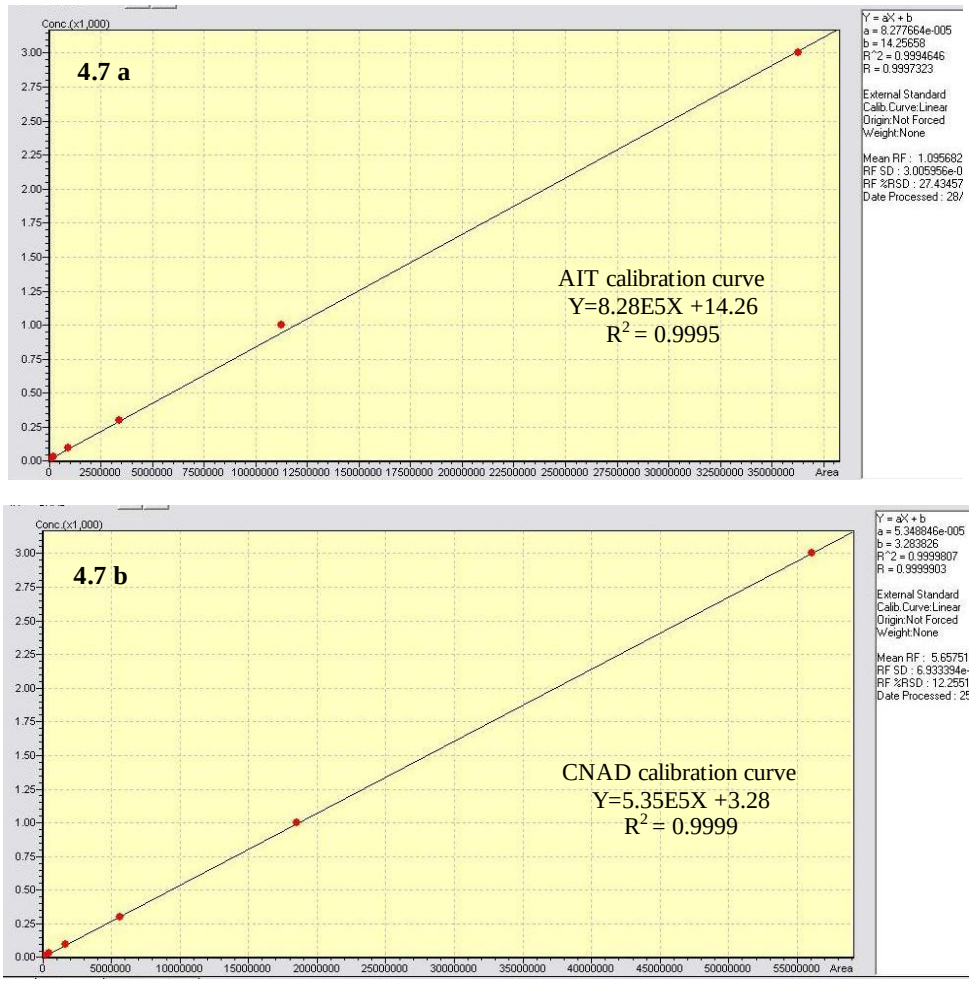


FIGURE 4.7 A & B: **Calibration curves of AIT (4.7 a) and CNAD (4.7 b) determined by GC-FID quantification.**

4.3 Results and Discussion

4.3.1 MSN Characterisation

4.3.1.1TEM

MSNs were imaged with bright field TEM in different orientations to determine the shape and dimension of the particles as well as the pores. Mesopores showed high rotational symmetry about the centre axis in a hexagonal arrangement (a central pore surrounded by six equidistant pores) when imaged through the axis of the central pore, which was denoted as "spot contrast" view (Figures 4.8 and 4.10). In the "line contrast" view, MSNs displayed line array of pores running through the entire volume of the nanoparticle when the electron beam was perpendicular to the centre axis (Figures 4.8 and 4.9). From such images, a synthesised MSN may be described as a polyhedron with constituent pore channels arranged in cubic order. It is common for MSNs with pores orientated with the electron beam (spot contrast view) to show a more circular projection as compared to those with pores orientated transversely across the beam (line contrast view), which appear more elongated.

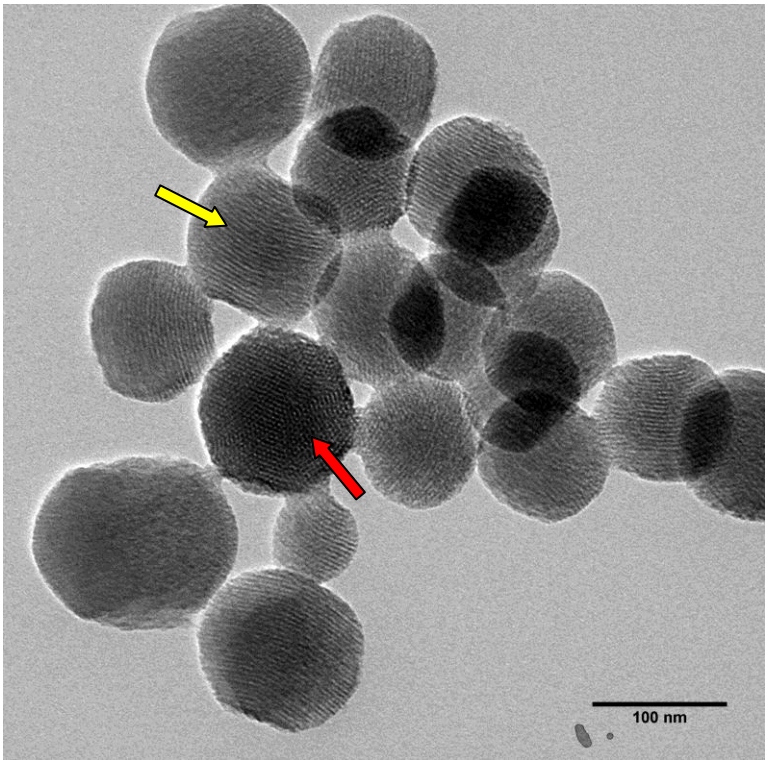


FIGURE 4.8: **Typical TEM image of MSNs. Red arrow: MSN in spot contrast view, imaged with pores orientated along the electron beam; spherical in shape. Yellow arrow: MSN in spot contrast view, imaged with pores orientated transversely across the electron beam; elongated "kidney" shape.**

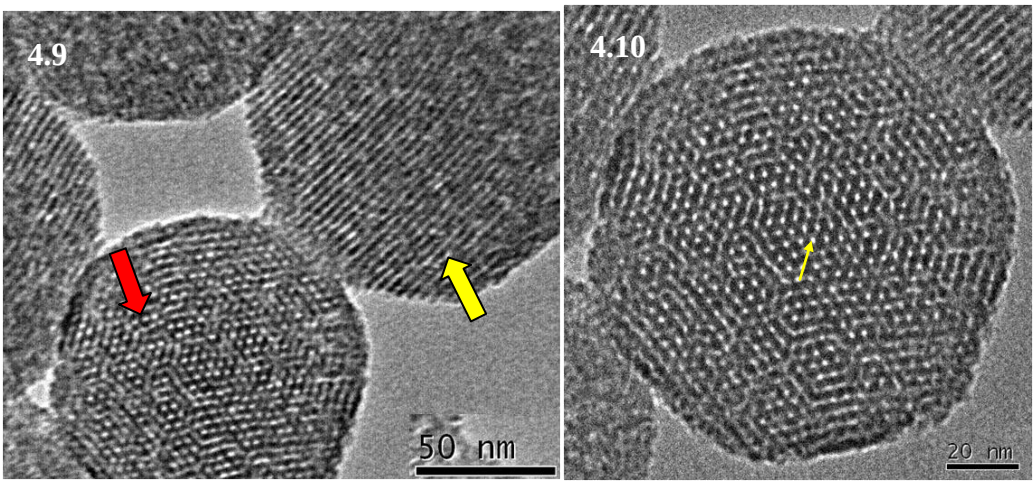


FIGURE 4.9: **TEM image displaying two adjacent MSNs, one in spot contrast view (red arrow) with pores arranged hexagonally, and the other (yellow arrow) with line array of pores running through the entire volume of the nanoparticle.**

FIGURE 4.10: **TEM image of an MSN showing pores aligned in a hexagonal pattern, arrow pointing to the centre axis.**

4.3.1.2 Quantitative Analysis of Particle Size

MSN particle size was measured employing three techniques: TEM, Disc Centrifuge, and NanoSight™. MSN pore size was determined using TEM and nitrogen sorption isotherms (Gemini™ VI Surface Area Analyzer).

4.3.1.2.1 TEM

As explained in the Methods and Materials portion of this chapter, particle diameters were measured using the histograms generated by building a contrast profile along selected regions on TEM images. The distribution of nanoparticle size is displayed in Figure 4.11. Mean particle size was 103.64 ± 18.78 nm in diameter, n = 140. The average aspect ratio was determined to be 1.12. The size distribution of the MSNs follows a unimodal Gaussian curve with standard deviation of 18.78, which means the synthesis method was robust and reproducible, yielding particles of similar size with expected deviation.

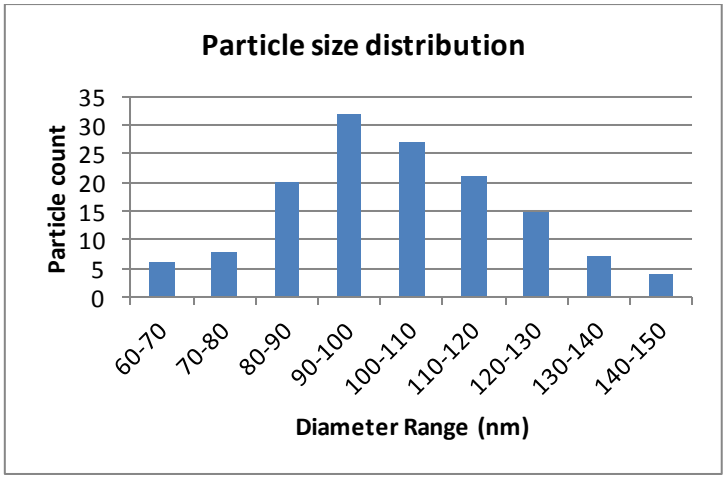


FIGURE 4.11: **Size distribution of MSNs obtained from measurements of TEM images.**

4.3.2.2 CPS Disc Centrifuge™ and NanoSight™

Data obtained using CPS Disc Centrifuge™ are shown in Figure 4.12, showing peaks at 125.38 ± 0.001 nm, which are comparable to the measurements obtained from TEM images. Particle size measurements obtained from this technique are commonly larger than

diameters measured from TEM images due to agglomeration of nanoparticles during disc centrifuge photosedimentometric analysis.

Using NanoSight™, the peak of size distribution was 102 ± 48 nm (Figure 4.13). This is consistent with values obtained from TEM images.

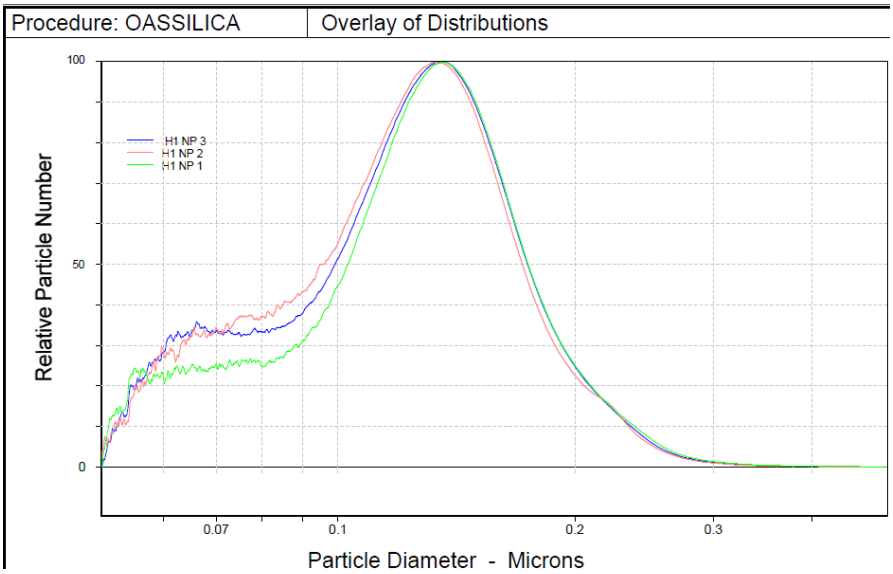


FIGURE 4.12: **Overlay of size distribution of MSNs obtained from CPS Disc Centrifuge™.**

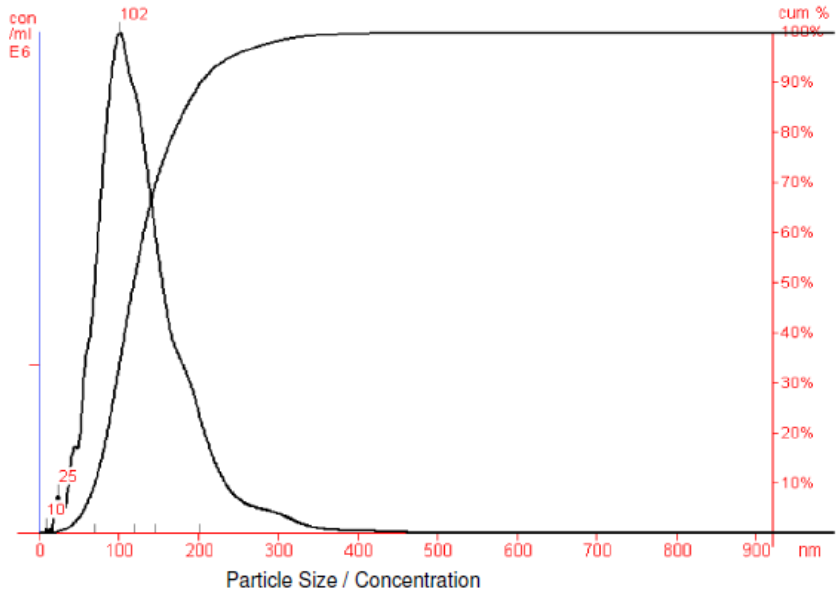


FIGURE 4.13: **Particle size vs. concentration plot created by Nanoparticle Tracking Analysis software from NanoSight™ analysis.**

4.3.1.3 Quantitative Analysis of Porosity and Surface Area

MSN pore size was determined using TEM and nitrogen sorption isotherms (Gemini™ VI Surface Area Analyzer).

4.3.1.3.1 TEM

MSN pores were measured from TEM images using the same protocol as that for determining particle size. Mean pore size was 2.03 ± 0.19 nm in diameter, n = 170 from 15 different nanoparticles. Mean channel width was 2.02 ± 0.17 nm in diameter, n = 70 from 15 different nanoparticles. Pore size and channel width measurements are highly consistently with each other, and the low standard deviations for both are indicative of the uniformity and regularity of the mesopores.

4.3.1.3.2 Nitrogen sorption isotherm

Using the Gemini™ VI Surface Area Analyzer, porosity was determined based on the BJH theory and surface area was determined based on the BET theory. The nitrogen sorption isotherm (Figure 4.14) of the MSNs is typical of mesoporous solids (Nandiyanto *et al.*, 2009). This type IV isotherm shows appreciable porosity, where N_2 condensation inside the mesopores are observed based on the adsorption step at $P/P_0 \sim 0.35$ (inflection point in Figure 4.14 a). In contrast, non-porous solids would yield flat isotherms indicating less N_2 adsorption. The mean pore size obtained from BJH adsorption theory was 2.78 nm in diameter (red peak, Figure 4.14 b) and from the BJH desorption was 2.82 nm in diameter (green inflection point, Figure 4.14 b). These values are slightly larger than diameters measured from TEM images, which could be considered more accurate due to the agglomeration of the nanoparticles during porosity assessment and also due to the limitations of the BJH theory itself.

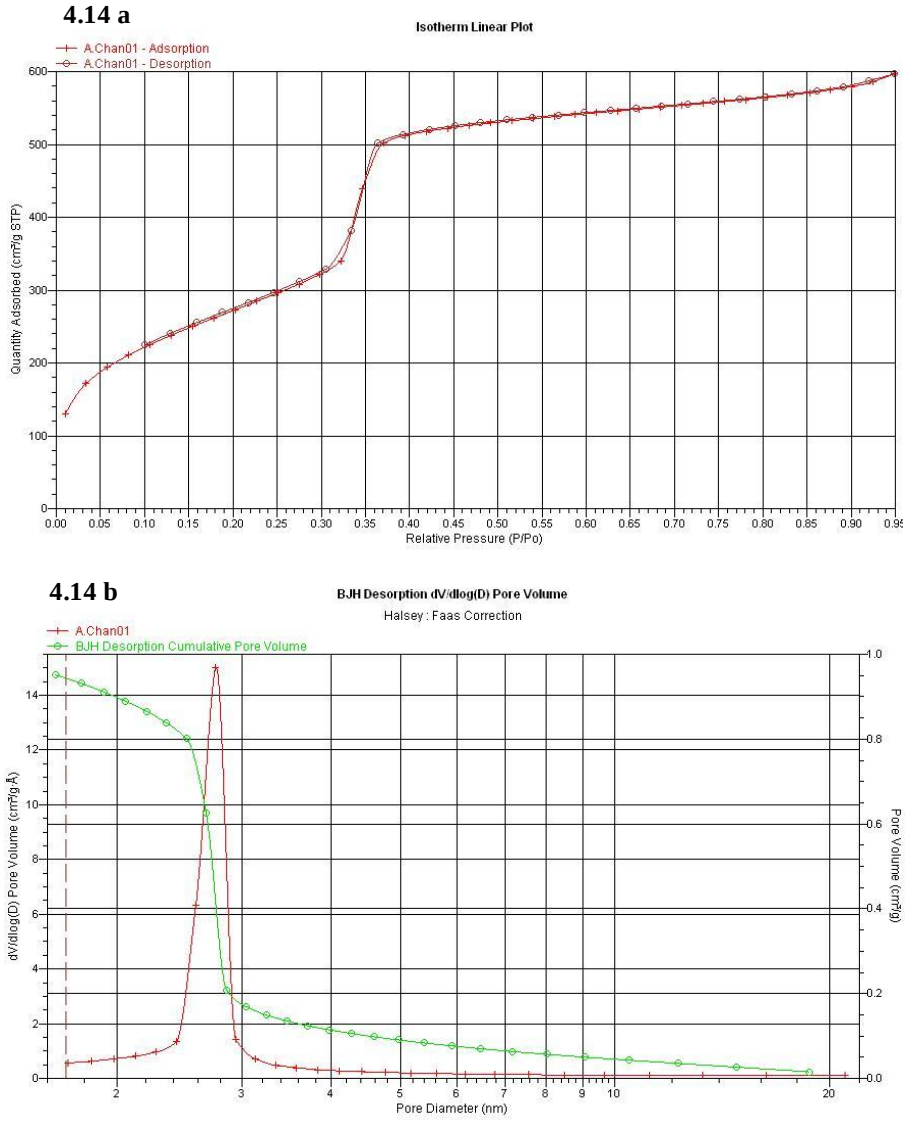
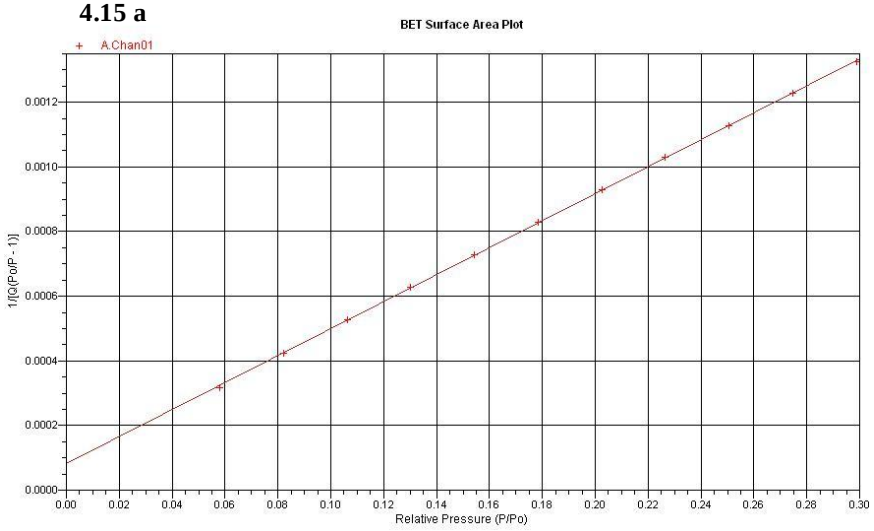


***FIGURE 4.14 A & B*: BET nitrogen sorption isotherms of synthesised MSNs (4.14 a). BJH nitrogen sorption for MSN pore size determination (4.14 b).**

The surface area of the MSNs is 1022.7755 ± 3.22 m²/g based on the multilayer BET theory, and 1671.2809 ± 66.67 m²/g based on the monolayer Langmuir theory. Plots obtained from both theories are represented below in Figures 4.15 a and 4.15 b, respectively.

4.15 a



4.15 b

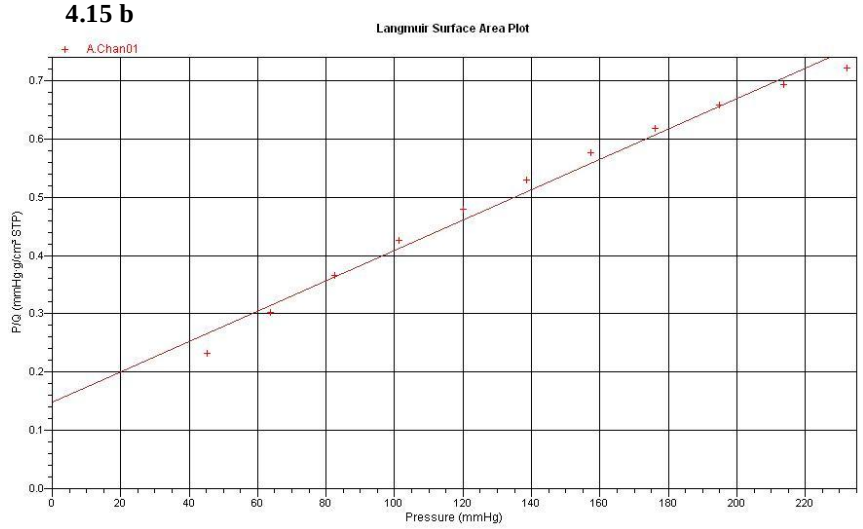


***FIGURE 4.15 A & B*: Surface area plots of synthesised MSNs obtained from the BET theory (4.15 a) and the Langmuir theory (4.15 b).**

4.3.2 Release of Guest Molecules

4.3.2.1 Calcein

Using the experimentally-derived calibration curve that related fluorescence to calcein concentration (described in Section 4.2.4.1), fluorescence values recorded over 12 h from 200 µl aliquots of 20mg calcein-loaded MSNs in 1.5 ml PBS were translated into mg/ml calcein. The resulting release profile of calcein is presented in Figure 4.16.

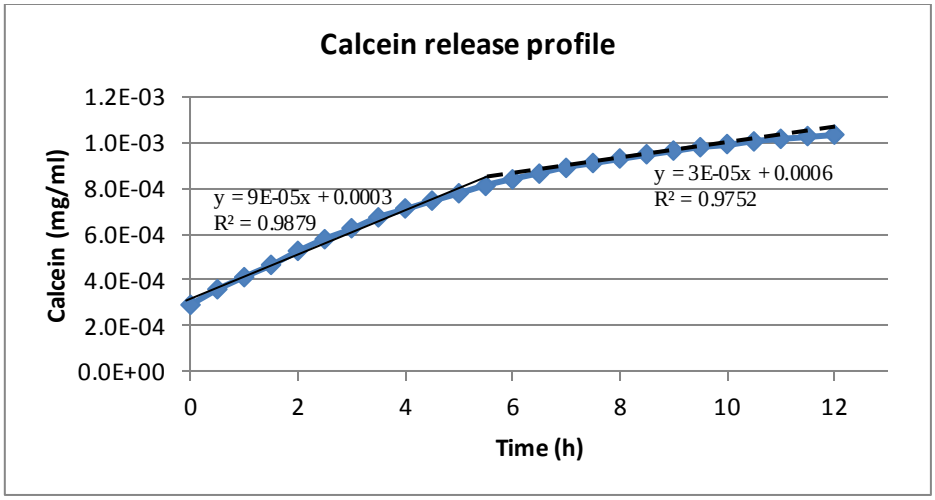


FIGURE 4.16: **Release profile of calcein from 200 µl aliquots of 20 mg calcein-loaded MSNs in 1.5 ml PBS. Two distinct trend lines accompanied by respective equations that describe each of them shows the two rates of release.**

The profile showed a gradual increase of calcein in solution over time with no spike in release at any point. The rate of release remained constant from 0 to 5.5 h (slope m = 9E-5, R^2 = 0.9878) (Figure 4.14), then decelerated at 5.5 h and remained relatively stable until 12 h (m = 3E-5, R^2 = 0.9752). Sustained release of calcein from synthesised MSNs seemed to be achieved, therefore experiments progressed onto the loading of MSNs with the plant compounds AIT and CNAD.

4.3.2.2 AIT

GC-FID analyses using the established method as described in Section 4.2.3 for AIT generated chromatographs similar to Figure 4.17. The AIT compound eluted at ~ 6.668 min (retention time of AIT), and the large peak beginning at ~ 2.65 min referred to the EtOAc solvent, since the presence of this peak was observed even in blank samples containing only EtOAc.

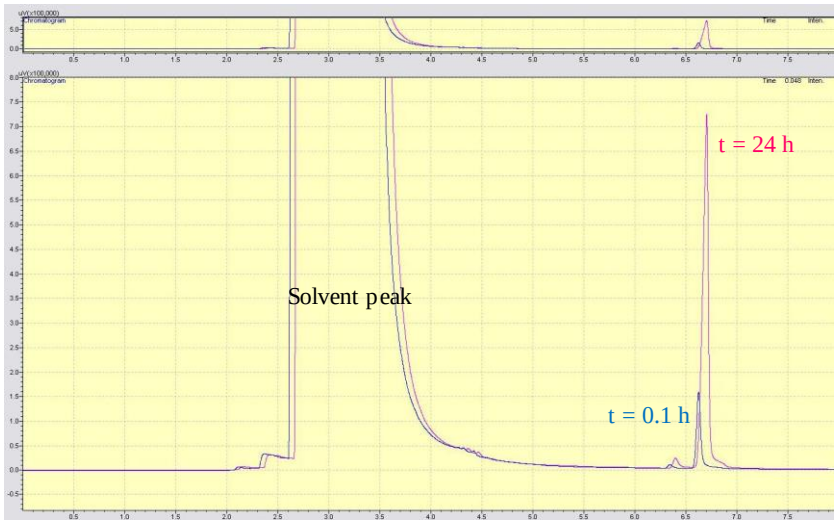


FIGURE 4.17: **Overlay of two chromatographs obtained via GC-FID analysis of AIT at t = 0.1 h and t = 24 h; AIT retention time ~ 6.668 min.**

Employing the experimentally-derived GC-FID calibration curve of AIT (as described in Section 4.2.3), AUCs of relevant peaks were translated into concentrations of AIT detected in solution. The resulting release profile of AIT is presented in Figure 4.18.

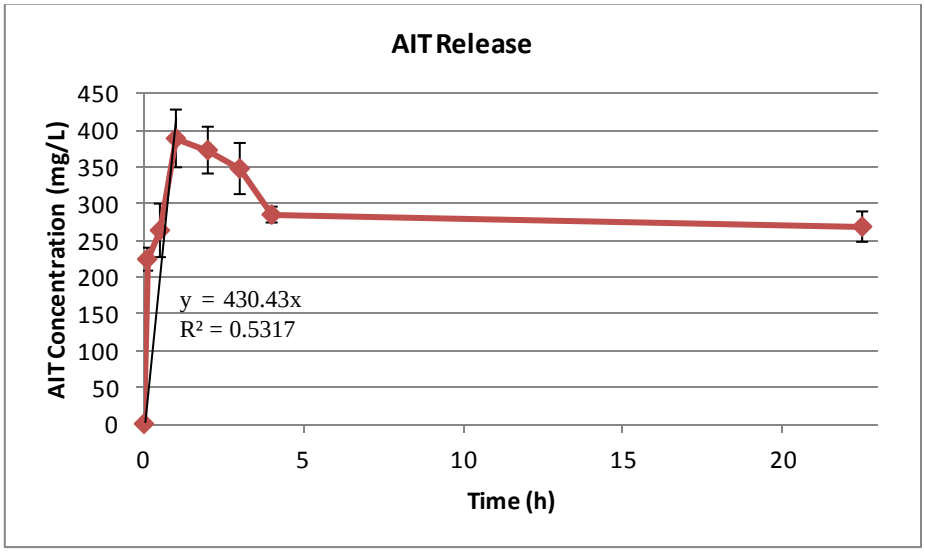


FIGURE 4.18: **AIT release profile from 20 mg AIT-loaded MSNs in 10 ml PBS. Error bars represent ± SD.**

4.3.2.3 CNAD

GC-FID analyses for CNAD generated chromatographs similar to Figure 4.19. Retention time of CNAD was ~ 7.078 min, and the large peak beginning at ~ 2 min referred

to the EtOAc solvent, since the presence of this peak was observed even in blank samples containing only EtOAc.

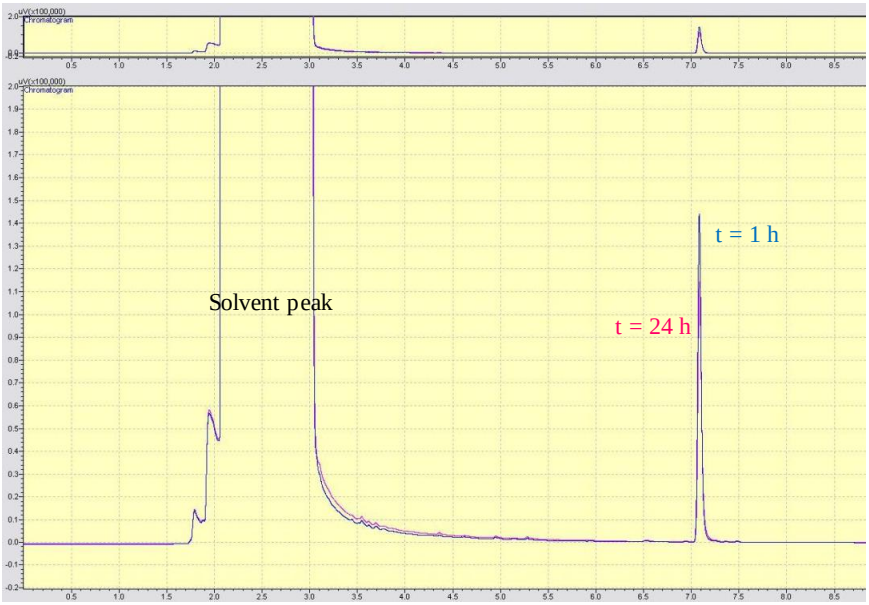


FIGURE 4.19: **Overlay of two chromatographs obtained via GC-FID analysis of CNAD at t = 1 h and t = 24 h; CNAD retention time ~ 7.078 min.**

Employing the GC-FID calibration curve of CNAD, AUCs of relevant peaks were translated into concentrations of CNAD in detected solution. The resulting release profile of CNAD is presented in Figure 4.20.

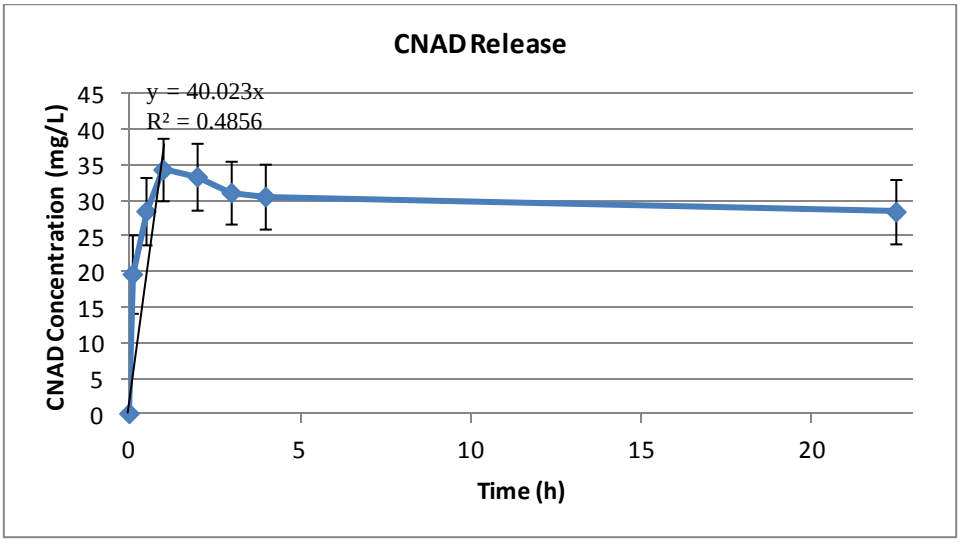


FIGURE 4.20: **Release profile of CNAD from 20 mg CNAD-loaded MSNs in 10 ml PBS. Error bars represent ± SD.**

The release of both AIT and CNAD from MSNs was rapid at the start, reaching peak concentrations at 1 h (AIT: mean of 362.7 mg/L, CNAD: mean of 34.3 mg/L). The high initial rates of release (AIT: 430.43 mg/L/h, CNAD: 40.02 mg/L/h) may have been due to the extreme concentration gradient established from within the pores and outside the pores in the external solution. Slight and gradual decreases in concentration were detected from 1 to 24 h for both compounds. This decrease was most likely attributed to the highly volatile nature of both plant compounds, since both are easily lost from the system via spontaneous vaporisation (explained in more detail in Chapter 1 and 2). Release of AIT or CNAD may have still persisted from 1 h onwards, but the compounds' rate of escape into the atmosphere may have been greater than the rate of their release from the MSNs. Without sustained release of the plant compounds from MSNs compensating for the loss through vaporisation, the concentrations of AIT and CNAD at 24 h may have been much lower than those detected in these experiments.

Much higher concentrations of AIT were detected in solution than CNAD (approximately ten-fold higher) as a result of diffusive release from the same amount of MSNs (20 mg). This may have been due to a combination of several factors: 1) AIT, a C_3-N-C linear molecule with molar mass of 99.15 g/mol, is a smaller molecule than CNAD, a C_9 molecule with an aromatic ring structure with molar mass of 132.16 g/mol, and therefore more AIT molecules can be housed in the mesopores of MSNs as compared to CNAD molecules; 2) again, because AIT is a smaller molecule than CNAD, AIT may have been released more readily from the pore openings due to less physical self-obstruction than CNAD had; 3) because AIT is more volatile and hydrophobic than CNAD, AIT may have preferentially diffused into the pores of the MSNs more effectively than CNAD did in order to partition away from the aqueous PBS solution during loading; and 4) because AIT is more "sticky" and hydrophobic than CNAD, AIT may have adhered onto the surface of the MSNs

more strongly than CNAD did (even after three washes with 50:50 (vol:vol) methanol:DW, and therefore the amount of AIT or CNAD detected to be released from the pores actually included release from the surfaces of the MSNs as well. The release profiles of AIT and CNAD were quite distinct from that of calcein, which is not surprising since the physicochemical properties of the plant compounds and the fluorescent dye are quite different.

4.3.3 Conclusion

Data from this study demonstrated that the sol-gel method of MSN synthesis yielded uniform and regular nanoparticles of ~ 100 nm in diameter with pores of ~ 2 nm in diameter. Furthermore, results of loading and release experiments using calcein, AIT, and CNAD as guest molecules showed that MSNs facilitated sustained release and maintenance of these compounds in solution.

Chapter Five

5. Improving Antimicrobial Efficacy of AIT and CNAD via MSN Encapsulation and Delivery

5.1 Introduction

The focus of this chapter is to test the hypothesis that employing MSNs as a delivery system would enhance the bacterial-killing efficacy of AIT and CNAD as compared to their antibacterial activity as free agents, when used at the same concentrations and conditions. Because of the hydrophobicity and volatile nature of plant compounds, the hypothesis that loading AIT and CNAD inside mesopores of MSNs would increase their antimicrobial activity was formed based on the following logic: (i) MSNs can provide physical protection around volatile guest molecules to minimise their loss through rapid and spontaneous vaporisation, (ii) MSNs' high surface area-to-volume ratio can help to maximise the bioavailability of their guest compounds during exposure to microbes, and (iii) MSNs can mitigate the problem of immiscibility of hydrophobic compounds in aqueous environments because they can freely disperse evenly in solution without the use of additional emulsifiers or solvents.

In this study, both planktonic and biofilm bacteria were subjected to AIT and CNAD in free form as well as encapsulated in MSNs. Biofilms comprise a major portion of unwanted microbial growth (biofouling) in water-related industries, including purification, desalination, and temperature control systems (Ludensky, 2003; Yasunori *et al.*, 2007), causing blockages and reducing efficiencies. Hence, in order to properly assess whether this

MSN-mediated approach of delivering plant compounds could be a novel and effective anti-biofouling strategy, it is important to study both planktonic and biofilm response to AIT and CNAD treatments.

Several methods of assessing planktonic and biofilm bacterial viability that were employed in this study are detailed below. The aim of this chapter was to determine (i) whether or not and (ii) to what degree MSNs improve the antimicrobial activities of AIT and CNAD when the plant compounds are used at fixed concentrations.

5.1.1 Viability Assays for Planktonic Bacteria

5.1.1.1 Miles and Misra Method

The Miles and Misra method is a microbiological technique to determine the number of colony forming units (CFUs) in a bacterial suspension when the quantity of bacteria is unknown (Hedges, 2002). This technique is equally precise, more efficient, and less resource-consuming than conventional plate count methods that utilise spreaders or glass beads (Hedges, 2002). In this method, ten-fold serial dilutions of bacterial suspensions are prepared using sterile PBS as diluent. Using a calibrated pipette 2.5 cm above the surface of agar medium, a small volume of each diluted suspension is carefully dropped onto the growth medium to form a continuous, circular droplet on the surface of the agar. It is important that the pipette tip does not touch the agar and that the plates are left upright and undisturbed so that droplets of inocula are allowed to spread naturally and be absorbed properly before incubation. Resulting colonies are counted in the dilution at which the highest number of full-size discrete colonies is visible. CFU values from the original bacterial sample are then calculated using the following equation:

CFU/ml = (average number of colonies) x (dilution factor) x (volume dispensed onto agar)

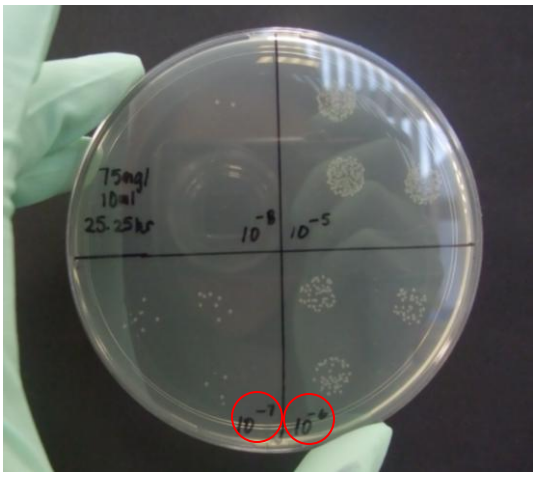


FIGURE 5.1: **Miles and Misra method: dilutions of *E. coli* on nutrient agar. Circled dilutions produced discrete, countable colonies. Photo by Andrea Chan.**

5.1.1.2 LIVE/DEAD® *Bac*Light™ Bacterial Viability Staining

This fluorescence-based method employs two nucleic acid stains to assess bacterial viability: the green-fluorescent SYTO® 9 stain and the red-fluorescent propidium iodide (PI) stain from the LIVE/DEAD® *Bac*Light™ Bacterial Viability Staining Kit (Molecular Probes®, Invitrogen™, US). The two stains penetrate healthy bacterial cells differentially: SYTO® 9 stain labels both live and dead cells, whereas PI stain penetrates only bacteria with damaged cell membranes, outcompeting SYTO® 9 fluorescence when both dyes are present (Molecular Probes® Invitrogen™, 2004). Thus, live bacteria with intact membranes fluoresce green, while dead bacteria with compromised membranes fluoresce red. Both SYTO® 9 and PI are DNA intercalating agents that have low intrinsic fluorescence when not bound to nucleic acids, but show a large fluorescence enhancement upon binding to DNA and/or RNA (Molecular Probes® Invitrogen™, 2004, 2011). The excitation/emission maxima is 480/500 nm for SYTO® 9 and 490/635 nm for PI, respectively. Results from this assay can be reached quantitatively using a fluorescence microplate reader and qualitatively/visually via fluorescence microscope.

5.1.1.3 Transmission Electron Microscopy (TEM)

For qualitative results, TEM can be used to visually image bacterial samples that have undergone antimicrobial treatment (Eltsov & Zuber, 2006). The technique is as described in Chapter 4, Section 4.1.3.1. Bacteria along with the MSNs they have been treated with can be visualised together using TEM.

5.1.2 Biofilm Analysis

5.1.2.1 Crystal violet assay

Crystal violet ($C_{25}N_3H_{30}Cl$) is a blue-violet dye commonly used in histological staining and Gram staining (stains peptidoglycan layer of Gram-positive bacteria). In aqueous solution at neutral pH, the dye's absorbance maximum is at 590 nm (Adams & Rosenstein, 1914). Since most cells are colourless, crystal violet is commonly used to stain cell cultures (both mammalian and microbial) and microbial biofilms to make them more visible for examination (Djordjevic, Wiedmann, & McLandsborough, 2002; Nassar, Li, & Gregory, 2011). In this present study, crystal violet was used to assess the degree to which various antimicrobial treatments inhibited the formation and attachment of biofilms on the bottom of tissue culture plates.

5.1.2.2 Confocal Laser Scanning Microscopy (CLSM)

Confocal laser scanning microscopy (CLSM) is an imaging modality for acquiring high-resolution optical images with depth selectivity (Pawley, 2006). It is a technique widely used in cell biology and microbiology, and in this present study CLSM was useful for assessing the lethal effects of various antimicrobial treatments on preformed biofilms (Takenaka, Iwaku, & Hoshino, 2001; Wagner, Ivleva, Haisch, Niessner, & Horn, 2009). The key feature of CLSM is optical sectioning, the ability to obtain images from selected depths (Fellers & Davidson, 2007). Specimens are scanned point-by-point with a focused laser beam

at specific depths, and three-dimensional images are subsequently constructed by compiling individual horizontal "slices" or "planes" (known as *z* stacks) together using associated software. This is useful for topological and surface profiling as well as interior imaging of internal structures. CLSM enables direct, noninvasive, serial optical sectioning of intact, living specimens with thickness to them (Fellers & Davidson, 2007). Biological samples are often fluorescently stained for visualisation. In combination with differential fluorescence staining with SYTO® 9 and PI, CLSM can be used to qualitatively assess the viability of preformed biofilms that has been exposed to designated treatment(s) (Suzuki, Fujikura, Higashiyama, & Takata, 1997).

In CLSM, a laser beam passes through a light source aperture and is then focused by an objective lens onto a small volume within the specimen. The objective lens re-collects scattered, reflected, and fluorescent light from the illuminated spot. A beam splitter then directs a portion of the light through the detector aperture (a pinhole) into a detector, which in fluorescence confocal microscopy will have a filter that selectively passes the fluorescent emission wavelengths while blocking the original excitation wavelength (Pawley, 2006). The detector is typically a photomultiplier tube that is highly sensitive to UV, visible, and near-infrared light, which functions by multiplying the current produced by incident light by as much as 100 million times. The detector aperture blocks any light that does not originate from the focal point. Because of this obstruction of out-of-focus light CLSM not only generates sharper images than conventional fluorescence microscopy does, but also is also able to obtain images at specific depths within the sample (Pawley, 2006).

The light originating from an illuminated volume within the sample represents one pixel of the resulting image, and the brightness of a pixel relates to the intensity of detected light. Images of various focal planes at different depths can be collected, and a three-dimensional picture of the sample can be achieved by assembling a stack of these two-

dimensional images from successive focal planes (Pawley, 2006). The laser beam scans across a horizontal plane at a particular depth within a sample by using oscillating dichromatic mirror(s) of which the scanning speed can be controlled. Slower scans result in better signal-to-noise ratio, generating better contrast and higher resolution.

In this technique, the detector pinhole aperture is CONjugate to the FOCAL point within the sample, and hence the name *CONFOCAL* Laser Scanning Microscopy.

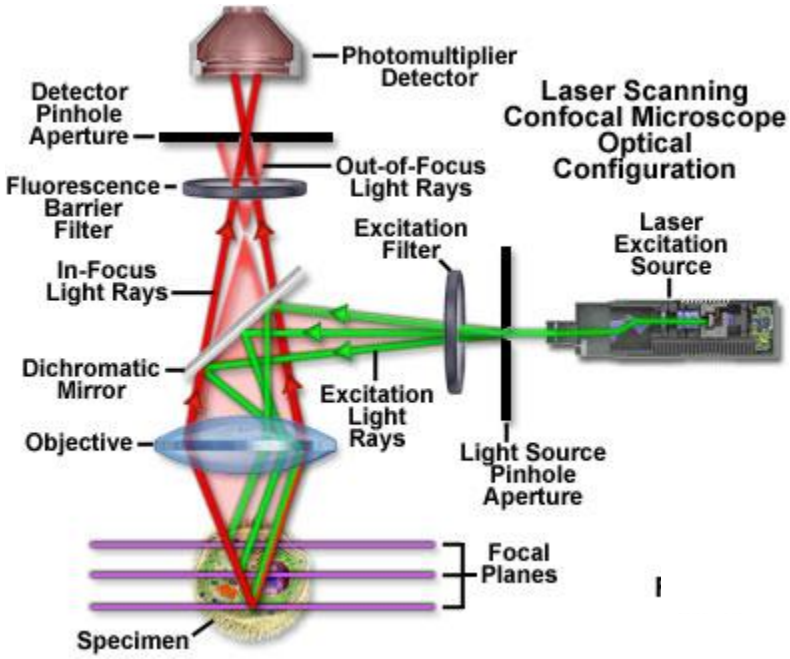


***FIGURE 5.2:* Principles of confocal laser scanning microscopy (CLSM).**

(Schematic from Olympus Microscopy Resource Center, available at http://www.olympusmicro.com/primer/techniques/confocal/confocalintro.html)

5.1.2.3 Mature Biofilms

Bio-Blok®100 (EXPO-NET Danmark A/S, Denmark) are polyethylene lattice matrices manufactured to support biofilm growth for the purpose of wastewater treatment (CAP Technology; Expo-Net Danmark). Such matrices can sustain viable biofilm growth for weeks and months. In this present study, Bio-Blok®100 material was used to cultivate mature biofilms, to which various antimicrobial treatments were applied. The wet weight of treated

biofilms was then measured to assess ability of each treatment to dislodge or detach biofilm cells and associated EPS from the substrata.

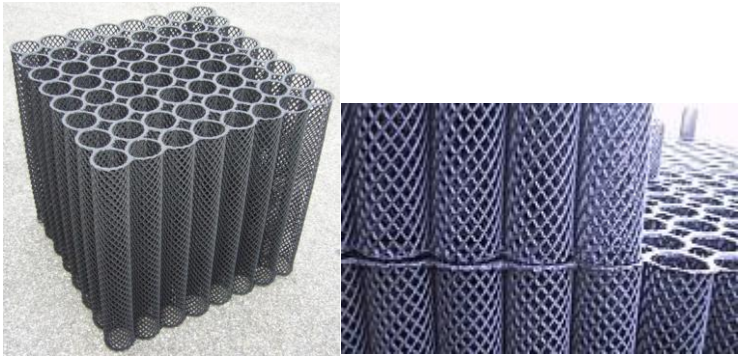


FIGURE 5.3: **Bio-Blok®100 matrices for growing mature biofilms.**

(Images from EXPO-NET, http://www.expo-net.dk)/

5.1.3 Aims and Objectives

The objectives of this chapter were:

(i) to assess and compare the antimicrobial efficacy of AIT and CNAD as free oils versus the two compounds entrapped and delivered via MSNs against planktonic *E. coli* employing the Miles and Misra plate count method, the LIVE/DEAD® *Bac*Light™ Bacterial viability staining method, and TEM imaging.

(ii) to evaluate the effects of AIT and CNAD on initial biofilm formation and adherence of *P. aeruginosa* using crystal violet staining in 96-well microplates.

(iii) to assess and compare the effects of AIT and CNAD in free form versus the two compounds entrapped and delivered by MSNs against 48 h-old *P. aeruginosa* biofilms via LIVE/DEAD® *Bac*Light™ Bacterial viability staining and CLSM.

(iv) To evaluate and compare the effects of AIT and CNAD in free form versus the two compounds entrapped and delivered via MSNs against 60 day-old *P. aeruginosa* biofilms by measuring the wet weight of biofilms grown on polyethylene matrices.

5.2 Materials and Methods

5.2.1 Escherichia coli Culture Conditions

E. coli (NCIMB 8879) cultures were prepared by streaking a frozen glycerol stock (-80˚C) onto nutrient agar (NA) (Sigma-Aldrich Company Ltd., Dorset, UK) and were left to grow for 16 h at 37°C until visible colonies appeared. One healthy colony was then picked to start a primary seed culture in 5 ml sterile nutrient broth (NB) (Sigma-Aldrich, UK). After growth for 6 h at 37˚C with 150 rpm agitation, the seed culture was added to 100 ml sterile NB and incubated at 37°C with 150 rpm agitation until it reached mid-exponential growth phase. The resulting culture was harvested, washed twice with PBS (Sigma-Aldrich, UK), and then resuspended in PBS. The turbidity of the *E. coli* suspension was adjusted to match 0.5 McFarland standard (OD_{600} = 0.132), which corresponds to bacterial density of 10^8 CFU/ml.

5.2.2 Calibration curve for LIVE/DEAD® BacLight™ Bacterial Viability Stain

A calibration curve for Syto® 9 and PI stains was established by analysing green : red fluorescence ratios of *E. coli* suspensions at known viabilities. In a 50-ml sterile centrifuge tube (Fisher Scientific Ltd., Loughborough, UK), a 45 ml *E. coli* culture (grown as described above without the wash steps) was harvested and concentrated by centrifugation at 3,000 rpm for 20 min. Supernatant was carefully removed and the cell pellet was resuspended in 4 ml PBS. One ml of this cell suspension was added to each of two 50-ml centrifuge tubes containing either 20 ml PBS for live bacteria or 20 ml 70% isopropyl alcohol (IPA) for killed bacteria. Both samples were incubated at room temperature for 1 h with mixing by inversion every 10 min, and then centrifuged at 3,000 rpm for 20 min. Supernatant was removed and the pellets were washed once in 20 ml fresh PBS. Both samples were resuspended in 20 ml

PBS, and OD_{600} of both were further adjusted to ~0.07 with PBS as diluent. Five different proportions of live : dead cells were then prepared (Table 5.1) using varying volumes of the resulting live-cell suspension and the IPA-killed cell suspension, yielding a total volume of 2 ml for each mixture.

TABLE 5.1: **Volumes of live- and dead-cell suspensions combined to achieve various proportions of live : dead cells.**

PERCENT LIVE BACTERIA (%)	VOLUME OF LIVE-CELL SUSPENSION (ML)	VOLUME OF DEAD-CELL SUSPENSION (ML)
100	2	0
90	1.8	0.2
50	1	1
10	0.2	1.8
0	0	2

A 2X Syto® 9-PI stock stain solution was prepared by adding 30 µl 3.34 mM Syto® 9 and 30 µl 20 mM PI to 9.94 ml DW (Molecular Probes® Invitrogen™, 2004). Each of the bacterial suspension mixtures (100 µl) was dispensed into wells of a 96-well flat-bottom black microplate (Nunc, UK), with each sample prepared in triplicate. In the same wells, 100 µl of the 2X stock stain solution was added, yielding a total volume of 200 µl in each well. Contents were thoroughly mixed by pipetting up and down, and then incubated at room temperature for 15 min in the dark to fluorescently stain the cells.

Fluorescence was measured using a Synergy HT Multi-detection Microplate Reader (Bio-Tek, UK) at excitation wavelength of 485/20 nm and emission wavelengths of 528/20 nm for live cells (green) and 645/20 nm for dead cells (red). Each sample was measured three times, and the mean green : red fluorescence ratios were calculated for each proportion of live : dead bacteria. The data is fit to a straight line using linear regression analysis, yielding a model described by the equation $y = 0.0686x + 0.06981$ with an R^2 value of 0.9974 (Figure 5.4).

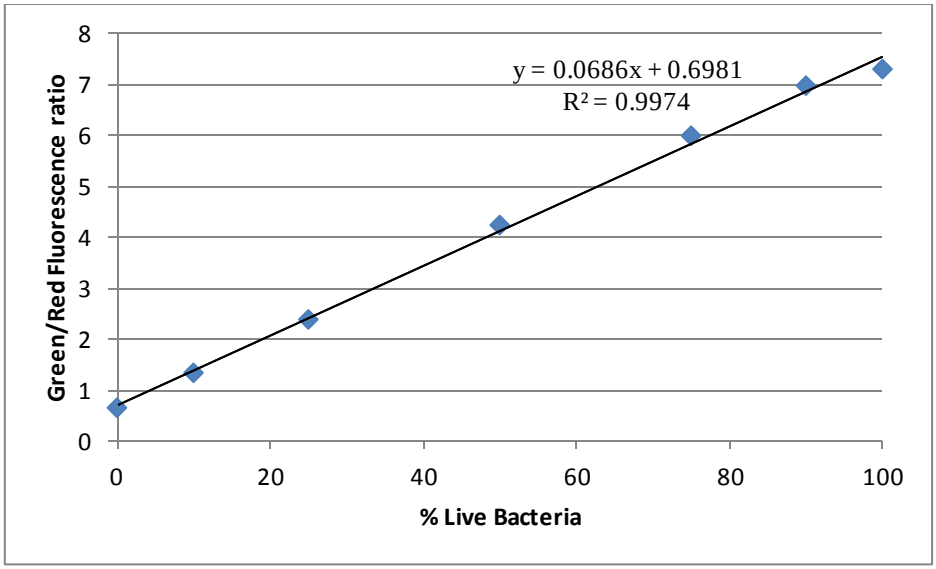


FIGURE 5.4: **Calibration curve for the green : red fluorescence ratios of five different proportions of live *E. coli* cells. Each point represents the mean of three samples, with each sample measured three times. The line is a least-squares fit of the relationship between % live bacteria (*x*) and green : red ratio (*y*).**

5.2.3 Effect on Planktonic Bacteria

From the AIT- and CNAD-loaded MSN release studies performed previously (described in detail in Chapter 4), it was experimentally established that the maximum concentrations detected in solution as a result of being released from 2 mg/ml of loaded MSNs were 362.7 mg/L for AIT and 34.8 mg/L for CNAD (Figures 4.18 and 4.20 in Chapter 4). To directly compare the killing efficiencies of AIT and CNAD in free form versus encapsulated in pores of MSNs when used at the same concentrations, *E. coli* cells were subjected to treatments of 362.7 mg/L AIT and 34.8 mg/L CNAD (both as free agents), which served as reference controls. Bacterial viability after such treatments was assessed using both the Miles and Misra plate count method and LIVE/DEAD® *Bac*Light™ bacterial viability staining.

In sterile 50-ml centrifuge tubes, 10-ml aliquots of an *E. coli* suspension, grown and adjusted as described above in Section 5.2.1, were each incubated with the following treatments for 18 h at 32˚C with 120 rpm agitation: (i) no treatment (negative control), (ii)

362.7 mg/L AIT, (iii) 2 mg/ml AIT-loaded MSNs, (iv) 1 mg/ml AIT-loaded MSNs, (v) 34.8 mg/L CNAD, (vi) 2 mg/ml CNAD-loaded MSNs, and (vii) 1 mg/ml CNAD-loaded MSNs. Three biological replicates were prepared for each treatment. For samples being treated with loaded MSNs, the impregnation of MSNs with AIT and CNAD was done directly prior to exposure to the bacterial suspensions. The protocol for loading MSNs with AIT and CNAD is described in Section 4.2.3 of Chapter 4. *E. coli* cells were exposed to the saturated MSNs immediately after the last wash step with PBS. After incubation, each sample was split into two equal and homogeneous aliquots, one for plate count experiments and one for differential fluorescent staining.

5.2.3.1 Miles and Misra Plate Count Method

For the Miles and Misra plate count method, treated *E. coli* and control samples were serially diluted 10-fold using sterile PBS, yielding dilutions ranging from 10^{-1} to 10^{-7} of the original sample. Twenty µl of the 10^{-4}, 10^{-5}, 10^{-6}, and 10^{-7} diluted suspensions were carefully pipetted onto NA media. Each dilution series is plated at least three times for statistical soundness. Agar plates were left undisturbed at room temperature for 15 min to allow for the droplets of inocula to diffuse and be absorbed evenly before overnight incubation at 37°C. The resulting colonies, typically countable at the 10^{-6} and 10^{-7} dilution, were counted using Stuart™ SC6PLUS colony counter. The mean CFU/ml values resulting from the various treatments were calculated using the following equation:

CFU per ml = (average number of colonies) x (dilution factor) x (1000 µl/ 20 µl)

5.2.3.2 Bacterial Viability Fluorescent Staining

For the LIVE/DEAD® *Bac*Light™ bacterial viability staining method, a 2X stock stain solution was prepared as described earlier in Section 5.2.2 (30 µl 3.34 mM Syto® 9 and 30 µl 20 mM PI in 9.94 ml DW) (Molecular Probes® Invitrogen™, 2004). Treated *E. coli* and

control samples were diluted 10-fold, and 100 µl of each sample was dispensed into a 96-well flat-bottom black microplate (Nunc, UK). Triplicates were prepared for each replicate of each treatment. In the same wells, 100 µl of the 2X stock stain solution was added, yielding a total volume of 200 µl in each well. Contents were thoroughly mixed by pipetting up and down, and then incubated at room temperature for 15 min in the dark to fluorescently stain the cells.

Fluorescence was measured using a Synergy HT Multi-detection Microplate Reader (Bio-Tek, UK) at excitation wavelength of 485/20 nm and emission wavelengths of 528/20 nm for live cells (green) and 645/20 nm for dead cells (red). Each sample was measured three times, and the mean green : red fluorescence ratios were calculated for each treatment.

5.2.3.3 TEM Imaging

Ten ml aliquots of an *E. coli* suspension, grown and adjusted as described above in Section 5.2.1, were each incubated with 1) no treatment (negative control), 2) 2 mg/ml empty MSNs, 3) 2 mg/ml AIT-loaded MSNs, and 4) 2 mg/ml CNAD-loaded MSNs for 18 h at 32˚C with 120 rpm agitation. After treatment, *E. coli* suspensions were centrifuged for 10 min at 3000 rpm, washed, resuspended in 5 ml DW, then then further diluted 150-fold with DW. Resulting samples were imaged via TEM with JEOL JEM 2010 operating at 200 kV for bright field imaging. Specimens were prepared by drop-casting 10 µl of each diluted sample onto holey carbon-coated TEM copper grids (carbon film on 3mm 300 mesh, Agar Scientific, UK), allowing them to air dry overnight before imaging. Triplicates were prepared for each treatment.

5.2.4 Pseudomonas aeruginosa Culture Conditions

Pseudomonas aeruginosa (NCIMB 950) cultures were prepared by streaking frozen glycerol stocks (-80˚C) onto tryptic soy agar (TSA) (Sigma-Aldrich, UK) and incubated at 37˚C for 16 h. Following incubation, a single colony was inoculated into 100 ml sterile

tryptic soy broth (TSB) (Sigma-Aldrich, UK) and incubated at 37°C with 150 rpm agitation until it reached mid-exponential growth phase. The resulting culture was harvested, washed twice with PBS (Sigma-Aldrich, UK), and then resuspended in PBS. The turbidity of the *P. aeruginosa* suspension was adjusted to match 0.5 McFarland standard (OD_{600} = 0.132), which corresponds to bacterial density of 10^8 CFU/ml.

5.2.5 Effect on Bacterial Biofilms

5.2.5.1 Biofilm Formation and Adherence Assay

The effects of varying concentrations of AIT (ranging from 2500 mg/L to 78.125 mg/L) and CNAD (ranging from 2500 mg/L to 156.25 mg/L) on adherence and the biofilm-forming ability of *P. aeruginosa* were evaluated in 96-well tissue culture microplates (Corning® CellBIND® 96 well clear flat bottom polystyrene microplate) as follows. Stock solutions of 5000 mg/L of AIT and CNAD were prepared in 0.0002% (w/v) crystal violet-TSB solution (crystal violet from Sigma-Aldrich, UK). The AIT and CNAD stock solutions were serially diluted by a factor of two with 0.0002% crystal violet-TSB solution across columns of a microplate, with 100 µl in each well. One hundred µl of the *P. aeruginosa* suspension prepared as described earlier (turbidity adjusted to 0.5 McFarland units) were then dispensed into each well, resulting in final concentrations of AIT ranging from 2500 mg/L to 78.125 mg/L, and of CNAD ranging from 2500 mg/L to 156.25 mg/L. Crystal violet (0.0002%)-TSB solution without AIT or CNAD plus *P. aeruginosa* inoculum served as positive control, the same crystal violet-TSB solution plus sterile PBS with no inoculum served as negative control. Inoculated microtitre plates were sealed with microporous tape sheets (AirPore® Tape Sheets, Qiagen, UK) incubated in 35˚C for 24 h in a static incubator.

During the course of incubation, the biofilms that had formed in permitting concentrations of each compound were stained with the crystal violet present in the TSB

growth media. This crystal violet staining method was modified and optimised from assays previously employed in other published studies (Ding *et al.*, 2011; Soumya *et al.*, 2011). After incubation, liquid in the wells were carefully removed and all wells were washed twice with sterile DW to remove any planktonic or loosely associated bacteria. Quantitative analysis of biofilm formation was performed by dispensing 150 µl of 95% ethanol in all wells and allowing 15 min to de-stain the crystal violet-stained biofilms. One hundred µl from each well was then transferred to a new microplate and the absorbance at 590 nm (A_{590}) of dissolved crystal violet was measured with a Synergy HT Multi-detection Microplate Reader (Bio-Tek, UK). The assay was repeated three times for both compounds, with eight technical replicates for each concentration of AIT and CNAD per assay. As a measure of efficacy, relative biofilm formation in treated wells was expressed as percentages of the untreated negative control: (mean A_{590} of treated wells/mean A_{590} of control wells) X 100.

5.2.5.2 CLSM Imaging of Preformed Biofilms

CLSM was used to visualise *P. aeruginosa* biofilms grown in sterile FluoroDish™ tissue and cell culture dishes (35 mm diam) with cover glass bottom (23 mm diam) (World Precision Instruments, UK). Control biofilms were grown for 48 h at 30˚C in 2 ml sterile 10% TSB in PBS with $^{1}/_{100}$ (vol/vol) *P. aeruginosa* inocula prepared as described above (turbidity adjusted to 0.5 McFarland units). After 24 h of growth, media in the culture dish was removed and carefully replaced with fresh sterile 10% TSB in PBS so as not to disturb the biofilm forming on the surface of the cover glass. This was done not only to provide fresh nutrients to support growth of nascent biofilm, but also to remove any planktonic cells in the spent media so they did not compete with the biofilm cells for nutrients. Confluent and adherent biofilms were visible after 48 h of growth. At this point, the preformed biofilms were subjected to various treatments listed in Table 5.2 (2 ml for each) for 24 h, with PBS as the solvent. Control samples treated with 2 ml sterile PBS.

TABLE 5.2: **The various treatments that *P. aeruginosa* biofilms were subjected to prior to CLSM imaging.**

TREATMENT			
AIT	AIT-LOADED MSNS	CNAD	CNAD-LOADED MSNS
600 mg/L	2 mg/ml	600 mg/L	2 mg/ml
350 mg/L	1 mg/ml	350 mg/L	1 mg/ml
	0.5 mg/ml	35 mg/L	0.5 mg/ml

CLSM images were collected directly from the cover glass at the bottom of the cell culture dish using a Zeiss LSM 510 Meta confocal microscope (Carl Zeiss MicroImaging GmbH, Jena, Germany) with a 1.2-numerical-aperture C-Apochromat 40X water immersion lens (Carl Zeiss MicroImaging GmbH, Jena, Germany). Before imaging, biofilms were stained with 1:1 v:v mixture of Syto® 9 and PI dyes from the LIVE/DEAD® *Bac*Light™ bacterial viability kit (Molecular Probes®, Invitrogen™, US). Stock stain solution was prepared by dissolving 30 µl 3.34 mM Syto® 9 and 30 µl 20 mM PI in 9.94 ml DW (similar to the 2X stock stain solution prepared previously for fluorescence spectroscopy). Biofilm samples were stained with 1 ml stock dye solution for 15 min in the dark in order to fluorescently stain the cells, then washed once with PBS to remove any excess dye.

Biofilm samples were excited with a 488-nm line from a 30-mW Ar ion laser operating with a tube current of 6.1 A attenuated to 0.3 to 0.7% of full power in multitrack mode. Fluorescence emission was detected with 500- to 530-nm (green, alive) and a 585- to 615-nm (red, dead) band-pass filers. Three-dimensional (3D) were collected over square areas with image size of 1024 x 1024 pixels (76.8 X 76.8 µm) in *x* and *y* with variable *z* since the thickness of each biofilm differed from one another due to the intrinsic variance of biological samples and the different types of treatment each biofilm was subjected to. Pixel spacing was 70 nm and pixel dwell time was 1.6 µs.

Three biological replicates were prepared for each treatment, each was imaged at three different locations of the biofilm (at the least), and the entire experiment was repeated

four separate times. CLSM images were rendered using Zeiss LSM Image Browser Version 4.2.0.121 software.

5.2.5.3 Biomass Reduction of Mature, Adherent Biofilms

5.2.5.3.1 Establishing Mature Biofilms

The apparatus for growing *P. aeruginosa* biofilms were constructed as follows: Bio-Blok®100 (EXPO-NET Danmark A/S, Denmark), a polyethylene lattice matrix manufactured to support bacterial growth for the purpose of wastewater treatment, was cut into fifteen uniform rectangular coupons weighing 2 g each. Each coupon was placed snuggly inside a 50-ml centrifuge tube. Two 4-mm diam holes were drilled on caps of the fifteen 50-ml centrifuge tubes, through which two 12-cm segments of silicone airline tubing (Marina® Hagen®, UK) were inserted, one being the inlet for aeration and the other being the outlet. The modified caps were placed back on the centrifuge tubes, and the assembled apparatuses were sterilised by autoclave. After sterilisation, sterile cellulose membrane syringe filters with pore size of 0.22 µm (Millipore Millex MCE sterile 33 mm 0.22 µm syringe filters) were fitted onto all the exposed ends of the tubing (Figure 5.5).

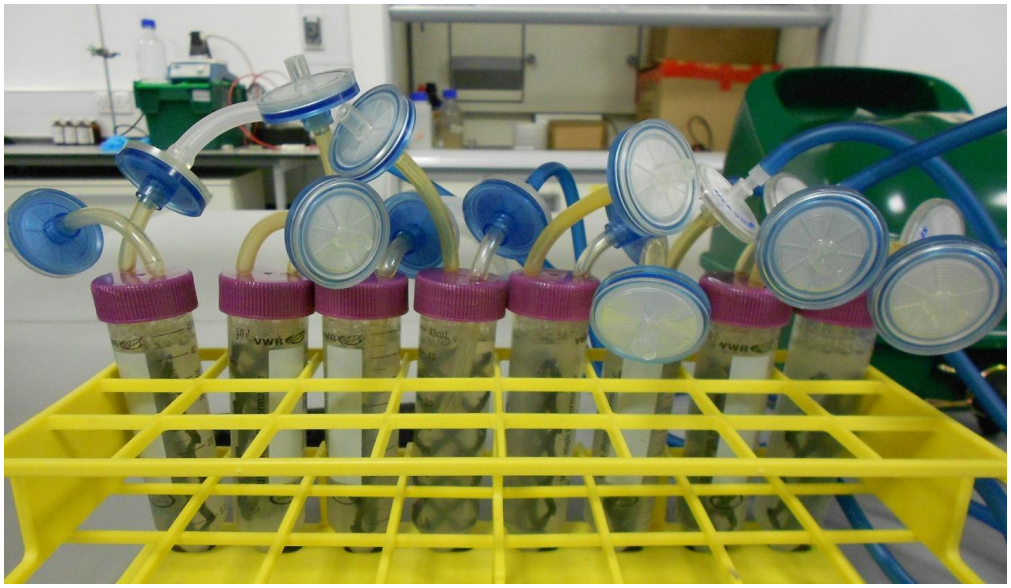


FIGURE 5.5: **Apparatuses used to grow 60-day old biofilms, constructed using Bio-Blok®100 polyethylene material, 50-ml centrifuge tubes, silicone tubing, and cellulose membrane syringe filters. Photo by Andrea Chan.**

Three independent cultures of *P. aeruginosa* were propagated until mid-exponential growth phase, then washed and resuspended in PBS (as described earlier) with final OD_{600} = 0.695. Under aseptic conditions, three separate 300-ml aliquots of sterile 10% TSB were inoculated with $^{1}/_{100}$ (vol/vol) of their respective *P. aeruginosa* suspensions. To yield six sets of biological triplicates, 6 aliquots of 40 ml inoculated media from each of the three separate cultures were dispensed into each biofilm-growing apparatus. One end of an 80-cm segment of silicone tubing was then fitted onto one of the two syringe filters on each of the setups, while the other end of the tubing was attached to an outlet of an air pump (Blagdon® 65 Koi Air Pump with 18X valved metal air divider). All 18 apparatuses were supplied with air by a single air pump with multiple outlet ports; valves on each outlet were adjusted so that air flow rate was uniform across all setups (Figure 5.6). With regular replenishment of fresh 3 ml 10% TSB every three days, bacterial cells were left to grow, to adhere to the Bio-Blok® material, and to form eventual biofilms for 60 days in total.

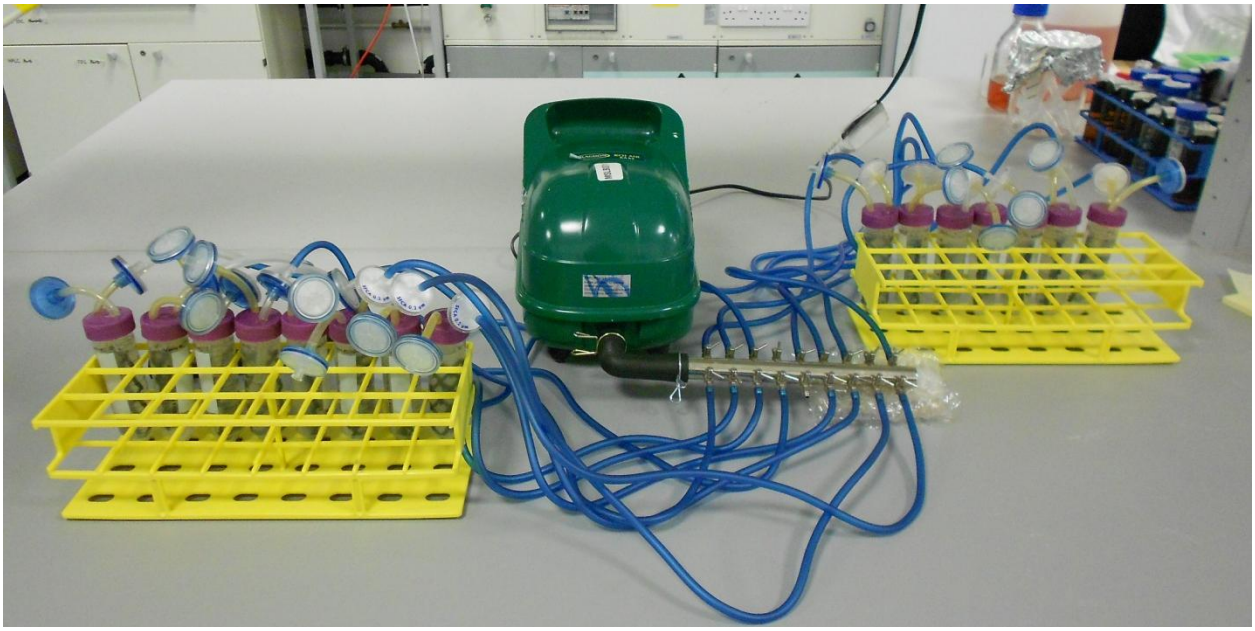


FIGURE 5.6: **Biofilm-growing setup consisting of a series of apparatuses connected to a multi-valve air pump for aeration. Photo by Andrea Chan.**

5.2.5.3.2 Exposing preformed biofilms to various treatments

On day 60, solutions of AIT and CNAD were added to setups containing mature biofilms (triplicates for each compound), yielding final concentration of 350 mg/L for AIT, and 350 mg/L and 35 mg/L for CNAD. Additionally, preformed biofilms were treated with either 2 mg/ml AIT-loaded MSNs or 2 mg/ml CNAD-loaded MSNs, also in triplicates for both. Three of the biofilm setups were left untreated to serve as negative controls. In order to properly compare the activity of AIT as a free agent versus encapsulated in MSNS, the concentration 350 mg/L was chosen as an approximation of the maximum concentration of AIT detected (362.7 mg/L) as a result of being released from 2 mg/ml of AIT-loaded MSNs (Chapter 4). For the same reason, 35 mg/L CNAD was chosen as an approximation of the maximum CNAD concentration detected (34.8 mg/L) as a result of being released from 2 mg/ml of CNAD-loaded MSNs. CNAD at 350 mg/L was also included in this assay in order to directly compare the anti-biofilm effects of AIT and CNAD when used at the same concentration. After 24 h exposure to the various treatments, the Bio-Blok® coupons, with attached biofilms, were taken out of the vessels and left to drip dry for 10 min. Each Bio-

Blok® coupon was then weighed, and the efficacy of AIT and CNAD against 60-day old *P. aeruginosa* biofilms was reflected in the degree of reduction in wet weight of treated samples as compared to the untreated negative controls. Since the starting mass of the Bio-Blok® coupons was 2 g each, the wet weight of the biofilm alone was calculated by subtracting 2 g from the total mass obtained.

5.2.6 Statistical Analysis

F-test, *t*-test and ANOVA followed by Tukey's test were applied when appropriate. *P* values of 0.05 were used to determine statistical significance.

5.3 Results and Discussion

5.3.1 Planktonic Bacteria

5.3.1.1 AIT-treated Bacteria: Plate Count Assay

Exposing planktonic *E. coli* to 2 mg/ml and 1 mg/ml AIT-loaded MSNs along with 362.7 mg/L AIT as a reference control over the course of 18 h produced plate count results presented in Figure 5.7. Resulting colonies could be counted from dilutions of 10^{-4} to 10^{-7} of the planktonic bacteria after designated treatments. Mean CFU/ml values were calculated from colony counts resulting from all technical and biological replicates. Once CFU/ml values were calculated, data was converted to percentages of the untreated, negative control.

As mentioned before, in order to directly compare the killing efficiency of AIT in free form versus encapsulated in MSNs, *E. coli* cells were subjected to treatments of 362.7 mg/L AIT, which was the experimentally established maximum concentration detected as a result of being released from 2 mg/ml of AIT-loaded MSNs (Chapter 4). At the 1 h time point, 2 mg/ml AIT-loaded MSNs yielded significantly lower colony counts as compared to both the negative control (by approximately 40%) and the reference control (by approximately 20%) ($P \leq 0.05$) (Figure 5.7). Exposure to 1 mg/ml AIT-loaded MSNs for 1 h resulted in approximately 20% reduction in CFU/ml as compared to the negative control ($P \leq 0.05$), but did not yield significantly different results as compared to the reference control (Figure 5.7). Since 2 mg/ml AIT-loaded MSNs released a maximum of 362.7 mg/L AIT in solution, it would be reasonable to derive that 1 mg/ml AIT-loaded MSNs would release ($^1/_2$)X 362.7 mg/L AIT, which is 181.35 mg/L AIT. Based on present experimental data, it can be concluded that only 181.35 mg/L AIT encapsulated in MSNs (equivalent to 1 mg/ml MSNs) was required to kill the same amount of planktonic bacteria as twice that amount of AIT (362.7 mg/L) in free form after 1 h of treatment. Furthermore, 2 mg/ml AIT-loaded MSNs

(equivalent to 362.7 mg/L AIT) killed twice the amount of bacteria than 362.7 mg/L AIT in free form did after 1 h of treatment. These findings collectively suggest that employing MSNs as a delivery system doubled the antibacterial efficacy of free form AIT after 1 h of exposure.

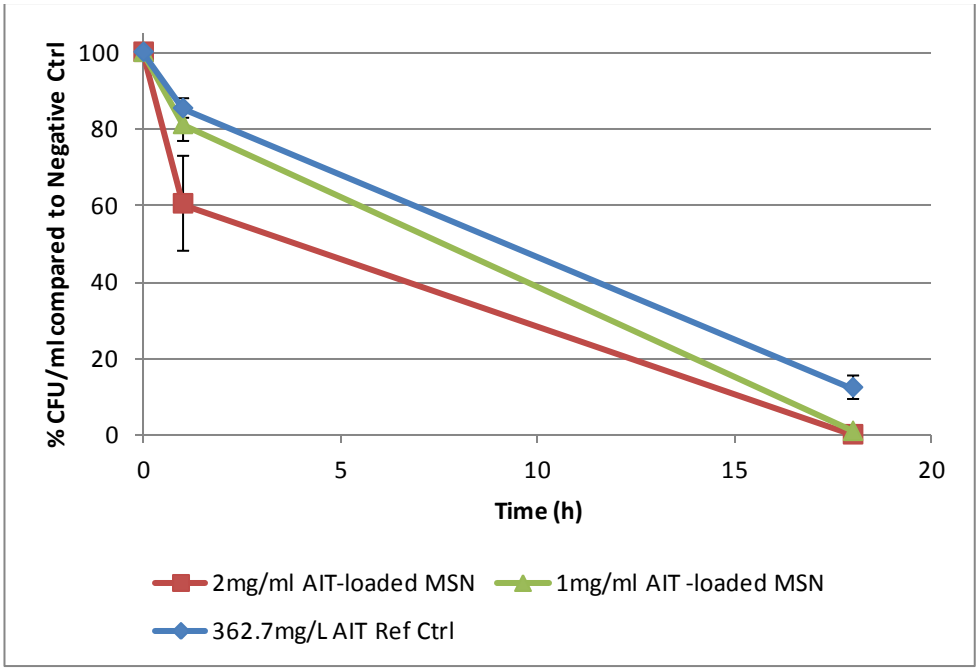


FIGURE 5.7: **Miles and Misra plate count assay after exposing planktonic *E. coli to* various AIT treatments for 0 h, 1 h, and 18 h. CFU/ml values are expressed as percentages of the negative control. Error bars represent ± standard deviation (SD). Data represents the mean and SD of biological and technical triplicate samples.**

At the 18 h time point, the negative control samples experimentally yielded (2.365 ± 0.037) X 10^9 CFU/ml *E. coli*. Both 2 mg/ml and 1 mg/ml AIT-loaded MSNs killed essentially all planktonic bacteria in the system, yielding approximately 0% culturable colonies as compared to the negative control. Free form AIT at 362.7 mg/L was able to inhibit > 85% bacterial colonies as compared to the untreated control after 18 h; however, it was significantly less effective than both 2 mg/ml and 1 mg/ml AIT-loaded MSNs ($P \leq 0.05$). Presuming with reason that 181.35 mg/L AIT was the maximum concentration released by 1 mg/ml AIT-loaded MSNs, it can be concluded that 362.7 mg/L AIT in free form was

significantly less effective (by approximately 10%) in killing planktonic bacteria than half that concentration (181.35 mg/L AIT) encapsulated in MSNs ($P \leq 0.05$).

Although 2 mg/ml AIT-loaded MSNs resulted in significantly lower CFU/ml values than 1 mg/ml AIT-loaded MSNs at the 1 h time point, these two treatments were equally as effective in killing the *E. coli* cells after more prolonged exposure (18 h). Thus, when employing MSNs as a delivery system for 18 h, it can be deduced that the concentration of AIT needed to eradicate a suspension consisting of approximately 2.365 X 10^9 CFU/ml planktonic *E. coli* would be ≤ 181.35 mg/L. After just 1 h of exposure, 2 mg/ml AIT-loaded MSNs were able to reduce culturable colonies by ~ 40%, whereas 1 mg/ml AIT-loaded MSN only reduced colony counts by ~ 20% (which is 50% less effective than 2 mg/ml AIT-loaded MSNs); on the other hand, after 18 h of treatment, 1 mg/ml AIT-loaded MSNs were able to kill essentially all bacteria in the system, exhibiting the same effectiveness as twice that amount (2 mg/ml) of loaded MSNs did. Based on present experimental data, the degree of antibacterial efficacy was not solely dependent on the amount of AIT-loaded MSNs employed at any given time; but rather, the killing efficiency of AIT-loaded MSNs was also a function of treatment time.

The microencapsulation of AIT in gum arabic (hardened sap from acacia trees) and chitosan (polysaccharide derived from cell walls of fungi and exoskeletons of arthropods and insects) in order to overcome its poor solubility and volatility has been reported in the context of food preservation (Chacon, Buffo, & Holley, 2006; Ko, Jeon, & Park, 2012; Ko, Kim, & Park, 2012). In addition to the distinction in application between aforementioned studies and our present work (food storage versus sustainable anti-biofouling strategy), methods and results also differed in several ways. Firstly, previous studies entrapped AIT in the cores of micro-sized capsules made of organic plant exudate that were irregular, non-spherical, and rock-like (Chacon *et al.*, 2006; Ko, Jeon, *et al.*, 2012; Ko, Kim, *et al.*, 2012), whereas our

current study employs nanosized, uniform, spherical, inorganic particles with mesopores in which AIT was stored for delivery. Secondly, AIT release and antimicrobial activity was assessed after two to over three weeks at lower-than-ambient temperatures (4ºC and 10ºC) (Chacon *et al.*, 2006; Ko, Kim, *et al.*, 2012), while we assessed the same parameters in the course of 18 hours at near-optimal bacterial growth temperature (32ºC). Also, contrary to our current work in which Gram-negative bacteria were used as targets, Ko, Kim, & Park, 2012, evaluated the bactericidal activity of encapsulated AIT against Gram-positive bacteria, which are generally more susceptible to antimicrobial treatment than Gram-negative bacteria (S.P. Denyer & Maillard, 2002; Mann *et al.*, 2000; Mayaud *et al.*, 2008).

Chacon *et al.*, 2006, did not directly compare the effectiveness of AIT in free form versus AIT encapsulated in freeze-dried or spray-dried sap wall material, which was achieved presently by assessing AIT as a free agent and AIT as guest molecules loaded in MSNs. Furthermore, compared to previous published works, Chacon *et al.*, 2006, reported the overall antibacterial efficacy against *E. coli* was reduced when delivered from gum acacia microcapsules than when freely volatised in the food package (Chacon *et al.*, 2006), whereas in this present study, encapsulation and delivery using MSNs significantly improved antimicrobial efficacy of AIT.

AIT in gelatin-gum arabic cross-linked with tannic acid microspheres have also been achieved for oral delivery of AIT as a nutraceutical formulation (Z. Q. Zhang, Pan, & Chung, 2011). In addition to differences in application and size scale as compared to our study, assessment of antimicrobial activity, which was an integral objective in our present research, was not a part of the work of Zhang *et al.*, 2011.

A few reports of AIT microencapsulation inside central cavities of the following organic compounds have also been published for the purpose of food storage and flavour

retention/controlled slow release: modified starches (carbohydrates comprised of a large number of glucose units), α- and β-cyclodextrins (cyclic oligosaccharides produced from starch), and maltodextrin (oligosaccharide produced from starch) (Piercey *et al.*, 2012; Plackett, Ghanbari-Siahkali, & Szente, 2007; Ratanasiriwat, Worawattanamateekul, & Klaypradit, 2013; Yamamoto, Neoh, Honbou, Yoshii, & Furuta, 2012). In these studies, inclusion complexes with AIT as the core were synthesised via microencapsulation methods in which an active and sensitive ingredient are coated with a thin layer of another wall material via transformation of emulsions into a dry powder in the micro-scale. These reports differ from our present work in application (food preservation versus novel anti-biofouling approach), materials (organic emulsifiers versus inorganic silica), synthesis methods (emulsion microencapsulation versus sol-gel particle synthesis followed by AIT loading), and size scale (micro versus nano).

5.3.1.2 CNAD-treated Bacteria: Plate Count Assay

The plate count assay was also performed after planktonic *E. coli* was exposed to 2 mg/ml CNAD-loaded MSNs and 34.8 mg/L CNAD over the course of 18 h, producing results presented in Figure 5.8. Resulting colonies were countable from 10^{-5} to 10^{-7} dilutions of the planktonic bacteria after designated treatments. Mean CFU/ml values were calculated from colony counts resulting from all technical and biological replicates. Once CFU/ml values were calculated, data was converted to percentages of the untreated, negative control.

As in the case of AIT, in order to directly compare the killing efficiency of CNAD in free form versus encapsulated in MSNs, *E. coli* cells were subjected to treatments of 34.8 mg/L CNAD as a reference control, which was the experimentally-established maximum concentration detected as a result of being released from 2 mg/ml of CNAD-loaded MSNs (Chapter 4). At both 1 h and 18 h, 2 mg/ml CNAD-loaded MSNs yielded significantly lower

colony counts as compared to both the negative control (by > 15% at 1 h; by approximately 50% at 18 h) and the reference control (by approximately 15% at both 1 h and 18 h) ($P \leq 0.05$) (Figure 5.8). At 1 h, exposure to 34.8 mg/L CNAD reference control did not yield significantly different results as compared to the negative control; exposure at the same concentration for 18 h resulted in approximately 35% reduction in CFU/ml as compared the negative control ($P \leq 0.05$) (Figure 5.8).

When compared to CNAD in free form, it appears that the employment of MSNs as a delivery vehicle for CNAD significantly enhanced its antibacterial efficiency during the first hour of exposure. From 1h to 18 h, on the other hand, CNAD-loaded MSNS and CNAD in free form exhibited the same rate of kill. This is evident in the slopes (m) of both samples from 0 h to 1 h and from 1 h to 18 h, which is a reflection of rates of CFU/ml reduction. From 0 h to 1 h, 34.8 mg/L CNAD reference control produced a slope of -2.68, whereas 2 mg/ml CNAD-loaded MSNs produced a slope of -16.60. This indicates that when colony counts were normalised to those of the negative control, 2 mg/ml CNAD-loaded MSNs killed planktonic bacteria at a rate that was over 6X faster than that of 34.8 mg/L CNAD in free form within the first hour of exposure. In contrast, 34.8 mg/L CNAD and 2 mg/ml CNAD-loaded MSNs produced similar slope values from 1 h to 18 h of exposure, yielding m = -32 for 34.8 mg/L CNAD and m = -33.81 for 2 mg/ml CNAD-loaded MSNs. This indicates that both treatments reduced colony counts at similar rates during this time. The same conclusion can be drawn from a different perspective of the same data, which is presented in Figure 5.9. Instead of normalising to the negative control, CFU/ml values produced by 2 mg/ml CNAD-loaded MSNs were normalised to the 34.8 mg/L CNAD reference control. From this data, no significant difference was observed between the colony count percentage at 1 h and 18 h (79.56% of reference control at 1 h, 76.75% at 18 h), which means that the degree to which the employment of MSNs improved CNAD's antibacterial activity as compared to the use of

it in free form remained the same at 1 h and 18 h. Therefore, it can be concluded that 2 mg/ml CNAD-loaded MSNs and 34.8 mg/L CNAD exhibited similar antibacterial efficiencies from 1 h to 18 h, reducing colony counts at similar rates. It is important to note that because data was not collected at any other intermediate time points between 1 h and 18 h, it cannot be concluded that the rate of kill between 2 mg/ml CNAD-loaded MSNs and 34.8 mg/L CNAD in free form became congruous precisely at the 1 h time point.

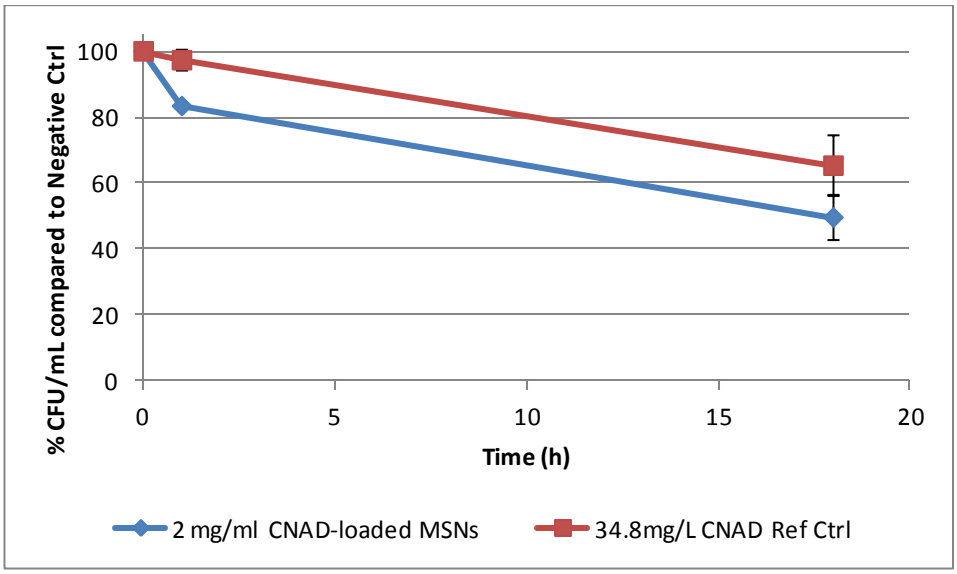


FIGURE 5.8: **Miles and Misra plate count assay after exposing planktonic *E. coli* to various CNAD treatments for 0 h, 1 h, and 18 h. CFU/ml values are expressed as percentages of the negative control. Error bars represent ± SD. Data represents the mean and SD of biological and technical triplicate samples.**

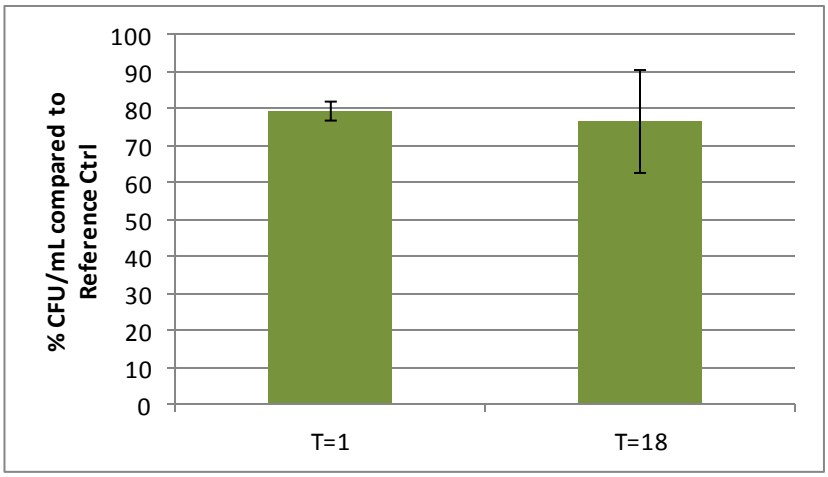


FIGURE 5.9: **Colony counts expressed as CFU/ml obtained from the plate count assay after exposing planktonic *E. coli* to 2 mg/ml CNAD-loaded MSNs for 1 h and 18 h. CFU/ml values are expressed as percentages of the reference control (34.8 mg/L CNAD in free form). Error bars represent ± SD. Data represents the mean and SD of biological and technical triplicate samples.**

As mentioned before the negative control samples experimentally yielded (2.365 ± 0.037) X 10^9 CFU/ml *E. coli* at the 18 h time point. Thus, it can be deduced from present experimental data that the maximum concentration of CNAD-loaded MSNs needed to kill 50% of a suspension consisting of approximately 2.365 X 10^9 CFU/ml planktonic *E. coli* (median lethal concentration (LC_{50})) would be 2 mg/ml.

CNAD entrapment in nanosized vectors made of the synthetic polymer poly(lactide-*co*-glycolic acid) (PLGA) has been reported for the purpose of improving antimicrobial efficiency in food systems (Gomes *et al.*, 2011). Unlike the CNAD-loaded MSNs synthesised and employed in our study, CNAD-loaded PLGA nanoparticles were capsules with a liquid core surrounded by a solid shell. Such CNAD-loaded PLGA nanospheres were able to inhibit Gram-negative (*Salmonella* spp.) and Gram-positive (*Listeria* spp.) at 20 to 10 mg/ml, which were concentrations five to ten times higher than the effective concentration in our study when treating similar amount of bacteria. CNAD release profile from PLGA matrix was similar to that of our present study, showing an initial burst followed by a slower rate of release. Apart from application, synthesis methods, and antimicrobial efficiency achieved, conclusions drawn from Gomes *et al.*, 2011 and our work were aligned, showing that encapsulation of hydrophobic CNAD could improve antimicrobial efficacy.

As with AIT, organic materials such as gum arabic, oleoresins (soft hydrocarbon plant secretions), chitosan, pectin (structural heteropolysaccharide in plant cell walls), maltodextrin, and starches (Brasil, Gomes, Puerta-Gomez, Castell-Perez, & Moreira, 2012; Hill, Gomes, & Taylor, 2013; I. H. Kim *et al.*, 2013; Mantilla, Castell-Perez, Gomes, & Moreira, 2013; Vaidya, Bhosale, & Singhal, 2006; Y. Wang *et al.*, 2013) have been employed as encapsulants for the microencapsulation of CNAD in the context of food preservation and retention/gradual release of cinnamon flavour. These reports differ from our

present work in application (food preservation versus novel anti-biofouling strategy), materials (organic emulsifiers versus inorganic silica), synthesis methods (emulsion microencapsulation versus particle sol-gel synthesis followed by CNAD loading), and size scale (micro versus nano). Of these reports, only three have assessed CNAD-loaded microcapsules for antimicrobial activity (Brasil *et al.*, 2012; Hill *et al.*, 2013; Mantilla *et al.*, 2013). Although all three reported good biocidal efficacy, only one of the three claimed higher antimicrobial efficiency when CNAD was encapsulated rather than in free form (Hill *et al.*, 2013).

5.3.1.3 AIT-treated Bacteria: LIVE/DEAD® *Bac*Light™ Bacterial Viability Staining Assay

In addition to the Miles and Misra plate count method, viability of planktonic *E. coli* cells after various AIT and CNAD treatments were examined using the LIVE/DEAD® *Bac*Light™ bacterial viability stains. As mentioned previously, a calibration curve for Syto® 9 and PI stains was established by analysing green : red fluorescence ratios of *E. coli* suspensions at known viabilities, which yielded a straight line model described by the equation $y = 0.0686x + 0.06981$ with an R^2 value of 0.9974 (Figure 5.4).

After bacterial suspensions were treated with 2 mg/ml and 1 mg/ml AIT-loaded MSNs along with 362.7 mg/L AIT as a reference control over the course of 18 h, percentage of live cells in suspension after each treatment was calculated using the calibration equation. Data was then converted to percentages of the untreated, negative control. Results are presented in Figure 5.10.

At the 1 h time point, 2 mg/ml AIT-loaded MSNs killed a significantly larger fraction of cells than 1 mg/ml AIT-loaded MSNs (by approximately 15%), the reference control (by approximately 40%), and the negative control (by approximately 70%) ($P \leq 0.05$) (Figure

5.10). This directly correlates with the results of the plate count assay (Figure 5.7). Similarly, 1 mg/ml AIT-loaded MSNs at the 1 h time point also yielded significantly lower percentage of live cells as compared to the reference control (by approximately 17%) and the negative control (by approximately 45%) ($P \leq 0.05$) (Figure 5.10). However, this is not fully in line with results obtained from the plate count assay, where 1 mg/ml AIT-loaded MSNs did not kill a significantly larger fraction of planktonic bacteria than the reference control did (Figure 5.7). Apart from the intrinsic variance in sensitivity between the plate count method and the LIVE/DEAD® fluorescent staining, other possible reasons as to why these results did not fully align are further detailed below.

There was no significant difference between the proportions of viable cells remaining as a result of exposure to 2 mg/ml and 1 mg/ml AIT-loaded MSNs for 18 h. At this time point, treatment with 2 mg/ml and 1 mg/ml AIT-loaded MSNs yielded approximately 95% and 85% less live cells than the negative control, respectively. Taking standard error of the data into consideration, both 2 mg/ml and 1 mg/ml AIT-loaded MSNs killed essentially all planktonic *E. coli* in the system. This directly correlates with the results of the plate count assay (Figure 5.7).

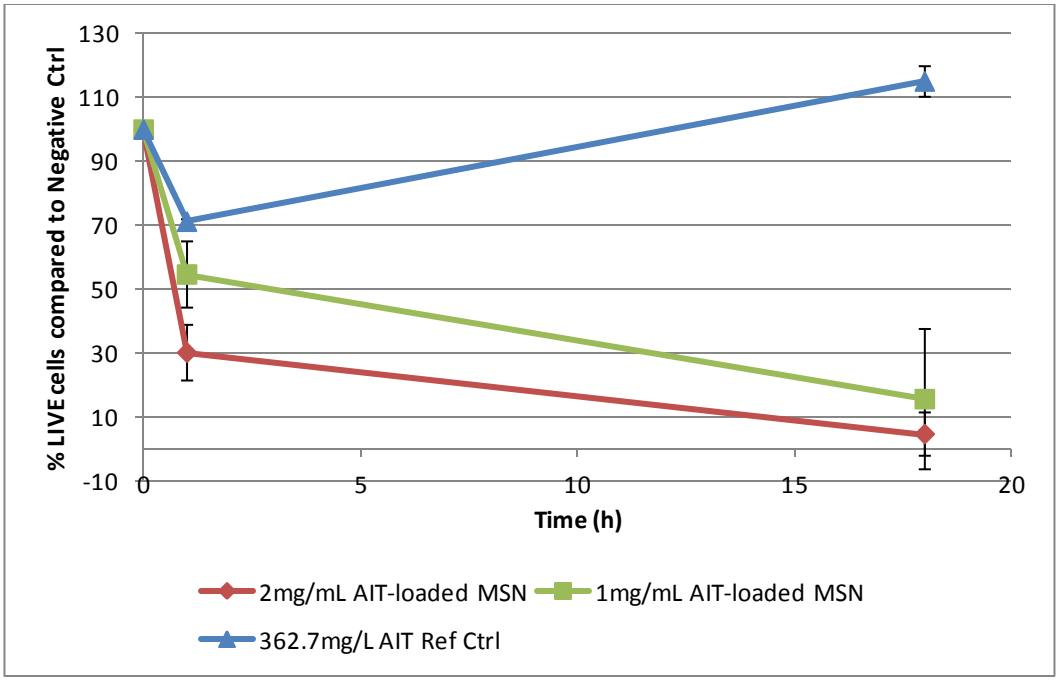


FIGURE 5.10: **LIVE/DEAD® *Bac*Light™ bacterial viability staining assay after exposing planktonic *E. coli* to various AIT treatments for 0 h, 1 h, and 18 h. Percentage of live cells resulting from each treatment are expressed in comparison to the negative control. Error bars represent ± SD. Data represents the mean and SD of biological and technical triplicate samples.**

Treatment with the reference control of 362.7 mg/L AIT yielded interesting results in this assay at the 18 h time point. The ratio of green : red fluorescence obtained in samples treated with 362.7 mg/L AIT for 18 h correlated to viability of approximately 115% as compared to the negative control. Superficially, these results may indicate that 362.7 mg/L AIT stimulated bacterial growth after 18 h of exposure. However, taking supportive data from the plate count assay into account for a more in-depth analysis, 362.7 mg/L AIT did in fact reduce a large fraction of sub-culturable planktonic bacteria as compared to the negative control at this time point. This was not reflected in the LIVE/DEAD® fluorescent staining assay due to several possible reasons.

5.3.1.3.1 Sequestration of PI via Reaction with Isothiocyanates

Firstly, the red-fluorescent PI dye molecules (molecular weight of 668.39 g/mol) (Figure 5.11) used to stain dead bacteria in the LIVE/DEAD® fluorescent staining assay are excellent nucleophiles consisting of iodide ions and primary amine groups that may readily

react with isothiocyanate compounds (ITCs) (Figure 5.11) and their degradation products (Podhradský, Drobnica, & Kristian, 1979). ITCs are unstable in aqueous conditions and prone to reactions with nucleophiles (Podhradský *et al.*, 1979). Of these nucleophilic substitution reactions, ITCs are highly selective for primary amines in other compounds (Hermanson, 2008; Jobbagy & Kiraly, 1966) to form stable thiourea products. This reaction involves attack of the nucleophile on the electrophilic central carbon of the isothiocyanate group, resulting in electron shift and proton loss which creates a thiourea linkage between the ITC and the amine with no leaving group involved (Figure 5.12) (Hermanson, 2008). In addition, iodides present in PI molecules are highly nucleophilic anions that may readily undergo nucleophilic substitution reactions with ITCs and their degradation products as well.

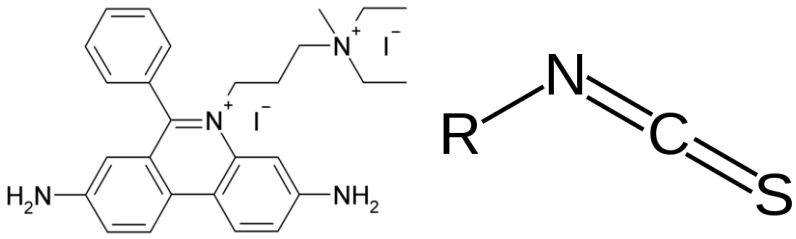


FIGURE 5.11: **Chemical structure of propidium iodide (left) and an isothiocyanate compound (right).**

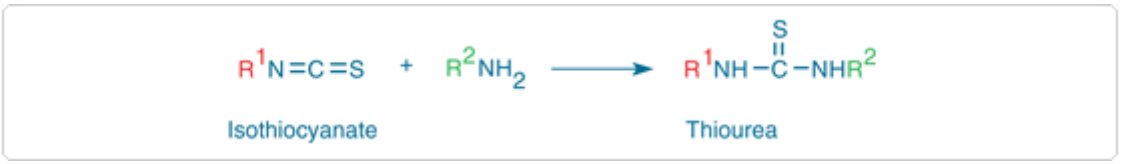


FIGURE 5.12: **Isothiocyanates (ITCs) react with primary amines in other compounds to form stable thiourea products. This reaction involves attack of the nucleophile on the electrophilic central carbon of the isothiocyanate group, resulting in electron shift and proton loss which creates a thiourea linkage between the ITC and the amine with no leaving group involved.**

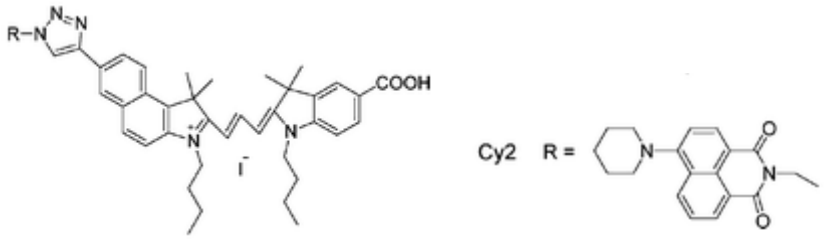


FIGURE 5.13: **Chemical structure of the cyanine dye Cy2. SYTO® 9 is a cyanine dye likely to resemble Cy2 due to their similar excitation/emission wavelengths.**

In the case of 362.7 mg/L AIT treatment, reaction between PI and AIT would sequester PI for conversion into thiourea products, rendering it unavailable for viability staining. In contrast, green-fluorescent SYTO® 9 is a cynanine dye (likely to resemble the closed chain Cy2 dye due to their similar excitation/emission wavelengths, Figure 5.13) that is likely to be unreactive with ITCs. Although the SYTO® 9 molecule does have potentially nucleophilic centres (e.g. areas with nitrogen or oxygen), such possible reactive sites are relatively unavailable from a stereochemical perspective, due to the molecule's large size (molecular weight of 700 – 1100+ g/mol) and complex ring structures. The high probability of PI (and not SYTO® 9) reacting with AIT in the reference control sample is one possible reason that the green : red fluorescence ratio after 18 h of treatment with 362.7 mg/L AIT was skewed since a lower amount of PI than expected was available for staining while the expected amount of SYTO® 9 remained. This erroneous fluorescence ratio would therefore result in false bacterial viability of over 100% as compared to the negative control.

This phenomenon was unlikely to be observed in either of the two AIT-loaded MSN samples. This is because AIT was gradually released from the MSNs in a controlled manner and therefore, only a small amount of AIT was available in solution at any given time point, unlike the 362.7 mg/L AIT reference control where a relatively larger volume of AIT was simultaneously available to undergo reaction with PI during staining. Furthermore, since MSNs protect AIT from degradation while housed inside the mesopores, less degradation

products would have been available in solution to react and to sequester the PI in AIT-loaded MSN samples when compared to the reference control containing free form 362.7 mg/L AIT.

5.3.1.3.2 Artifacts of LIVE/DEAD® Fluorescent Staining: Detection of Green Fluorescence is More Sensitive than Red Fluorescence

Secondly, because binding of SYTO® 9 to double-stranded nucleic acids is cooperative (Molecular Probes® Invitrogen™, 2011), it is more efficient in saturating DNA at low concentrations than PI. Also, SYTO® 9 is cell membrane permeant while PI can only penetrate damaged membranes. Furthermore, the molar absorptivity of SYTO® 9 (extinction coefficient of SYTO® 9 > 50,000 $cm^{-1}M^{-1}$) is over ten-fold greater than that of PI (extinction coefficient of PI = 5,900 $cm^{-1}M^{-1}$) (Molecular Probes® Invitrogen™, 2011) . Collectively, these factors contribute to the detection of green fluorescence, indicating live cells, to be more sensitive than that of red fluorescence, indicating dead cells. Coupled with the likelihood of reaction between PI and AIT, the fluorescence ratio may likely be erroneously biased towards green, therefore resulting in unreliable outcome of bacterial viability being > 100% of the negative control after 18 h of 362.7 mg/L AIT treatment. To a lesser degree, these considerations may also explain why results from the plate count method and LIVE/DEAD® fluorescent staining do not fully correlate for samples treated with 1 mg/ml AIT-loaded MSNs for 1 h, as mentioned above. `

5.3.1.3.3 Viable but Nonculturable State of Bacteria

Although PI sequestration by reaction with AIT and the artifacts of LIVE/DEAD® staining of these particular samples are possible, the most likely and conceivable reason for the unexpected results at 18 h is that a fraction of the planktonic bacteria were damaged to the degree of being viable but nonculturable (VBNC) after exposure to 362.7 mg/L AIT. Bacteria in the VBNC state typically lose culturability on standard growth media and do not divide, yet they remain viable and metabolically active at very low levels (Oliver, 2005; Steck,

2006). It is important to note that the VBNC state differs significantly from the starvation survival state, wherein cells also dramatically decrease in metabolism, but otherwise remain fully culturable (Oliver, 1999). Bacteria become VBNC as a response to environmental stress that might otherwise be lethal if cells did not enter this dormant state, and in the present case this stress was the exposure to 362.7 mg/L AIT for 18 h. Furthermore, it has been well documented that *E. coli* is a bacterial species known to enter the VBNC state (Makino *et al.*, 2000; Oliver, 2005), and that the viability of nonculturable cells can be determined by establishing the presence of intact cytoplasmic membrane using LIVE/DEAD® *Bac*Light™ bacterial viability stains (Breeuwer & Abee, 2000; McFeters, Yu, Pyle, & Stewart, 1995; Oliver, 1993), both of which are relevant factors in present experiments.

Exposure to 362.7 mg/L AIT may have actually induced a portion of planktonic cells to recover and/or proliferate as a bacterial survival tactic between the 1 h and 18 h time point (sub-inhibitory concentrations of antimicrobial agents are often known to activate bacterial defence mechanisms such as increased division and/or biofilm formation (Hoffman *et al.*, 2005; Lopez & Blazquez, 2009), but these newly-generated cells may be in the VBNC state after being stressed. As a result, this population would have tested as being live/viable in the bacterial viability staining assay since their membranes were intact, but at the same time would have indicated as being dead/nonviable in the plate count experiment since they were unable to develop into colonies on culture media. Therefore, the VBNC phenomenon of bacteria is highly possible explanation for the discrepancy in viabilities of the reference control at 18 h observed in the plate count method and the LIVE/DEAD® fluorescent staining assay.

Although dormant, VBNC cells are potentially capable of regaining normal metabolic activity and returning to a culurable state after resuscitation (Oliver, 2005; Steck, 2006). This physiological state of bacteria is better specified as “nonculturable by routinely employed

methods" since VBNC cells can restore their ability to develop into colonies under certain environmental conditions that induce recovery and resuscitation. Based on results of these two complementary bacterial viability tests, it can be deduced that after 18 h, employment of MSNs as a delivery system for AIT successfully killed the exposed planktonic bacteria, whereas free form AIT rendered a large fraction of cells VBNC, which is much less effective in the antimicrobial sense since VBNC cells are able to regain the ability to grow and become virulent once again.

It is very likely that the reasons for the disparity in viabilities of the reference control at 18 h observed between the plate count method and the LIVE/DEAD® fluorescent staining assay are multidimensional (Figure 5.14), comprising of a combination of any and/or all the possible explanations detailed above. Nevertheless, present experiments demonstrated that the use of MSNs as delivery vehicles for AIT significantly enhanced the bacterial lethality as compared to AIT used in free form.

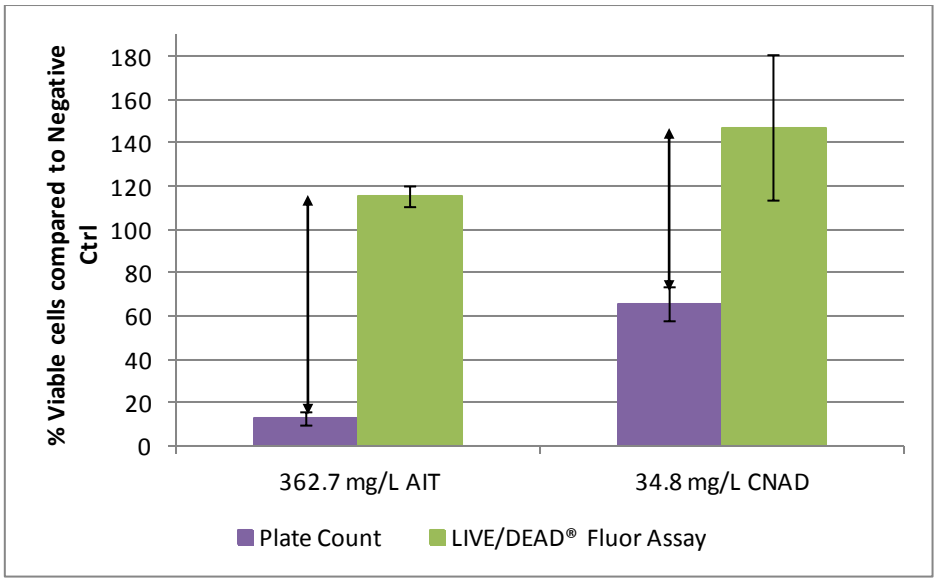


FIGURE 5.14: **Discrepancy in bacterial viabilities obtained from the plate count method and the LIVE/DEAD® fluorescent staining assay for AIT and CNAD reference controls after 18 h of exposure. Disparity between results from the two methods, as indicated by the black arrows, may be due to (i) intrinsic variance in sensitivity between the two viability assays, (ii) PI sequestration, (iii) artifacts of LIVE/DEAD® fluorescent staining, and most importantly (iv) viable but nonculturable (VBNC) state of bacteria.**

5.3.1.4 CNAD-treated Bacteria: LIVE/DEAD® *Bac*Light™ Bacterial Viability Staining Assay

LIVE/DEAD® fluorescent staining was also performed after planktonic *E. coli* was exposed to 2 mg/ml CNAD-loaded MSNs and 34.8 mg/L CNAD as reference control over the course of 18 h. Similar to the case of AIT treatments, percentage of live cells in suspension after each treatment was calculated using the calibration equation. Data was then converted to percentages of the untreated, negative control. Results are presented in Figure 5.15.

At the 1 h time point, 2 mg/ml CNAD-loaded MSNs killed a significantly larger fraction of cells (over 35% in both cases) than both the reference and the negative control respectively ($P \leq 0.05$) (Figure 5.15), which directly correlates with the results of the plate count assay (Figure 5.8). Exposure to 34.8 mg/L CNAD for 1 h did not yield significantly different results as compared to the negative control (Figure 5.15), which also aligns with data from plate count experiments (Figure 5.8).

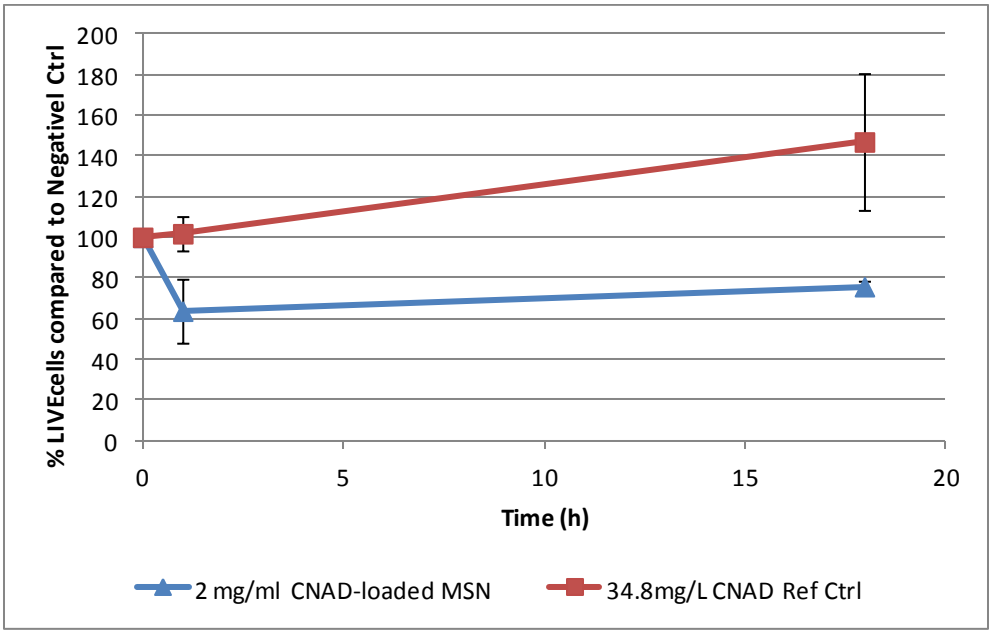


FIGURE 5.15: **LIVE/DEAD® *Bac*Light™ Bacterial Viability Staining assay after exposing planktonic *E. coli* to various CNAD treatments for 0 h, 1 h, and 18 h. Percentage of live cells resulting from each treatment are expressed in comparison to the negative control. Error bars represent ± SD. Data represents the mean and SD of biological and technical triplicate samples.**

There was no significant difference between the proportions of viable cells remaining as a result of exposure to 2 mg/ml CNAD-loaded MSNs for 1 h and 18 h. Treatment with CNAD-loaded MSNs for 1 h and 18 h yielded mean values of approximately 36% and 25% less live cells than the negative control, respectively. Taking into account the standard error of the mean for both time points, CNAD-loaded MSNs did not further reduce planktonic cell viability between 1 and 18 h of exposure, which means that the major portion of lethal activity took place between 0 and 1 h. This is not fully in line with results obtained from the plate count assay, where exposure to 2 mg/ml CNAD-loaded MSNs for 18 h killed a significantly larger fraction of planktonic bacteria as compared to 1 h of exposure (Figure 5.8). Apart from the intrinsic variance in sensitivity between the plate count method and the LIVE/DEAD® staining, other possible reasons as to why these results did not fully align are the same as those detailed above in Sections 5.3.1.3.2 and 5.3.1.3.3.

5.3.1.4.1 Reaction between PI and Aldehydes cause Increased Red Fluorescence

As with PI's propensity to react with isothiocyanates (as explained in Section 5.3.1.3.1), it is also prone to react with aldehydes (Rohr & Kaffenbergerber, 1993). Since PI is a good nucleophile consisting of iodide ions and primary amine groups, it may readily undergo nucelophilic addition with the aldehyde group of the CNAD molecule where the nucleophilic species of the PI molecule would form a new bond with the electrophilic carbon of the aldehyde group (Carey & Giuliano, 2013). It has been reported that immediate reaction of PI with with aldehyde groups occurs when the two species are introduced to each other, causing a sharp increase of fluorescence intensity of PI (Rohr & Kaffenbergerber, 1993). A likely reaction mechanism between PI and an aldehyde-containing molecule is shown in Figure 5.16, where PI (I) reacts with aldehydes via intermediate products to form a modified fluorochrome called azomethine (II). The resulting modified fluorochrome is characterised by

two additional conjugated double bonds, which will cause or contribute to the increase in red fluorescence emission.

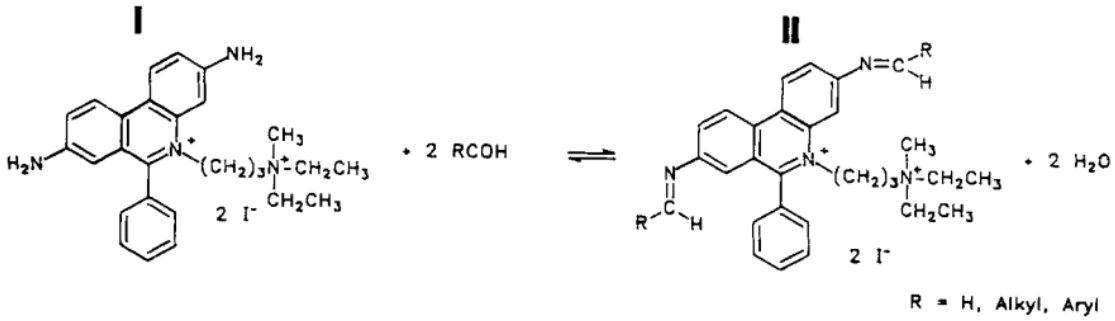


FIGURE 5.16: **Reaction mechanism of PI (I) with aldehyde-containing compounds to form a modified fluorochrome called azomethine (II).**

(Schematic from Rohr, E.L. and Kaffenberger, W., 1993)

In the case of 34.8 mg/L CNAD treatment, reaction between PI and CNAD would increase red fluorescence signal, indicating more dead cells than was actually present. In contrast, green-fluorescent SYTO® 9 is likely to be unreactive with aldehyde groups. As explained previously, although the SYTO® 9 molecule does have potentially nucleophilic centres, such possible reactive sites are relatively unavailable stereochemically due to the molecule's large size (molecular weight of 700 – 1100+ g/mol) and complex ring structures. The high probability of PI (and not SYTO® 9) reacting with CNAD in the reference control sample may contribute to the inaccuracy of green : red fluorescence ratio obtained after 1 h and 18 h of treatment with 34.8 mg/L CNAD. This erroneous fluorescence ratio would therefore result in false bacterial viability biased toward containing a larger amount of dead cells than in actuality. It's important to note that this artifact of increased red fluorescence intensity when PI and CNAD react is the opposite effect hypothesised in the case of PI reacting with AIT, wherein PI is sequestered by AIT and therefore unavailable for staining dead cells. Bacterial viability of cells treated with 34.8 mg/L CNAD for 18 h was reported to be well over 100% (145 ± 33.62%) as compared to the negative control in this assay, but this

figure may even be higher due to the falsely inflated proportion of dead cells reported due to PI modification via reaction with CNAD.

This phenomenon was unlikely to be observed in the CNAD-loaded MSN samples. This is because CNAD was gradually released from the MSNs in a controlled manner and therefore, only a very small amount of CNAD was available in solution at any given time point. Therefore, unlike the reference control where the entire amount of 34.8 mg/L CNAD was available all at once to undergo reaction with PI during staining, only small concentrations of CNAD were available at any given moment, and that small amount was unlikely to have remained in solution long enough for PI to react with it due to CNAD's high volatility (especially in such low amounts).

5.3.1.4 LIVE/DEAD® CNAD (Continued)

Treatment with the reference control yielded interesting results in this assay at the 18 h time point. The ratio of green : red fluorescence obtained in samples treated with 34.8 mg/L CNAD for 18 h correlated to mean viability of approximately 145% of the negative control. These results may indicate that 34.8 mg/L CNAD stimulated bacterial growth after 18 h of exposure, especially since this treatment yielded bacterial viability that was quite significantly above 100% as compared to the negative control ($P \leq 0.05$). It is important to note that the probability of induced bacterial growth as a result of exposure to 34.8 mg/L CNAD for 18 h is higher than that of 18 h treatment with 362.7 mg/L AIT for two reasons. Firstly, sub-inhibitory concentrations of antimicrobial agents are often known to activate bacterial defence mechanisms such as increased growth (Lopez & Blazquez, 2009). In this case, 34.8 mg/L of CNAD is considered a low and sub-inhibitory amount since it is less than half the MIC and MBC of CNAD against planktonic *E. coli*, whereas 362.7 mg/L AIT is not a sub-inhibitory concentration since it more than twice the MIC and MBC of AIT (Chapter 2,

Table 2.3). These concentrations of the two plant compounds were selected as reference controls because they correlated to the experimentally-established maximum concentration detected as a result of being released from 2 mg/ml of loaded MSNs (Chapter 4).

Secondly, the disparity in bacterial viability between the negative control and treatment with 34.8 g/L CNAD for 18 h (145 ± 33.62% live cells as compared to negative control) was significantly greater than the discrepancy resulting from the negative control and 18 h exposure to 362.7 mg/L AIT (115.02 ± 4.78% live cells as compared to negative control). The effect that the artifacts of LIVE/DEAD® staining had on distorting bacterial viability in this assay was only limited. Also, possible chemical reaction between PI and CNAD may have even deflated the percent live cells reported. Because of this significant difference in viability between 34.8 mg/L CNAD and the negative control at 18 h, it is likely that the major contributing factor was in fact induced growth.

In contrast, similar to the case with treatment of 362.7 mg/L AIT, data from the plate count assay indicate that 34.8 mg/L CNAD did in fact reduce a large fraction of sub-culturable planktonic bacteria as compared to the negative control at 18 h. By cross referencing results from this fluorescent staining assay with those of the plate count experiments (Figure 5.8), it can be deduced that a large fraction of planktonic cells that proliferated in the 34.8 mg/L CNAD reference control were in the VBNC state after 18 h.

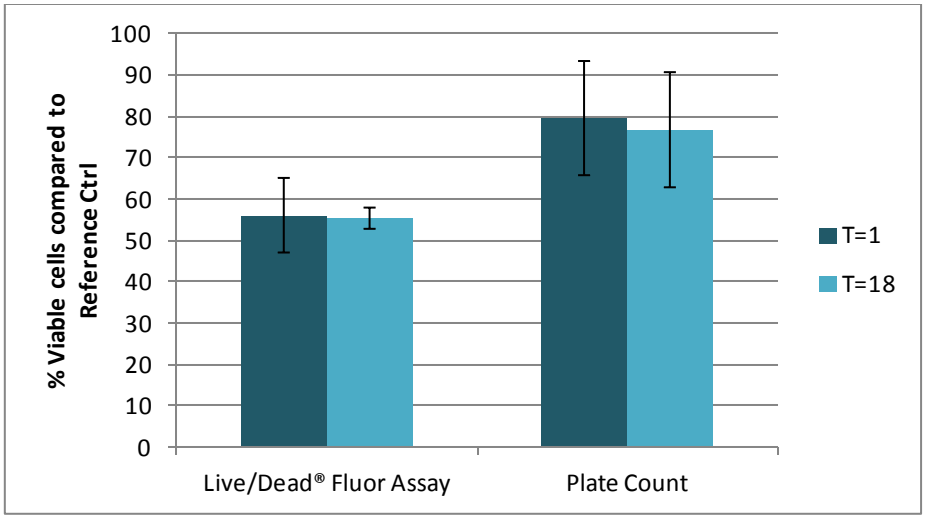


FIGURE 5.17: **Bacterial viabilities obtained from the LIVE/DEAD® fluorescent staining assay and the plate count assay after exposing planktonic *E. coli* to 2 mg/ml CNAD-loaded MSNs for 1 h and 18 h. Values are expressed as percentages of the reference control (34.8 mg/L CNAD in free form). Error bars represent ± SD. Data represents the mean and SD of biological and technical triplicate samples.**

When compared to CNAD in free form, it appears that the employment of MSNs as a delivery vehicle for CNAD significantly enhanced its antibacterial efficiency during the first hour of exposure. From 1 to 18 h, on the other hand, CNAD-loaded MSNS and CNAD in free form exhibited the same rate of bacterial inhibition. This is exactly in line with results from the plate count method (Figure 5.8). The slopes (m) in Figure 5.15 depicting bacterial viabilities at different time points reflect the rate of change (reduction or increase) in viability over time as result of various CNAD treatments. From the 1 h to 18 h time point, 34.8 mg/L CNAD and 2 mg/ml CNAD-loaded MSNs produced similar slopes, yielding m = 2.65 for 34.8 mg/L CNAD and m = 0.71 for 2 mg/ml CNAD-loaded MSNs. This indicates that both treatments impacted viability at similar rates during this time. The same conclusion can be drawn from a different perspective of the same data, which is presented in Figure 5.17. Instead of normalising to the negative control, bacterial viabilities resulting from 2 mg/ml CNAD-loaded MSNs were normalised to the 34.8 mg/L CNAD reference control. From this data, no significant difference was observed between the percentages of viability at 1 h and 18 h for both the plate count assay (79.56% of reference control at 1 h, 76.75% at 18 h) and the LIVE/DEAD® fluorescent staining assay (56.07% of reference control at 1 h, 55.34% at

18 h), which means that the degree to which the employment of MSNs improved CNAD's antibacterial activity as compared to the use of it in free form remained the same at 1 h and 18 h. Therefore, as corroborated by two bacterial viability assays, it can be concluded that 2 mg/ml CNAD-loaded MSNs and 34.8 mg/L CNAD exhibited similar antibacterial efficiencies from 1 h to 18 h. As mentioned before, it is important to note that because data was not collected at any other intermediate time points between 1 h and 18 h, it cannot be concluded that the rate of kill between 2 mg/ml CNAD-loaded MSNs and 34.8 mg/L CNAD in free form became congruous precisely at the 1 h time point.

5.3.1.5 TEM Images of *E. coli* Treated with AIT- and CNAD-loaded MSNs

Planktonic *E. coli* treated with AIT- and CNAD-loaded MSNs, along with empty MSNs (vehicle control) and no treatment (negative control), were imaged with bright field TEM; resulting images are displayed in Figures 5.18 and 5.20, respectively. As expected, the negative controls (Figure 5.18) show healthy, rod-shaped bacteria undergoing asexual reproduction and cell division (binary fission) in some cases (Campbell *et al.*, 2008a, 2008e).

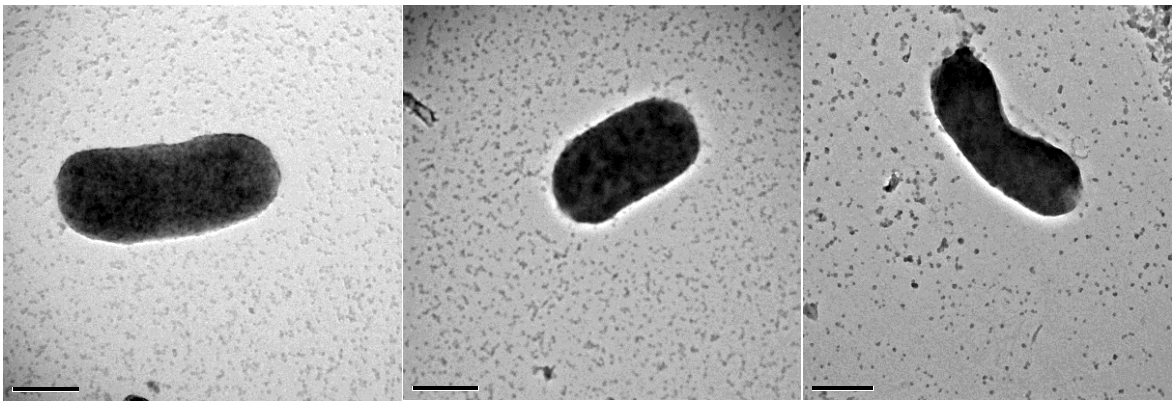


FIGURE 5.18: **TEM images of planktonic *E. coli* (negative control). One representative image was chosen from each triplicated sample. Scale bars represent 0.2 µm.**



FIGURE 5.19: **Representative TEM image of *E. coli* undergoing binary fission.**

(Image from Dr. Karl J. Roberts' Lecture and Laboratory Notes on Microbiology, Prince George's Community College; available at http://academic.pgcc.edu/~kroberts/Lecture/Chapter%206/fission.html)

Treatment with unloaded MSNs also yielded healthy cells in bacillus morphology (Figure 5.20), but bacteria appeared slightly larger and relatively more spherical rather than elongated as compared to those in the negative control, likely a bacterial reaction induced by the presence of foreign but nontoxic objects in the media (empty MSNs). Also, cells did not appear to be dividing after this treatment, unlike cells in the negative controls.

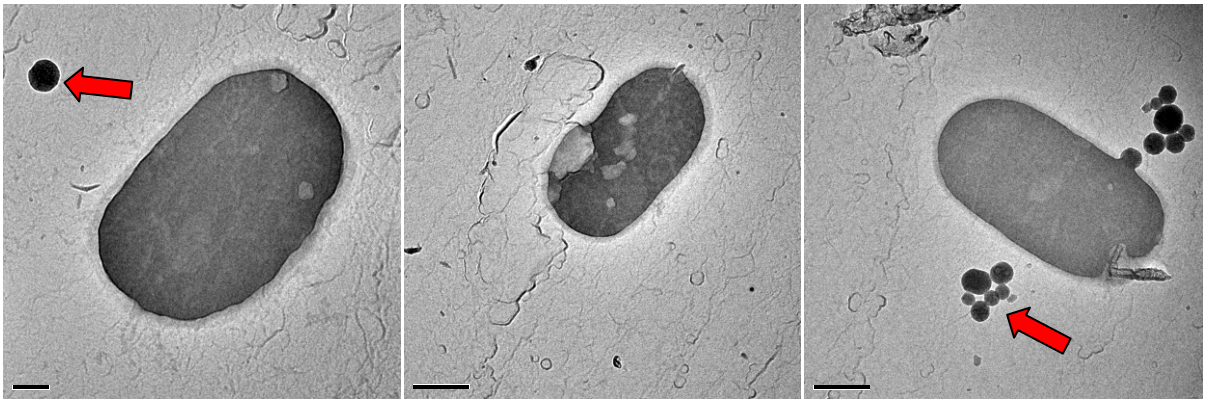


FIGURE 5.20: **TEM images of planktonic *E. coli* exposed to 2 mg/ml empty MSNs (vehicle control). One representative image was chosen from each triplicated sample. Red arrows indicate empty MSNs. Scale bars represent 0.2 µm.**

E. coli treated with 2 mg/ml AIT- and CNAD-loaded MSNs appeared stressed and flaccid (Figures 5.21 and 5.22) when compared to healthy bacteria in the negative controls. These cells were likely experiencing plasmolysis, a phenomenon where the cytoplasmic membrane shrinks and pulls away from the cell wall due to loss of water from inside the cell (Figure 5.23). Halo-like shadows surrounding the shrunken cytoplasm, which is probably the

bacterial cell wall, can be seen in Figures 5.21 and 5.22. Typically, turgor pressure exists on the interior of a bacterial cell, which is caused by osmotic flow of water from outside into the cell since there is higher solute concentration intracellularly due to active transport (Abedon, 1998; Campbell *et al.*, 2008c). Plasmolysis occurs when bacteria are in a hypertonic environment, wherein water exits the cell via osmosis and turgor pressure is lost to the degree where the cytoplasm peels away from the cell wall (Figure 5.23) (Abedon, 1998; Voet, Voet, & Pratt, 2001). Eventually, plasmolysis can lead to the complete collapse of the cell wall (cytorrhysis) and subsequent cell death (Campbell *et al.*, 2008c; Voet *et al.*, 2001), which is likely the case in these *E. coli* suspensions treated with AIT- and CNAD-loaded MSNs.

From these TEM images, there was no endocytosis of the MSNs or any specific association between the nanoparticles and the cells. The MSNs seemed to act solely as a delivery vehicle, delivering and unloading the plant compounds without entering the cells.

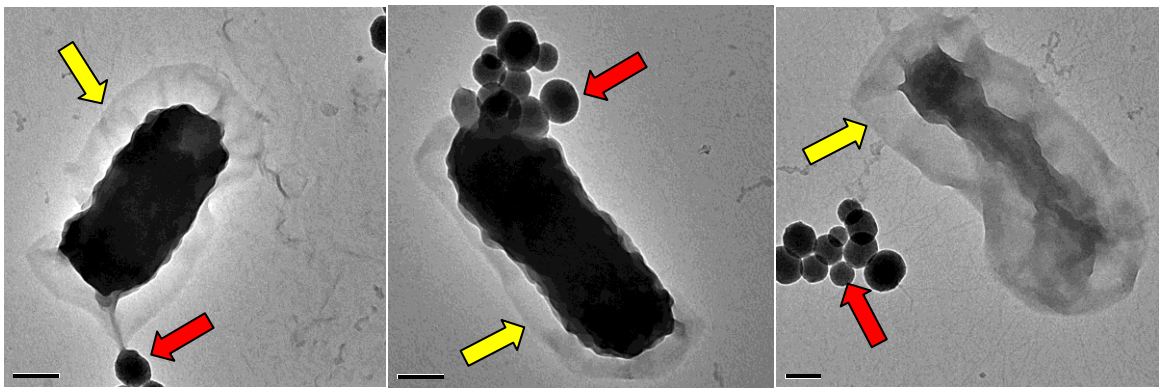


FIGURE 5.21: **TEM images of planktonic *E. coli* exposed to 2 mg/ml AIT-loaded MSNs. One representative image was chosen from each triplicated sample. Red arrows indicate MSNs; yellow arrows indicate cell walls from which the cytoplasm has shrunken away from. Scale bars represent 0.2 µm.**

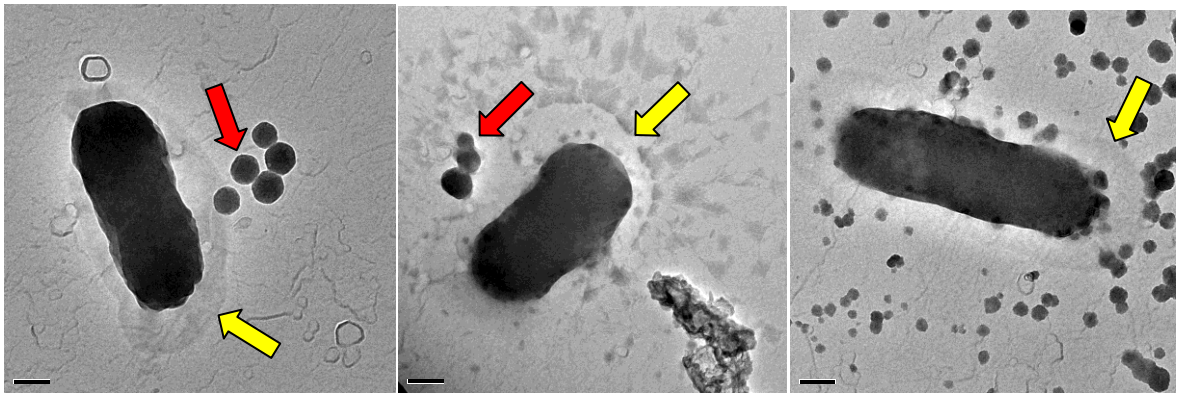


FIGURE 5.22: **TEM images of planktonic *E. coli* exposed to 2 mg/ml CNAD-loaded MSNs. One representative image was chosen from each triplicated sample. Red arrows indicate MSNs; yellow arrows indicate cell walls from which the cytoplasm has shrunken away from. Scale bars represent 0.2 µm.**

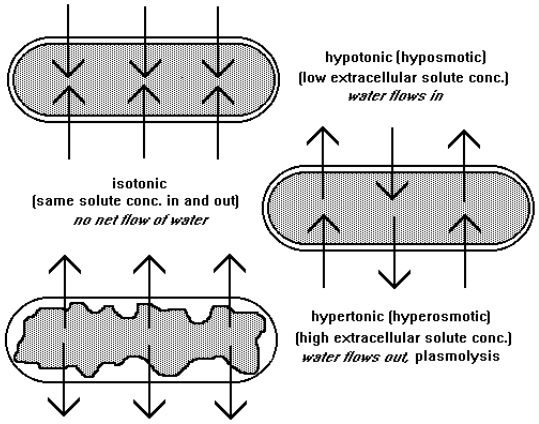


FIGURE 5.23: **Schematic of the movement of water in and out of bacterial cells by osmosis. Plasmolysis occurs in hypertonic environments, causing water to exit the cell and cytoplasm to shrink away from the cell wall.**

(Schematic from Dr. Stephen T. Abedon's Lecture Notes on Microbiology, Ohio State University; available at http://www.mansfield.ohio-state.edu/~sabedon/biol1080.htm)

5.3.2 Biofilm Bacteria

5.3.2.1 Biofilm Formation/Adherence Assay

Results from the biofilm formation and adherence assay using crystal violet are presented in Figure 5.24. Relative biofilm development in treated samples is expressed as percentages of the negative control. There were no significant differences between the four highest concentrations of AIT tested (312.5, 625, 1250, and 2500 mg/L); in the case of CNAD, the same was true for the three highest concentrations evaluated (625, 1250, and

2500 mg/L). Since there were no significant improvements in activity beyond 312.5 mg/L for AIT, it can be deduced that 312.5 mg/L AIT yielded maximum anti-biofilm-forming activity, resulting in > 80% reduction in biofilm biomass development as compared to untreated negative controls. The same inference can be drawn for CNAD at 625 mg/L; no significant decrease in biofilm generation was observed at concentrations above 625 mg/L CNAD, and thus it can be inferred that CNAD at ≥ 625 mg/L yielded maximum inhibitory activity, causing > 80% reduction in biofilm formation as compared to positive controls.

No significant differences between the anti-biofilm-forming effects between the two different compounds were detected at concentrations ranging from 625 to 2500 mg/L. Based on present experimental data, it can be extrapolated that AIT and CNAD at concentrations ≥ 625 mg/L would inhibit biofilm formation with similar efficacies.

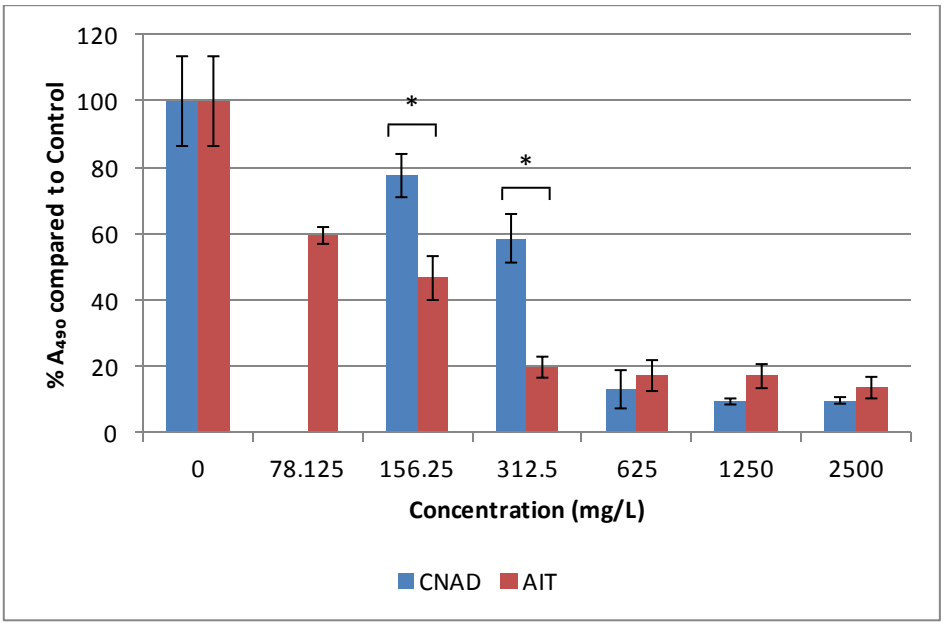


***FIGURE 5.24*: Effects of AIT and CNAD on *P. aeruginosa* biofilm formation in 24 h. Relative biofilm development in treated samples are expressed as percentages of the negative control. Data for 78.125 mg/L CNAD are intentionally unavailable because assay was not performed at this concentration. Error bars represent ± SD. Asterisks (*) denote significant difference ($P \leq 0.05$). The data represents the mean and SD of two independent experiments performed three times, with eight technical replicates for each concentration of AIT and CNAD per experiment.**

Observable differences in the ability to inhibit biofilm formation occurred at 312.5 and 156.25 mg/L between the two plant compounds. At 312.5 mg/L, AIT was significantly

more effective in decreasing the occurrence of biofilm biomass than CNAD at the same concentration ($P \leq 0.05$) by approximately two-fold. Similarly, 156.25 mg/L AIT significantly stunted biofilm formation more effectively than 156.25 mg/L CNAD ($P \leq 0.05$) by over two-fold. Although the two compounds differ in molecular weight, AIT would still be more efficacious in inhibiting biofilm development than CNAD from an equal molar basis if concentrations were converted to molar values (molar mass: 99.15 g/mol for AIT, 132.16 g/mol for CNAD).

AIT at 312.5 mg/L was equally as effective in disrupting biofilm formation as 2500 mg/L AIT, a concentration 8X 312.5 mg/L. In contrast, 312.5 mg/L CNAD inhibited biofilm development approximately five times less effectively than 625 mg/L CNAD, a concentration 2X 312.5 mg/L.

The lowest concentration of AIT resulting in significant disparity of biofilm development occurred between 312.5 mg/L and 156.25 mg/L; as for CNAD, this occurred between 625 mg/L and 312.5 mg/L, which is one dilution step less than that of AIT. Furthermore, experimental data suggests that the median lethal concentration (LC_{50}) of AIT was approximately 156.25 mg/L, reducing biofilm biomass by 53.36%, whereas the LC_{50} of CNAD was closer to 312.5 mg/L, reducing biofilm biomass by 42.37% (at 156.25 mg/L, CNAD reduced 22.46%). In fact, 78.125 mg/L AIT stunted biofilm formation with the same efficacy as 312.5 mg/L CNAD did (reducing biofilm biomass by approximately 40% in both cases) even though the concentration of CNAD employed was 4X that of AIT. The results from this assay collectively suggest AIT was more efficacious in inhibiting biofilm formation and adherence than CNAD.

Only one report has been published regarding the assessment of the effects of AIT on biofilm formation and inhibition of preformed biofilm (Zou, Woo, & Ahn, 2012). In that

study, biofilm forming ability and associated gene expression patterns of Gram-negative *Salmonella* Typhimurium exposed to a sublethal concentration of AIT (0.69 mg/ml) were characterised. Zou, *et al.*, 2012, reported the MIC of AIT against planktonic *S.* Typhimurium was found to be 1.28 mg/ml (MIC of AIT against Gram-negative *E. coli* and *P. aeruginosa* was found to be 156.25 mg/L for both species in our present work (Chapter 2, Section 2.3.2)) and concluded that sublethal concentration of AIT did not accelerate cellular and molecular mechanisms of biofilm formation (Zou *et al.*, 2012). This study differed from our present work in two major aspects: 1) target bacteria (*S.* Typhimurium versus *P. aeruginosa*) and 2) objectives (to characterise cellular, molecular, physicochemical, and gene expression properties of bacteria upon exposure to AIT versus assessment of antimicrobial efficacy of AIT delivered in free form and entrapped in MSNs).

More reports regarding the antimicrobial activity of CNAD against biofilms have been published than that of AIT, typically revolving applications such as food preservation and food-borne pathogen control (de Oliveira, Brugnera, do Nascimento, Batista, & Piccoli, 2012; Nostro *et al.*, 2012; Upadhyay, Upadhyaya, Kollanoor-Johny, & Venkitanarayanan, 2013), disease and infection control (Amalaradjou, Narayanan, Baskaran, & Venkitanarayanan, 2010; Jia, Xue, Duan, & Shao, 2011; Nuryastuti *et al.*, 2009), and exploration of CNAD's effects on gene expression and quorum sensing ability (Brackman, Cos, Maes, Nelis, & Coenye, 2011; Jia *et al.*, 2011). Reports with biomedical applications focused mainly on preventing biofilm formation on indwelling medical devices such as catheters and implants (Nuryastuti *et al.*, 2009; Zodrow, Schiffman, & Elimelech, 2012). Some previous reports have assessed anti-biofilm activity of CNAD when applied on surfaces of specific material (e.g. stainless steel, urinary catheters) (de Oliveira *et al.*, 2012) and when incorporated in polymeric (polyethylene-co-vinylacetate) films for food packaging (Nostro *et al.*, 2012) or poly(lactic-*co*-glycolic acid) (PLGA) films for infectious disease prevention

(Zodrow *et al.*, 2012). Although target applications and target species (from yeast to pathogenic/non-pathogenic Gram-positive and Gram-negative bacteria) differ from study to study, all published works reported good efficacy against biofilm formation and/or against preformed biofilm, which correlates to findings from our present study.

5.3.2.2 Detachment and Viability of 48 h-Old Biofilms (CLSM)

The effects of various AIT and CNAD treatments on pre-existing, 48 h-old biofilms were studied using CLSM after treated samples were stained with LIVE/DEAD® *Bac*Light™ Bacterial Viability Stain. Maximum intensity projections of CLSM stack images are presented in Figures 5.26 to 5.31. Scale bars in all images are 10 µm. Images are 76.8 x 76.8 µm in *x* and *y* axes with variable *z* (indicated for each image stack and in Figure 5.25) since the thickness of each biofilm differed from one another due to the intrinsic variance between biological samples and the different types of treatment each biofilm was subjected to.

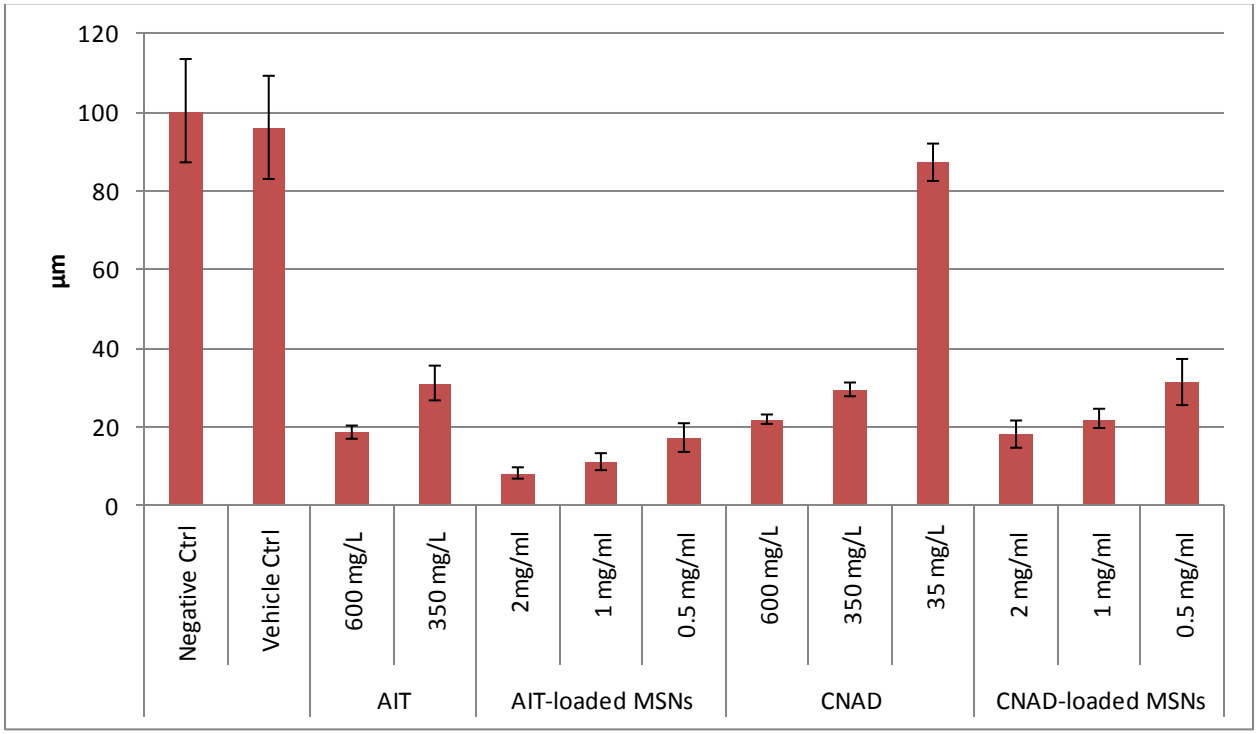


FIGURE 5.25: **Thickness of 48 h-old *P. aeruginosa* biofilms (*z* axis of 3D CLSM image stacks) resulting from various treatments for 24 h. Error bars represent ± SD. The data represents the mean and SD of images from four independent imaging sessions, each session consisting of three biological replicates, with each replicate imaged at three different locations of the biofilm (at the least).**

There was no observable difference between the negative control samples and the vehicle control samples (24 h treatment with 2 mg/ml empty MSNs); both control samples were highly viable, as indicated by the dense green fluorescence signals with hardly any red fluorescence signals in Figures 5.26 A to D with 5.27 A to D, with mean biofilm thickness of 100.25 ± 13.13 µm for the negative control and 96 ± 13.12 µm for the vehicle control. Empty, unloaded MSNs had negligible effect on preformed *P. aeruginosa* biofilms.

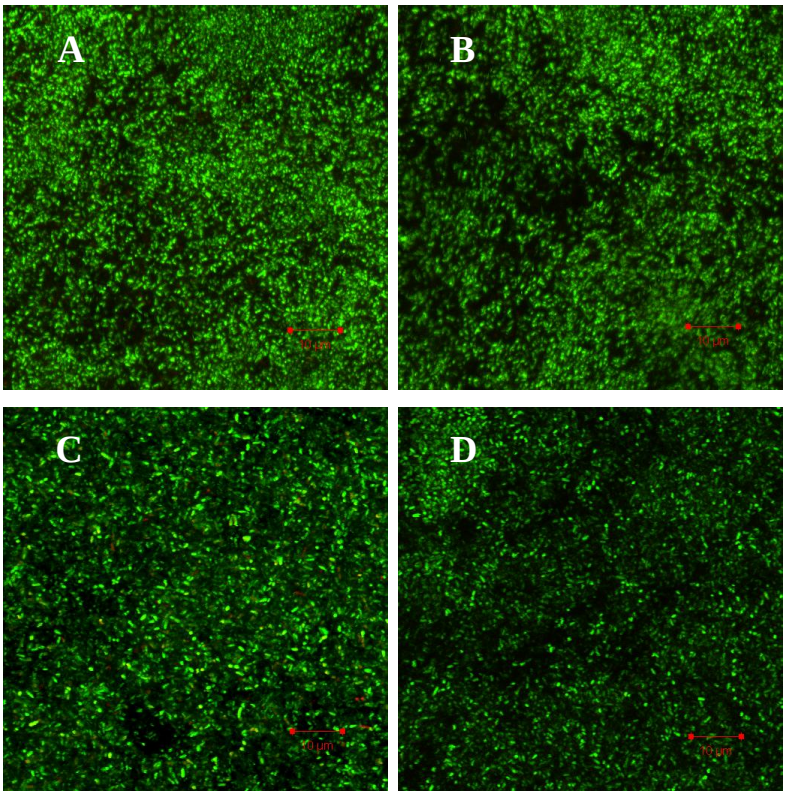


FIGURE 5.26 (A TO D): **Maximum intensity projections of CLSM image stacks of negative control *P. aeruginosa* biofilms grown for 72 h at 30˚C in 2 ml 10% TSB in PBS, stained directly prior to CLSM with LIVE/DEAD® *Bac*Light™ Bacterial Viability Stain (SYTO® 9, green = live cells, PI, red = dead cells). One representative image was chosen from each of four independent imaging sessions, each session consisting of three biological replicates, with each replicate imaged at three different locations of the biofilm (at the least). Thickness of biofilm in *z* axis (µm): A= 98, B = 83, C = 113.5, and D = 106.5, Scale bar 10 µm in all CLSM images presented in this chapter.**

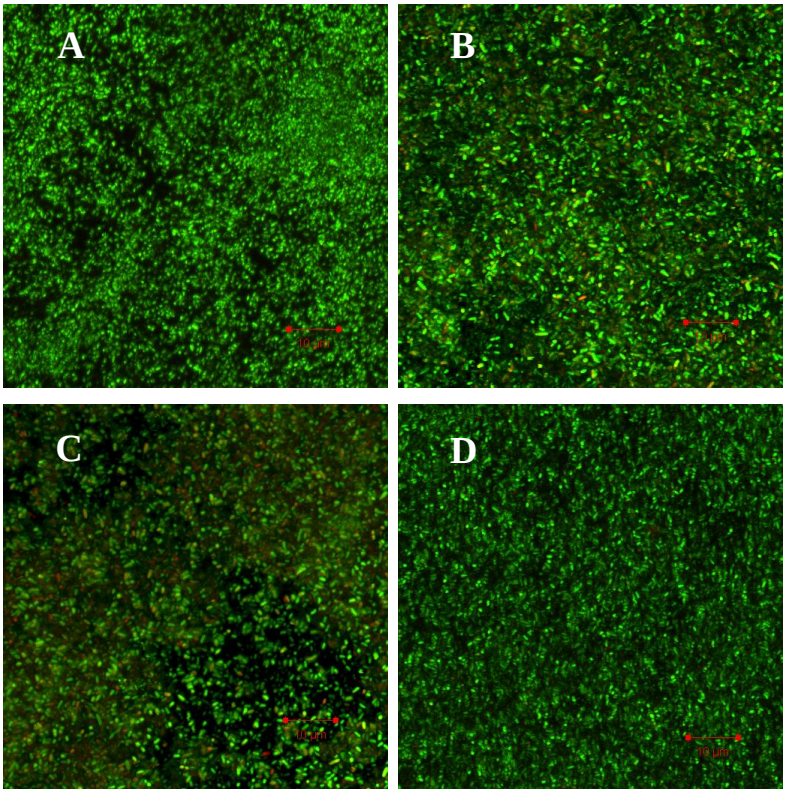


FIGURE 5.27 (A TO D): **Maximum intensity projections of CLSM image stacks of 48 h-old vehicle control *P. aeruginosa* biofilms treated for 24 h with 2 mg/ml empty/unloaded MSNs, stained directly prior to CLSM with LIVE/DEAD® Viability Stain (SYTO® 9, green = live cells, PI, red = dead cells). One representative image was chosen from each of four independent imaging sessions, each session consisting of three biological replicates, with each replicate imaged at three different locations of the biofilm (at the least). Thickness of biofilm in *z* axis (µm): A= 115.5, B = 87, C = 90.5, and D = 91.**

P. aeruginosa biofilms were subjected various treatments listed in Table 5.2 (presented again below) for 24 h. Both AIT and CNAD at concentration of 600 mg/L were selected because results from the biofilm formation and adherence assay (Section 5.3.2.1) indicate that 625 mg/L of both compounds (approximated to 600 mg/L in CLSM experiments here) yielded maximum anti-biofilm-forming activity, resulting in > 80% reduction in biofilm biomass development as compared to untreated negative controls (Figure 5.25). Furthermore, in order to compare the anti-biofilm efficacies of the two plant compounds in free form versus encapsulated in MSNs, biofilms were treated with 350 mg/L AIT, 350 mg/L CNAD, and 35 mg/L CNAD since 362.7 mg/L AIT and 34.8 mg/L CNAD were the experimentally-established maximum concentrations detected as a result of being released from 2 mg/ml of loaded MSNs (Chapter 4). Concentration of 362.7 mg/L AIT and 34.8 mg/L CNAD were

approximated to 350 mg/L AIT and 35 mg/L CNAD, respectively. Additionally, 350 mg/L CNAD was also included in order to directly compare the anti-biofilm efficacies of the two compounds when used at the same concentration.

TABLE 5.2: **Various treatments that preformed biofilms were subjected to prior to CLSM imaging.**

TREATMENT			
AIT	AIT-LOADED MSNS	CNAD	CNAD-LOADED MSNS
600 mg/L	2 mg/ml	600 mg/L	2 mg/ml
350 mg/L	1 mg/ml	350 mg/L	1 mg/ml
	0.5 mg/ml	35 mg/L	0.5 mg/ml

5.3.2.2.1 AIT Treatment

Treatment with 600 mg/L and 350 mg/L AIT significantly reduced the viability (compare Figures 5.28 A to H with 5.26 A to D) and thickness of the biofilms as compared to the negative controls ($P \leq 0.05$), resulting in mean *z* axis values of 18.5 ± 1.63 μm and 31 ± 4.42 μm, respectively (Figure 5.25). Treatment with 600 mg/L AIT not only dramatically reduced the number of bacteria present in the biofilm, as indicated by the relatively sparse signals of green fluorescence in Figures 5.28 A to D, but also killed a large portion of the remaining bacteria, as indicated by the abundance of red fluorescence signals in those same images. Treatment with 350 mg/L AIT resulted in thicker, denser biofilms with more constituent bacteria as compared to 600 mg/L treatment (compared Figures 5.28 E to H with A to D); thus, 350 mg/L AIT was significantly less effective than 600 mg/L AIT in removing and killing bacterial biofilms. As compared to the negative controls (compared Figures 5.28 E to H with 5.26 A to D), 350 mg/L AIT removed a significant amount of biofilm cells and effectively killed a portion of the adherent bacteria (indicated by the presence and abundance of red fluorescence signals), which shows that although not as efficient as 600 mg/L AIT, 350 mg/L AIT treatment was effective in dissociating and killing biofilms.

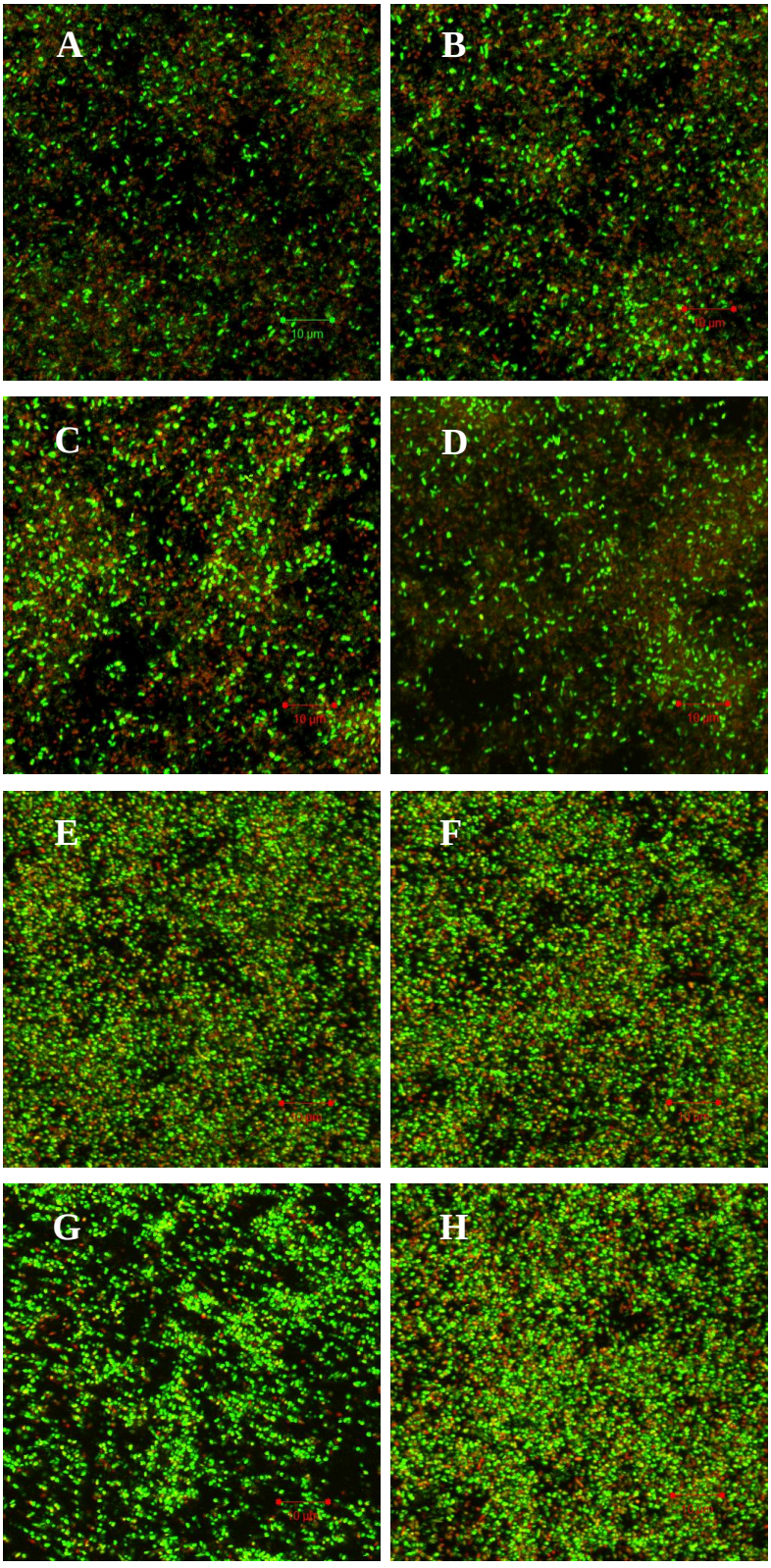


FIGURE 5.28 (A TO H): **Maximum intensity projections of CLSM image stacks of 48 h-old *P. aeruginosa* biofilms treated for 24 h with 2 ml of 600 mg/L AIT (A to D) and 350 mg/L AIT (E to H), stained with LIVE/DEAD® Viability Stain (SYTO® 9, green = live cells, PI, red = dead cells). One representative image was chosen from each of four independent imaging sessions, each session consisting of three biological replicates, with each replicate imaged at three different locations of the biofilm (at the least). Thickness of biofilm in *z* axis (µm): A= 20.5, B = 16.5, C = 19, D = 18, E = 36.5, F = 29.5, G = 26, and H = 32.**

Treatment with 2 mg/ml, 1 mg/ml, and 0.5 mg/ml AIT-loaded MSNs (Figures 5.29 A to L) significantly reduced the thickness and the amount of constituent bacteria of the biofilms as compared to the negative controls (Figures 5.26 A to D), the vehicle controls (Figures 5.27 A to D), as well as samples exposed to 600 mg/L and 350 mg/L AIT (Figures 5.28 A to H) ($P \leq 0.05$), resulting in mean *z* axis values of 8.125 ± 1.44 µm, 11 ± 2.16 µm, and 17.125 ± 3.65 µm, respectively (Figure 5.25). Two mg/ml AIT-loaded MSNs yielded the thinnest and the least bacterially dense biofilms of all AIT-treated samples. Biofilms treated with 1 mg/ml AIT-loaded MSNs were denser with bacteria and more viable cells than those treated with 2 mg/ml AIT-loaded MSNs (compared Figures 5.29 E to H with 5.29 A to D), and the same is the case for 0.5 mg/ml AIT-loaded MSNs (Figures 5.29 I to L) compared with the other two aforementioned concentrations of AIT-loaded MSNs (Figures 5.29 A to H). The remaining biofilm bacteria in samples treated with AIT-loaded MSNs at any concentration were mostly viable with a small fraction of residual dead cells, as indicated by the presence of red fluorescence.

It is important to note that color is a function of the human visual system, and each colour has an intrinsic luminance or visually perceived brightness normalised to the standard of white light (Poynton, 2003). It may be more difficult to perceive red fluorescence than green fluorescence in the CLSM images presented here because the colour green is ~ 90% of white light, whereas red is ~ 30% of white light. This means that the colour red is humanly perceived to be "dimmer" or "murkier" than the colour green in dark field images (Poynton, 2003) and therefore, it may appear that the abundance of green fluorescence signal is higher than that of red fluorescence signal even if the two signals are equal.

Additionally, because binding of SYTO® 9 (green fluorescence) to nucleic acids is cooperative (Molecular Probes® Invitrogen™, 2011), it is more efficient in saturating DNA at low concentrations than PI (red fluorescence). Furthermore, the molar absorptivity of SYTO®

9 (extinction coefficient of SYTO® 9 > 50,000 $cm^{-1}M^{-1}$) is over ten-fold greater than that of PI (extinction coefficient of PI = 5,900 $cm^{-1}M^{-1}$) (Molecular Probes® Invitrogen™, 2011). Together, these two factors contribute to the detection of green fluorescence to be more sensitive than that of red fluorescence.

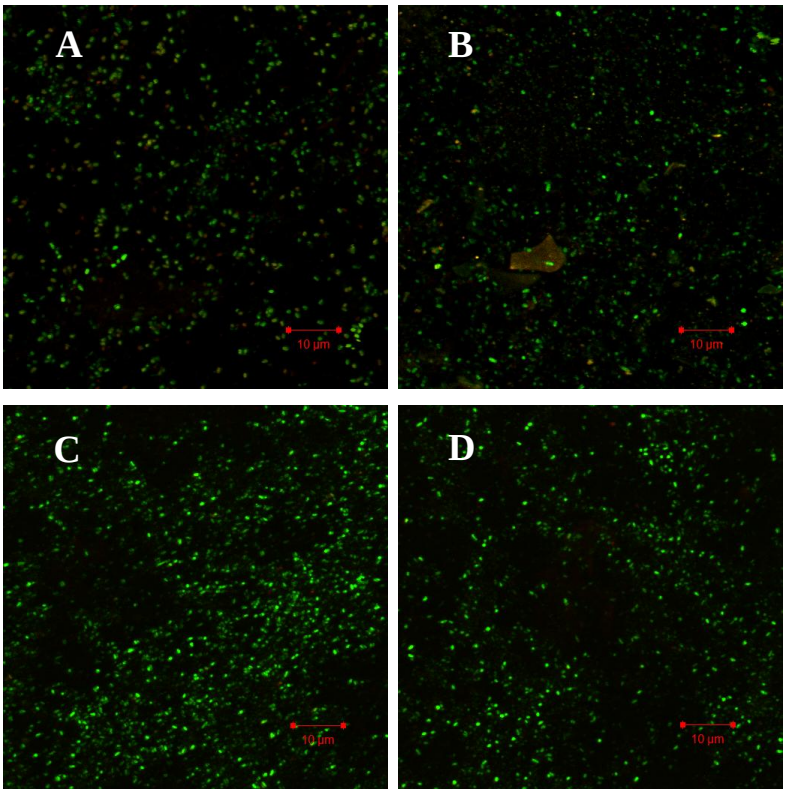


FIGURE 5.29 (A TO D): **Maximum intensity projections of CLSM image stacks of 48 h-old *P. aeruginosa* biofilms treated for 24 h with 2 ml of 2 mg/ml AIT-loaded MSNs, stained with LIVE/DEAD® Viability Stain (SYTO® 9, green = live cells, PI, red = dead cells). One representative image was chosen from each of four independent imaging sessions, each session consisting of three biological replicates, with each replicate imaged at three different locations of the biofilm (at the least). Thickness of biofilm in *z* axis (µm): A= 8.5, B = 7, C = 10, D = 7.**

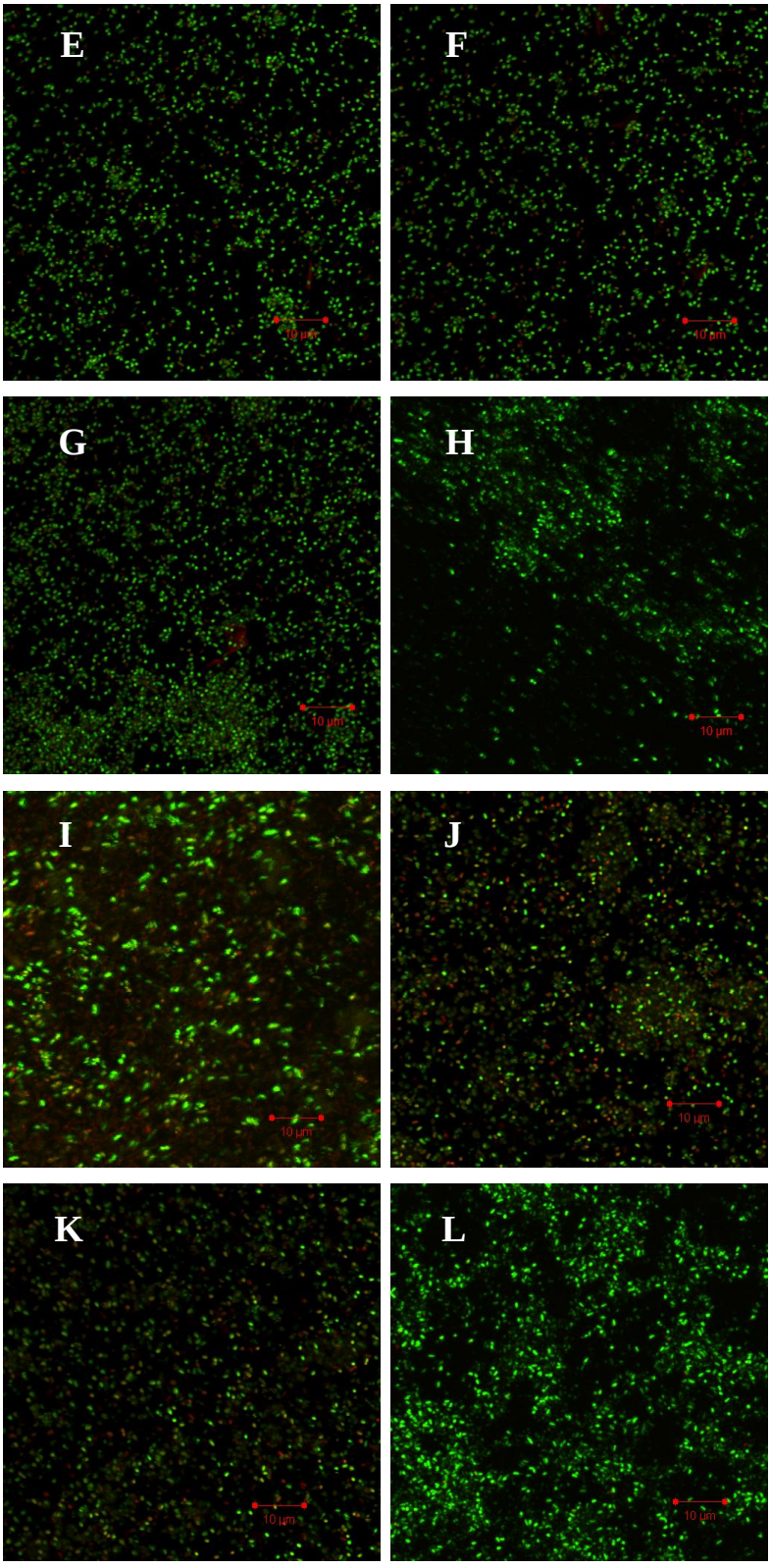


FIGURE 5.29 (E TO L): **Maximum intensity projections of CLSM image stacks of 48 h-old *P. aeruginosa* biofilms treated for 24 h with 2 ml of 1 mg/ml (E to H) and 0.5 mg/ml (I to L) AIT-loaded MSNs, stained with LIVE/DEAD® Viability Stain (SYTO® 9, green = live cells, PI, red = dead cells). One representative image was chosen from each of four independent imaging sessions, each session consisting of three biological replicates, with each replicate imaged at three different locations of the biofilm (at the least). Thickness of biofilm in *z* axis (µm): E= 11, F = 10, G = 14, H = 9, I = 15.5, J = 18, K = 16, and L = 19.**

Employment of 2 mg/ml AIT-loaded MSNs was approximately equivalent to exposure to 350 mg/L AIT. However, treatment with 2 mg/ml AIT-loaded MSNs was significantly more effective in detaching and killing biofilm bacteria than 350 mg/L and even 600 mg/L AIT in free form, which is evident in the CLSM images (compare Figures 5.29 A to D with 5.28 A to H) and in the average thickness of biofilms from the two treatments (Figure 5.25). Although there were more dead cells present in samples treated with 350 mg/L and 600 mg/L AIT (Figures 5.28 A to H), there are much less remaining cells overall in the biofilms when treated with 2 mg/ml and 1 mg/ml AIT-loaded MSNs. This means that treatment with AIT-loaded MSNs at these two concentrations was more effective than the free form in dissociating adherent cells from the biofilm and/or killing constituent cells first and then causing detachment (or a combination of both). Even exposure to 0.5 mg/ml AIT-loaded MSNs, which presumably would be approximately equivalent to treatment with (¼)X 350 mg/L AIT, resulted in significantly thinner and less bacterially dense biofilms than 350 mg/L AIT (compare Figures 5.28 E to H with 5.29 I to L). In fact, the biofilm thickness resulting from exposure to 0.5 mg/ml AIT-loaded MSNs (theoretically equivalent to 87.5 mg/L AIT treatment) was similar to that detected after exposure to 600 mg/L AIT, which were 17.125 ± 3.65 µm and 18.5 ± 1.68 µm, respectively. Furthermore, cell density and abundance of green and red fluorescence signals between the two cases were also similar. Therefore, it can be concluded that 0.5 mg/ml AIT-loaded MSNs had similar efficacy in detaching and killing bacterial biofilms as 600 mg/L AIT in free form.

CLSM images of biofilms treated with 0.5 mg/L AIT-loaded MSNs were more variable, mostly in the intensity and size of green fluorescence signals, than samples treated with other AIT treatments, with or without MSNs. The four images of this sample (Figures 5.29 I to L) obtained from four independent imaging sessions are not as congruent as images of the negative control, vehicle control, and other AIT-treated samples. Nevertheless, the

biofilm thickness of the four replicates was consistent, and the density and abundance of green fluorescence in the images were also similar to one another.

5.3.2.2.2 CNAD Treatment

For CNAD treatments, 600 mg/L and 350 mg/L CNAD significantly reduced the thickness of the biofilms as compared to the negative controls ($P \leq 0.05$), resulting in mean *z* axis values of 21.8 ± 1.19 µm and 29.375 ± 1.75 µm, respectively, Also, these two treatments effectively killed almost all remaining bacteria present in the biofilms, as indicated by the scarcity of green fluorescence and abundance of red fluorescence in Figures 5.30 A to H. Treatment with 350 mg/L CNAD resulted in thicker biofilms as compared to 600 mg/L treatment, but the viability of the remaining cells are quite comparable in both cases (compare Figures 5.30 E to H with A to D). There was a slightly larger amount of green fluorescence after exposure to 350 mg/L CNAD than to 600 mg/L CNAD; thus, it can be concluded that 350 mg/L CNAD was slightly less effective in dissociating and killing biofilms than 600 mg/L CNAD.

There was no significant difference in biofilm thickness between samples treated with free form AIT and CNAD at the same concentrations (600 mg/L and 350 mg/L; Figure 5.19). However, the majority of (if not close to all) remaining biofilm cells were dead after exposure to CNAD (Figures 5.30 A to H), whereas residual bacteria present after exposure to AIT were much more viable (5.29 A to H). Therefore, it can be concluded that while equally effective in detaching adherent biofilm cells, CNAD was more effective than AIT in killing the remaining adherent bacteria when both were used in free form at the same concentration.

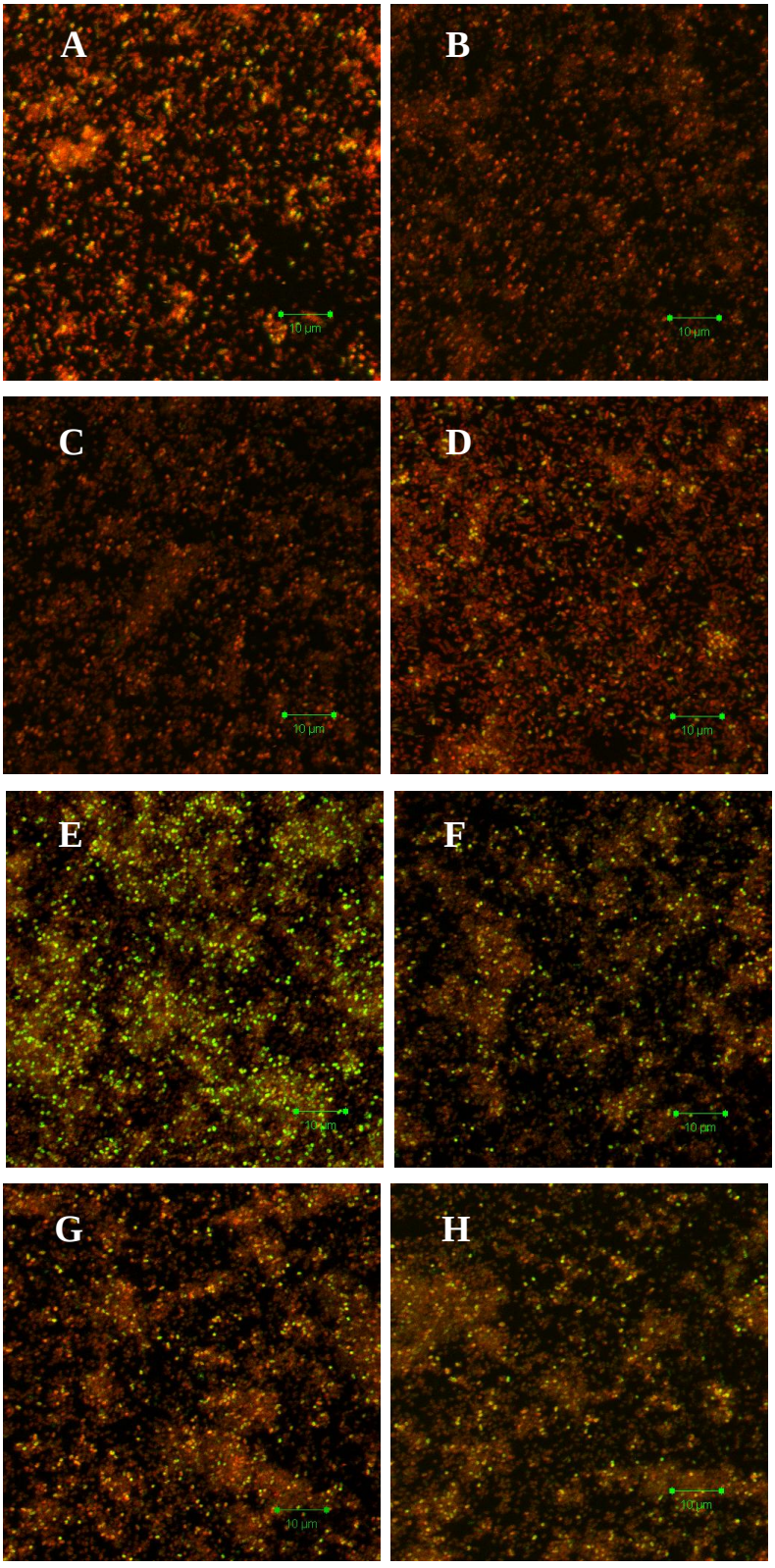


FIGURE 5.30 (A TO H): **Maximum intensity projections of CLSM image stacks of 48 h-old *P. aeruginosa* biofilms treated for 24 h with 2 ml of 600 mg/L CNAD (A to D) and 350 mg/L CNAD (E to H), stained with LIVE/DEAD® Viability Stain (SYTO® 9, green = live cells, PI, red = dead cells). One representative image was chosen from each of four independent imaging sessions, each session consisting of three biological replicates, with each replicate imaged at three different locations of the biofilm (at the least). Thickness of biofilm in *z* axis (µm): A= 21.5, B = 21.5, C = 20.7, D = 23.5, E = 29, F = 29, G = 30.5, and H = 29.**

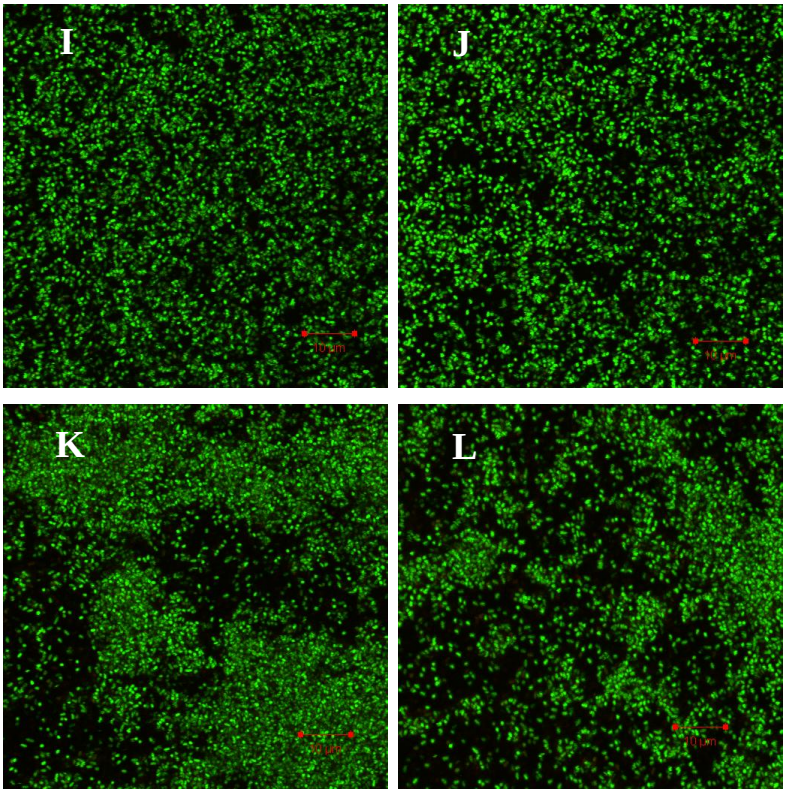


FIGURE 5.30 (I TO L): **Maximum intensity projections of CLSM image stacks of 48 h-old *P. aeruginosa* biofilms treated for 24 h with 2 ml of 35 mg/L CNAD, stained with LIVE/DEAD® Viability Stain (SYTO® 9, green = live cells, PI, red = dead cells). One representative image was chosen from each of four independent imaging sessions, each session consisting of three biological replicates, with each replicate imaged at three different locations of the biofilm (at the least). Thickness of biofilm in *z* axis (µm): I = 83, J = 89, K = 96.5, and L = 80.**

There was no observable difference between negative control samples and samples treated with 35 mg/L CNAD; both were highly viable (dense green fluorescence signals with hardly any red fluorescence signals) with mean biofilm thickness of 100.25 ± 13.13 µm for the negative control and 87.125 ± 4.75 µm for 35 mg/L CNAD (compare Figures 5.26 A to D with 5.30 I to L). It can be concluded that 35 mg/L CNAD had negligible effect of preformed *P. aeruginosa* biofilms.

Employment of 2 mg/ml CNAD-loaded MSNs was approximately equivalent to exposure to 35 mg/L CNAD. However, treatment with 2 mg/ml, and even 1 mg/ml and 0.5 mg/ml CNAD-loaded MSNs were significantly more effective in detaching and killing biofilm bacteria than 35 mg/L CNAD in free form. This is evident in the CLSM images

(compare Figures 5.31 A to H with 5.30 I to L) and in the average thickness of biofilms of each treatment (Figure 5.25). The biofilm cells that remained after treatment with 2 mg/ml and 1 mg/ml were sparse and mostly dead with a small fraction of live cells scattered throughout, as indicated by the abundance of red fluorescence signals and the relatively low occurrence of green fluorescence signals in Figures 5.31 A to H. In contrast, samples treated with 0.5 mg/ml CNAD-loaded MSNs were relatively denser, thicker, and more viable, as indicated by the higher occurrence of green fluorescence and lower amount red fluorescence (Figures 5.31 I to L).

There was no significant difference between biofilm thickness resulting from exposure to 2 mg/ml and 1 mg/ml CNAD-loaded MSNs, which were 18 ± 3.46 μm and 22 ± 2.45 μm, respectively (Figure 5.25). Furthermore, from qualitative analysis of CLSM images (Figures 5.31 A to H), there was no observable difference in viability and cell density between 2 mg/ml versus 1 mg/ml CNAD-loaded MSNs. These two treatments yielded significantly thinner biofilms than treatment with 350 mg/L CNAD did (29.375 ± 1.75 μm) ($P \leq 0.05$). CNAD at 350 mg/L is theoretically a concentration equivalent to the employment of 10X 2mg/ml and 20X 1 mg/ml CNAD-loaded MSNs, yet 350 mg/L CNAD was less effective in dissociating biofilm bacteria than both 2 mg/ml and 1 mg/ml CNAD-loaded MSNs. As for the viability of the remaining biofilm cells, CLSM images show that the abundance of red fluorescence signals in all three treatments were all similar to one another (compare Figures 5.30 E to H with 5.31 A to H), suggesting that 350 mg/L AIT, 2 mg/ml and 1 mg/ml CNAD-loaded MSNs were equally effective in killing residual adherent bacteria. It is important to note that the intensity of red fluorescence in 350 mg/L AIT images were higher than that in 2 mg/ml and 1 mg/ml CNAD-loaded MSNS images. This was due to the intrinsic variance between different biological samples and artifacts from different types of

treatment, but the abundance and density of the red fluorescence signals between the three treatments were in fact comparable.

Two mg/ml and 1 mg/ml CNAD-loaded MSNs yielded similar biofilm thickness to samples treated with 600 mg/L CNAD (21.8 ±1.19 μm). However, the remaining cells in biofilms subjected to 600 mg/L CNAD were essentially all killed, while 2 mg/ml and 1 mg/ml CNAD-loaded MSN treatments resulted in a relatively more viable cells. This suggests that while 600 mg/L CNAD, 2 mg/ml and 1 mg/ml CNAD-loaded MSNs were all equally efficacious in dissociating adherent cells from biofilms, 600 mg/L CNAD in free form was more effective than the other two treatments in killing the remaining adherent bacteria.

Exposure to 0.5 mg/ml CNAD-loaded MSNs resulted in similar biofilm thickness to 350 mg/L CNAD treatment, with *z* values of 31.25 ± 5.87 μm and 29.375 ± 1.75 μm, respectively. Employment of 0.5 mg/ml CNAD-loaded MSNs is theoretically equivalent to exposure to (¼)X 35 mg/L CNAD in free form, yet 350 mg/L (10X 35 mg/L) CNAD and 0.5 mg/ml CNAD-loaded MSNs displayed similar efficacies in reducing biofilm biomass. In contrast, CLSM images of these two treatments show that 350 mg/L CNAD was much more effective in killing the remaining adherent cells than 0.5 mg/ml CNAD-loaded MSNs was, as indicated in the larger amount of red fluorescence signals in the former than the latter (compare Figures 5.30 E to H with 5.31 I to L).

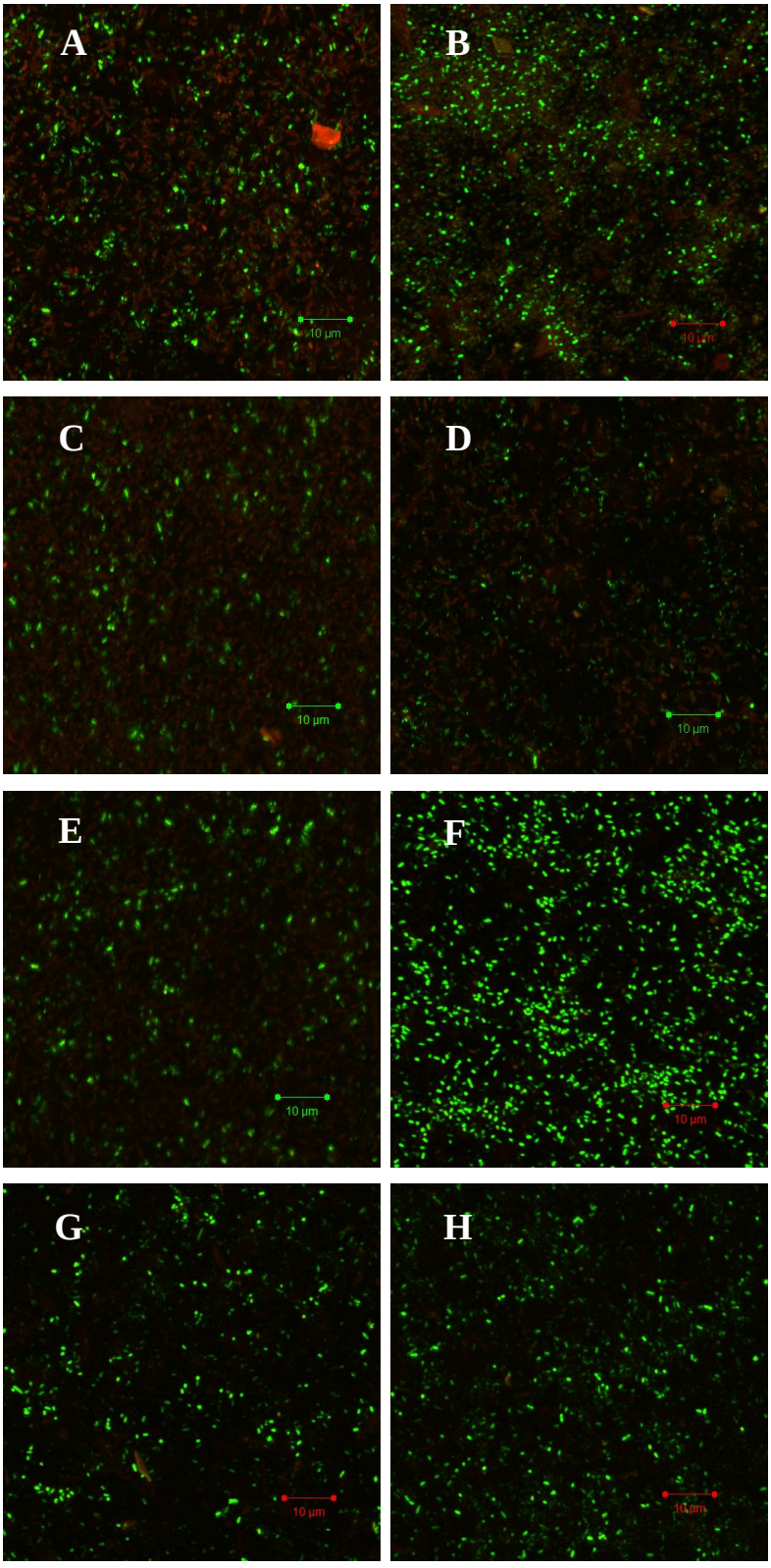


FIGURE 5.31 (A TO H): **Maximum intensity projections of CLSM image stacks of 48 h-old *P. aeruginosa* biofilms treated for 24 h with 2 ml of 2 mg/ml (A to D) and 1 mg/ml (E to H) CNAD-loaded MSNs, stained with LIVE/DEAD® Viability Stain (SYTO® 9, green = live cells, PI, red = dead cells). One representative image was chosen from each of four independent imaging sessions, each session consisting of three biological replicates, with each replicate imaged at three different locations of the biofilm (at the least). Thickness of biofilm in *z* axis (µm): A= 23, B = 17, C = 17, D = 15, E = 20, F = 23, G = 20, and H = 25.**

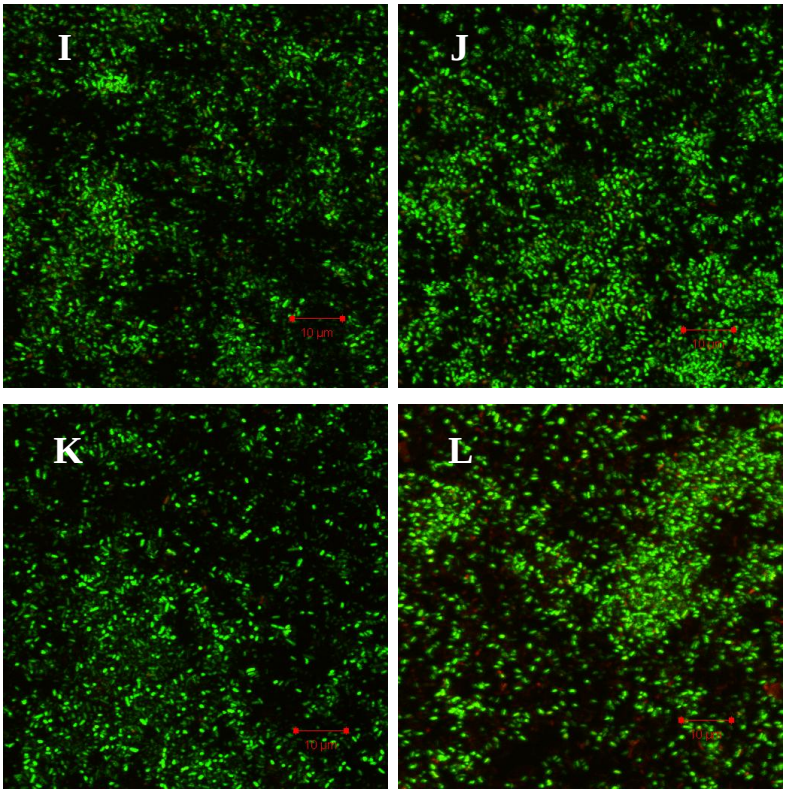


FIGURE 5.31 (I TO L): **Maximum intensity projections of CLSM image stacks of 48 h-old *P. aeruginosa* biofilms treated for 24 h with 2 ml of 0.5 mg/ml CNAD-loaded MSNs, stained with LIVE/DEAD® Viability Stain (SYTO® 9, green = live cells, PI, red = dead cells). One representative image was chosen from each of four independent imaging sessions, each session consisting of three biological replicates, with each replicate imaged at three different locations of the biofilm (at the least). Thickness of biofilm in *z* axis (µm): I = 25, J = 30, K = 36.5, and L = 23.5.**

Biofilms generated from treatment with AIT-loaded MSNs were significantly thinner than those resulting from CNAD-loaded MSN treatment when compared at the same concentrations (2 mg/ml, 1 mg/ml, and 0.5 mg/ml) ($P \leq 0.05$; Figure 5.32). This directly correlates with general findings of almost all previous viability tests performed in this study, wherein AIT was more effective than CNAD in inhibiting and killing bacteria when used at the same concentrations.

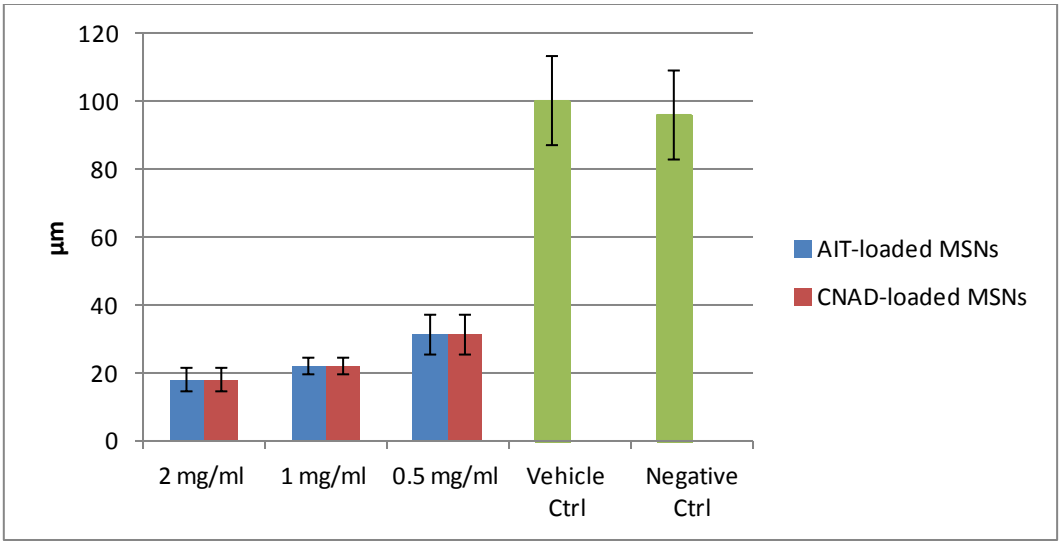


***FIGURE 5.32*: Thickness of 48 h-old *P. aeruginosa* biofilms (*z* axis of 3D CLSM image stacks) resulting from exposure to various concentrations of AIT-loaded and CNAD-loaded MSNs for 24 h. Error bars represent ± SD. The data represents the mean and SD of images from four independent imaging sessions, each session consisting of three biological replicates, with each replicate imaged at three different locations of the biofilm (at the least).**

However, as mentioned previously, there was no significant difference in biofilm thickness between samples treated with free form AIT and CNAD at the same concentrations (600 mg/L and 350 mg/L). Furthermore, the majority of remaining bacteria were dead after exposure to CNAD (Figures 5.30 A to H), whereas residual cells present after exposure to AIT were much more viable (5.29 A to H). This contradicts results from the bulk of previous viability assays. A probable explanation for free form CNAD to perform better than AIT in dissociating and killing biofilm cells is the difference in volatility between the two compounds. The vapour pressure of AIT (4.6 mm/Hg at 25˚C) is greater than that of CNAD (0.03 mm/Hg at 25˚C), meaning a greater amount of AIT compared to CNAD would have been lost from the system into the atmosphere during the 24 h incubation period due to volatisation (T.-T. Liu & Yang, 2010). This would leave a smaller quantity of AIT than expected in the system to react with biofilm cells, thus this lowered bioavailability of AIT compared to CNAD may be the reason CNAD appeared to be more effective than AIT in killing the remaining adherent bacteria when both were used in free form at the same concentration. Since AIT is more volatile than CNAD, AIT would greatly benefit (even more

so than CNAD) from being encapsulated in pores of MSNs for protection and stabilisation in order to harness the full antimicrobial and antibiofilm potential of the compound. This is evident in the disparity in biofilm thickness and viability generated from AIT-loaded MSN treatment versus CNAD-loaded MSN treatment.

5.3.2.3 Biomass Reduction of Mature, Adherent Biofilms

In this assay, the efficacy of AIT and CNAD against 60 day-old *P. aeruginosa* biofilms was reflected in the degree of reduction in wet weight of treated samples as compared to the untreated negative controls and vehicle controls (empty MSNs) after treatment for 24 h. As mentioned before, the starting mass of the Bio-Blok® polyethylene coupons to which the biofilms adhered weighed 2 g each, therefore the wet weight of the resulting biofilm alone was calculated by subtracting 2 g from the total mass obtained. Results are displayed in Figure 5.33. Photos depicting the most extreme results (negative control and treatment with 2 mg/ml AIT-loaded MSNs) are presented in Figure 5.34.

There was no significant difference between resulting biomass of the negative control samples and the vehicle control samples. Empty, unloaded MSNs had negligible effect on preformed, 60-day old *P. aeruginosa* biofilms.

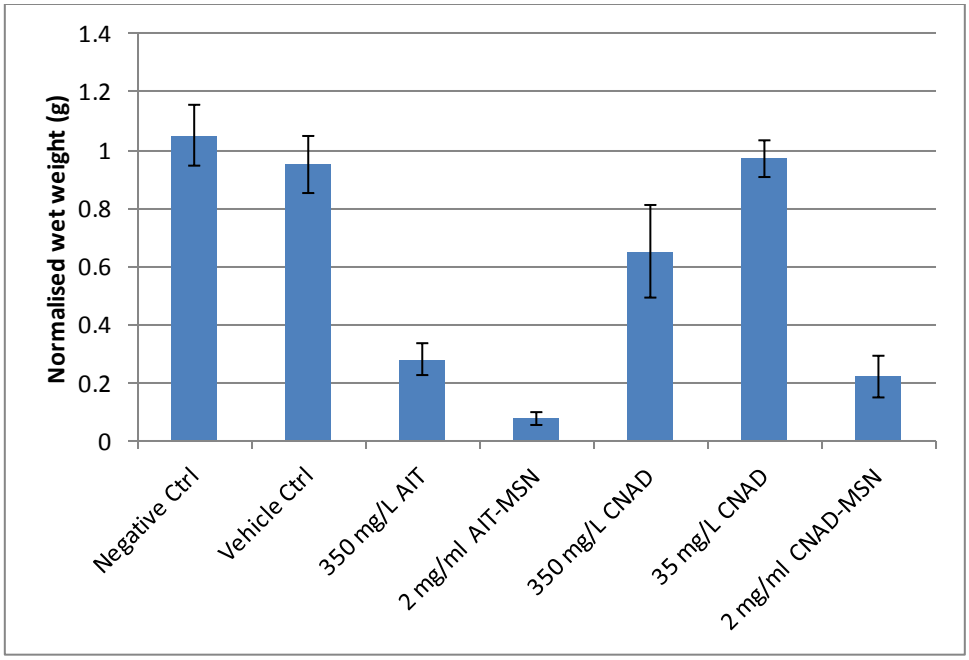


FIGURE 5.33: **Wet weight of 60 day-old *P. aeruginosa* biofilms after various treatments for 24 h. Mass of resulting biofilms were calculated by subtracting 2 g (mass of each Bio-Blok® substratum) from total mass obtained from weighing Bio-Blok® coupons with biofilms attached. The data represents the mean and SD of biological and technical triplicate samples.**

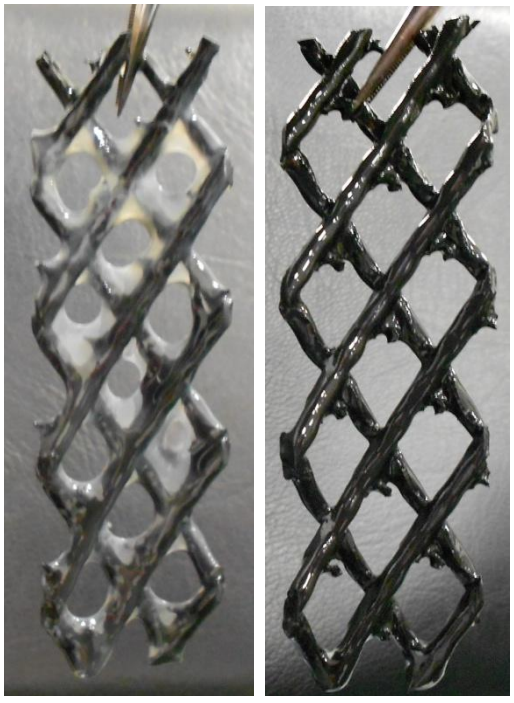


FIGURE 5.34: **Photos of 60 day-old *P. aeruginosa* biofilms grown on Bio-Blok® polyethylene coupons: negative control (left) and treatment with 2 mg/ml AIT-loaded MSN (right). Photos by Andrea Chan.**

Under the assumption that the maximum concentration of AIT and CNAD released from 2 mg/ml loaded MSNs were ~350 mg/L and ~35 mg/L respectively (Chapter 4), both compounds encapsulated in MSNs (2 mg/ml for both) were significantly more effective in reducing biofilm biomass than AIT (350 mg/L) and CNAD (35 mg/L) as free agents ($P \leq 0.05$). AIT at 350 mg/L caused approximately 70% of adherent biofilm to detach and/or perish, whereas 2 mg/ml AIT-loaded MSNs essentially removed and/or killed all of the mature biofilm developed over 60 days. In the case of CNAD, 35 mg/L CNAD had no significant effect on the mass of attached biofilm, whereas 2 mg/ml CNAD-loaded MSNs caused approximately 80% reduction in biofilm biomass. When the same amount of AIT-loaded and CNAD-loaded MSNs (2 mg/ml for both) were employed, the AIT-loaded variety was significantly more effective (by about 20%) in killing and/or dissociating mature biofilms from the polyethylene substrata than the CNAD-loaded variety ($P \leq 0.05$). Additionally, when the same concentration of both plant compounds (350 mg/L for both) were employed, AIT reduced a significantly larger amount of adherent biofilm (~70%) than CNAD was able to (55%) ($P \leq 0.05$).

Results from this assay suggest AIT was more efficacious in reducing the biomass of mature, adherent biofilms than CNAD. Furthermore, the approach of encapsulating both plant compounds in MSNs significantly improved both their abilities to kill and/or dissociate mature biofilms attached onto substrata. This finding supports the hypothesis that employing MSNs as a delivery system would enhance the antimicrobial/anti-biofilm efficacy of AIT and CNAD as compared to their activity as free agents, when used at the same concentrations, and would be a very good way to exploit a broad range of biocides whose applications are limited by being exceptionally volatile.

5.3.3 Conclusion

The Miles and Misra plate count experiment tested the antibacterial efficacies of AIT and CNAD both in free form and encapsulated in MSNs against planktonic *E. coli* suspensions harvested at mid-exponential growth phase. This assay demonstrated the following:

- Employing MSNs as a delivery system doubled the antibacterial efficacy of 362.7 mg/L AIT in free form after 1 h of exposure
- Both 2 mg/ml and 1 mg/ml AIT-loaded MSNs killed essentially all planktonic *E. coli* in the system (2.365 X 10^9 CFU/ml) after 18 h
- 362.7 mg/L AIT was significantly less effective in killing planktonic *E. coli* than half that concentration (181.35 mg/L AIT) encapsulated in MSNs ($P \leq 0.05$)
- Employing MSNs as a delivery system significantly reduced colony counts (by approximately 15%) as compared to 34.8 mg/L CNAD in free form at both 1 h and 18 h
- 2 mg/ml CNAD-loaded MSNs killed planktonic *E. coli* at a rate that was over 6X faster than that of 34.8 mg/L CNAD in free form within the first hour of exposure, but both reduced colony counts at similar rates from 1 h to 18 h
- 2 mg/ml CNAD-loaded MSNs killed 50% of 2.365 X 10^9 CFU/ml planktonic *E. coli*

The LIVE/DEAD® *Bac*Light™ bacterial viability staining assay also tested the antibacterial efficacies of both compounds in free form and in MSNs against planktonic *E. coli* suspensions harvested at mid-exponential growth phase. This assay demonstrated the following:

- Both 2 mg/ml and 1 mg/ml AIT-loaded MSNs killed essentially all planktonic *E. coli* in the system after 18 h; results correlate with those from plate count experiment

- After 1 h, 2 mg/ml and 1 mg/ml AIT-loaded MSNs significantly lower percentage of live cells as compared to 362.7 mg/L AIT by 40% and 17%, respectively
- 2 mg/ml CNAD-loaded MSNs killed a significantly larger fraction (over 35%) of cells than 34.8 mg/L CNAD after 1 h, but it did not further lower the proportion of viable cells after 18 h

The biofilm formation/adherence assay using crystal violet in microtitre plates assessed the anti-biofilm-forming efficacies of AIT and CNAD in free form. This assay demonstrated that 312.5 mg/L AIT and 625 mg/L CNAD yielded maximum anti-biofilm-forming activity, resulting in > 80% reduction in biofilm biomass development as compared to negative controls.

The experiment using CLSM for analysis assessed the efficacies of AIT and CNAD both in free form and encapsulated in MSNs against preformed, 48 h-old *P. aeruginosa* biofilms. This assay demonstrated that the ability of both compounds to dissociate and to kill constituent biofilm cells was significantly enhanced by the employment of MSNs as a delivery system.

Lastly, the experiment using Bio-Blok® polyethylene matrices tested the ability of both compounds in free form and encapsulated in MSNs to reduce the biomass of mature, 60 day-old *P. aeruginosa* biofilms. This assay demonstrated that AIT and CNAD were able to detach significantly larger amount of adherent biofilm when encapsulated in MSNs as compared to their use in free form.

Chapter Six

6. LACTOSE-CAPPED MSNS FOR DIRECTED, ON-COMMAND RELEASE OF AIT AND CNAD

6.1 Introduction

The employment of hexagonally-ordered MSNs to deliver plant compounds for antimicrobial applications, as described in the previous chapter, conforms to traditional delivery systems currently more commonly trailed in medical applications that release entrapped cargo via diffusion. To further optimise these nanoscale silica containers for more sophisticated, on-command delivery applications, gate-like scaffoldings that are stimuli-responsive can be incorporated on the external surface to act as detachable caps over mesopores storing guest compounds within the MSNs. Several silica mesoporous materials (not necessarily in the nanoscale) with control release properties containing different gate-like structures have been reported (Bernardos *et al.*, 2010; C. Park, Kim, *et al.*, 2009; C. Park, Lee, *et al.*, 2009; Trewyn *et al.*, 2007). Such systems are sensitive to light, pH, or redox changes as triggers for de-capping the pores.

The first capped mesoporous silica support utilised light to de-cap coumarin molecules attached to pore outlets via reversible photodimerisation (Mal, Fujiwara, & Tanaka, 2003). Various photochemical gated systems have since been developed using cis-trans isomerisation of azobenzene moieties (Angelos, Vhoi, Vögtle, De Cola, & Zink, 2007; Lu, Choi, Tamanoi, & Zink, 2008; Mal, Fujikura, Tanaka, Taguchi, & Matsukata, 2003), light-induced dissociation of α-cyclodextrin with azobenzene groups (N. Liu *et al.*, 2004; C. Park, Lee, *et al.*, 2009), and photo-switchable transformation of spiropyran-merocynine

complexes (Aznar *et al.*, 2007). pH is another effective approach to control the release of cargo within mesoporous silica material. pH-sensitive systems include silica particles functionalised with polyamines, carboxylates, pseudorotaxanes, complexes with cucurbit(6)uril, cucurbit(7)uril, and α-cyclodextrins, amphiphilic diblock polymers, and iron(II,III) oxide (Angelos, Yang, Patel, Stoddart, & Zink, 2008; Bernardos *et al.*, 2008; Casasús *et al.*, 2008; Casasús *et al.*, 2004; Mei *et al.*, 2012; Nguyen *et al.*, 2006; C. Park, Oh, Lee, & Kim, 2007; Tao & Fu, 2012). Moreover, dual pH- and photosensitive release has been achieved in mesoporous silica material capped with boronic acid-functionalised gold nanoparticles (Aznar, Marcos, Martiñez-Máñez, *et al.*, 2009). Changes in redox conditions are also commonly used for on-command delivery. Such materials include those capped with cadmium sulfide, gold, and paramagnetic iron oxide nanoparticles, as well as rotaxanes and pseudorotaxanes containing redox-active moieties, attached (Lai *et al.*, 2003; Slowing, Trewyn, Giri, & Lin, 2007; Trewyn *et al.*, 2007).

In addition to examples mentioned above, other external stimuli used to trigger de-capping include temperature (Fu *et al.*, 2003) and the presence of certain ligands (Coll *et al.*, 2007). Temperature-responsive silica nanocontainers include those functionalised with zwitterionic sulfobetaine copolymers (Sun, Yu, Hong, & Pan, 2012), α-cyclodextrin rings hinged on azobenzene axles (Yan *et al.*, 2013), and thermosensitive hydrogel (Kang *et al.*, 2012). Ligand-responsive systems include DNA-functionalised silica nanoparticles triggered by mercuric ion (Y. Zhang *et al.*, 2012) and superparamagnetic iron oxide nanoparticle-capped silica microspheres that respond to EDTA and sodium citrate (Teng *et al.*, 2012). Despite these efforts in developing controlled release silica using pore gatekeepers, there are some drawbacks to these nascent delivery systems, such as 1) the requirement of being in non-aqueous environment, 2) complex synthesis methods, and 3) use of external triggers that are difficult to apply.

Apart from external stimuli, selective delivery induced by target cells or biomolecules themselves have also been reported. One example involves antibody-gated mesoporous nanoparticles that are specifically de-capped in the presence of the corresponding antigen (Climent *et al.*, 2009). Other such delivery systems utilise the presence of specific degradative enzymes to cleave the functionalised substrate off for de-capping. This includes 1) protein avidin gatekeepers on biotinylated silica particles being cleaved off upon addition of the protease trypsin, which hydrolyses the attached avidin to de-cap the pores (Schlossbauer, Kecht, & Bein, 2009), and 2) β-cyclodextrin caps on silica nanoparticles being de-capped in the presence of α-amylase, which hydrolyses the cyclodextrin core (C. Park, Kim, *et al.*, 2009).

In the present work, the MSNs containing gate-like scaffolds as pore caps synthesised for on-command release of entrapped AIT and CNAD are of the enzyme-substrate category described above. Herein, pore caps functionalised over pore outlets would be carbohydrate molecules, and the de-capping mechanism would exploit the metabolic activity of target microorganisms themselves. Carbohydrates/saccharides are the major source of energy in microbes and crucial components in biosynthesis and other cellular functions (Campbell *et al.*, 2008b). The ability to metabolise different types of saccharides to yield energy is specific to each organism (Palcu & Popescu, 2005). This study capitalised on the distinct ability to utilise lactose as a carbon source, which is specific to *E. coli* (and some other enteric bacteria) but not to other bacterial species.

6.1.1 Lactose and the Lac Operon

Lactose is a disaccharide sugar formed from the monosaccharides galactose and glucose linked together via β-1→4 glycosidic bond (Figure 6.1) (Linko, 1982). *E. coli* characteristically possesses the *lac* operon, which is a cluster of genes under a single

promoter that enables the transport and metabolism of lactose (Shuman & Silhavy, 2003). The operon consists of three adjacent structural genes, *lacZ*, *lacY*, and *lacA*, which encode the enzymes β-galactosidase, β-galactoside permease, and β-galactoside transacetylase, respectively (Shuman & Silhavy, 2003). β-galactosidase (LacZ) is an intracellular enzyme that hydrolyses lactose into glucose and galactose by rupturing the glycosidic bond that links the two monosaccharides; lactose permease (LacY) is a cytoplasmic membrane-bound transport protein that pumps lactose into the cell, and β-galactoside transacetylase (LacA) is an enzyme that transfers an acetyl group from acetyl-CoA to β-galactosides.

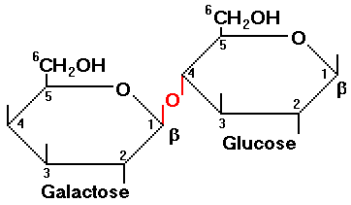


FIGURE 6.1: **The disaccharide lactose molecule, consisting of galactose and glucose linked by a β-1→4 glycosidic bond.**

Expression of these structural genes is under two regulatory mechanisms to ensure that the enzymes are only produced when lactose is available (Figure 6.2) (Görke & Stülke, 2008). The first control involves a constitutively expressed regulatory *lacI* gene that codes for a lactose repressor protein in the absence of lactose. The lactose repressor binds to the operator of the *lac* operon to inhibit RNA polymerase from binding to the promoter of the *lac* operon, therefore inhibiting its expression (Lewis, 2005; Shuman & Silhavy, 2003). In the presence of lactose, allolactose (a lactose metabolite) binds to the allosteric repressor protein and inactivates it by changing its conformation. The lactose repressor is thus unable to bind to the operator, allowing RNA polymerase to transcribe the structural *lac* genes (Lewis, 2005).

The second mechanism involves the cyclic adenosine monophosphate (cAMP)-bound catabolite activator protein (CAP), which facilitates the binding of RNA polymerase to the promoter of the *lac* operon when activated (Busby & Ebright, 2001). cAMP is a signal

molecule whose concentration is inversely proportional to that of glucose available (Campbell *et al.*, 2008d). The binding of cAMP to CAP activates the complex to bind to the CAP binding site, a 16 bp regulatory region upstream from the promoter and operator of the *lac* operon (Busby & Ebright, 2001; Shuman & Silhavy, 2003). This binding activates the transcription of the *lac* operon genes by assisting RNA polymerase binding. Thus, when glucose concentration is low, cAMP concentration is subsequently high, and the CAP engages the *lac* operon to enhance its transcription.

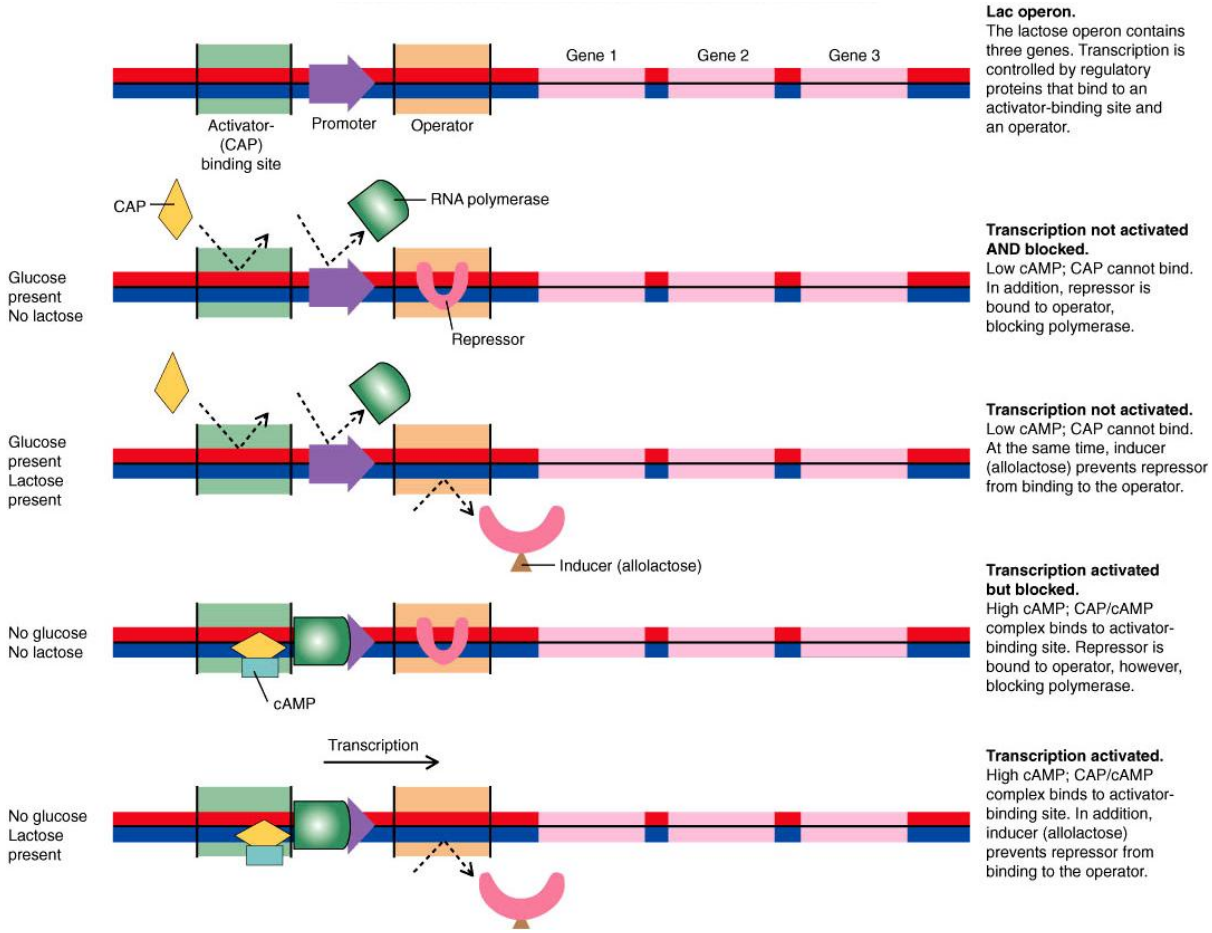


FIGURE 6.2: **The *lac* operon and its two regulatory mechanisms in the presence and absence of glucose and lactose. Gene 1, 2, and 3 represent *lacZ*, *lacY*, and *lacA*, respectively.**

(Schematic from Lecture on Microbial Genetics, Bakersfield College; available at http://www2.bakersfieldcollege.edu/bio16/images/lacoperon.jpg)

6.1.2 Trialkoxysilane Lactose Derivative as Gatekeepers

Herein, lactose in the form of its corresponding alkoxysilane derivative was anchored onto the external surface of MSNs to serve as mesopore caps (Bernardos *et al.*, 2009). MSNs were synthesised as described according to Hom *et al.*, 2010 in Chapter 4 (Hom *et al.*, 2010), except that particle surfaces were not functionalised with phosphonate groups (as described in Section 4.2.1) so as to not interfere with the functionalisation of the lactose gatekeepers. The trialkoxysilane lactose derivative was synthesised by reacting lactose monohydrate with 3-aminopropyltiethoxysilane (APTS) in ethanol (Figure 6.3) (Bernardos *et al.*, 2009).

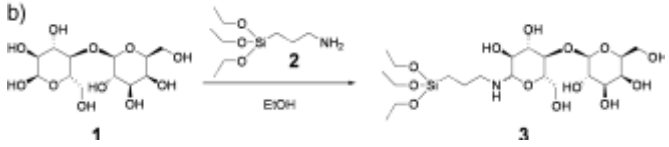


FIGURE 6.3: **Synthesis of the trialkoxysilane lactose derivative (3) from reacting lactose monohydrate (1) with 3-aminopropyltiethoxysilane (2) in ethanol.**

(Schematic from Bernardos, A. *et al. Enzyme-Responsive Controlled Release Using Mesoporous Silica Supports Capped with Lactose*. Angewandte Chemie International Edition, 2009. **48** (32): 5884-5887)

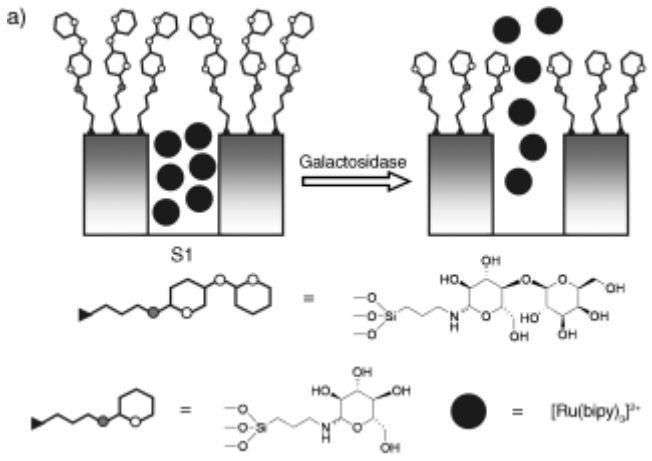


FIGURE 6.4: **Schematic of MSNs capped with trialkoxysilane lactose derivatives and the galactosidase-triggered de-capping action caused by the hydrolysis of the functionalised lactose, which releases the galactose portion and leaves only the glucose moiety anchored to the surface.**

(Schematic from Bernardos, A. *et al. Enzyme-Responsive Controlled Release Using Mesoporous Silica Supports Capped with Lactose*. Angewandte Chemie International Edition, 2009. **48** (32): 5884-5887)

Functionalising lactose derivative molecules on MSNs would inhibit the release of guest compounds via a network of dissacharides linked by dense hydrogen bonding around the mesopore outlets (Figure 6.4). The lateral hydrogen bonding will sterically cap the pores and thus, keep guest compounds loaded inside from leaching out through simple diffusion (Bernardos *et al.*, 2009; Bernardos *et al.*, 2010). Deliberate de-capping and controlled delivery of cargo within MSNs would be triggered by the presence of β-galactosidase, either supplied by addition of the isolated enzyme itself or by endogenous production from organisms that possess the *lac* operon (e.g. *E. coli*). β-galactosidase would cleave the lactose molecule, releasing the galactose fragment and leaving the glucose moiety attached on the surface of the MSN (Figure 6.4) (Bernardos *et al.*, 2009).

6.1.3 β-Galactosidase

β-galactosidase is a glycoside hydrolase enzyme that catalyses the hydrolysis of β-galactosides, which are a class of molecules containing the monosaccharide galactose linked to a functional group via a glycosidic bond (Shuman & Silhavy, 2003). This enzyme is endogenously produced by the *lacZ* gene in *E. coli* when lactose concentration is high and glucose availability is low (Shuman & Silhavy, 2003). Galactosides are categorised as α- or β-galactosides based on whether the glycosidic bond is located below or above the plane of the galactose residue, respectively (Wikipedia, 2013). Lactose is a β-galactoside containing a glucose molecule in which the glycosidic bond lies above the plane of the galactose molecule (Figure 6.1).

The enzyme β-galactosidase cleaves the β-glycosidic linkage between a galactose and its organic functional group, and in the case of lactose it hydrolyses the disaccharide into its constituent monosaccharides, galactose and glucose. The presence of this enzyme would

break the 1→4 glycosidic bonds of the lactose caps and hence de-cap the mesopores of MSNs, allowing the release of guest compounds inside.

6.1.4 Dye-Loading in MSNs Prior to Capping

The ruthenium dye tris(2,2'-bipyridyl)ruthenium(II) chloride ($[Ru(bpy)_3]Cl_2$) was selected as a model compound to be loaded into lactose-capped MSNs so as to replicate and validate the previously published work done by Bernardos, *et al.*, 2009, in which the authors successfully demonstrated the enzyme-triggered release of the ruthenium dye (Bernardos *et al.*, 2009). $[Ru(bpy)_3]Cl_2$ is a red-orange crystalline salt wherein the optical properties of the cation $[Ru(bpy)_3]^{2+}$ are of particular interest because its release from the MSN pores can easily be monitored by either absorbance readings at 452 ± 3 nm or fluorescence readings with excitation at 454 nm and emission at 610 nm over time (Montalti, Cedi, Prodi, & Gandolfi 2006).

6.1.5 AIT- and CNAD-Loading in MSNs Prior to Capping

The loading of MSNs with AIT and CNAD prior to lactose functionalisation was performed to test whether capping the pores with the disaccharide to entrap the two plant compounds as guest cargo was feasible. The protocol for loading AIT and CNAD was the same as described in Section 4.2.3 of Chapter 4, with the exception that the loaded nanoparticles were not washed after centrifugation. Instead, AIT- and CNAD-loaded MSNs were subjected to capping with trialkoxysilane lactose molecules directly after excess AIT and CNAD in the supernatant was removed.

6.1.6 Aims and Objectives

The objectives of this study were (i) to functionalise trialkoxysilane lactose onto the surface of MSNs to serve as pore caps and to characterise their size, (ii) to load ($[Ru(bpy)_3]Cl_2$) dye within the mesopores of the MSNS, then to cap with lactose derivative, and finally to trigger dye release using β-galactosidase, (iii) to prove that this delivery system was selective and specific only to bacterial species that are able to metabolise lactose, and (iv) to assess the *E. coli* killing efficiency of lactose-capped, AIT- and CNAD-loaded MSNs triggered by the target bacteria themselves.

6.2 Materials and Methods

6.2.1 Synthesis of MSN Scaffold

MSNs were synthesised via hot hydrolysis in an aqueous, base-catalysed sol-gel system as described in Hom *et al.*, 2010, with some modifications (also described in Chapter 4, Section 4.2.1). In a typical synthesis, 200 mg cetyltrimethylammonium bromide (CTAB) (99%, Sigma Aldrich, UK) was dissolved in a 96 ml DW and 700 µl 2M NaOH in a 250-ml round-bottom flask at 80˚C (pH 12.4) with stirring at 500 rpm. Once the temperature stabilised, 1 ml silica precursor tetraethylorthosilicate (TEOS) (Sigma Aldrich, UK) was added into the system. Unlike the synthesis method described in Section 4.2.1, phosphonate groups were not incorporated in the reaction so as to keep the silica surface unmodified. After stirring for 2 h at 80˚C, the suspension was centrifuged at 9000 rpm for 5 min. The resulting nanoparticles were washed twice with methanol (Sigma Aldrich, UK). The surfactant CTAB was subsequently removed by refluxing in 40 ml methanol plus 2 ml 37% hydrochloric acid (HCl) (Aldrich, UK) overnight at 80˚C using a water-cooled coil condenser.

6.2.2 Synthesis of Trialkoxysilane Lactose Derivative

The capping molecule, a lactose derivative, was synthesised as described in Bernardos, *et al.*, 2009. Briefly, 5.85 ml of 25 mmol 3-aminopropyltriethoxysilane (APTS) in ethanol (Sigma Aldrich, UK) was added to a suspension of 5.4 g D-lactose monohydrate (Sigma Aldrich, UK) in 244.15 ml absolute ethanol to give 250 ml total reaction volume. The reaction mixture was stirred in a 500-ml round bottom flask at 500 rpm at room temperature for 24 h, then heated to 60ºC for 30 min. The resulting product was transferred to five separate 50-ml centrifuge tubes and centrifuged at 9000 rpm for 8 min. The lactose alkoxysilane derivative was collected by discarding the supernatant, dried in a desiccator overnight, and then ground into a fine white powder using a mortar and pestle.

6.2.3 Loading and Subsequent Lactose-Capping of MSNs

Using a 100-ml round bottom flask, 0.5 g MSNs without any surface modifications (from Section 6.2.1) was added to 20 ml DW and probe-sonicated for 3 min at 5 sec intervals. Subsequently, 0.3 g of the dye $[Ru(bpy)_3]Cl_2$ (Sigma Aldrich, UK) was added to the MSN suspension and stirred at 500 rpm at room temperature for 24 h in an inert atmosphere. To achieve this, the reaction mixture was continuously flushed with nitrogen gas (N_2) using a latex balloon filled with N_2 attached to a 5-ml syringe that pierced through the rubber stopper sealing the reaction flask.

The protocol for loading MSNs (0.5 g in this case) with AIT and CNAD is described in Section 4.2.3 of Chapter 4, with the exception that the loaded MSNs were not washed after centrifugation and the removal of supernatant. The AIT- and CNAD-loaded MSNs that were pelleted were subsequently resuspended in 20 ml DW in a 100-ml round bottom flask.

After loading each respective compound ($[Ru(bpy)_3]Cl_2$, AIT, and CNAD) into the pores of the MSNs, 3.61 g trialkoxysilane lactose derivative (from Section 6.2.2) suspended in 10 ml DW was added to the loaded-MSN suspension and stirred for another 5.5 h to achieve capping. Finally, the resulting solid was carefully filtered off using two stacked pieces of 3 µm particle retention filter paper (44 Ashless Circles, 110 mm diam, Whatman, Fisher Scientific Ltd., Loughborough, UK) and then washed once with DW directly on the filter paper in a vacuum filter funnel system. The resulting loaded and capped MSNs on filter papers were dried at 40ºC overnight in covered petri dishes and then collected by scraping with a small spatula.

6.2.4 Characterisation of Dye-Loaded, Lactose-Capped MSNs using CPS Disc Centrifuge™

The CPS Disc Centrifuge™ operated with fluids that formed a density gradient inside the disc. Aqueous solutions ranging from 4% to 12% sucrose were prepared with DW, and the density gradient was created by injecting 2 ml of each solution into the disc in order of decreasing concentration. This allowed the sedimentation of the MSNs to remain stable.

With the disc centrifuge set to 24,000 rpm, the instrument was calibrated against known particle size standards before analysing MSN samples. Dilute suspensions of MSNs (200 µl aliquots) were injected into the instrument with a syringe, and three separate samples from three independent syntheses were measured.

6.2.5 Dye-Release Study: Enzyme-Triggered De-Capping of MSNs

6.2.5.1 Calibration Curve

A calibration curve of the ruthenium dye $[Ru(bpy)_3]Cl_2$ was established by measuring the fluorescence signal of five standard samples of known concentrations prepared in PBS (Table 6.1). Triplicate samples were prepared for each concentration and readings were undertaken in a 96-well flat-bottom black microplate (Nunc, UK), with 200 µl of sample dispensed in each well.

TABLE 6.1: **Calibration curve for the fluorescence of $[Ru(bpy)_3]Cl_2$**

$[Ru(bpy)_3]Cl_2$ concentration (mg/L)	**Fluorescence**
0	155
5	8886
10	17300
20	34000
35	59333

Fluorescence was measured using a Synergy HT Multi-detection Microplate Reader (Bio-Tek, UK) at excitation and emission wavelengths of 485/20 nm and 590/35 nm, respectively. The data was fit to a straight line using linear regression analysis, yielding a model described by the equation $y = 1686.5x + 323.48$ with an R^2 value of 1 (Figure 6.5).

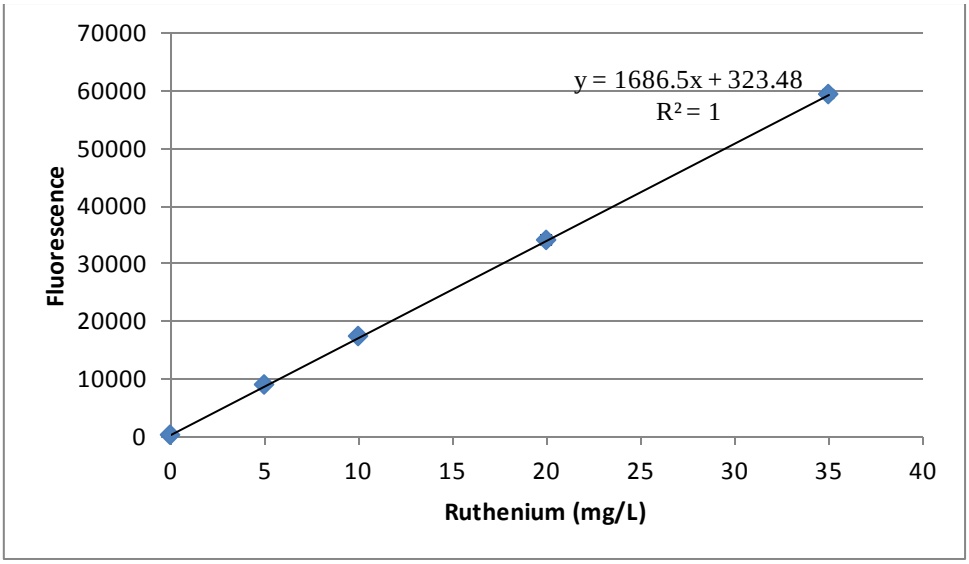


FIGURE 6.5: **Calibration curve for the fluorescence of $[Ru(bpy)_3]Cl_2$. Each point represents the mean of three samples, with each sample measured three times. Error bars represent ± SD. The line is a least-squares fit of the relationship between concentration of $[Ru(bpy)_3]Cl_2$ (*x*) and fluorescence value (*y*).**

6.2.3.2 Loading and Release of Ruthenium Dye $[Ru(bpy)_3]Cl_2$

Using a 25-ml centrifuge tube, 10 mg of dried $[Ru(bpy)_3]Cl_2$-loaded MSNs were suspended in 19 ml DW and bath-sonicated briefly to break up any agglomerated nanoparticles. To the suspension, 6 ml of 100 unit/ml stock of commercially-obtained β-galactosidase from *E. coli* (Grade VIII, Sigma Aldrich, UK) was added, resulting in a total reaction volume of 25 ml. For negative control samples, 6 ml of DW was added instead of the enzyme stock.

Enzymatic hydrolysis of the lactose gatekeepers were carried out in a shaking incubator with 60 rpm agitation at 37ºC, since the optimum functional temperature of β-galactosidase from *E. coli* is 37ºC (the optimal growth temperature of *E. coli*). A 650 µl

aliquot from both sample and negative control was retrieved every hour for six hours and centrifuged for 2 min at each sampling to pellet the MSNs. Triplicates of 200 µl supernatant was then transferred to wells of a black 96-well microplate, with total volume of 600 µl supernatant from both the sample and the negative control. Using a Synergy HT Multi-detection Microplate Reader (Bio-Tek, UK), fluorescence was measured at excitation and emission wavelengths of 485/20 nm and 590/35 nm, respectively. After each sampling, the supernatant inside wells of 96-well microplate after optical readings and the pelleted MSNs (in resuspended state) were returned to their corresponding reaction tubes to be further incubated. This was done to ensure future samples remained accurate and neither concentrated nor diluted by the removal of MSNs and the decrease in reaction volume. After sampling every hour for six hours, readings were taken at 24 h and 48 h as well.

This protocol for evaluating the de-capping of the lactose gatekeeper and the release of the entrapped dye differed from that published by Bernardos, *et al.*, 2009 in two aspects. Firstly, the commercially-purchased β-galactosidase used in this study was from *E. coli*, while the enzyme used in literature was from the yeast species *Kluyveromyces lactis* (Bernardos *et al.*, 2009) . Enzyme from *E. coli* was chosen instead because of relevance, since this work ultimately aimed to assess the de-capping ability of endogenously produced β-galactosidase from bacterial species possessing the *lac* operon. Secondly, the lactose-capped mesoporous silica materials used by Bernardos, *et al.* were not in the nanoscale, but rather large silica "supports" that far exceeded 100 nm in diameter (Bernardos *et al.*, 2009). In this study, lactose scaffoldings were anchored to mesoporous silica nanoparticles synthesised and characterised as described in Chapter 4.

6.2.6 Bacterial Growth using Trialkoxysilane Lactose Derivative as Carbon Source

E. coli (NCIMB 8879) and *Pseudomonas aeruginosa* cultures were prepared by streaking a frozen glycerol stock (-80˚C) onto nutrient agar (NA) (Sigma-Aldrich Company Ltd., Dorset, UK) which were left to grow for 16 h at 37°C until visible colonies appeared. One healthy colony from each species was then picked to start respective primary seed cultures in 5 ml sterile lysogeny broth (LB) (Sigma-Aldrich, UK). After growth for 6 h at 37˚C with 150 rpm agitation, the seed cultures were added to 100 ml sterile LB and incubated at 37°C with 150 rpm agitation until they reached mid-exponential growth phase. The resulting cultures were harvested, washed twice with PBS (Sigma-Aldrich, UK), and then resuspended in PBS. The turbidity of the bacterial suspension was adjusted to match 0.5 McFarland standard (OD_{600} = 0.132), which corresponds to bacterial density of 10^8 CFU/ml.

M9 minimal media was used to assess the ability of *E. coli* and *P. aeruginosa* to metabolise trialkoxysilane lactose derivative as a carbon source. M9 media contains the minimum nutrients required for bacterial growth, typically lacking in amino acids (Green & Sambrook, 2012) . In this study, M9 media was supplemented with a single variable agent, the carbon source, to test whether these two bacterial species could assimilate the lactose derivative without other supplementary elements that may support growth.

M9 media was prepared by initially making stock solutions as follows. All individual components purchased from Sigma-Aldrich Company Ltd., Dorset, UK.

1. A stock solution of 10X M9 salts was prepared by adding the following to 1 L DW:

COMPONENTS	AMOUNT
Na_2HPO_4 (anhydrous)	60 g
KH_2PO_4	30 g
NaCl	5 g
NH_4Cl	10 g

pH of solution was adjusted to 7.4 with 10 M NaOH, then sterilised with autoclave.

2. A 10 ml stock solution of 1 M $MgSO_4$, sterilised with autoclave.
3. A 10 ml stock solution of 1 M $CaCl_2$, sterilised with autoclave.
4. A 20% (w/v) glucose solution as carbon source, filter sterilised with 250-ml Nalgene® sterilisation filter unit with cellulose nitrate membrane, 0.2 µm pore size (VWR, Leicestershire, UK).
5. A 20% (w/v) trialkoxysilane lactose derivative solution as carbon source, filter sterilised with 250-ml Nalgene® sterilisation filter unit with cellulose nitrate membrane, 0.2 µm pore size (VWR, Leicestershire, UK).

One L of 1X M9 broth media supplemented with either 2 mg/L glucose or 2 mg/L trialkoxysilane lactose derivative was prepared as follows, using stock solutions prepared as described above.

COMPONENTS	VOLUME
10X M9 salts	100 ml
1M $MgSO_4$	2 ml
1M $CaCl_2$	0.1 ml
20% Glucose or Trialkoxysilane lactose derivative	10 ml
Autoclaved DW	887.9 ml

Using sterile 250-ml Erlenmeyer flasks, aliquots of 50 ml M9 broth media supplemented with 2 mg/L glucose or lactose derivative were inoculated with 50 µl of either the *E. coli* or *P. aeruginosa* suspension, which were grown and adjusted to 0.5 McFarland units as described above. Inoculated cultures were incubated at 32ºC with 120 rpm agitation.

OD_{600} was measured at various time points until 24 h as a measurement of bacterial growth and hence, indication of bacteria's ability to utilise either sugar as the sole carbon source.

The ability of *E. coli* to metabolise lactose derivative even at low concentrations was assessed by monitoring *E. coli* growth in M9 minimal media supplemented with varying amounts of trialkoxysilane lactose derivative. This was pertinent because the amount of lactose derivative gatekeepers available on MSN surface for bacterial assimilation may be quite low; therefore, it is important to test whether *E. coli* would be able to hydrolyse the anchored dissacharrides and utilize them as a carbon source when only small amounts were present. To test this, 1 L of 1X M9 broth media supplemented with a range of 2-fold diluted amounts of trialkoxysilane lactose derivative (from 2 g/L to 15.625 mg/L) was prepared as follows, using stock solutions prepared as described previously.

COMPONENTS	**VOLUME**
10X M9 salts	100 ml
1M $MgSO_4$	2 ml
1M $CaCl_2$	0.1 ml
20% Trialkoxysilane lactose derivative	Variable (from 10 ml to 78.125 µl)
Autoclaved DW	Variable (from 887.9 ml to 897.8 ml)

Using sterile 250-ml Erlenmeyer flasks, aliquots of 50 ml M9 broth media supplemented with varying concentrations of lactose derivative were inoculated with 50 µl of *E. coli* suspension, grown and adjusted to 0.5 McFarland units as described above. Inoculated cultures were incubated at 32ºC with 120 rpm agitation. OD_{600} was measured at various time points as a measurement of bacterial growth and hence, indication of bacteria's ability to metabolise trialkoxysilane lactose derivative as a carbon source.

Bacterial growth was reflected as a function of turbidity, and OD_{600} values of bacterial cultures were measured with a UV-2450 UV-Vis spectrophotometer (Shimadzu Ltd., Manchester, UK).

6.2.7 Employment of Lactose-Capped, AIT- and CNAD-loaded MSNs to Kill Bacteria

E. coli viability after treatment with AIT- and CNAD-loaded, lactose-capped MSNs was used to determine the ability of endogenous β-galactosidase from *E. coli* to hydrolyse and de-cap the lactose gatekeepers and trigger the bacteria's own killing. In sterile 50-ml centrifuge tubes, 10-ml aliquots of *E. coli* suspensions, grown and suspended in PBS as described above in Section 6.2.6 (with turbidity adjusted to 0.5 MacFarland standard), were each incubated with the following treatments for 18 h at 35˚C with 120 rpm agitation: 1) no treatment (negative control), 2) 2 mg/ml lactose-capped AIT-loaded MSNs, 3) 2 mg/ml lactose-capped CNAD-loaded MSNs, and 4) 2 mg/ml lactose-capped unloaded MSNs. Three biological replicates were prepared for each treatment. After incubation, the Miles and Misra plate count assay was performed to assess bacterial viability.

In the plate count method, samples were serially diluted 10-fold using sterile PBS, yielding dilutions ranging from 10^{-1} to 10^{-7} of the original sample. Twenty µl of the 10^{-4}, 10^{-5}, 10^{-6}, and 10^{-7} diluted suspensions were carefully pipetted onto nutrient agar (Sigma Aldrich, UK). Each dilution series was plated at least three times for statistical soundness. Agar plates were left undisturbed at room temperature for 15 min to allow for the droplets of inocula to diffuse and be absorbed evenly before overnight incubation at 37˚C. The resulting colonies, typically countable at the 10^{-6} and 10^{-7} dilution, were counted using Stuart™ SC6PLUS colony counter. The mean CFU/ml values resulting from the various treatments were calculated using the following equation:

CFU per ml = (average number of colonies) x (dilution factor) x (1000 µl/ 20 µl)

6.3 Results and Discussion

6.3.1 CPS Disc Centrifuge™

Data obtained using CPS Disc Centrifuge™ to characterise MSNs with trialkoxysilane lactose derivative modification on particle surface are presented in Figure 6.6, which shows the mean particle diameter to be 124.48 ± 0.001 nm, which is comparable to the measurements obtained from MSNs without lactose gatekeepers (Chapter 4, Section 4.3.2.2). Particle size measurements obtained from this technique are commonly larger than true diameters due to agglomeration of nanoparticles during disc centrifuge photosedimentometric analysis.

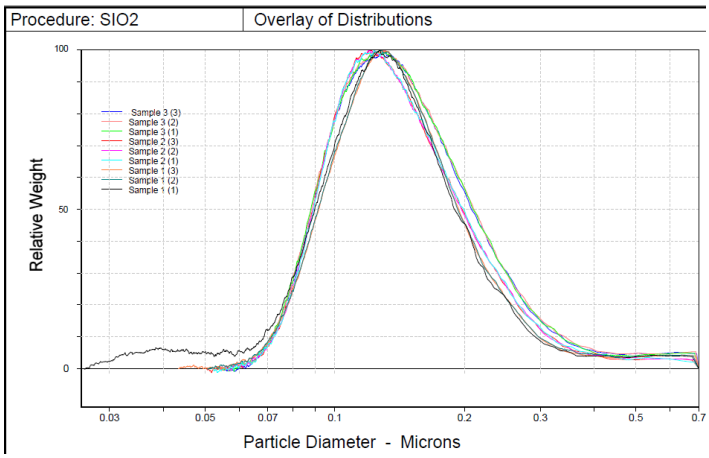


FIGURE 6.6: **Overlay of size distribution of MSNs functionalised with trialkoxysilane lactose pore caps obtained from CPS Disc Centrifuge™.**

6.3.2 Enzyme-triggered De-capping and Release of Ruthenium Dye $[Ru(bpy)_3]Cl_2$

The release profile of $[Ru(bpy)_3]Cl_2$ upon addition of commercially-obtained β-galactosidase from *E. coli* is presented in Figure 6.7. Using the experimentally-derived calibration curve that related fluorescence to $[Ru(bpy)_3]Cl_2$ concentration (described in Section 6.2.5.1), fluorescence values obtained over 48 h were translated into mg/L $[Ru(bpy)_3]Cl_2$.

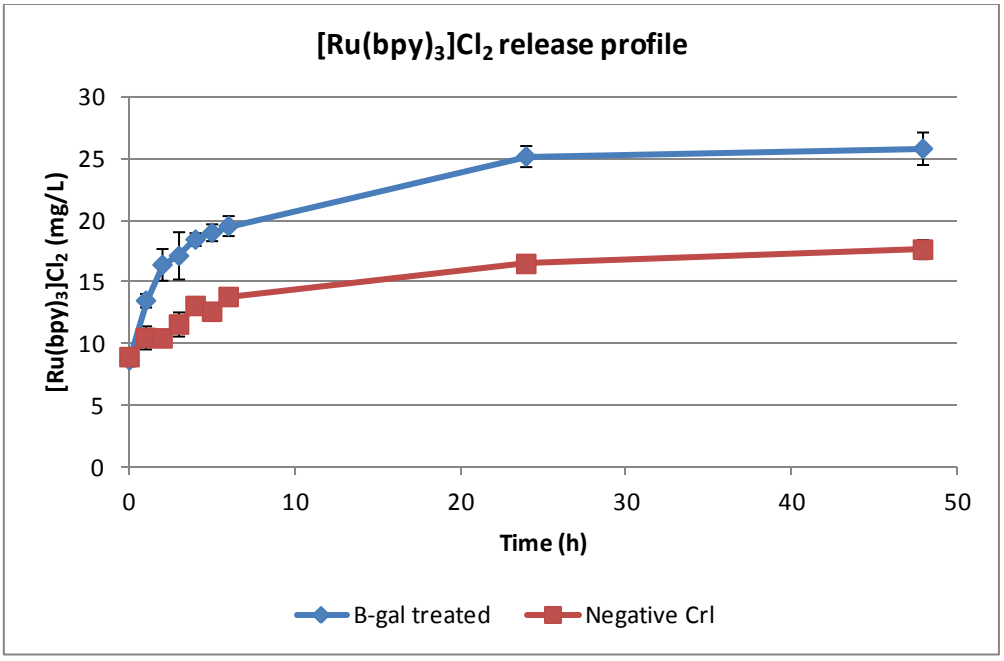


FIGURE 6.7: **Release profile of $[Ru(bpy)_3]Cl_2$ from lactose-capped MSNs, in the presence and absence of β-galactosidase. Error bars represent ± SD.**

In both the presence and absence of β-galactosidase, the release profile showed a continuous increase of $[Ru(bpy)_3]Cl_2$ in solution over time with no spikes at any point. In the presence of β-galactosidase, the delivery of ruthenium dye was appreciable, with relatively rapid rate of release from 0 to 2 h (slope m = 3.87, R^2 = 0.9789) (Figure 6.7), which then decelerated at 2 h and remained relatively stable until the 24 h time point (m = 0.3268 from 3 h to 24 h, R^2 = 0.9967). Thereafter, the concentration of the $[Ru(bpy)_3]Cl_2$ reached a steady plateau from 24 h to 48 h, with negligible release but a sustained amount detected during this span of time. This indicates that maximum delivery of $[Ru(bpy)_3]Cl_2$ was reached at 24 h via enzyme-triggered de-capping of lactose gatekeepers grafted on MSNs as delivery vehicles.

The rate of dye release in the negative control was slow (as compared to the enzyme-treated samples) and steady for the first six hours (m = 0.66, R^2 = 0.9159) before reaching an inappreciable rate from 6 h to 48 h (m = 0.089, R^2 = 0.9086).

Treatment with β-galactosidase yielded significantly greater concentrations of $[Ru(bpy)_3]Cl_2$ than no treatment for all time points ($P \leq 0.05$) and ultimately resulted in over

1.5X $[Ru(bpy)_3]Cl_2$ content as compared to that of the negative control after 48 h. The slight increase of dye detected in the absence of the enzyme was most likely to have been due to 1) diffusive leakage from within the mesopores that were not capped securely or properly and/or 2) the release of residual dye that remained on the surface of the MSNs after dye-loading. In contrast, the significant increase of $[Ru(bpy)_3]Cl_2$ in the β-galactosidase-treated samples was most likely to have been due to the enzyme-driven rupture of glycosidic bonds within the lactose caps, resulting in successful de-capping and subsequent controlled delivery of the dye, which was not observed in the negative control.

6.3.3 Bacterial Growth using Trialkoxysilane Lactose Derivative as Carbon Source

Growth curves of *E. coli* and *P. aeruginosa* using either 2 g/L glucose or 2 g/L trialkoxysilane lactose derivative as the sole carbon source are presented in Figures 6.8 and 6.9. *E. coli* successfully metabolised both types of saccharides and proliferated into turbid cultures by 24 h in both cases. The mid-exponential growth phase was delayed by several hours when lactose derivative was supplemented as compared to when glucose was used, but the *E. coli* grew appreciably in both cases, reaching comparable OD_{600} values at the 24 h time point. *P. aeruginosa* was able to assimilate glucose and successfully grew into turbid cultures by 24 h. However, no growth was detected when *P. aeruginosa* was supplemented with lactose derivative as the sole carbon source, indicating that this species was unable to metabolise and breakdown this disaccharide molecule. These findings were expected, since 1) glucose is a universal carbon source for most all bacterial species, including *E. coli* and *P. aeruginosa* (Palcu & Popescu, 2005), 2) the *lac* operon is known to exist in *E. coli* (Shuman & Silhavy, 2003), and therefore it is expected that this species is readily able to utilise lactose for as a source of energy for cellular functions, and 3) *P. aeruginosa* lacks the *lac* genes that make lactose metabolism possible , therefore it is expected that this species would not grow

when only lactose is available. It is important to note that the lactose molecules used in these experiments have been derivatised, so for de-capping purposes it was a promising finding that *E. coli* was able to metabolise this form of the disaccharide.

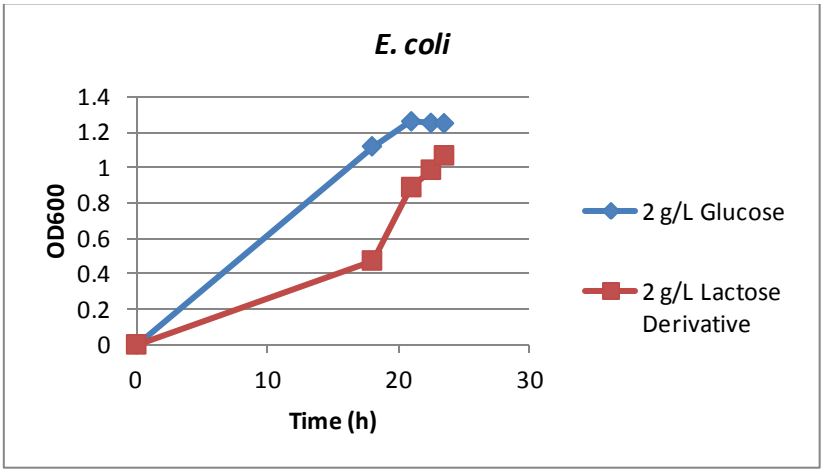


***FIGURE 6.8: E. coli* growth curve using either 2 g/L glucose or 2 g/L trialkoxysilane lactose derivative as carbon source.**

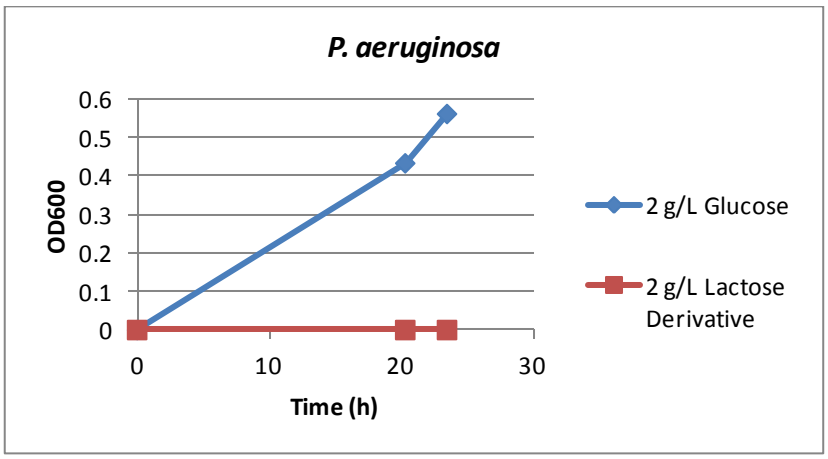


***FIGURE 6.9: P. aeruginosa* growth curve using either 2 g/L glucose or 2 g/L trialkoxysilane lactose derivative as carbon source.**

E. coli growth curves using varying concentrations of trialkoxysilane lactose derivative are presented in Figure 6.10. Results show that *E. coli* was able to utilise the derivatised disaccharide for proliferation even when low levels of the sugar were available. Detectable growth was detected at lactose derivative concentration as low as 125 mg/L and possibly even at 62.5 mg/L.

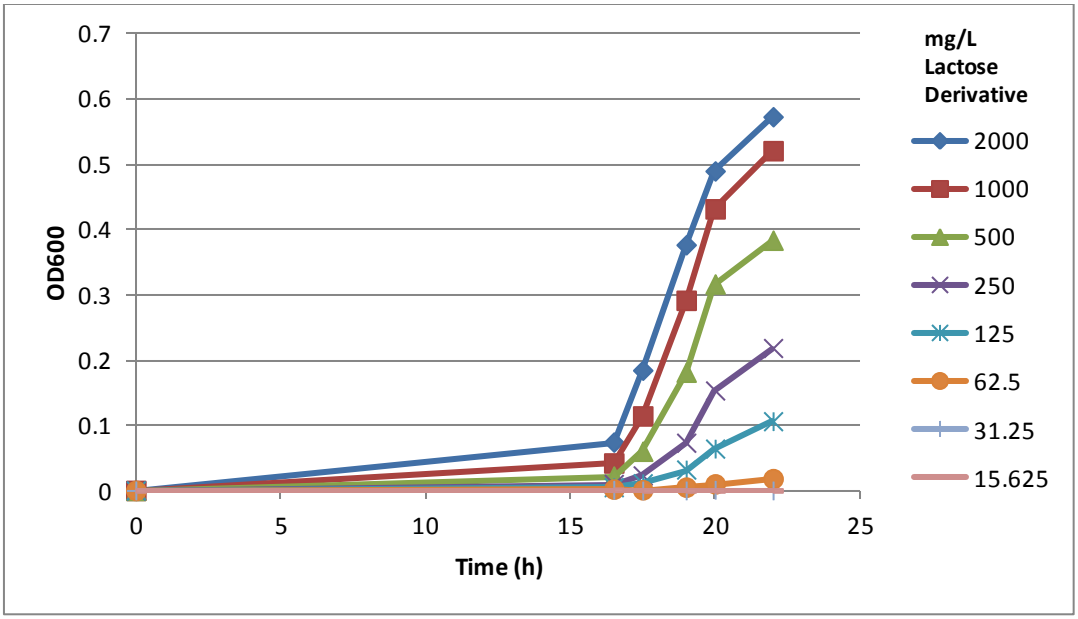


***FIGURE 6.10: E. coli* growth over 22 h using trialkoxysilane lactose derivative as sole carbon source.**

Collectively, these growth experiments using two different bacterial species showed that selective and directed delivery of guest compounds housed within lactose-capped MSNs was possible via de-capping mechanism triggered only by target microbes of a particular strain themselves. Bacterial communities consisting of species that were unable to metabolise the compound serving as pore gatekeepers (in this case, *P. aeruginosa* was unable to metabolise lactose) presumably would not induce any release of entrapped compounds. Since enzyme-directed, on-command release of $[Ru(bpy)_3]Cl_2$ from MSNs capped with trialkoxysilane lactose derivative was successfully achieved and assimilation of lactose was by *E. coli* was detected even at low levels of lactose, experiments progressed onto the loading lactose-functionalised MSNs with AIT and CNAD and the de-capping of the dissacharide gatekeepers using endogenous β-galactosidase from *E. coli*.

6.3.4 Employment of Lactose-Capped, AIT- and CNAD-loaded MSNs to Kill Bacteria

Exposing *E. coli* to 2 mg/ml lactose-capped, AIT- and CNAD-loaded MSNs along with 2 mg/ml lactose-capped, unloaded MSNs for 18 h produced plate count results presented

in Figure 6.11. Resulting colonies could be counted from dilutions of 10^{-4} to 10^{-7} of the bacteria after designated treatments. Mean CFU/ml values were calculated from colony counts resulting from all technical and biological replicates. Once CFU/ml values were calculated, data was converted to percentages of the untreated, negative control.

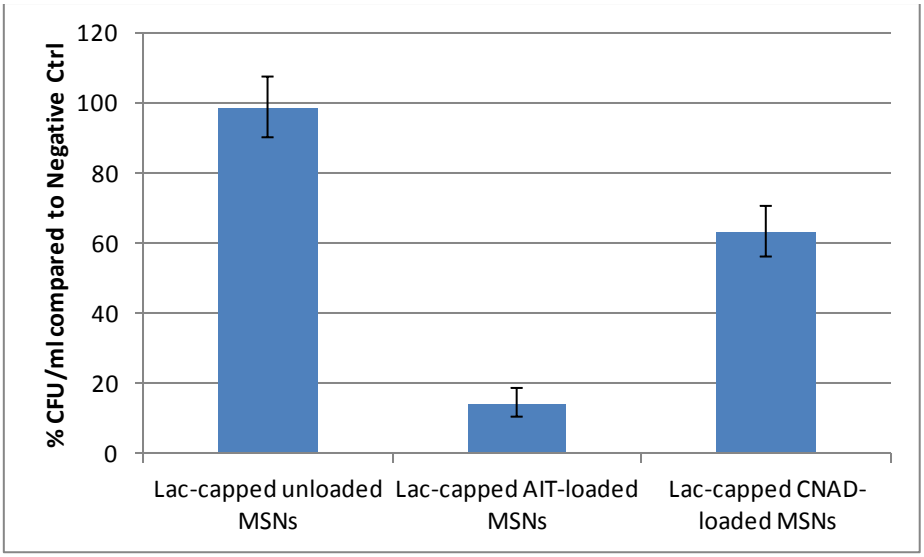


FIGURE 6.11: **Miles and Misra plate count assay after exposing *E. coli* to 2 mg/ml lactose-capped, AIT-/CNAD-loaded and unloaded MSNs for 18 h. CFU/ml values are expressed as percentages of the negative control. Error bars represent ± SD. Data represents the mean and SD of biological and technical triplicate samples.**

The negative control samples experimentally yielded (2.734 ± 0.056) X 10^9 CFU/ml *E. coli*. Both AIT- and CNAD-loaded varieties of the lactose-capped MSNs significantly reduced the number of culturable colonies as compared to the negative control and the lactose-capped, unloaded MSNs ($P \leq 0.05$). Capped AIT-loaded MSNs reduced colony count by approximately 85% of both the negative control and the unloaded MSNs, while capped CNAD-loaded versions reduced it by approximately 40%. Capped unloaded MSNs did not yield significantly different amount of colonies as compared to the negative control and at times, induced a slight increase in colony count, which was expected since (i) empty MSNs are non-toxic to cells and (ii) the lactose derivative grafted on MSN surface may have provided a small dose of nutrients to sustain a slight bit of growth.

From these findings, it can be concluded that (i) treatment with 2 mg/ml lactose-capped AIT-loaded MSNs was significantly more effective in killing *E. coli* than 2 mg/ml lactose capped CNAD-loaded MSNs ($P \leq 0.05$, the former reducing almost twice the number of colonies than the latter), and (ii) the antimicrobial action of lactose-capped, AIT- and CNAD-loaded MSNs was attributed to the biocidal capacity of the plant compounds alone. Also, appreciable reduction in culturable cells in both treatments is indication that β-galactosidase produced endogenously by *E. coli* successfully cleaved and de-capped the lactose gatekeepers, thus enabling the antimicrobial compounds entrapped inside to diffuse out.

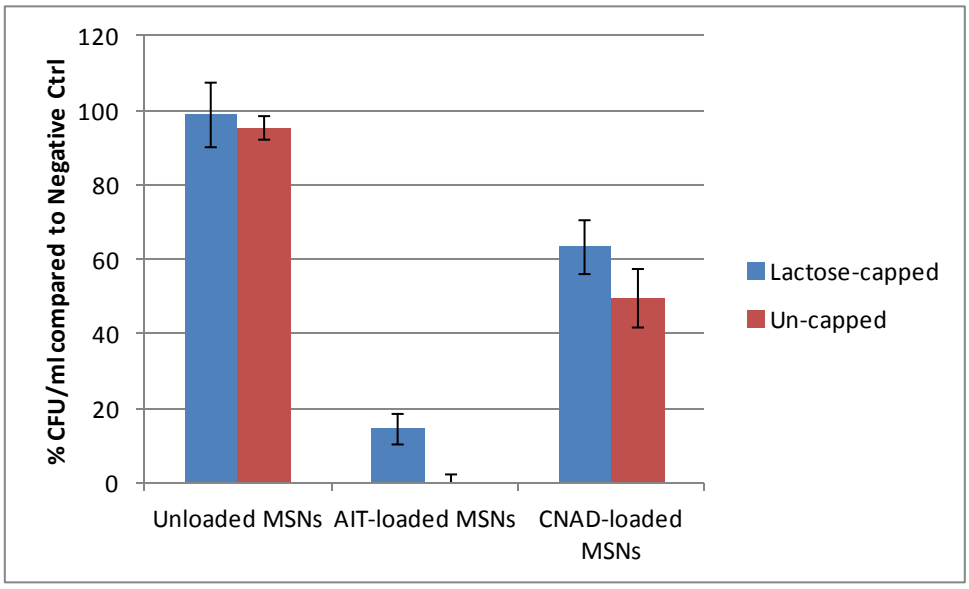


FIGURE 6.12: **Miles and Misra plate count assay after exposing *E. coli* to 2 mg/ml of various designated MSN treatements for 18 h. CFU/ml values are expressed as percentages of the negative control. Error bars represent ± SD. Data represents the mean and SD of biological and technical triplicate samples.**

A comparison between the results from Miles and Misra plate count assays using un-capped (from Chapter 5) and lactose-capped MSNs loaded with designated compounds is presented in Figure 6.12. Lactose attachment did not affect the viability of cells when MSNs were empty, as seen by the lack of significant difference in colony count between treatment with capped MSNs, uncapped MSNs, and the negative control. For both AIT- and CNAD-loaded MSNs, the un-capped variety reduced a significantly larger fraction of cells ($P \leq 0.05$)

than the lactose-capped variety in both cases. This is likely to have been due to the < 100% de-capping efficiency of the lactose-capped MSNs by the *E. coli* cells, causing a lower amount of either plant compound (as compared to the amount delivered by their uncapped counterparts) to diffuse out and be available for killing. Also, a small volume of AIT and CNAD may have leached out during the capping step, resulting in lower amounts of both compounds entrapped in the MSNs as compared to the case when capping with lactose was skipped. This may also have been a contributing factor in the disparity in killing between capped and uncapped MSNs. Although significantly different, results from capped and uncapped versions were relatively comparable, which indicated that grafting lactose derivatives on MSN surface did not dramatically disrupt the antimicrobial activity of the AIT- and CNAD-delivery systems.

6.3.5 Conclusion

Herein, surface modification of trialkoxysilane lactose derivative as mesopore caps on MSNs proved to be a suitable method for targeted delivery of entrapped compounds. The inability of *P. aeruginosa* to metabolise the lactose derivative showed that this delivery strategy was targeted and specific. The anchored lactose gatekeeper was a sugar that could only be metabolised by specific bacterial species and the entrapped compounds were antimicrobially-active AIT and CNAD, so this delivery system successfully served as a targeted "Trojan horse," self-killing approach to inhibiting *E. coli*.

Chapter Seven

7. DISCUSSION

7.1 Discussion

Biofouling occurs when undesired microbial adhesion and biofilm formation impedes a substrate's function when immersed in a liquid matrix (Chapman *et al.*, 2010; Weir *et al.*, 2008). It is a ubiquitous problem in engineered systems, especially water-based technological processes, ranging from water temperature control to desalination and purification (D. Kim *et al.*, 2009; Ludensky, 2003). Biofouling and associated biofilm formation cause contamination, biocorrosion and essential damage of materials, occlusion of pipes, inactivation of probes and sensors, congestion and biodegradation of membranes, increase in frictional resistance, and impedance of heat exchange and diffusion in fluid systems (Bernhard, 2003; Weir *et al.*, 2008). These adverse effects lead to health hazards, increase in energy consumption, more frequent maintenance of equipment, and significant decrease in overall productivity, all of which means higher operational costs and substantial harm to the environment.

Stiffening regulations regarding the use of biocides have stimulated interest in investigating alternatives to current conventional antimicrobial strategies. The Council of the European Union announced that the body would tighten controls on biocidal products by implementing the "*Regulation of the European Parliament and of the Council concerning the making available on the market and use of biocidal products*," which has been in effect since 1st Sep 2013 (PE-CONS 3/12) (European Parliament, 2012; European Union, 2012). The purpose of this regulation is to ensure biocides comply with a high level of protection for both human and animal health and the environment. The regulation states: (i) its

"precautionary principle to ensure that the manufacturing and making available on the market of active substances and biocidal products do not result in harmful effects on human or animal health or unacceptable effects on the environment," and (ii) its purpose to "grant, cancel, or modify authorisations as appropriate" (European Parliament, 2012). The active substances on the European Union list are to be regularly examined to take account of developments in science and technology.

Current anti-biofouling strategies have significant limitations, which include the generation of toxic and carcinogenic by-products, dangerous bioaccumulation in humans and animals, indiscriminate reaction and corrosion of surrounding materials and the environment, and the ever evolving problem of development of biocide resistance (Bernhard, 2003; Davies, 2003; D. Kim *et al.*, 2009). Alternative and effective methods of controlling biofouling are highly desired because present-day solutions are not sustainable.

In this present study, antimicrobial efficacies of plant-derived compounds were assessed against various species of planktonic bacteria as well as different types of biofilms at various maturity stages. The antiseptic properties of plant EOs and their constituent compounds have been recognised for many thousands of year (Jones, 1996). Currently, interest in utilising EOs and their active constituents has gained some momentum in areas of controlling diseases, infections, and agricultural/food spoilage (Burt, 2004; Fux *et al.*, 2005; Mahmoud *et al.*, 2004; Sylvestre *et al.*, 2006). However, plant-derived compounds have not been explored in the context of anti-biofouling. Plant secondary metabolites could potentially serve as effective alternatives to conventional antimicrobial and anti-biofouling agents because they effectively inhibit microorganisms without conferring resistance (S. Chao *et al.*, 2008) whilst being non-toxic to humans and the environment as well as non-damaging to surrounding materials.

Herein, two particular plant-derived compounds, AIT and CNAD, were extensively evaluated for their antimicrobial activity against vagile and biofilm bacteria. Experimentally, both compounds displayed excellent inhibitory activity as compared to other plant-derived compounds in several antimicrobial susceptibility tests, with AIT yielding MICs of 156.25 mg/L and MBCs of 156.25 to 312.5 mg/L, and CNAD yielding MICs of 78.125 to 156.25 mg/L and MBCs of 78.125 to 312.5 mg/L. Thus, these two plant secondary metabolites were selected as test compounds in subsequent experiments.

7.1 Whole-Cell *Lux*-Based Biosensors to Assess Antimicrobial Mechanism of Action

The antimicrobial mode of attack by AIT and CNAD were explored using two complementary whole-cell biosensors designed to detect metabolic and DNA damage, respectively. This is the first reported study to employ a *lux*-based biosensor assay (*E. coli* HB101_pUCD607_*lux*) coupled with parallel plate count experiments to demonstrate that AIT and CNAD not only damaged cell membranes, but also disrupted cellular metabolism and energy production in bacteria. It is also the first to use genotoxicity-sensing whole-cell bioreporters (*A. baylyi* ADP1_*recA*_*lux*) to demonstrate that neither AIT nor CNAD induced expression of the universal DNA repair gene, *recA*. This suggests that AIT and CNAD were not genotoxic. As an antimicrobial agent, it is advantageous that the compound be genetically non-damaging so that toxicity towards higher multicellular organisms and resistance development via mutagenesis can be minimised.

Lux-based bacterial whole-cell biosensors have been previously employed to detect the presence, bioavailablity, and biodegradation of environment pollutants in soil and water samples, which include metals (e.g. Zn, Cd, Cu, Pb, and Ag) and chemical toxicants (e.g. toluene, hydrogen peroxide, and phenolic compounds) (Dams, Biswas, Olesiejuk, Fernandes,

& Christofi, 2011; Simpson *et al.*, 1998; Song *et al.*, 2009; Tiensing *et al.*, 2001). Employing whole-cell biosensors for the detection of environmental contaminants is relevant to this current study because our aim is to employ plant secondary metabolites to combat biofouling in engineered systems that ultimately impact the environment. However, what sets this present work apart from previous studies is that this was the first reported study to employ whole-cell biosensors (consisting of signal transducers of any type) to elucidate the mechanism of action of antimicrobial compounds of any sort. A journal article has been published in the Journal of Microbiological Methods regarding the aforementioned biosensor work done in this portion of our study (Chan, Ager, & Thompson, 2013).

7.2 MSNs as a Delivery Platform

Despite the antimicrobial potential of both natural plant compounds, their hydrophobicity, volatile nature, and low solubility in aqueous environments prevent them from reaching their maximum inhibitory capacity. In this regard, MSNs may be promising candidates for the stabilisation and delivery of natural compounds in order to improve their antimicrobial effect.

In recent years, MSNs have received growing scientific interest as carriers for many applications, most prevalent being drug delivery, gene therapy, bio-imaging, and enzyme immobilisation (Barbé *et al.*, 2004; Hom *et al.*, 2010; Ispas *et al.*, 2009; Lu *et al.*, 2007). The attraction of MSNs for biomedical applications is attributed to their unique properties, which include: good biocompatibility; high surface area for high bioavailability of guest compounds; uniform pore size and distribution; ordered cylindrical porous network for free diffusion of entrapped molecules; protective framework to stabilise volatiles; tuneable pore and particle size to maximise cell association or endocytosis; modifiable/functionalisable particle and pore surfaces; thermal, chemical, and mechanical stability (Hom *et al.*, 2010;

Liong *et al.*, 2008; Lu *et al.*, 2007; Trewyn *et al.*, 2007). One published study reported the exploitation of many of these key features to develop a versatile multifunctional MSN delivery system for hydrophobic anticancer drugs, with dual-imaging capability (fluorescence and magnetic resonance) and surface conjugation with a cancer-specific targeting component (folic acid) to increase uptake into cancer cells (Liong *et al.*, 2008). Similar success with storage and transport of hydrophobic anticancer drugs camptothecin, paclitaxel, and doxorubicin was achieved by employing MSNs to overcome the insolubility problem (Lu *et al.*, 2007; Vivero-Escoto, Slowing, Wu, & Lin, 2009).

Another report took advantage of MSNs' biocompatibility and highly functionalisable silica surface to deliver small interfering RNA (siRNA) in human cells to shut down specific gene function for treatment of genetic diseases (gene therapy) (Hom *et al.*, 2010; Xia *et al.*, 2009). This was achieved via surface modification with phosphonate compounds (THPMP, see Chapter 4) to reduce particle aggregation, plus the functionalisation of positively charged organic adjuncts (polyethyleneimine) to enhance cellular uptake and effectively bind negatively charged nucleic acids (Hom *et al.*, 2010; Xia *et al.*, 2009).

The use of MSNs to immobilise and deliver enzymes for bio-industrial purposes has also been reported (F. Wang *et al.*, 2010). Wang, *et* al., 2010, successfully increased storage stability and temperature endurance of laccase by immobilising the enzyme on Cu^{2+}-chelated MSNs. Laccases are copper-containing oxidase enzymes that have been used in biosensors, biofuel cells, bioremediation, and sustainable wastewater treatment (F. Wang *et al.*, 2010). These enzymes are very strongly inhibited by common reagents, anions, and metal ions. Thus, enhancing the bioactivity of laccase via a stabilising delivery system using MSNs would be beneficial for industrial applications. This work is similar in its target application as our present study, which is focused on an environmentally-sustainable, industrial, and engineering angle.

This present study is the first to report the utilisation of MSNs for the delivery of plant-derived compounds in any context. Like certain anticancer drugs (e.g. camptothecin, paclitaxel, and doxorubicin) (Liong *et al.*, 2008; Lu *et al.*, 2007; Vivero-Escoto *et al.*, 2009), plant secondary metabolites such as AIT and CNAD are hydrophobic and insoluble in aqueous environment, and thus poorly distributed and isolated from target microbes when employed as antimicrobial agents. To overcome this, emulsifiers or surfactants are often used, but the full antimicrobial potential of plant compounds is often muted by the use of such solvents (Barbé *et al.*, 2004). MSNs would mitigate this problem by eliminating the need for additional solvents. As carriers, MSNs would increase the bioavailability and enhance dispersion of plant compounds since MSNs are intrinsically hydrophilic and can freely disperse in aqueous solutions. Thus, MSNs could enhance the transport of hydrophobic agents such as AIT and CNAD to target cells.

Like siRNA or laccase (Hom *et al.*, 2010; F. Wang *et al.*, 2010), AIT and CNAD are unstable: siRNA is highly susceptible to nuclease degradation in biological fluids, laccase is highly unstable at pH 7.0 and breaks down progressively with increase in temperature beyond 30˚C, and AIT and CNAD are highly volatile and prone to degradation in water. The scaffolds that form the cylindrical pores within MSNs act as physical, protective barriers that surround volatile and/or unstable guest molecules (Trewyn *et al.*, 2007), decreasing their degradation in aqueous environment and minimising loss through vaporisation. This is highly advantageous because significant amounts of AIT and CNAD are normally lost through spontaneous vaporisation. The high surface area-to-volume ratio along with MSNs' accessible reaction sites on pore surfaces also helps to maximise the bioavailability of the loaded compound during its exposure to target cells.

Having MSNs act as physical shields would enhance the efficiency and effectiveness of each antimicrobial treatment by retaining more of the loaded agent in the system. Thus,

lower amounts of the biocidal agent would be needed per dose because less of it would be lost through vaporisation and/or nonspecific diffusion to areas with no target microbes. Treating bacteria with a biocidal agent that is more than the necessary amount leads to greater risk that persister cells would acquire resistance to the larger amount of agent applied. The surviving persister cells would then respond by further strengthening their resistance and repopulating with new cells that possess the same heightened resistant phenotypes as the parent persister cells (vertical gene transfer). Therefore, exposing target bacteria to lower dosages of an antimicrobial agent would reduce the opportunity for the development and augmentation of resistance, which is a valuable advantage to using MSNs as delivery vehicles of antimicrobials.

7.3 Controlled Release by Capped MSNs

It is highly desirable to design delivery systems that respond to external triggers and release the loaded compounds at specific sites. Premature and/or indiscriminate release of active compounds may lower the dosage and efficacy against target cells or tissue, and may even cause serious adverse effects in cases such as the delivery of toxic anti-tumour/chemotherapy drugs (Trewyn *et al.*, 2007). Several reports have been published regarding the incorporation of pore caps on MSNs for on-command release of entrapped molecules via external stimuli. Gatekeepers that have been successfully functionalised onto mesoporous silica material include azobenzene moieties, polyamines, carboxylates, rotaxanes/pseudorotaxanes, complexes with cucurbit(6,7)uril, proteins (e.g. avidin), α- and β-cyclodextrins, and various types of nanoparticles (i.e. iron(II,III) oxide, cadmium sulphide, and gold) (Angelos *et al.*, 2007; Aznar, Marcos, Martiñez-Máñez, *et al.*, 2009; Bernardos *et al.*, 2008; Casasús *et al.*, 2008; Fu *et al.*, 2003; Kang *et al.*, 2012; Lai *et al.*, 2003; Lu *et al.*, 2008; Mal, Fujiwara, *et al.*, 2003; Mei *et al.*, 2012; Schlossbauer *et al.*, 2009; Slowing *et al.*, 2007; Sun *et al.*, 2012; Teng *et al.*, 2012; Trewyn *et al.*, 2007). Stimuli-responsive strategies

for such delivery systems include light, pH, temperature, redox, electrochemical, ultrasonic, enzyme-induced, ligand-induced, and chemical-induced triggers.

This current study incorporated lactose molecules as enzyme-cleavable, selectively-metabolisable gatekeepers on MSNs for controlled release of entrapped antimicrobial agents. The ability to metabolise different types of saccharides/carbohydrates to yield energy is specific to each organism (Palcu & Popescu, 2005). Herein, lactose was employed as a model capping agent to demonstrate that selective de-capping and directed release antimicrobial compounds could be achieved via exploitation of the distinct ability to metabolise lactose by one species of bacteria and not another. This present study modelled and modified the method of anchoring lactose molecules to silica surface from Bernardos, *et al.*, 2009, in which silane groups were added to disaccharide molecules to allow for Si-Si bonds to form between the lactose and the surface of amorphous, microscale mesoporous silica support (Bernardos *et al.*, 2009).

As with the work described presently, several previous studies have also utilised carbohydrates/saccharides as pore caps. Capped MSNs with β-cyclodextrin (β-CD) (a cyclic oligosaccharide) as gatekeepers have been successfully fabricated, with the β-CD cap linked to an ester stalk that is either photo-cleavable or degradable by lipase or esterase enzymes. (C. Park, Kim, *et al.*, 2009; C. Park, Lee, *et al.*, 2009). Pores were de-capped in the presence of the α-amylase enzyme, which hydrolysed the β-CD molecules. The same occurred upon exposure to light, lipase, or esterase, which degraded the stalk portion of the gatekeeper.

Another example in which saccharide caps were employed would be the surface conjugation of various mixtures of carbohydrate polymers (glucose, maltose, oligosaccharides, and polysaccahrides) on MSNs serving as biodegradable gatekeepers (Bernardos *et al.*, 2010). The de-capping mechanism of these saccharide-capped MSNs was

achieved either by β-D-glalactosidase or pancreatin (a mixture of several digestive enzymes) via the hydrolysis of 1→4 glycosidic bonds in the starches.

A third example of employing carbohydrate-related compounds as gatekeepers would be the functionalisation of gluconamide onto non-spherical microscale mesoporous silica material, where the delivery of cargo was selectively inhibited via association of borate anions with the appended saccharide derivatives to form boronate ester pore caps (Aznar, Coll, *et al.*, 2009). The de-capping mechanism was pH-sensitive, wherein acidic pH (pH = 3.0) would hydrolyse the boroester derivative. The same authors also reported the synthesis of a similar mesoporous silica delivery system in which borate-functionalised gold nanoparticles inhibited release of cargo by forming boroester bonds with polyalcohols (sugar alcohols) appended on the silica surface (Aznar, Marcos, Martínez-Máñez, *et al.*, 2009). De-capping was achieved via decrease in pH or exposure to laser light (locally heating the gold nanoparticles), both causing the cleavage of boronic ester linkages.

Although our present study focused on the exploitation of saccharides as pore cap components on silica solids just as previous published works have done, the size scale (micro- versus nanoscale), the intended applications (delivery of therapeutics versus delivery of antimicrobial agents), and the de-capping mechanisms the for such systems are vastly different. The novelty of our work is the entrapment of volatile and unstable plant antimicrobial agents within capped mesoporous silica nanospheres in order to (i) harness and maximise antimicrobial activity of the plant-derived antimicrobial compounds per dose, and (ii) to engineer an antimicrobial system that provides on-command and directed delivery of biocidal compounds based on the targets themselves or the microenvironment they create.

As inventors working with Oxford University's technology transfer unit Isis Innovation Ltd., we (Andrea C. Chan, Prof. Ian P. Thompson, and Dr. Helen Townley) have

submitted an official patent application (application number GB 1317293.7) entitled "Methods, Materials and Products for Delivering Biocides." The patent application encompasses a delivery system for biocides being targeted toward a specific microorganism or microbial community comprising (i) a core material, (ii) a biocide suitable for combating the targeted microorganism, (iii) the biocide being located within or on the core material, and (iv) a capping material applied to the core material so as to contain the biocide within or on the core material, and to enable exposure of the biocide when the capping material is broken down or opened up; wherein the capping material comprises a degradable material selected such as to be desirable to, and consumable by, the microorganism being targeted.

7.4 Strategies to Combat Biofilms

Much of the research done in prevention, removal, and killing of bacterial biofilms are either in the dental/medical field (Cramton *et al.*, 2001; Nassar *et al.*, 2011) or for industrial applications (Ludensky, 2003). Of greater relevance and interest to this present study are efforts against industrial biofilms and biofouling. Some strategies to overcome biofouling involve surface modification of substrata susceptible to biofilm adherence (with hydrophilic materials, self-polishing copolymers, fouling release coatings like silicone, etc.), mechanical disruption, and electrochemical methods (Weir *et al.*, 2008). Other approaches include novel biocidal and bacteriostatic agents, and more recently, nanoparticles. Plant essential oils and their constituent active compounds have gained scientific attention for combating biofilms mainly from the small scale, food preservation angle (Delaquis & Mazza, 1995). Work involving precious-metal (Au, Ag) and metal oxide (ZnO, TiO_2, CuO, Fe_2O_3) nanoparticles have also been done to assess their anti-biofilm efficacy because of their ability to produce reactive oxygen species that damage cell and biofilm components (Li *et al.*, 2008).

Another current approach to inhibit biofilms is to disrupt quorum sensing between constituent cells of a biofilm community (Cady *et al.*, 2012). Quorum sensing is chemical signalling in biofilms that involve the release of small diffusible signalling molecules (e.g. oligopeptides, n-acyl homoserine lactones, autoinducers) by biofilm bacteria that induces transcription of specific genes and enables coordination of bacterial behaviour at the population level, increasing protection and resistance to antagonistic treatments (Davies, 2003; Miller & Bassler, 2001). Quorum sensing inhibition (QSI) may have the potential to mitigate the development of antibacterial resistance in biofilms (Cady *et al.*, 2012).

Anti-biofilm strategies involving delivery of antimicrobial agents via nanoparticles have also been reported. A combination of poly(lactic-*co*-glycolic acid) (PLGA) and alginate nanoparticles has been employed to release therapeutic doses of drugs to treat biofilm-related diseases (H. Ma & Bryers, 2012). Although the general strategy of exploiting nanomaterials for delivery of antimicrobial agents to combat biofilms have been previously executed, the novelty of our present work lies in the complete design using mesoporous silica nanospheres to deliver plant secondary metabolites for the purpose of killing biofilm bacteria in engineered systems.

7.5 Future Work

The capped MSN system for the delivery of plant antimicrobials developed in this present work can be further customised and engineered. Firstly, in addition to AIT and CNAD, other plant-derived compounds and sensitive antimicrobial agents would also benefit from being protected and entrapped in the mesopores of MSNs since they may be hydrophobic, volatile, or prone to degradation. Improving the dispersity of biocidal compounds and their retention in water through storage and transport within MSNs would improve their activity, antimicrobial or otherwise, in aqueous environments. Thus, one

possible next step could be expanding the types of antimicrobial compounds to be loaded within MSNs.

Secondly, other metabolisable saccharides or combinations of saccharides could be derivatised with silane groups and attached onto MSN surface as gatekeepers over mesopores. Lactose served as a proof-of-concept that MSNs could be functionalised with gatekeepers that allowed for the release of entrapped compounds only when specific stimuli or targets were present. This design can be expanded to include other selectively assimilated nutrients or carbohydrates such as xylose, which is metabolisable only by organisms possessing relevant pathways.

Conjugating functional groups to internal pore surfaces can also further enhance this system. Compounds can be housed within MSNs via physical adsorption, electrostatic interactions between the molecule and silica support, or chemical binding (Ispas *et al.*, 2009). By tailoring the size and chemistry of pores to match the structure and chemistry of guest molecules, the loading efficiency and release profile can be controlled and optimised.

Assessing the efficacy of this loaded-MSN antimicrobial system against a community consisting of mixed bacterial species would be valuable in the future since heterogeneous microbial populations are more realistic in practical application. So far in our work, the inhibitory activity of this delivery system has only been evaluated against cultures and biofilms of a single species.

Magnetic separation technology is a promising strategy for recovering paramagnetic MSNs using an external magnetic field for recycled use (F. Wang *et al.*, 2010). Magnetic elements like copper have been chelated to MSNs, making them magnetic. The ability to remove biocides once it has killed target cells is significantly advantageous because it reduces the cells' exposure to the biocide, thus lowering the chance of spontaneous or

elevated levels of resistance. Also, having the MSNs be magnetic enables them to be dragged through the biofilm matrix so that they can release their biocidal cargo even in the depths of the biofilm.

The sophistication of our current lactose-capped, AIT-or CNAD-loaded MSNs could be enhanced by incorporating magnetic separation technology, wherein a magnetite core would be included so that once the plant-secondary metabolites have been unloaded, the empty and de-capped MSNs can be quickly removed, retrieved, re-loaded with active compounds, and re-capped. This would be an excellent feature to further improve the sustainability of this antimicrobial strategy since the same MSNs can be used multiple times. Thus, fabricating magnetically separable, loaded and capped MSNs would be of significant advantage and environmental benefit in the future.

7.6 Conclusion

The use of stimuli-responsive MSNs loaded with a plant-derived antimicrobial compounds developed in this study was an elegant system that can be highly effective in treating unwanted bacteria in industrial sectors. These MSNs were designed to respond to external stimuli intelligently, with gatekeepers that degrade only in the vicinity of certain target bacterial cells. This system of transporting biocidal agents would alleviate the problem of over-saturating the system with high amounts of antimicrobial agents, which can confer resistance and also corrode materials.

The technology developed presently can be expanded to broader applications. Traditional biocides and other nonconventional antimicrobial agents could also benefit from the directed and on-command transport to target microbes that this capped-MSN delivery technology provides. Other capping materials can also be incorporated in order to tailor the de-capping trigger to appropriate external stimuli or microorganism being targeted.

Ultimately, the technology developed presently would improve the efficacy and efficiency of a loaded biocidal agent while minimising the amount of it used per dose, and hence opportunity for resistance development would also be reduced.

As free agents alone, AIT and CNAD proved to be highly effective against Gram-negative and Gram-positive, planktonic and biofilm bacteria. Employing complementary *lux*-based whole cell biosensors was a novel and effective method developed presently to elucidate the mechanism of kill for both compounds. The biocidal activities of AIT and CNAD were enhanced significantly when they were loaded into MSNs for protection and sustained release. This antimicrobial strategy is one that would be substantially more sustainable and resourceful than conventional methods because (i) at antimicrobially-active concentrations, plant-derived antimicrobials are neutral to humans and the environment since they are sourced from nature, (ii) chance of resistance development is lowered because exposure to antimicrobial pressure is minimised while inhibitory efficacy is maximised per dose, and (iii) the inert silica delivery vehicles can be recycled and reused, which would minimise cost of repetitive production, materials used, and waste generated. Thus, the complete AIT- or CNAD-loaded, lactose-capped MSNs delivery complex proved to be an effective, well-engineered, and environmentally conscientious system for killing planktonic and biofilm bacteria.

REFERENCES

Abedon, S. T. (1998). Lecure Notes on Microbiology, from http://www.mansfield.ohio-state.edu/~sabedon/biol1080.htm

Adams, E. Q., & Rosenstein, L. (1914). The color and ionization of crystal-violet. *Journal of American Chemical Society, 36*(7), 1452–1473.

Al-Ahmad, M., Abdul Aleem, F. A., Mutiri, A., & Ubaisy, A. (2000). Biofuoling in RO membrane systems Part 1: Fundamentals and control. *Desalination, 132*(1), 173-179.

Alil, S. M., Khan, A. A., Ahmed, I., Musaddiq, M., Ahmed, K. S., Polasa, H., . . . Ahmed, N. (2005). Antimicrobial activities of Eugenol and cinnamaldehyde against human gastric pathogen *Helicobacter pylori*. *Annals of Clinical Microbiology and Antimicrobials 4*(20).

Amalaradjou, M. A. R., Narayanan, A., Baskaran, S. A., & Venkitanarayanan, K. (2010). Antibiofilm effect of *trans*-cinnamaldehyde on uropathogenic *Escherichia coli*. *Journal of Urology 184*(1), 358-363.

Anderl, J. N., Franklin, M. J., & Stewart, P. S. (2000). Role of antibiotic penetration limitation in *Klebsiella pneumonia* biofilm resistance to ampicillin and ciprofloxacin. *Antimicrobial Agents and Chemotherapy, 44*, 1818-1824.

Andrews, J. M. (2001). Determination of minimum inhibitory concentrations. *Journal of Antimicrobial Chemotherapy, 28*(1), 5-16.

Andrews, J. M. (2001). The development of the BSAC (British Society for Antimicrobial Chemotherapy) standardized method of disk diffusion testing. *Journal of Antimicrobial Chemotherapy 48*, 5-16.

Angelos, S., Vhoi, E., Vögtle, F., De Cola, L., & Zink, J. I. (2007). Photo-driven expulsion of molecules from mesostructured silica nanoparticles. *Journal of Physical Chemistry, 111*, 6589-6592.

Angelos, S., Yang, Y.-W., Patel, K., Stoddart, J. F., & Zink, J. I. (2008). pH-responsive supramolecular nanovalves based on cucurbit[6]uril pseudorotaxanes. *Angewandte Chemie, International Edition, 47*, 2222–2226.

Aruoma, O. I., Spencer, J. P., Rossi, R., Aeschbach, R., Khan, A., Mahmood, N., . . . Halliwell, B. (1996). An evaluation of the antioxidant and antiviral action of extracts of rosemary and Provencal herbs. *Food and Chemical Toxicology, 34*, 449-456.

Aznar, E., Casasús, R., García-Acosta, B., Marcos, M. D., Martínez-Máñez, R., Sancenón, F., . . . Amorós, P. (2007). Photochemical and chemical two-channel control of functional nanogated hybrid architectures. *Advanced Materials, 19*, 2228-2231.

Aznar, E., Coll, C., Marcos, M. D., Martínez-Máñez, R., Sancenón, F., Soto, J., . . . Ruiz, E. (2009). Borate-driven gatelike scaffolding using mesoporous materials functionalised with saccharides. *Chemistry - A European Journal, 15*(28), 6877-6888.

Aznar, E., Marcos, M. D., Martiñez-Máñez, R., Sancenón, F., Soto, J., Amorós, P., & Guillem, C. (2009). pH- and photo-switched release of guest molecules from mesoporous silica supports. *Journal of American Chemical Society, 131*, 6833–6843.

Aznar, E., Marcos, M. D., Martínez-Máñez, R., Sancenón, F., Soto, J., Amorós, P., & Guillem, C. (2009). pH- and photo-switched release of guest molecules from mesoporous silica supports. *Journal of the American Chemical Society, 131*(19), 6933-6843.

Baldwin, T. O. (1996). Firefly luciferase: the structure is known, but the mystery remains. *Structure 4*(3), 223-228.

Baldwin, T. O., Christopher, J. A., Raushel, F. M., Sinclair, J. F., Ziegler, M. M., Fisher, A. J., & Rayment, I. (1995). Structure of bacterial luciferase. *Current Opinion in Structural Biology, 5*(6), 798-809.

Barbé, C., Barlett, J., Kong, L., Finnie, K., Lin, H. Q., Larkin, M., . . . Calleja, G. (2004). Silica particles: a novel drug-delivery system. *Advanced Materials 16*, 1959-1966.

Barrett, E. p., Joyner, L. G., & Halenda, P. P. (1951). The determination of pore volume and area distributions in porous substances. I. Computations from nitrogen isotherms. *Journal of American Chemical Society, 73*(1), 373-380.

Batchelor, G. K. (1967) *An Introduction to Fluid Dynamics* (pp. 229, 233). Cambridge, UK: Cambridge University Press.

Belas, R., Milehem, A., Cohn, D., Hilmen, M., Simon, M., & Silverman, M. (1982). Bacterial bioluminescence: Isolation and expression of the luciferase genes from *Vibrio harveyi*. *Science, 218*, 791-793.

Ben-Israel, O., Ben-Israel, H., & Ulitzur, S. (1998). Identification and quantification of toxic chemicals by use of *Escherichia coli* carrying *lux* genes fused to stress promoters. *Applied and Environmental Microbiology, 64*(11), 4346-4352.

Ben Arfa, A., Combes, S., Preziosi-Belloy, L., Gontard, N., & Chalier, P. (2006). Antimicrobial activity of carvacrol related to its chemical structure. *Letters is Applied Microbiology 43*, 149-154.

Bernardos, A., Aznar, E., Coll, C., Martiñez-Máñez, R., Barat, J. M., Marcos, M. D., . . . Soto, J. (2008). Controlled release of vitamin B_2 using mesoporous materials functionalized with amine-bearing gate-like scaffoldings. *Journal of Controlled Release, 131*, 181-189.

Bernardos, A., Aznar, E., Marcos, M. D., Martínez-Máñez, R., Sancenón, F., Soto, J., . . . Amoros, P. (2009). Enzyme-responsive controlled release using mesoporous silica supports capped with lactose. *Angewandte Chemie, 48*(5884-5887).

Bernardos, A., Mondragon, L., Aznar, E., Marcos, M. D., Martínez-Máñez, R., Sancenón, F., . . . Amorós, P. (2010). Enzyme-responsive intracellular controlled release using nanometric silica mesoporous supports capped with "saccharides". *Acs Nano, 4*(11), 6353-6368.

Bernhard, M. (2003). Approaches to prevention, removal and killing of biofilms. *International Biodeterioration and Biodegradation 51* 249-253.

Brackman, G., Cos, P., Maes, L., Nelis, H. J., & Coenye, T. (2011). Quorum sensing inhibitors increase the susceptibility of bacterial biofilms to antibiotics *in vitro* and *in vivo*. *Antimicrobial Agents and Chemotherapy, 55*(6), 2655-2661

Brasil, I. M., Gomes, C., Puerta-Gomez, A., Castell-Perez, M. E., & Moreira, R. G. (2012). Polysaccharide-based multilayered antimicrobial edible coating enhances quality of fresh-cut papaya. *LWT - Food Science and Technology, 47*, 39-45.

Breeuwer, P., & Abee, T. (2000). Assessment of viability of microorganisms employing fluorescence techniques. *International Journal of Food Microbiology, 55*, 193-200.

Brown, M. R., Allison, D. G., & Gilbert, P. (1988). Resistance of bacterial biofilms to antibiotics: a growth-rate related effect? . *Journal of Antimicrobial Chemotherapy 30*, 521-527.

Brown, M. R. W., & Gilbert, P. (1993). Sensitivity of biofilms to antibiotic agents. *Journal of Applied Bacteriology 74*, 87s-97s.

Brunauer, S., Emmett, P. H., & Teller, E. (1938). Adsorption of Gases in Multimolecular Layers. *Journal of American Chemical Society, 60*(2), 309-319.

Burlage, R. S., & Kuo, C. T. (1994). Living biosensors for the management and manipulation of microbial consortia. *Annual Review of Microbiology, 48*, 291-309.

Burt, S. A. (2004). Essential oils: their antibacterial properties and potential applications in foods: a review. *International Journal of Food Microbiology 94*, 223-253.

Busby, S., & Ebright, R. H. (2001). Transcription activation by catabolite activator protein (CAP). *Journal of Molecular Biology, 293*, 199–213.

Buschini, A., Carboni, P., Furlini, M., Poli, P., & Rossi, C. (2004). Sodium hypochlorite-, chlorine dioxide- and peracetic acid-induced genotoxicity detected by the Comet assay and *Saccharomyces cerevisiae* D7 tests. *Mutagenesis 19*(2), 157-162.

Cady, N. C., McKean, K. A., Behnke, J., Kubec, R., Mosier, A. P., Kasper, S. H., . . . Musah, R. A. (2012). Inhibition of biofilm fomation, quorum sensing and infection in *Pseudomonas aeruginosa* by natural products-inspired organosulfur compounds. *PLoS ONE, 7*(6), e38492.

Calsamiglia, S., Busquet, M., Cardozo, P. W., Castillejos, L., & Ferret, A. (2007). Essential oils as modifiers of rumen microbial fermentation. *Journal of Dairy Science, 90*(6), 2580-2595.

Campbell, N. A., Reece, J. B., Urry, L. A., Cain, M., Wasserman, S. A., Minorsky, P. V., & Jackson, R. B. (2008a). Cell Cycle *Biology* (Eighth ed.): Benjamin Cummings.

Campbell, N. A., Reece, J. B., Urry, L. A., Cain, M., Wasserman, S. A., Minorsky, P. V., & Jackson, R. B. (2008b). Cellular Respiration *Biology* (Eigth ed.): Benjamin Cummings.

Campbell, N. A., Reece, J. B., Urry, L. A., Cain, M., Wasserman, S. A., Minorsky, P. V., & Jackson, R. B. (2008c). Membrane Structure and Function *Biology* (Eigth ed.): Benjamin Cummings.

Campbell, N. A., Reece, J. B., Urry, L. A., Cain, M., Wasserman, S. A., Minorsky, P. V., & Jackson, R. B. (2008d). Structure and Function of Macromolecules *Biology* (Eighth ed.): Benjamin Cummings.

Campbell, N. A., Reece, J. B., Urry, L. A., Cain, M., Wasserman, S. A., Minorsky, P. V., & Jackson, R. B. (2008e). A Tour of the Cell *Biology* (Eighth ed.): Benjamin Cummings.

CAP Technology, U. K. Biological wastewater treatment with BIOBLOK®, from http://www.captechnology.co.uk/pdf/cap_design.pdf

Carey, F. A., & Giuliano, G. (2013). Aldehydes and Ketones. Nucleophilic Addition to C=O *Organic Chemistry* (Ninth ed.): McGraw-Hill.

Carr, B., Hole, P., Malloy, A., Smith, J., Weld, A., & Warren, J. (2008). *The real-time, simultaneous analysis of nanoparticle size, zeta potential, count, asymmetry and fluorescence in liquids*. Paper presented at the Particle Synthesis, Characterization, and Particle-Based Advanced Materials, Orlando, Florida.

Carr, B., & Wright, M. (2013). NTA Applied to Nanoparticles and Nanomaterials Production and Analysis *Nanoparticle Tracking Analysis: A Review of Applications and Usage 2010-2012*. London, UK: NanoSight Ltd.

Casasús, R., Climent, E., Marcos, M. D., Martiñez-Máñez, R., Sancenón, F., Soto, J., . . . Ruiz, E. (2008). Dual aperture control on pH- and anion-driven supramolecular nanoscopic hybrid gate-like ensembles. *Journal of American Chemical Society, 130*, 1903-1917.

Casasús, R., Marcos, M. D., Martiñez-Máñez, R., Ros-Lis, J. V., Soto, J., Villaescusa, L. A., . . . Latorre, J. (2004). Toward the development of ionically controlled nanoscopic molecular gates. *Journal of American Chemical Society, 126*, 8612-8613.

Chacon, P. A., Buffo, R. A., & Holley, R. A. (2006). Inhibitory effects of microencapsulated allyl isothiocyanate (AIT) against Escherichia coli O157:H7 in refrigerated, nitrogen packed, finely chopped beef. *International Journal of Food Microbiology, 107*, 231-237.

Chan, A. C., Ager, D., & Thompson, I. P. (2013). Resolving the mechanism of bacterial inhibition by plant secondary metabolites employing a combination of whole-cell biosensors. *Journal of Microbiological Methods, 93*(3), 209-217.

Chao, S., Young, G., C., O., & Nakaoka, K. (2008). Inhibition of methicillin-resistant *Staphylococcus aureus* (MRSA) by essential oils. *Flavour and Fragrance Journal, 23*, 444-449.

Chao, S. C., Young, D. G., & Oberg, C. J. (2000). Screening for inhibitory activity of essential oils on selected bacteria, fungi and viruses. *Journal of Essential Oil Research, 12*(5), 539-649.

Chapman, J., Weir, E., & Regan, F. (2010). Period four metal nanoparticles on the inhibition of biofouling. *Colloids and Surfaces B: Biointerfaces, 78*, 208-216.

Chen, Z., Yang, H., & Pavletich, N. P. (2008). Mechanism of homologous recombination from the RecA–ssDNA/dsDNA structures. *Nature, 453*(7194), 489-494.

Cheow, W. S., Chang, M. W., & Hadinoto, K. (2010). Antibacterial efficacy of inhalable levoflaxin-loaded polymeric nanoparticles against *E.coli* biofilm cells: The effect of antibiotic release profile. *Pharmaceutical Research 27*, 1597-1609.

Chuanchuen, R., Karkhoff-Schweizer, R. R., & Schweizer, H. P. (2003). High-level triclosan resistance in *Pseudomonas aeruginosa* is solely a result of efflux. *American Journal of Infection Control, 31*(2), 124-147.

Climent, E., Bernardos, A., Martínez-Máñez, R., Maquieira, A., Marcos, M. D., Pastor-Navarro, N., . . . Amorós, P. (2009). Controlled delivery systems using antibody-capped mesoporous nanocontainers. *Journal of American Chemical Society, 131*, 14075–14080.

Clinical and Laboratory Standards Institute, C. (2009a). Methods for dilution antimicrobial suceptibility tests for bacteria that grow aerobically; approved standard (Eighth ed., Vol. 29). USA: Clinical and Laboratory Standards Institute.

Clinical and Laboratory Standards Institute, C. (2009b). Performance standards for antimicobial disk susceptibility tests; approved standard (tenth ed., Vol. 29): Clinical and Laboratory Standards Institute.

Close, D., Xu, T., Smartt, A., Rogers, A., Crossley, R., Price, S., . . . G., S. (2012). The evolution of the bacterial luciferase gene cassette (lux) as a real-time bioreporter. *Sensors, 12*, 732-752.

Cochran, W. L., McFeters, G. A., & Stewart, P. S. (2000). Reduced susceptibility of thin *Pseudomonas aeruginosa* biofilms to hydrogen peroxide and monochloramine. *Journal of Applied Microbiology 88*, 22-30.

Coll, C., Casasús, R., Aznar, E., Marcos, M. D., Martínez-Máñez, R., Sancenón, F., . . . Amorós, P. (2007). Nanoscopic hybrid systems with a polarity-controlled gate-like scaffolding for the colorimetric signalling of long-chain carboxylates. *Chemical Communications*, 1957–1959.

Conlon, K. M., Humphreys, H., & O'Gara, J. P. (2002). *icaR* encodes a transcriptional repressor involved in environmental regulation of ica operon expression and biofilm formation in Staphylococcus epidermidis. *Journal of Bacteriology 184*, 4400-4408.

CPS Instruments Inc., E. CPS Disc Centrifuge Nano Particle Size Analysis General Brochure. Retrieved from http://www.cpsinstruments.eu/pdf/General%20Brochure.pdf

CPS Instruments Inc., E. (2005). CPS Disc Centrifuge Operating Manual, from http://www.cpsinstruments.eu/pdf/Manual.pdf

Cramton, S. E., Ulrich, M., Gotz, F., & Doring, G. (2001). Anaerobic conditions induce expression of polysaccharide intercellular adhesin in *Staphylococcus aureus* and *Staphylococcus epidermidis*. *Infection and Immunity 69*, 4079-4085.

Dams, R. I., Biswas, A., Olesiejuk, A., Fernandes, T., & Christofi, N. (2011). Silver nanotoxicity using a light-emitting biosensor *Pseudomonas putida* isolated from a wastewater treatment plant. *Journal of Hazardous Materials, 195*, 68-72.

Davey, M. F., & O'Toole, G. A. (2000). Microbial biofilms: from ecology to molecular genetics. *Microbiology and Molecular Biology Reviews, 64*(4), 847-867.

Davies, D. G. (2003). Understanding biofilm resistance to antibacterial agents. *Nature Reviews Drug Discovery, 2*, 114-122.

Davis, M. E. (2002). Ordered porous materials for emerging applications. *Nature 417*, 813-821.

de Oliveira, M. M. M., Brugnera, D. F., do Nascimento, J. A., Batista, N. N., & Piccoli, R. H. (2012). Cinnamon essential oil and cinnamaldehyde in the control of bacterial biofilms formed on stainless steel surfaces. *European Food Research and Technology, 234*(5), 821-832

Delaquis, P. J., & Mazza, G. (1995). Antimicrobial properties of isothiocyanates in food preservation. *Food Technology 49* 73-84.

Denyer, S. P. (1995). Mechanisms of action of antibacterial biocides. *International Biodeterioration and Biodegradation 36*, 227-245.

Denyer, S. P., & Maillard, J.-Y. (2002). Cellular impermeability and uptake of biocides and antibiotics in Gram-negative bacteria. *Journal of Applied Microbiology 92*, 35s-45s.

Department for Environment, F. a. R. A. (1995). *Waste Management, The Duty of Care, A Code of Practice*. London, UK: Stationary Office.

Didry, N., Dubreuil, L., & Pinkas, M. (1994). Activity of thymol, carvacrol, cinnamaldehyde and eugenol on oral bacteria. *Pharmaceutica Acta Helvetiae, 69*, 25-28.

Ding, X., Yin, B., Qian, L., Zeng, Z., Yang, Z., Li, H., . . . Zhou, S. (2011). Screening for novel quorum-sensing inhibitors to interfere with the formation of *Pseudomonas aeruginosa* biofilm. *Journal of Medical Microbiology, 60*, 1827-1834.

Djordjevic, D., Wiedmann, M., & McLandsborough, L. A. (2002). Microtiter plate assay for assessment of *Listria monocytogenes* biofilm formation. *Applied and Environmental Microbiology, 68*(6), 2950-2958.

Dorman, H. J. D., & Deans, S. G. (2000). Antimicrobial agents from plants: antibacterial activity of plan volatile oils. *Journal of Applied Microbiology 88*, 308-316.

Elsmore, R. G., P., Ludensky, M., & Coulburn, J. (1999). Biofilms in paper manufacturing *Biofilms: The Good, the Bad and the Ugly* (pp. 129-139). Cardiff: Bioline Press.

Eltsov, M., & Zuber, B. (2006). Minireview: Transmission electron microscopy of the bacterial nucleoid. *Journal of Structural Biology, 156*, 246-254.

Regulation of the European Parliament and of the Council concerning the making available on the market and use of biocidal products (2012).

European Union, C. o. t. (2012). Council tightens controls on biocidal products. *9757/12*, from http://www.consilium.europa.eu/uedocs/cms_data/docs/pressdata/en/envir/130111.pdf

Expo-Net Danmark, A. S. General information about BIO-BLOK®, from http://www.expo-net.dk/Standard/Produkter/Akvakultur/Generel%20information%20om%20BIO-BLOK.aspx

Fellers, T. J., & Davidson, M. W. (2007). Introduction to Confocal Microscopy. *Olympus Fluoview Resource Center*.

Fiss, E. M., Rule, K. L., & Vikesland, P. J. (2007). Formation of chloroform and other chlorinated byproducts by chlorination of triclosan-containing antibacterial products. *Environmental Science & Technology, 41*(7), 2387–2394.

Freeman, W. M., Walker, S. J., & Vrana, K. E. (1999). Quantitative RT-PCR: pitfalls and potential. *BioTechniques, 26*(1), 112-122, 124-125.

Friedman, M., Henika, P. R., & Mandrell, R. E. (2002). Bacericidal activities of plant essential oils and some of their isolated consitutents against *Campylobacter jejuni, Escherichia coli, Listeria monocytogenes,* and *Salmonella enterica*. *Journal of Food Protection, 65*(1545-1560).

Fu, Q., Rao, G. V. R., Ista, L. K., Wu, Y., Andrzejewski, B. P., Sklar, L. A., . . . López, G. P. (2003). Control of molecular transport through stimuli-responsive ordered mesoporous materials. *Advanced Materials, 15*, 1262–1266.

Fultz, B., & Howe, J. (2007). *Transmission Electron Microscopy and Diffractometry of Materials*: Springer.

Fux, C. A., Costerton, J. W., Stewart, P. S., & Stoodley, P. (2005). Survival strategies of infectious biofilms. *Trends in Microbiology 13*, 34-30.

Gallucci, M. N., Oliva, M., Casero, C., Dambolena, J., Luna, A., Zygadlo, J., & Demo, M. (2009). Antimicrobial combined action of terpenes against the food-borne microorganisms *Escherichia coli, Staphylococcus aureus* and *Bacillus cereus*. *Flavour and Fragrance Journal 24*, 348-354.

Gilbert, P., Das, J., & Foley, I. (1997). Biofilms susceptibility to antibiotics. *Advances in Dental Research 11*, 160-167.

Gill, A. O., & Holley, R. A. (2006). Inhibition of membrane bound ATPases of *Escherichia coli* and *Listeria monocytogenes* by plant oil aromatics. *International Journal of Food Microbiology, 111*, 170-174.

Gomes, C., R.G., M., & Castell-Perez, E. (2011). Poly(DL-lactide-co-glycolide) (PLGA) nanoparticles with entrapped *trans*-cinnamaldehyde and eugenol for antimicrobial delivery applications. *Journal of Food Science, 76*(2), N16-N24.

Görke, B., & Stülke, J. (2008). Carbon catabolite repression in bacteria: many ways to make the most out of nutrients. *Nature Reviews Genetics, 6*(8), 613–624.

Green, M. R., & Sambrook, J. (2012). Isolation and quantification of DNA *Molecular Cloning, A Laboratory Manual* (Fourth ed., Vol. 1): Cold Spring Harbor Laboratory Press.

Halasz, I., & Schneider, W. (1961). Quantitative gas chromatographic analysis of hydrocarbons with capillary column and flame ionization detector. *Analytical Chemistry, 33*(8), 978-982.

Harris, D. C. (1999). Gas Chromatography *Quantitative chemical analysis* (Fifth ed., pp. 675–712): W.H. Freeman and Company.

Heath, R. J., Rubin, J. R., Holland, D. R., Zhang, E., Snow, M. E., & Rock, C. O. (1999). Mechanism of triclosan inhibition of bacterial fatty acid synthesis. *Journal of Biological Chemistry, 274*(16), 11110-11114.

Hedges, A. J. (2002). Estimating the precision of serial dilutions and viable bacterial counts. *International Journal of Food Microbiology 76*(3), 207-214.

Heikkila, T., Salonen, J., Tuura, J., Hamdy, M. S., Mul, G., Kumar, N., . . . Lehto, V.-P. (2007). Mesoporous silica material TUD-1 as a drug delivery system. *Pharmaceutical Nanotechnology, 331*, 133-138.

Helander, I. M., Alakomi, H.-L., Latva-Kala, K., Mattila-Sandholm, T., Pol, I., Smid, E. J., . . . von Wright, A. (1998). Characterization of the action of essential oil components on Gram-negative bacteria. *Journal of Agricultural and Food Chemistry 46*, 3590-3595.

Hengge-Aronis, R. (1996). Regulation of gene expression during entry into stationary phase *Escherichia coli and Salmonella: cellular and molecular biology, 2nd ed.* (pp. 1497-1512). Washington, DC: ASM Press.

Hermanson, G. T. (2008). Bioconjugate Chemistry *Bioconjugate Techniques* (Second ed.).

Hewitt, D., Mulcahy, D., Ralston, J., & Wilkinson, G. T. (1991). Rapid particle sizing by photosedimentometry. *Measurement Science and Technology, 2*(4), 271.

Higson, S. (2004). *Analytical Chemistry*. Oxford, UK: Oxford University Press.

Hill, L. E., Gomes, C., & Taylor, T. M. (2013). Characterization of beta-cyclodextrin inclusion complexes containing essential oils (trans-cinnamaldehyde, eugenol, cinnamon bark, and clove bud extracts) for antimicrobial delivery applications. *LWT - Food Science and Technology, 51*, 86-93.

Hoffman, L. R., D'Argenio, D. A., MacCoss, M. J., Zhang, Z., Jones, R. A., & Miller, S. I. (2005). Aminoglycoside antibiotics induce bacterial biofilm formation. *Nature, 436*(7054), 1171-1175.

Hom, C., Lu, J., Liong, M., Luo, H., Li, Z., Zink, J. I., & Tamanoi, F. (2010). Mesoporous silica nanoparticles facilitate delivery of siRNA to shutdown signaling pathways in mammalian cells. *Small, 6*, 1185-1190.

Honoré, N., & Cole, S. T. (1994). Streptomycin resistance in mycobacteria. *Antimicrobial Agents and Chemotherapy, 38*(2), 238-242.

Huang, W. E., Huang, L., Preston, G. M., Naylor, M., Carr, J. P., Li, Y., . . . Wang, H. (2006). Quantitative in situ assay of salicylic acid in tobacco leaves using a genetically modified biosensor strain of *Acinetobacter* sp. ADP1. *Plant Journal, 46*(6), 1073-1083.

Inouye, S., Abe, S., Yamaguchi, H., & Asakura, M. (2003). Comparative study of antimicrobial and cytotoxic effects of selected essential oils by gaseous and solution contacts. *The International Journal of Aromatherapy, 13*(1), 33-41.

Inouye, S., Takizawa, T., & Yamaguchi, H. (2001). Antibacterial activity of essential oils and their major constituents against respiratory tract pathogens by gaseous contact. *Journal of Antimicrobial Chemotherapy, 47*, 565-573.

Ispas, C., Sokolov, I., & Andreescu, S. (2009). Enzyme-functionalized mesoporous silica for bioanalytical applications. *Analytical and Bioanalytical Chemistry 393*, 543-554.

Jia, P., Xue, Y. J., Duan, X. J., & Shao, S. H. (2011). Effect of cinnamaldehyde on biofilm formation and sarA expression by methicillin-resistant *Staphylococcus aureus*. *Letters in Applied Microbiology, 53*(4), 409-416

Jobbagy, A., & Kiraly, K. (1966). Chemical characterization of fluorescein isothiocyanate- protein conjugates. *Biochimica et Biophysica Acta, 124*(1), 166-175.

Jones, F. A. (1996). Herbs - useful plants. Their role in history and today. *European Journal of Gastroenterology & hepatology, 8*, 1227-1231.

Jorgensen, J. H., & Ferraro, M. J. (2009). Antimicrobial susceptibility testing: a review of general principles and contemporary practices. *Clinical Infectious Diseases: an official publication of the Infectious Diseases Society of America, 49*(11), 1749-1755.

Kalemba, D., & Kunicka, A. (2003). Antibacterial and antifungal properties of essential oils. *Current Medicinal Chemistry, 10*(10), 813-829.

Kang, X., Cheng, Z., Yang, D., Ma, P., Shang, M., Peng, C., . . . Lin, J. (2012). Drug delivery: design and synthesis of multifunctional drug carriers based on luminescent rattle-type mesoporous silica microspheres with a thermosensitive hydrogel as a controlled switch. *Advanced Functional Materials, 22*(7), 1539.

Kawabata, M., Kawabata, T., & Nishibori, M. (2005). Role of recA/RAD51 family proteins in mammals. *Acta Medica Okayama, 59*(1), 1-9.

Kawakishi, S., & Kaneko, T. (1987). Interactions of proteins with allyl isothiocyanate. *Journal of Agricultural and Food Chemistry, 35*, 85-88.

Keane, A., Phoenix, P., Ghoshal, S., & Lau, P. C. K. (2002). Exposing culprit organic pollutants: a review. *Journal of Microbiological Methods, 49*, 103-119.

Kim, D., Jung, S., Sohn, J., Kim, H., & Lee, S. (2009). Biocide application for controlling biofouling of SWRO membranes – an overview. *Desalination 238*, 43-52.

Kim, I. H., Han, J., Na, J. H., Chang, P. S., Chung, M. S., Park, K. H., & Min, S. C. (2013). Insect-resistant food packaging film development using cinnamon oil and microencapsulation technologies. *Journal of Food Science, 78*(2), E229-E237.

Knobloch, K., Weigand, H., Weis, N., Schwarm, H.-M., & Vigenschow, H. (1986). Action of terpenoids on energy metabolism. In E. J. Brunke (Ed.), *Progress in Essential Oil Research: 16th International Symposium on Essential Oils* (pp. 429-445). Berlin DeGruyter.

Knopp, D., Tang, D., & Niessner, R. (2009). Review: bioanalytical applications of biomolecule-functionalized nanometer-sized doped silica particles. *Analytica Chimica Acta., 647*(1), 14-30.

Knowles, J. R. (1980). Enzyme-catalyzed phosphoryl transfer reactions. *Annual Review of Biochemistry, 49*, 877-919.

Ko, J. A., Jeon, J. Y., & Park, H. J. (2012). Preparation and characterization of allyl isothiocyanate microcapsules by spray drying. *Journal of Food Biochemistry, 36*(3), 255-261.

Ko, J. A., Kim, W. Y., & Park, H. J. (2012). Effects of microencapsulated Allyl isothiocyanate (AITC) on the extension of the shelf-life of Kimchi. *International Journal of Food Microbiology, 153*(1-2), 92-98.

Koroch, A., Juliana, H. R., & Zygadio, J. A. (2007). Bioactivity of essential oils and their components. In R. G. Berger (Ed.), *Flavours and Fragrances Chemistry, Bioproccessing and Sustainability* (pp. 87-115). Berlin: Springer Verlag.

Kucers, A., Bennett, N. M., & Kemp, R. J. (1997). *Kucers' The Use of Antibiotics* (Vol. 5th edition). Oxford Butterworth-Heinemann

Kurita, N., Miyaji, M., Kurane, R., Takahara, Y., & Ichimura, K. (1979). Antifungal acitivity of molecular orbital energies of aldehyde compounds from oils of higher plants. *Agriculture and Biological Chemistry, 43*, 2365-2371.

Kurita, N., Miyaji, M., Kurane, R., Takahara, Y., & Ichimura, K. (1981). Antifungal activity of components of essential oils. *Agricultural Biology and Chemistry, 45*, 945-952.

Kurvet, I., Ivask, A., Bondarenko, O., Sihtmäe, M., & Kahru, A. (2011). *LuxCDABE*-transformed constitutively bioluminescent *Escherichia coli* for toxicity screening: comparison with naturally luminous *Vibrio fischeri Sensors, 11*, 7865-7878.

Kwon, Y. N., & Leckie, J. O. (2006). Hypochlorite degradation of crosslinked polyamide membranes — II. Changes in hydrogen bonding behavior and performance. *Journal of Membrane Science, 282*, 456–464.

Lai, C.-Y., Trewyn, B. G., Jeftinija, D. M., Jeftinija, K., Xu, S., Jeftinija, S., & Lin, V. S.-Y. (2003). A mesoporous silica nanosphere-based carrier system with chemically removable CdS nanoparticle caps for stimuli-responsive controlled release of neurotransmitters and drug molecules. *Journal of American Chemical Society, 125*, 4451–4459.

Leddy, N. (2012). *Surface Area and Porosity.* Paper presented at the Centre for Microscopy and Analysis (CMA) Analytical Workshop

Lewis, M. (2005). The lac repressor. *Comptes Rendus Biologies, 328*(6), 521-548.

Li, Q., Mahendra, S., Lyon, D. Y., Brunet, L., Liga, M. V., & Li, D. (2008). Antimicrobial nanomaterials for water disinfection and microbial control: Potential applications and implications. *Water Research, 42*, 4591-4602.

Lin, C. M., Preston, J. F., & Wei, C. I. (2000). Antibacterial mechanism of allyl isothiocyanate. *Journal of Food Protection, 63*(6), 727-734.

Lin, Y.-S., & Haynes, C. L. (2009). Synthesis and characterization of biocompatible and size-tunable multifunctional porous silica nanoparticles. *Chemistry of Materials, 21*, 3979-3986.

Linko, P. (1982). Lactose and lactitol. In G. G. Birch & K. J. Parker (Eds.), *Natural Sweeteners* (pp. 109–132). London and New Jersey: Applied Science Publishers.

Liong, M., Lu, J., Kovochich, M., Xia, T., Ruehm, S. G., Nel, A. E., . . . Zink, J. I. (2008). Multifunctional inorganic nanoparticles for imaging, targeting, and drug delivery. *Acs Nano, 2*, 889-896.

Little, J. W. (1984). Autodigestion of lexA and phage lambda repressors. *Proceedings of the National Academy of Sciences Of USA, 81*(5), 1375–1379.

Liu, C. S., Cham, T. M., Yang, C. H., Chang, H. W., Chen, C. H., & Chuang, L. Y. (2007). Antibacterial properties of Chinese herbal medicines against nosocomial antibiotic resistant strains of *Pseudomonas aeruginosa* in Taiwan. *The American Journal of Chinese Medicine, 35*(6), 1047-1060.

Liu, N., Dunphy, D., Atanassov, P., Bunge, S. D., Chen, Z., López, G. P., . . . Brinker, C. J. (2004). Photoregulation of mass transport through a photoresponsive azobenzene-modified nanoporous membrane. *Nano Letters, 4*, 551-554.

Liu, T.-T., & Yang, T.-S. (2010). Stability and antimicrobial activity of allyl isothiocyanate during long-term storage in an oil-in-water emulsion. *Journal of Food Science, 75*(5), C445-451.

Liu, Y., Li, J., Qiu, X., & Burda, C. (2007). Bactericidal activity of nitrogen-doped metal oxide nanocatalysts and the influence of bacterial extracellular polymeric substances (EPS). *Journal of Applied Microbiology 107*, 1193-1201.

Lopez-Ramirez, J. A., Sahuquillo, S., Sales, D., & Quiroga, J. M. (2003). Pre-treatment optimisation studies for secondary effluent reclamation with reverse osmosis. *Water Research, 37*, 1177–1184.

López, D., Vlamakis, H., & R., K. (2010). Biofilms. *Cold Spring Harbor Perspectives in Biology, 2*(7), a000398.

Lopez, E., & Blazquez, J. (2009). Effect of Subinhibitory Concentrations of Antibiotics on Intrachromosomal Homologous Recombination in *Escherichia coli*. *Antimicrobial Agents and Chemotherapy, 53*(8), 3411–3415.

Lu, J., Choi, E., Tamanoi, F., & Zink, J. I. (2008). Light-activated nanoimpeller-controlled drug release in cancer cells. *Small, 4*, 421-426.

Lu, J., Liong, M., Li, Z., Zink, J. I., & Tamanoi, F. (2010). Biocompatibility, biodistribution, and drug-delivery efficiency of mesoporous silica nanoparticles for cancer therapy in animals. *Small, 6*(1794-1805).

Lu, J., Liong, M., Zink, J. I., & Tamanoi, F. (2007). Mesoporous silica nanoparticles as delivery system for hydrophobic anticancer drugs. *Small, 3*(8), 1341-1346.

Luciano, F. B., & Holley, R. A. (2009). Enzymatic inhibiton of allyl isothiocyanate and factors affecting its antimicrobial action against *Escherichia coli* O157:H7. *International Journal of Food Microbiology, 131*, 240-245.

Luciano, F. B., Hosseinian, F. S., Beta, T., & Holley, R. A. (2008). Effect of free -SH containing compounds on allyl isothiocyanate antimicrobial activity against *Escherichia coli* O157:H7. *Journal of Food Science, 73*, 214-220.

Ludensky, M. (2003). Control and monitoring of biofilms in industrial application. *International Biodeterioration and Biodegradation 51*, 255-263.

Ma, H., & Bryers, J. D. (2012). *Anti-biofilm efficacy of biodegradable nanoparticles to delivery novel antimicrobial agents*. Paper presented at the American Institute of Chemical Engineers Annual Meeting 2012, Pittsburgh, PA.

Ma, L., Conover, M., Lu, H., Parsek, M. R., Bayles, K., & Wozniak, D. J. (2009). Assembly and development of the *Pseudomonas aeruginosa* biofilm matrix. *Public Library of Science Pathogens, 5*(3), 1-11.

Mah, T., & O'Toole, G. A. (2001). Mechanism of biofilm resistance to antibiotic agents. *Trends in Microbiology 9* 34-39.

Mahmoud, B. S. M., Yamazaki, K., Miyashita, K., Shin, I.-S., Chang, D.-S., & Tetsuya, S. (2004). Bacterial microflora of carp (*Cyprinus carpio*) and its shelf life extension by essential oil compounds. *Food Microbiology, 21*, 657-666.

Makino, S.-I., Kii, T., Asakura, H., Shirahata, T., Ikeda, T., Takeshi, K., & Itoh, K. (2000). Does enterohaemorrhagic *Escherichia coli* O157 enter the VNC state in salmon roe? *Applied and Environmental Microbiology, 66*, 5536-5539.

Mal, N. K., Fujikura, M., Tanaka, Y., Taguchi, T., & Matsukata, M. (2003). Photoswitched storage and release of guest molecules in the pore boid of coumarin-modified MCM-41. *Chemistry of Materials, 15*, 3385-3394.

Mal, N. K., Fujiwara, M., & Tanaka, Y. (2003). Photocontrolled reversible release of guest molecules from coumarin-modified mesoporous silica. *Nature, 421*(6921), 350-353.

Mann, C. M., Cox, S. D., & Markham, J. L. (2000). The outer membrane of *Pseudomonas aeruginosa* NCTC6749 contributes to its tolerance to essential oil of *Melaleuca alternifolia* (tea tree oil). *Letters in Applied Microbiology, 30*, 294-297.

Mann, C. M., & Markham, J. L. (1998). A new method for determining the minimum inhibitory concentration of essential oils. *Journal of Applied Microbiology, 84*, 538-544.

Mantilla, N., Castell-Perez, M. E., Gomes, C., & Moreira, R. G. (2013). Multilayered antimicrobial edible coating and its effect on quality and shelf-life of fresh-cut pineapple (Ananas comosus). *LWT - Food Science and Technology, 51*, 37-43.

Mayaud, L., Caricajo, A., Zhiri, A., & Aubert, G. (2008). Comparison of bacteriostatic and bactericidal activity of 13 essential oils against strains with varying sensitivity to antibiotics. *Letters in Applied Microbiology 47*, 167-173.

McCusker, L. B., Liebau, F., Engelhardf, G., & Schuth, F. (2003). NOMENCLATURE OF STRUCTURAL AND COMPOSITIONAL CHARACTERISTICS OF ORDERED MICROPOROUS AND MESOPOROUS MATERIALS WITH INORGANIC HOSTS: IUPAC recommentations 2001. *Microporous and Mesoporous Materials, 58*, 3-13.

McFeters, G. A., Yu, F. P., Pyle, B. H., & Stewart, P. S. (1995). Physiological assessment of bacteria using fluorochromes. *Journal of Microbiological Methods, 21*, 1-13.

Mei, X., Chen, D., Li, N., Xu, Q., Ge, J., Li, H., . . . Lu, J. (2012). Facile preparation of coating fluorescent hollow mesoporous silica nanoparticles with pH-sensitive amphiphilic diblock copolymer for controlled drug release and cell imaging. *Soft Matter, 8*, 5309-5316.

Meighen, E. A. (1991). Molecular biology of bacterial bioluminescence. *Microbiological Reviews, 55*, 123-142.

Metcalf & Eddy, I., Tchobanoglous, G., Burton, F., & Stensel, D. H. (2002). *Wastewater Engineering: Treatment and Resuse*. USA: McGraw-Hill Professional.

Micromeritics. (2013a). Gas Adsoprtion Theory Poster, from http://www.micromeritics.com/repository/files/gas_adsorption_theory_poster.pdf

Micromeritics. (2013b). Gemini VII Series Surface Area Analyzers Brochure, from http://www.micromeritics.com/Repository/Files/Gemini_VII_Brochure_1.pdf

Miller, M. B., & Bassler, B. L. (2001). Quorum sensing in bacteria. *Annual Review of Microbiology, 55*, 165-199.

Molecular Probes® Invitrogen™, L. T. (2004). LIVE/DEAD® BacLight™ Bacterial Viability Kits Product Information from http://probes.invitrogen.com/media/pis/mp07007.pdf

Molecular Probes® Invitrogen™, L. T. (2011). SYTO® Green-Fluorescent Nucleic Acid Stains, from http://tools.lifetechnologies.com/content/sfs/manuals/mp07572.pdf

Moleyar, V., & Narasimham, P. (1986). Antifungal activity of some essential oil components. *Food Microbiology, 3*, 331-336.

Montalti, M., Cedi, A., Prodi, L., & Gandolfi , M. T. (2006). *Handbook of Photochemistry* (Third ed.). Florida: CRC press.

Monzote, L., Montalvo, A. M., Scull, R., Miranda, M., & Abreu, J. (2007). Activity, toxicity and analysis of resistance of essential oil from *Chenopodium ambrosioides* after intraperitoneal, oral and intralesional administration in BALC/c mice infected with *Leishmania amazonensis*: a protein study. *Biomedicine & Pharmacotherapy, 61*, 148-153.

Nandiyanto, A. B. D., Kim, S.-G., Iskander, F., & Okuyama, K. (2009). Synthesis of spherical mesoporous silica nanoparticles with nanometer-size controllable pores and outer diameters. *Microporous and Mesoporous Materials, 120*, 447-453.

NanoSight, L. (2009). Applications of Nanoparticle Tracking Analysis (NTA) in nanoparticle research from http://www.nanosight.com

Nassar, H. M., Li, M., & Gregory, R. L. (2011). Effect of honey on *Streptococcus mutans* growth and biofilm formation. *Applied and Environmental Microbiology, 78*(2), 536-540.

Nedorostova, L., Kloucek, P., Kokoska, L., Stolcova, M., & Pulkrabek, J. (2009). Antimicrobial properties of selected essential oils in vapour phase against food borne bacteria *Food Control, 20*, 157-160.

Nguyen, T. D., Leung, K. C.-F., Liong, M., Pentecost, C. D., Stoddart, J. F., & Zink, J. I. (2006). Construction of a pH-driven supramolecular nanovalve. *Organic Letters, 8*, 3363-3366.

Nostro, A., Scaffaro, R., D'Arrigo, M., Botta, L., Filocamo, A., Marino, A., & Bisignano, G. (2012). Study on carvacrol and cinnamaldehyde polymeric films: mechanical properties, release kinetics and antibacterial and antibiofilm activities. *Applied Microbiology and Biotechnology, 96*(4), 1029-1038.

Nuryastuti, T., van der Mei, H. C., Busscher, H. J., Iravati, S., Aman, A. T., & Krom, B. P. (2009). Effect of cinnamon oil on icaA expression and biofilm formation by *Staphylococcus epidermidis*. *Applied and Environmental Microbiology, 75*(21), 6850-6855.

Odabasi, M. (2008). Halogenated volatile organic compounds from the use of chlorine-bleach-containing household products. *Environmental Science & Technology, 42*, 1445-1451.

Oliver, J. D. (1993). Formation of viable but nonculturable cells. In S. Kjelleberg (Ed.), *Starvation in Bacteria* (pp. 239-272). New York: Plenum Press.

Oliver, J. D. (1999). *The viable but nonculturable state and cellular resuscitation*. Paper presented at the 8th International Symposium on Microbial Ecology, Halifax, Canada.

Oliver, J. D. (2005). The viable but nonculturable state in bacteria. *Journal of Microbiology, 43*, 93-100.

Ouattara, B., Simard, R. E., Holley, R. A., Pitte, G. J. P., & Begin, A. (1997). Antibacterial activity of selected fatty acids and essential oils against six meat spoilage organisms. *International Journal of Food Microbiology 37*, 155-162.

Oussalah, M., Caillet, S., & Saucier, L. L., M. . (2007). Inhibitory effects of selected plant essential oils on growth of four pathogenic bacteria: *E. coli* O157:H7, *Salmonella Typhimurium, Staphylococcus aureus* and *Listeria monocytogenes*. *Food Control, 18*, 414-420.

Ozin, G. A., & Arsenault, A. C. (2005). Nanochemistry: a chemical approach to nanomaterials. *Royal Society of Chemistry*.

Palaniappan, K., & Holley, R. A. (2010). Use of natural antimicrobials to increase antibiotic susceptibility of drug resistant bacteria. *International Journal of Food Microbiology, 140*, 164-168.

Palcu, S., & Popescu, I. (2005). Experimental studies regarding the bacterial metabolism of sugars. *Agroalimentary Processes and Technologies, 11*(2), 315-320.

Park, C., Kim, H., Kim, S., & Kim, C. (2009). Enzyme responsive nanocontainers with cyclodextrin gatekeepers and synergistic effects in release of guests. *Journal of American Chemical Society, 131*, 16614-16615.

Park, C., Lee, K., & Kim, C. (2009). Photoresponsive cyclodextrin-covered nanocontainers and their sol-gel transition induced by molecular recognition. *Supramolecular Chemistry, 48*, 1275-1278.

Park, C., Oh, K., Lee, S. C., & Kim, C. (2007). Controlled release of guest molecules from mesoporous silica particles based on a pH-responsive polypseudorotaxane motif. *Angewandte Chemie, International Edition, 46*, 1455-1457.

Park, C. M., Taormina, P. J., & Beuchat, L. R. (2000). Efficacy of allyl isothiocyanate in killing enterohemorrhagic *Escherichia coli* O157:H7 on alfalfa seeds. *International Journal of Food Microbiology 56*, 13-20.

Patel, H., Tscheka, C., & Heerklotz, H. (2009). Characterizing vesicle leakage by fluorescence lifetime measurements. *Soft Matter, 5*(15), 2849-2851.

Pawley, J. B. (2006). *Handbook of Biological Confocal Microscopy* (Third ed.). Berlin: Springer.

Pei, R.-S., Zhou, F., Ji, B.-P., & Xu, J. (2009). Evaluation of combined effects of eugenol, cinnamaldehyde, thymol, and carvacrol against *E. coli* with an improved method. *Journal of Food Science, 74*, M379-383.

Perrins, J. C., Cooper, W. J., van Leeuwen, J. H., & Herwig, R. P. (2006). Ozonation of seawater from different locations: Formation and decay of total residual oxidant — implications for ballast water treatment. *Marine Pollution Bulletin, 52*, 1023–1033.

Piercey, M. J., Mazzanti, G., Budge, S. M., Delaquis, P. J., Paulson, A. T., & Truelstrup Hansen, L. (2012). Antimicrobial activity of cyclodextrin entrapped allyl isothiocyanate in a model system and packaged fresh-cut onions. *Food Microbiology, 30*, 213-218.

Plackett, D., Ghanbari-Siahkali, A., & Szente, L. (2007). Behavior of α- and β-cyclodextrin-encapsulated allyl isothiocyanate as slow-release additives in polylactide-co-polycaprolactone films. *Journal of Applied Polymer Science, 105*(5), 2850-2857.

Podhradský, D., Drobnica, L., & Kristian, P. (1979). Reactions of cysteine, its derivatives, glutathione coenzyme A, and dihydrolipoic acid with isothiocyanates. *Experientia, 35*(2), 154-155.

Poynton, C. A. (2003). Luminance and Lightness *Digital Video and HDTV: Algorithms and Interfaces* (pp. 203-207): Morgan Kaufmann.

Prabuseenivasan, S., Jayakumar, M., & Ignacimuthu, S. (2006). In vitro antibacterial activity of some plant essential oils. *BMC Complementary and Alternative Medicine 6*(39).

Rachid, S., Ohlsen, K., Witte, W., Hacker, J., & Ziebuhr, W. (2000). Effect of subinhibitory antibiotic concentration on polysaccharide intercellular adhesion expression in biofilm-forming *Staphylococcus epidermidis*. *Antimicrobial Agents and Chemotherapy 44*, 3357-3363.

Rao, K. S., El-Hami, K., Kodaki, T., Matsuhige, K., & Makino, K. (2005). A novel method for synthesis of silica nanoparticles. *Journal of Colloid and Interface Science*(289), 125-131.

Ratanasiriwat, P., Worawattanamateekul, W., & Klaypradit, W. (2013). Properties of encapsulated wasabi flavour and its application in canned food. *International Journal of Food Science & Technology, 48*, 749-757.

Ricart, M., Guasch, H., Alberch, M., Barceló, D., Bonnineau, C., Geiszinger, A., . . . Sabater, S. (2010). Triclosan persistence through wastewater treatment plants and its potential toxic effects on river biofilms. *Aquatic Toxicology, 100*(4), 346-353.

Rohr, E. L., & Kaffenbergerber, W. (1993). Fluorescence instability of propidium iodide-labelled microspheres in (para)formaldehyde *Cytometry*(14), 584-586.

Rule, K. L., Ebbett, V. R., & Vikesland, P. J. (2005). Formation of chloroform and chlorinated organics by free-chlorine-mediated oxidation of triclosan. *Environmental Science & Technology, 39*(9), 3176-3185.

Saeed, M. O., Jamaluddin, A. T., Tisan, I. A., Lawrence, D. A., Al-Amri, M. M., & Chida, K. (2000). Biofouling in seawater reverse osmosis plant on the Red Sea coast, Saudi Arabia. *Desalination 128*, 177-190.

Sambrook, J., & Russel, D. W. (2001). *Molecular Cloning: A Laboratory Manual* (Third ed.). Cold Spring Harbor, NY: Cold Spring Harbor Laboratory Press.

Schaule, G., & Flemming, H.-C. (1997). Biofilmme in Reistwassersystemenein übersehenes kontaminationspotential. *SOFW-Journal 123*, 391-397.

Schleifer, K. H., & Kandler, O. (1972). Peptidoglycan types of bacterial cell walls and their taxonomic implications. *BACTERIOLOGICAL REVIEWS, 36*(4), 407-477.

Schlossbauer, A., Kecht, J., & Bein, T. (2009). Biotin-avidin as a protease-responsive cap system for controlled guest release from colloidal mesoporous silica. *Angewandte Chemie, International Edition, 48*, 3092–3095.

Sherry, E., Boeck, H., & Warnke, P. H. (2001). Topical application of a new formulation of eucalyptus oil phytochemical clears methicillin-resistant *Staphylococcus aureus* infection. *American Journal of Infection Control, 29*, 346.

Shuman, H. A., & Silhavy, T. J. (2003). Microbial genetics: The art and design of genetic screens: *Escherichia coli. Nature Reviews Genetics, 4*, 419-431.

Sikkema, J., DeBont, J. A. M., & Poolman, B. (1994). Interactions of cyclic hydrocarbons with biological membranes. *Journal of Biological Chemistry 269*, 8022-8028.

Simpson, M. L., Sayler, G. S., Applegate, B. M., Ripp, S., Nivens, D. E., Paulus, M. J., & Jellison, G. E. (1998). Bioluminescent-bioreporter integrated circuits form novel whole-cell biosensors. *Trends in Biotechnology, 16*, 332-338.

Sing, K. (2001). The use of nitrogen adsorption for the characterisation of porous materials. *Colloids and Surfaces A: Physicochemical and Engineering Aspects, 187-188*, 3-9.

Slater-Radosti, C., Van Alle, G., Greenwood, R., Nicholas, R., Keller, P. M., DeWolf, W. E. J., . . . Jaworski, D. D. (2001). Biochemical and genetic characterization of the action of triclosan on *Staphylococcus aureus*. *Journal of Antimicrobial Chemotherapy, 48*(11-6).

Slowing, I. I., Trewyn, B. G., Giri, S., & Lin, V. S. Y. (2007). Misoporous silica nanoparticles for drug delivery and biosensing applications. *Advanced Functional Materials, 17*, 1225–1236.

Smith, W. T. (1994). *Human and Environmental Safety of Hypochlorite*. Paper presented at the Proceedings of the 3rd World Conference on Detergents: Global Perspectives.

Song, Y., Li, G., Thornton, S. F., Banwart, S. A., Lerner, D. N., & Huang, W. E. (2009). Optimization of bacterial whole cell bioreporters for toxicity assay of environmental samples. *Environmental Science & Technology, 43*, 7931-7938.

Soumya, E.-A., Saad, I. K., Hassan, L., Ghizlane, Z., Hind, M., & Adnane, R. (2011). Carvacrol and thymol components inhibiting *Pseudomoas aeruginosa* adherence and biofilm formation. *African Journal of Microbiology Research, 5*(20), 3229-3232.

Springer, B., Kidan, Y. G., Prammananan, T., Ellrott, K., Böttger, E. C., & Sander, P. (2001). Mechanisms of streptomycin resistance: selection of mutations in the 16S rRNA gene conferring resistance. *Antimicrobial Agents and Chemotherapy, 45*, 2877-2884.

Steck, T. R. (2006). Viable but nonculturable bacteria. *Encyclopedia of Life Sciences*, a0000407.

Stewart, P. S. (2002). Mechanisms of antibiotic resistance in bacterial biofilms. *International Journal of Microbiology, 292*, 107-113.

Stöber, W., Fink, A., & Johnston, P. G. (1968). Controlled growth of monodisperse silica spheres in micron size range. *Journal of Colloid and Interface Science, 26*, 62-69.

Suci, P. A., Mittelman, M. W., Yu, F. P., & Geesey, G. G. (1994). Investigation of ciprofloxacin penetration on *Pseudomonas aeuriginosa* biofilms. *Antimicrobial Agents and Chemotherapy 38*, 2125-2133.

Suhr, K. I., & Nielsen, P. V. (2003). Antifungal activity of essential oils evaluated by two different application techniques against rye break spoilage fungi. *Journal of Applied Microbiology, 94*, 665-674.

Sun, J. T., Yu, Z. Q., Hong, C. Y., & Pan, C. Y. (2012). Biocompatible zwitterionic sulfobetaine copolymer-coated mesoporous silica nanoparticles for temperature-responsive drug release. *Macromolecular Rapid Communications, 33*(9), 811-818.

Suzuki, T., Fujikura, K., Higashiyama, T., & Takata, K. (1997). DNA staining for fluorescence and laser confocal microscopy. *Journal of Histochemistry & Cytochemistry, 45*(1), 49-53.

Sylvestre, M., Pichette, A., Longtin, A., Nagau, F., & Legault, J. (2006). Essential oil analysis and anticancer activity of leaf essential oil of *Croton flavens L.* from Guadeloupe. *Ethnopharmacology, 103*, 99-102.

Takenaka, S., Iwaku, M., & Hoshino, E. (2001). Artificial *Pseudomonas aeruginosa* biofilms and confocal laser scanning microscopic analysis. *Journal of Infection and Chemotherapy, 7*, 87-93.

Tao, C., & Fu, J. (2012). pH-responsive nanovalves based on hollow mesoporous silica spheres for controlled release of corrosion inhibitor. *Nanotechnology, 23*(23), 235605.

Teng, Z., Zhu, X., Zheng, G., Zhang, F., Deng, Y., Xiu, L., . . . Zhao, D. (2012). Ligand exchange triggered controlled-release targeted drug delivery system based on core–shell superparamagnetic mesoporous microspheres capped with nanoparticles. *Journal of Materials Chemistry, 22*, 17677-17684.

Tiensing, T., Preston, S., Strachan, N., & Paton, G. I. (2001). Soil solution extraction techniques for microbial ecotoxicity testing: a comparative evaluation. *Journal of Environmental Monitoring, 3*, 91-96.

Trewyn, B. G., Nieweg, J. A., Zhao, Y., & Lin, V. S. Y. (2008). Biocompatible mesoporous silica nanoparticles with different morphologies for animal cell membrane, penetration. *Chemical Engineering Journal, 137*, 23-29.

Trewyn, B. G., Slowing, I. I., Giri, S., Chen, H.-T., & Lin, V. S. Y. (2007). Synthesis and functionalization of a mesoporous silica nanoparticles based on the sol-gel process and applications in controlled release. *Accounts of Chemical Research, 40*, 846-853.

Tunc, S., Chollet, E., Chalier, P., Preziosi-Belloy, L., & Gontard, N. (2007). Combined effect of volatile antimicrobial agents on the growth of *Penicillium notatum*. *International Journal of Food Microbiology, 113*, 263-270.

Turgis, M., Han, J., Caillet, S., & Lacroix, M. (2009). Antimicrobial activity of mustard essential oil against *Escherichia coli* O157:H7 and *Salmonella typhi*. *Food Control, 20*, 1073-1079.

Turner, A., Wilson, G., & Kaube, I. (1987). *Biosensors: Fundatmentals and Applications*. Oxford, UK: Oxford University Press.

Tyrovola, K., & Diamadopoulos, E. (2005). Bromate formation during ozonation of groundwater in coastal areas in Greece. *Desalination, 176*, 201-209.

Ultee, A., Bennik, M. H., & Moezelaar, R. (2002). The phenolic hydroxyl group of carvacrol is essential for action against the food-borne pathogen *Bacillus cereus*. *Applied Environmental Microbiology, 68*, 1561-1568.

Ultee, A., Kets, E. P. W., & Smid, E. J. (1999). Mechanisms of action of carvacrol on food borne pathogen *Bacillus cereus*. *Applied and Environmental Microbiology, 6*, 4606-4610.

Upadhyay, A., Upadhyaya, I., Kollanoor-Johny, A., & Venkitanarayanan, K. (2013). Antibiofilm effect of plant derived antimicrobials on *Listeria monocytogenes*. *Food Microbiology, 36*(1), 79-89.

US Environmental Protection Agency, E. (2010). *Triclosan facts.*

US Environmental Protection Agency, E. (2012). *Disinfection byproducts: a reference resource.*

US Food and Drug Administration, F. (2010). *Triclosan: What consumers should know.*

Vaidya, S., Bhosale, R., & Singhal, R. S. (2006). Microencapsulation of cinnamon oleoresin by spray drying using different wall materials. *Drying Technology, 24*(8), 983-992.

Van den Berg, M., Birnbaum, L. S., Denison, M., De Vito, M., Farland, W., Feeley, M., . . . Peterson, R. E. (2006). The 2005 World Health Organization re-evaluation of human and mammalian toxic equivalency factors for dioxins and dioxin-like compounds. *Toxicological Sciences, 93*(2), 223-241.

Veldhoen, N., Skirrow, R. C., Osachoff, H., Wigmore, H., Clapson, D. J., Gunderson, M., . . . Helbing, C. (2006). The bactericidal agent triclosan modulates thyroid hormone-associated gene expression and disrupts postembryonic anuran development. *Aquatic Toxicology, 80*(3), 217-227.

Vivero-Escoto, J. L., Slowing, I. I., Wu, C.-W., & Lin, V. S. Y. (2009). Photoinduced intracellular controlled release drug delivery in human cells by gold-capped mesoporous silica nanosphere. *Journal of American Chemical Society, 131*, 3462-3463.

Voet, D., Voet, J. G., & Pratt, C. W. (2001). *Fundamentals of Biochemistry*. New York: Wiley.

Wagner, M., Ivleva, N. P., Haisch, C., Niessner, R., & Horn, H. (2009). Combined use of confocal laser scanning microscopy (CLSM) and Raman microscopy (RM): Investigations on EPS - Matrix. *Water Research, 43*, 63-76.

Wang, F., Guo, C., Yang, L.-R., & Liu, C.-Z. (2010). Magnetic mesoporous silica nanoparticles: Fabrication and their laccase immobilization performance. *Bioresource Technology, 101*, 8931-8935.

Wang, Y., Li, H., Wu, X., Xu, X., Jin, Z., & Tian, Y. (2013). Acid-thermal dextrin prepared from rice starch: Structure and encapsulation properties. *International Journal of Biological Macromolecules, 60*, 178-180.

Warnke, P. H., Becker, S. T., Podschun, R., Sivananthan, S., Springer, I. N., Russo, P. A., . . . Sherry, E. (2009). The battle against multi-resistant strains: Renaissance of antimicrobial essential oils as a promising force to fight hospital-acquired infections. *Journal of Cranio-Maxillofacial Surgery, 3337*, 392-397.

Weir, E., Lawlor, A., A., W., & F., R. (2008). The use of nanoparticles in antimicrobial materials and their characterization. *The Analyst 133*, 835-845.

Wikipedia. (2013). Galactoside, from http://en.wikipedia.org/wiki/%CE%92-galactoside

Williams, D., & Carter, C. B. (1996). 1 – Basics. In P. Press (Ed.), *Transmission Electron Microscopy*.

Xia, T. A., Kovochich, M., Liong, M., Meng, H., Kabehie, S., George, S., . . . Nel, A. E. (2009). Polyethyleneimine coating enhances the cellular uptake of mesoporous silica nanoparticles and allows safe delivery of siRNA and DNA constructs. *Acs Nano, 3*, 3273-3286.

Yamamoto, C., Neoh, T. L., Honbou, H., Yoshii, H., & Furuta, T. (2012). Kinetic analysis and evaluation of controlled release of D-Limonene encapsulated in spray-dried cyclodextrin powder under linearly ramped humidity. *Drying Technology, 30*, 1283–1291.

Yan, H., Zhu, L., Kwok, A., Li, X., Ågren, H., & Zhao, Y. (2013). Photothermal-responsive [2]rotaxanes. *Royal Society of Chemistry Advances, 3*(7), 2341-2350.

Yasunori, T., Takaaki, N., & Kazuhiko, M. (2007). Monitoring of biofilm in cooling water system by measuring lactic acid consumption rate. *Biochemical Engineering Journal, 35*(1), 81-86.

Yu, L., Chen, W., & Mulchandani, A. (2006). Review: Microbial bioensors *Analytica Chimica Acta., 568*, 200-210.

Zhang, F., & Keasling, J. (2011). Biosensors and their applications in microbial metabolic engineering. *Trends in Microbiology, 19*(7), 323-329.

Zhang, H., Li, Z., Xu, P., Wang, L., Di, Y., Lin, K., & Xiao, F.-S. (2010). A facile two step synthesis of novel chrysanthemum-like mesoporous silica nanoparticles for controlled pyrene release. *Chemical Communications 46*, 6738-6785.

Zhang, Y., Yuan, Q., Chen, T., Zhang, X., Chen, Y., & Tan, W. (2012). DNA-capped mesoporous silica nanoparticles as an ion-responsive release system to determine the presence of mercury in aqueous solutions. *Analytical Chemistry, 84*(4), 1956-1962.

Zhang, Z. Q., Pan, C. H., & Chung, D. (2011). Tannic acid cross-linked gelatin-gum arabic coacervate microspheres for sustained release of allyl isothiocyanate: Characterization and in vitro release study. *Food Research International, 44*(4), 1000-1007.

Zhao, Q., Wang, C., Liu, Y., & Wang, S. (2007). Bacterial adhesion on the metal-polymer composite coatings. *International Journal of Adhesion and Adhesives, 27*(2), 85-91.

Zhu, Y., Fang, Y., Bordchardt, L., & Kaskel, S. (2011). PEGylated hollow mesoporous silica nanoparticles as potential drug delivery vehicles. *Microporous and Mesoporous Materials, 141*, 199-206.

Zodrow, K. R., Schiffman, J. D., & Elimelech, M. (2012). Biodegradable polymer (PLGA) coatings featuring cinnamaldehyde and carvacrol mitigate biofilm formation. *Langmuir, 28*(39), 13993-13999.

Zou, Y., Woo, J., & Ahn, J. (2012). Cellular and molecular responses of Salmonella Typhimurium to antimicrobial-induced stresses during the planktonic-to-biofilm transition. *Letters in Applied Microbiology, 55*(4), 274-282.